Optimization of Renewable Energy Systems

Thesis submitted in partial fulfillment of the requirements for the degree of

DOCTOR OF PHILOSOPHY

By

Debasis Maharana

Roll No: 156107002

Department of Chemical Engineering

Indian Institute of Technology Guwahati

Guwahati-781039, India

Optimization of Renewable Energy Systems

Debasis Maharana

Dedicated to my wife, without whom I would have never pursued this path…

Department of Chemical Engineering
Indian Institute of Technology Guwahati
Guwahati, Assam − 781039, India

Declaration

I hereby declare that the thesis is a presentation of my original research work done under the guidance of my thesis supervisor, Dr. Prakash Kotecha, Associate professor, Department of Chemical Engineering, Indian Institute of Technology Guwahati. Wherever contributions of others are involved, every effort is made to indicate this clearly, with due reference to the literature. The work documented in this thesis has not been submitted to any other University or Institute for the award of any degree or diploma.

Debasis Maharana
Roll No: 156107002
Department of Chemical Engineering
Indian Institute of Technology Guwahati
Guwahati 781039, India
Date: 04-11-2024

Department of Chemical Engineering
Indian Institute of Technology Guwahati
Guwahati 781039, India

CERTIFICATE

It is certified that the work reported in the thesis entitled "**Optimization of Renewable Energy Systems**", by **Debasis Maharana** for the award of the degree of Doctor of Philosophy has been carried out under my supervision. To the best of my knowledge, the work documented in this thesis has not been submitted to any other University or Institute for the award of any degree or diploma.

Dr. Prakash Kotecha
Associate Professor
Department of Chemical Engineering
Indian Institute of Technology Guwahati
Guwahati 781039, India
Date:

Acknowledgements

I want to express gratitude to my research supervisor, **Dr. Prakash Kotecha,** for providing me with guidance throughout the entire course of this work. I would also like to thank all my doctoral committee members, **Prof. Tamal Banerjee** (Department of Chemical Engineering), **Prof. Rajib Kumar Bhattacharjya** (Department of Civil Engineering), and **Dr. R. Anandalakshmi** (Department of Chemical Engineering) for their valuable suggestions throughout my research work. I am also thankful to all the faculty members and staff of the Chemical Engineering Department for their help at various stages.

I also want to acknowledge the contribution of **Dr. Tulika Bhattacharyya** for her help in developing the solar energy models.

I want to thank all of my lab mates and friends at IIT Guwahati for making my stay enjoyable. While I acknowledge that conducting research at an institution such as IIT Guwahati can be rather demanding, I have always drawn inspiration from adventurous travel. I will specially thank my friend **Varun** for encouraging me to explore the unexplored.

I am grateful to my family back home and my in-laws for believing in me and supporting me during my research journey. I will always be short of words to describe the support I received from my wife, **Remya** and my eldest brother **Bikash**, without them I would have never been able to achieve this success.

Lastly, I acknowledge and thank myself for my dedication, perseverance, and positive outlook, which have helped me overcome many challenges during this research.

Debasis Maharana

IIT Guwahati

Abstract

There has been a sustained effort to reduce reliance on fossil fuels by transitioning to carbon-neutral energy sources like solar, wind, and tidal power. Biofuels, recognized as a sustainable energy option, offer a promising solution for meeting fuel demands. Among renewable energy sources, solar power stands out as one of the most widely adopted due to its abundant availability, lower capital costs compared to other renewables, and more predictable output, in contrast to the variability of wind and tidal energy. In order to commercialize and ensure the profitability of biofuel and solar energy systems, careful decision-making is required at various stages. This thesis addresses these challenges by proposing efficient optimization strategies for designing biorefinery supply chain networks and solar energy-based systems.

Considering the biomass-based energy systems, the corresponding supply chain is a combinatorial optimization problem that requires optimal decisions at multiple stages. One of the primary decisions to improve the benefits of a biorefinery supply chain is to use economic processing technologies. However, due to design limitations, such technologies are often restricted by their maximum processing capacity. The literature related to the capacity planning of biorefineries uses the single-unit strategy where only a single process unit per selected technology is allowed to be installed for biomass processing, leading to suboptimal production plans. Secondly, various constraints at different supply chain echelons make the problem computationally expensive. Most literature models employ a MILP approach for determining the optimal parameters; however, these techniques often use binary variables to assist in identifying decisions related to active flow domains, technology selection, etc. Metaheuristic techniques have been widely adopted for solving such combinatorial problems as these techniques are good for reaching near-optimal solutions in a reasonable time. However, the procurement and distribution of biomass and biofuel require multiple equality

constraints for the mass balance that needs to be satisfied at various biofuel production stages in bio-refineries. Such restrictions often induce difficulties for metaheuristic techniques in holding on to the feasible search space.

In this thesis, first, a new solution strategy for the optimization of biomass to biofuel supply chain is proposed, which can be easily adapted to different metaheuristic techniques. An implicit constraint handling technique is used that reduces the complexities found due to equality-type constraints. This framework also utilizes the nonlinear relationship between plant capacity and capital cost using economics of scale. The proposed framework is tested using multiple metaheuristic techniques on a bio-refinery case study. The framework is extended to address the capacity restriction of biofuel production from profitable processes due to design limitations of processing technologies. The single-unit framework is integrated with a novel heuristic algorithm that can implement multiple units of a beneficial process to overcome plant capacity limitations. Multiple metaheuristic techniques were used to demonstrate the benefits of the multi-unit strategy over the single-unit strategy in a distributed biorefinery case study.

In order to extend the benefits of a multi-unit strategy for MILP-based models, this thesis proposed a distributed multi-unit MILP supply chain model for biorefineries capable of utilizing multiple technologies for each biomass. A single-unit superstructure from the literature is improved to accommodate decisions related to multiple technological choices for different biomass and extended to a multi-unit model by allowing the installation of more than one process unit of the selected technology. This study incorporated the investment and operational costs for biorefinery, and the efficacy of the proposed model is demonstrated in the case study using linear approximations for the capacity-dependent investment costs. Further, a multi-objective, multi-unit, multi-period supply chain model to harness the benefits

of the multi-unit strategy for periodic supply chain networks is proposed to demonstrate the benefits of multi-unit strategy on periodic supply chains.

The second part of the thesis focuses on the strategies for solar-based energy systems. In solar-based renewable energy systems, solar air collectors are commonly used for space heating, irrigation, greenhouses, grain drying, hot air generation, etc. Similarly, the solar water heating (SWH) system is one of the most efficient solar conversion technologies for water heating and cooling applications. The performance of the collector depends significantly on its geometrical optical and operational parameters, and optimization is the only method to find the best controlling parameters that will yield the best-performing efficiency. Designing solar collectors requires in-depth studies of governing concepts and parameters that affect the operational condition and assembly process. Advanced solution techniques for solving solar models are a common practice. Despite the performance and wide usage of solar collectors depending on the optimum design and operational parameters, there have been very few insights available in the literature regarding the optimization problem formulation, details on decision variables, details on constraint parameters, optimization algorithm, and defined parameters, etc. Also, various approximations in the heat transfer processes of the system are observed in the literature, which often leads to losses in real-world system efficiency.

This thesis first proposes an exergetic optimization framework of simple and finned flat plate solar air collectors to determine the optimal design and operational parameters for humid subtropical climatic conditions. A simulation program is developed for the solar energy model, energy, and exergetic calculations. The proposed model is optimized using a metaheuristic technique for maximum mean exergy efficiency in simple and finned solar air collectors. This thesis also proposes a multi-objective flat plate solar water collector model to

determine the optimal performance and design conditions for a humid subtropical region. The proposed model is validated with the data in the literature and optimized using multiple metaheuristic techniques. Studies are performed to evaluate the trade-off solutions between the conflicting objectives of maximizing exergy efficiency and minimizing the area of the absorber plate.

This thesis proposes novel optimization frameworks for biomass-based and solar-based energy systems. For biorefineries, it introduces an implicit constraint handling technique to help metaheuristic techniques determine feasible solutions and provides a multi-unit strategy to overcome capacity limitations and improve efficiency in supply chain design. For solar energy systems, it presents exergetic optimization models for solar air and water collectors, focusing on optimizing design and operational parameters. This thesis demonstrates the benefits of these approaches through case studies and encourages broader adoption in large-scale applications.

CONTENTS

List of Figures

List of Tables

Chapter 1
Introduction

Conventional fossil fuels meet a significant part of the global energy demand, and the extensive energy dependency has led to the depletion of their global reserve as these non-renewable sources take millions of years for their formation. In addition, the rising pollution levels also compelled us to search for clean and sustainable energy sources. Apart from the energy requirement, most stakeholders have made efforts to become self-reliant and break the monopoly of countries rich in conventional fossil fuels (Alpanda & Peralta-Alva, 2010). Renewable energy uses range from small-scale domestic applications to large-scale centralized energy distribution systems. However, capital intensiveness and lower productivity adversely affect the wider usage of such energy systems. These systems are comparatively new and need timely development of innovative ideas for replacing non-renewable energy sources in the future. The majority of the world's energy requirement is satisfied using fossil fuels due to their extensive usage in the transportation and industrial sectors.

There has been a constant effort to shift the energy demand from fossil fuel to carbon-neutral sources such as solar, wind, tidal, etc.; however, an immediate transition is impossible as fossil fuel contributes 84% of the global primary energy demand (Ritchie & Roser, 2020). A steady shift in energy dependency on fossil fuels will help the industrial and transportation sectors cover financial burdens when adapting to newer technologies. One possible alternative for the energy requirements is biofuels produced using biomass as feedstock. Among the other types of renewable energy sources, solar energy has emerged as one of the most widely used because it is significantly less dangerous, not as high in capital costs as tidal and geothermal energy resources, and reasonably foreseeable, unlike tides and wind. The commercialization of biofuel and solar energy-based systems requires optimal decisions in various implementation stages.

The technical viability of biofuel production requires optimal biofuel supply chain networks, whereas the solar energy-based system needs higher system efficiencies.

1.1. Biorefinery superstructure for producing biofuel

Biofuels generate fewer emissions than their non-renewable counterparts and are cleaner as they are inherently biodegradable. Mixing biofuel with fossil fuel is practiced nowadays to harness the benefits of biofuel, leading the way to the steady transition from fossil fuel to biofuel. Vehicles fuelled with ethanol–methanol–gasoline blends can reduce the emission of carbon monoxide and unburnt hydrocarbons compared to pure gasoline (Elfasakhany, 2015). Due to the increasing urge for alternative renewable energy, the potential of biorefineries to fulfill the energy requirement can be witnessed in the coming years. However, the concept of biorefinery is still in the development stage, and the complications in the trade-offs between various metrics are hindering the growth of biorefineries at commercial scales.

Castillo-Villar et al., (2017) analyzed the effect of variability in biomass supply and quality on the strategic and tactical level decisions for designing and planning a biofuel supply chain using a two-stage stochastic programming model. Poor biomass quality was observed to increase the total cost by 27%–31%. The challenges in the timely delivery of homogeneous feedstock to customers, considering biomass quality, seasonality, and weather-related supply restrictions, were highlighted by Gautam et al., (2017). A terminal in the forest biomass feedstock supply chain allowed delivery of feedstock 4–11% lower in moisture content while reducing procurement costs by 11–32%. Khishtandar (2019) proposed a fuzzy chance-constrained programming model to help decision-makers design a biogas supply chain network under the risks associated with uncertain biomass availability, biomass demand, and available workforce. Chandel et al. (2018) discussed the critical issues associated with the scale-up of biorefineries from pilot-scale operations. Several factors, such as process integration, selection

of products, clear-cut master plans, risk factors analysis, cost sensitivity analysis, safety & regulatory norms, and reproducible economic modeling play a pivotal role in the transition towards large-scale biorefineries. The sustainability criteria in designing a multi-echelon supply chain were discussed by Tirkolaee et al. (2020), where the proposed multi-objective mixed-integer linear programming (MOMILP) model was able to select sustainable suppliers for the supply chain. The facility disruptions in complex supply chains were studied by Hatefi et al. (2019), and a bi-objective model for reliable supply chain network design was proposed. The model considered minimizing total supply chain network cost and recovery time from disruptions as the objectives.

The biorefinery supply chain involves a network of biomass sources, processing units, and demand locations connected through upstream, midstream, and downstream linkages, respectively (Basile et al., 2022). The upstream involves biomass production and its logistics in harvesting sites to refineries, the midstream constitutes biofuel production in refineries, and the downstream activities involve the distribution of biofuels to the market from the refineries. Each hub of the network requires several strategic and operational decisions for a cost-effective and sustainable biorefinery supply chain on an industrial scale (Espinoza Pérez et al., 2017).

It is necessary to evaluate the economic viability by optimizing the complete bioenergy supply chain network (Geraili et al., 2016) to move towards large-scale production and consumption of biofuels and other bioenergy products. This would be accomplished by thoroughly examining biomass feedstock production to the biofuel distribution by appropriately addressing the strategic and tactical choices. The selection of the best choices for biomass sources, processing facilities, and demand centers would also be necessary to execute such a complicated structure effectively. The optimization at the planning stages of a biorefinery superstructure is essential for their efficient and sustainable operations. The usage of pre-

feasibility analysis for the setting of biorefineries (Ortiz-Sanchez et al., 2020), utilization of new efficiency measuring tools (Moncada B et al., 2016), and identifying limitations affecting the performance of a process or design (How & Lam, 2019) are observed to be helpful to the biorefineries in moving towards commercialization.

1.2. Solar collectors for harvesting solar energy

Solar energy is considered carbon-neutral, clean, renewable energy, which helps reduce CO2 emissions, contributes to climate change mitigation, and provides clean energy for the environment. One of the direct applications of solar energy includes solar air heaters which are commonly used for space heating, running irrigation, greenhouses, grain drying in agricultural fields, hot air generation in manufacturing industries, etc. Flat plate solar collectors are the most popular air heaters because of their simple, low-cost designs and easy installations. It was noted that solar air heaters suffer from low heat transfer coefficient and low thermal efficiency, and they can be improved by choosing high thermal conductivity extended surfaces (fins) as absorber plates. However, realizing the potentiality of simultaneous application of the first and the second law of thermodynamics in the analysis and design of thermal systems (Bejan, 2002), exergy investigation is carried out in flat plate solar air collectors to achieve better efficiency, better use of existing design and better sustainability.

Exergy analysis allows many of the limitations of energy analysis to be controlled. Torres-Reyes et al., (2001) presented a design method for flat plate solar air collectors based on minimum entropy generation. They concluded that the proposed design methodology based on the entropy generation and mass flow numbers could be used for any flat plate collector geometry. Naphon (2005) analyzed the performance of a double-pass solar air heater with longitudinal fins and reported that the thermal efficiency is directly proportional to the height and number of fins, whereas entropy generation is inversely the same. Mohseni-Languri et al.

(2009) experimentally analyzed the solar air heater to find the optimum mass flow rate for maximum exergy efficiency. The introduction of metallic obstacles like baffles or fins inside the flow path provides a larger heat transfer area, higher throughput rates, and greater turbulence, which enhances the heat transfer characteristic of the system. Alta et al. (2010) performed energy and exergy analysis on three different solar air heaters with and without fins and reported the superiority of exergy analysis over energy. Though higher energy efficiency can be achieved at larger air flow rates, an increase in air flow rate increases leakage rates, which further decreases exergy efficiency.

Similar to solar air heaters, the solar water heating (SWH) system is one of the most efficient solar conversion technologies for water heating (Wang et al., 2015), space heating (Lugo et al., 2019), and cooling applications (Shirazi et al., 2018). SWH employs a low temperature (< 250 °C) category solar collectors for heating/cooling applications as the main component. This category includes flat plate collectors and evacuated tube collectors for their simple design and lower cost. The COP of the absorption cooling system depends on wall glazing, optical properties, and design modifications of solar collectors (Sakoda & Suzuki, 1986). In the recent past, a common array of solar thermal collectors has been used to supply the required energy demand of an entire building (space heating, cooling, and hot water) as a solarcombi system. Sustar et al. (2015) analyzed a solarcombi system as a function of loads, size, and location and found that the largest incremental savings occur when domestic solar hot water (DSHW) loads are low, and space heating loads are high. Asaee et al., (2016) reported a 19% decrease in the energy consumption and greenhouse gas (GHG) emissions of the Canadian housing stock. The performance of solarcombi systems using flat plate solar collector (FPSC) and evacuated tube solar collector (ETSC) for a two-story building was analyzed by Nájera-Trejo et al. (2016) for their optimum performance. Heat pipe-based evacuated tube solar collectors (ETSCs) offer higher outlet temperatures and higher efficiencies in water heating systems (Chopra et al.,

2018). Katsaprakakis (2019) concluded that introducing a solar combi system in the swimming pool heating of Pancretan Stadium, Crete, Greece, reduced the primary energy consumption by 75.6%.

1.3. Targeted research gaps and objectives

This thesis broadly tries to contribute efficient optimization strategies to design two types of renewable energy systems: biorefinery supply chain networks and solar energy-based systems. The research gaps and proposed solutions for both systems are presented below in two separate sections.

1.3.1. Biorefinery superstructures

For biofuels to be competitive with conventional fossil fuels, their production needs to be optimal, and it should account for various factors such as the type of biomass to be used, the technology used to convert biomass into biofuel, and the location of the production facility of biomass. Apart from the chosen technology, the quantity of biofuel production depends on the capacity of the technology at the processing unit, and it directly impacts the revenue of the refinery. The restriction on processing capacities might compel the distributed biorefineries to process the biomass at less profitable locations. The requirement of domain constraints on the capacity of the selected technology at the processing units requires specific measures to address the investment and operational level decisions. The requirement of optimization in the bioenergy supply chain has encouraged researchers to propose models addressing various critical aspects such as biomass quality and availability, transportation, technology selection, market demand, etc. (Ponce-Ortega & Santibañez-Aguilar, 2019). Most of the models are optimized using mathematical programming techniques (Ba et al., 2016) and are often observed to adopt model approximations to avoid nonlinearity (Soren & Shastri, 2021). These models utilize binary variables for decision-making and struggle to reach the optima within a finite

time (Hà et al., 2014; Olivares-Benitez et al., 2013). The use of metaheuristic techniques eliminates the above hurdle by providing near-optimal solutions within limited computational resources, as these techniques do not demand the model to be postulated in canonical form. These techniques are well-known black-box optimization solvers and do not require prior problem information. The complexity of the bioenergy supply chain involving many constraints requires a better solution framework for utilizing the effectiveness of metaheuristic techniques. However, the absence of dedicated constraint-handling techniques makes it difficult for these techniques to determine feasible solutions and marks this area open for research (Ba et al., 2016; Deb, 2000).

This thesis tries to contribute efficient optimization strategies to design biorefinery supply chain networks. First, the challenge for the metaheuristic techniques in determining feasible solutions due to the presence of a large number of equality constraints involving multiple decision variables in the model is addressed by proposing a novel framework suitable for metaheuristic techniques to optimize the biomass-biofuel supply chain network. A repair operator is introduced to improve potential solutions that violate the bound constraints on the flow rates and the processing capacity. The solution structure followed in the proposed framework inherently satisfies the requirement of selecting a particular technology for processing specific biomass in the processing units. A nonlinear cost function dependent on the processing capacity is adopted to determine the setup cost for the processing units. The optimization framework provides decisions at various biofuel production stages, such as biomass flow rates between the source and different processing units, technology selection for available biomass, and fuel distribution among demand locations. The proposed framework is extended to include a heuristic mechanism that helps in the capacity planning of the biorefineries by implementing multiple units of profitable technology. In addition to the

domain corrections for biomass and biofuel flow rates, the framework also incorporates repair schemes in the capacity planning stage.

The majority of the biorefinery supply chain networks are optimized using mixed-integer linear programming (MILP) due to their extensive modeling capabilities and assured global optimum. The use of the multi-unit strategy with metaheuristic techniques is observed to help gain economic benefits in the biorefinery superstructure, which motivated the implementation of a multi-unit strategy-based MILP model for the biorefinery superstructure. In this context, a single-unit biorefinery supply chain network adapted from the literature is modified to support multiple technological choices for each type of biomass. In addition, domain constraints related to the capacity selection of the processing technologies and biofuel distributions are also integrated with the supply chain network. Subsequently, the single-unit model is upgraded by incorporating the multi-unit strategy. The efficacy of the multi-unit model is demonstrated in the biorefinery case study with linear approximations for the cost calculations.

The biorefineries require periodic assessment of the operational decisions due to significant variations in the seasonal availabilities of biomass. These networks often utilize storage structures to satisfy demand during low-harvesting seasons. The application of the multi-unit strategy helps to avoid dependencies on larger capacity processing units by efficiently utilizing smaller processing units in conjunction with the storage facilities. The smaller processing facilities are also suitable for seasons with low biomass availability, thus reducing the requirement for excessive product inventory, which is observed with large capacity processing units and lesser periodic operations. The effectiveness of the multi-period, multi-unit strategy is demonstrated on a multi-period distributed biorefinery supply chain network available in the literature, and the model is modified to accommodate multiple processing units of the selected technology. The model incorporates storage facilities at various production and distribution

hubs for storing unprocessed raw materials and unutilized products. The network features multiple periods over which the products can be sold in the markets. The proposed multi-unit strategy-based supply chain model is solved by considering economic and social objectives.

1.3.2. Solar collector models

Solar collector models involve complex nonlinear equations and are often optimized using advanced optimization techniques. Various articles available in the literature have mainly focused on identifying the objective function of the problem with its constraints and the lack of crucial details on optimization problem formulation, decision variables, constraint parameters, optimization algorithm, and other user-defined parameters. Additionally, the assumption considered on various operational parameters often leads to losses in real-world system efficiency. Optimization involving exergy analysis of solar collectors allows many of the limitations of energy analysis to be controlled, as the lost exergy is the reason for the process inefficiency of the system. This thesis proposes an exergetic optimization framework for simple and finned flat plate solar air collectors to determine the optimal design and operational parameters. The framework employs a model for energy and exergetic calculations of solar air collectors. Optimization studies were performed using two models of solar air collectors: (a) with a simple air collector and (b) with a finned-type air collector. The framework utilizes a novel optimization approach where a metaheuristic technique is used to optimize decision variables and the trust-region dogleg algorithm to determine thermodynamically feasible operating conditions. Additional penalty functions are used in the framework to avoid any thermodynamically impractical system conditions. This framework is extended by considering water as the working fluid, and an optimization framework for flat plate solar water collectors based on exergy analysis is proposed to determine the optimum absorber plate area and exergy

efficiency for humid subtropical climatic conditions. Multiple metaheuristic techniques are used to determine the maximum exergy efficiency by optimizing the plate area of the absorber, mass flow rate, and inlet temperature of the working fluid. The trade-off solutions between the conflicting objectives of maximizing exergy efficiency and minimizing the absorber plate area are analyzed using six multi-objective metaheuristic techniques.

1.3.3. Research objectives

The research gaps outlined in Sections 1.3.1 and 1.3.2 concerning the biorefinery supply chain and solar energy systems can be encapsulated as follows.

- **Metaheuristic Techniques for Bioenergy Supply Chain Optimization**: While metaheuristic techniques offer advantages in handling complex optimization problems in the bioenergy supply chain, there is a gap in their ability to determine feasible solutions due to the presence of numerous equality constraints involving multiple decision variables. This highlights the need for improved frameworks that can effectively utilize metaheuristics while ensuring solution feasibility.
- **Constraint Handling in Metaheuristic Optimization**: The absence of dedicated constraint-handling techniques in existing metaheuristic approaches creates challenges in finding feasible solutions for the bioenergy supply chain, particularly when dealing with domain constraints such as biomass and biofuel flow rates, processing capacities, and technology selection.
- **Incorporation of Multi-Unit Strategies in Supply Chain Models**: Although mixed-integer linear programming (MILP) models are widely used for optimizing biorefinery supply chains, there is limited exploration of multi-unit strategies that could enhance

economic efficiency. The integration of such strategies into supply chain models, particularly with metaheuristic techniques, remains underexplored.

- **Multi-Unit Strategies for Seasonal Variations and Storage Considerations**: There is a gap in addressing the operational challenges posed by seasonal variations in biomass availability. Existing models often overlook the benefits of using smaller processing units in conjunction with storage facilities to reduce dependencies on larger units and excessive inventory, particularly in multi-period distributed biorefinery networks.
- **Detailed optimization formulation of Solar Collectors**: Existing literature primarily focuses on identifying the objective function and constraints in solar collector optimization but lacks a detailed optimization formulation of the problem.
- **Use of a wide range of metaheuristic techniques:** The existing literature lacks the use of multiple metaheuristic techniques for solving solar energy models.
- **Limited Consideration of Exergetic Optimization**: There is a gap in integrating exergy analysis into optimization frameworks to improve the thermodynamic efficiency of solar collectors.

The proposed solutions against the above-discussed research gaps related to biorefineries and solar energy systems are summarized below and are considered as the objectives of the thesis.

- Developing an efficient framework using metaheuristic techniques for the supply chain network of biorefineries with nonlinear cost functions.
- To propose a multi-unit strategy-based framework for the biorefinery supply chain network addressing the capacity planning of processing technologies.
- Proposing a mixed-integer linear programming model integrated with the multi-unit strategy for enhancing the economic benefits of biorefinery superstructure.

- Developing a multi-objective, multi-period mixed-integer linear programming model incorporating the multi-unit strategy for a distributed storage-based biorefinery supply chain with economic and social benefits.
- Developing a single objective framework using metaheuristic techniques for solar air collectors.
- Developing a multi-objective framework for solar water collectors using metaheuristic techniques.

1.4. Organization of the thesis

Chapter 1 discusses motivation and briefly overviews the optimization strategies proposed in the thesis. In Chapter 2, an efficient single-unit framework using metaheuristic techniques for the supply chain network of biorefineries is proposed, and the benefits of the framework are demonstrated using multiple metaheuristic techniques. The single-unit framework is extended to a multi-unit framework, and its benefits over the single-unit framework are discussed in Chapter 3. Chapter 4 discusses the implementation of a multi-unit strategy-based MILP model for the biorefinery superstructure. Chapter 5 presents a MILP model for a multi-unit, multi-period distributed biorefinery supply chain network with storage facilities. Chapter 6 proposes an optimization framework for solar air collectors using metaheuristic techniques, and Chapter 7 discusses a multi-objective metaheuristic framework for solar water collectors. Finally, Chapter 8 summarizes the significant inferences drawn from this thesis and provides suggestions for future research.

Chapter 2

A novel optimization framework using metaheuristic techniques for biorefinery supply chain network

This chapter discusses a novel framework suitable for metaheuristic techniques to optimize the biorefinery supply chain involving nonlinear cost functions. The proposed framework introduces a repair operator to improve potential solutions that violate the constraints in flow rates and processing capacities. An implicit constraint handling technique is employed to satisfy the constraints involved in mass balances. The efficacy of the proposed formulation and strategies are demonstrated using multiple metaheuristic techniques in a biorefinery case study.

This chapter is structured as follows: Section 2.1 provides the literature review related to the application of metaheuristic techniques to bioenergy models and their challenges. Section 2.2 presents the problem description, and Section 2.3 details the mathematical model and the general metaheuristic approach for optimizing the supply chain network. Section 2.4 explains the proposed solution strategy to improve the performance of metaheuristic techniques and briefly highlights the features of the selected techniques. Section 2.5 provides details of the case studies used in this chapter. Section 2.6 provides a detailed analysis of the results and discusses the various benefits of the proposed strategy. The last section concludes the chapter by summarising the benefits of the proposed strategy and the overall performance of the metaheuristic techniques.

2.1. Background

The advancement towards large-scale production and use of biofuels and other bioenergy products requires assessing the economic feasibilities, systematic design, and optimization of the entire bioenergy supply chain network. In order to attain such an efficient system, proper analysis from the biomass feedstock production to the biofuel/bioenergy end-use and suitable

handling of strategic and tactical decisions is required (Struhs et al. 2020; Akhtari and Sowlati 2020). The successful implementation of such a complex structure requires multiple optimal decisions at various contact points, such as biomass sources, processing units, and demand centers.

Metaheuristic techniques are intelligent search methods that mimic the different ways of optimization occurring in nature. These methods are highly efficient in solving complex optimization models where the problems are considered NP-hard (Reche-López et al. 2009; Ayoub et al. 2009), or the optima cannot be easily obtained using convex optimization algorithms (Sarker, Wu, and Paudel 2019). Metaheuristic algorithms also help solve multimodal problems where traditional techniques get trapped in local optima (Schwefel 1993; Ge and Li 2018). Metaheuristics are also best suited for solving problems with multiple objectives (Hernández-Pérez et al. 2019). Metaheuristic techniques have been applied for solving biorefinery optimization models, such as determining optimal locations of mobile and fixed biorefineries in biomass to bio-oil model using genetic algorithm (Sadeghi and Haapala 2019), parameter optimization for methane production from microalgae using particle swarm optimization (Nassef et al. 2021), determining optimal placement and supply area for the biomass plant using binary honey bee foraging algorithm (Vera et al. 2010) and binary particle swarm optimization (Reche López et al. 2008), a decision support system for multi-biomass energy conversion in providing electricity, heating, and cooling using genetic algorithm and sequential quadratic programming (A. A. Rentizelas, Tatsiopoulos, and Tolis 2009) and so on. To the best of our knowledge, the availability of works utilizing metaheuristics to optimize the biorefinery supply chain from biomass source to demand satisfaction is scarce (Ba, Prins, and Prodhon 2016). The primary reason for this lacuna is the involvement of numerous constraints at various nodes of this superstructure, necessitating the extensive requirement of constraint

handling techniques. Conventionally, the metaheuristic techniques handle model constraints by assigning a worse fitness value to the infeasible solutions. The fitness of such solutions is usually determined using various penalty approaches (Deb 2000). Among the types of constraints, the equality constraints are hard-binding ones and often induce infeasibility in the solutions. These constraints often tighten the search space and force the metaheuristic techniques to restrict the search to an n-1 dimensional hyperplane for an n-dimensional constraint. The requirement of mass balancing at various distribution points translates into equality-type constraints in the biorefinery supply chain. A proper direction to handle the equality constraints in the models would aid the metaheuristics in providing various tactical and operational level optimal decisions.

A biorefinery utilizes different processing technologies to produce valuable products (Yue, You, and Snyder 2014; Bala et al. 2016) from the biomass procured from harvesting sites. The possibility of considering processing technology and biomass flow rate as decision variables inherently makes the model nonlinear and limits the likeliness of solving the model using linear optimization techniques. The decision variables representing the flow rate of raw materials and products have a discrete domain to avoid any value indicating an impractical flow rate, resulting in domain constraints. The above constraints are generally realized using binary variables in the mathematical model, exponentially increasing the computational complexity for expensive case studies. Additionally, the plant capital cost varies nonlinearly with the processing capacity (Bowling, Ponce-Ortega, and El-Halwagi 2011), which is crucial in utilizing economics of scale. These models often use approximations for the cost calculations to avoid complications and are optimized using linear solvers (Bowling, Ponce-Ortega, and El-Halwagi 2011; Soren and Shastri 2021; El-Halwagi et al. 2013). In this chapter, attempts were made to overcome these limitations by proposing a model devoid of binary variables and

suitable for metaheuristic techniques. The absence of additional variables for tackling the domain constraints and technology selection makes the model compact and dimensionally inexpensive. The strategy implicitly handles the equality type nonlinear mass balance constraints in converting the raw material into fuel, increasing the probability of determining feasible solutions using metaheuristic techniques. The model studied in this chapter has incorporated a nonlinear function for determining the capital cost required for implementing the processing units. Although metaheuristic techniques do not guarantee the determination of global optima, they are highly efficient in solving complex nonlinear optimization problems (Ge and Li 2018; Aguitoni et al. 2018). Thus, their usage is justified to handle the nonlinearity arising at the product processing stage of biorefineries and in determining plant capital cost.

2.2. Problem statement

The bio-fuel supply chain model (El-Halwagi et al. 2013) satisfies the biofuel demand of users located at various geographical locations using multiple processing plants. The processing plants are categorized as the main processing unit with greater processing capacities near biomass sources and secondary processing units with smaller capacities installed close to the demand locations. The biofuel demand of the users can be satisfied by (i) the main processing unit, (ii) the secondary processing units, and (iii) a combination of main and secondary processing units.

A generalized superstructure for the biomass-to-biofuel supply chain network is provided in Fig 2.1. The superstructure requires decisions at various biofuel production stages, such as biomass flow rates between the source and different processing plants, technology selection for available biomass, and fuel distribution between demand locations. The cost of biomass depends on the feedstock type and its quality, whereas transportation cost varies with transport

mode and distance between various hubs. The plant setup and yearly processing costs of specific biomass depend on the type of technology used and the capacity of the plant. The objective of the optimization model is to minimize the total cost while satisfying the demand for plant life.

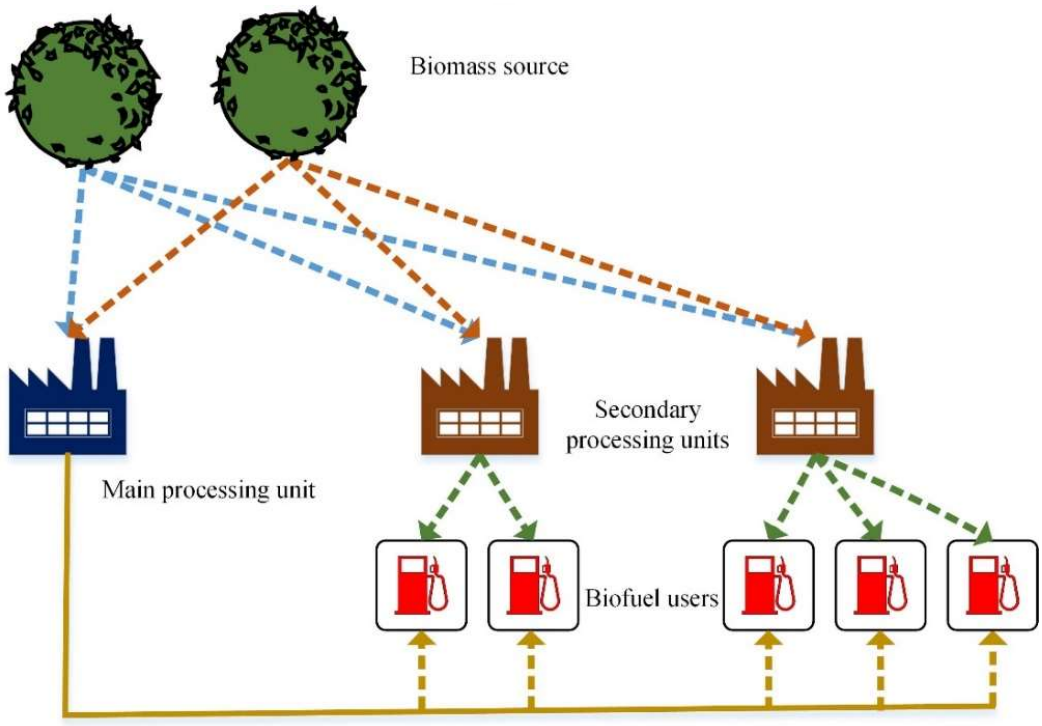

Fig 2.1 Generic superstructure of the biomass-biofuel supply chain

Nomenclature

Sets

H	Set representing the harvesting sites
I	Set representing the type of biomass
J	Set representing the secondary processing units
D_j	Set representing the users are secondary location j
T_i	Set representing the available conversion technologies for biomass (i)

Indexes

i	Index of biomass source $i \in I$
j	Index of secondary location $j \in J$
d	Index of users corresponding to j^{th} secondary location, $d \in D_j$
t	Index of conversion technologies for i^{th} raw material type, $t \in T_i$

Parameters

$A_{h,i}$	Total biomass (i) available at harvesting site (h)
$B_{h,i}$	Unit cost of biomass (i) from harvesting source (h)
$CAP_i^{Main-Min}$	Minimum processing capacity at the main processing unit for i^{th} biomass
$CAP_i^{Main-Max}$	Maximum processing capacity at the main processing unit for i^{th} biomass
$Ct_{h,i}^{Bio-Main}$	Transportation cost of biomass (i) from harvesting source (h) to the main processing unit
$Ct_{h,i,j}^{Bio-Sec}$	Transportation cost of biomass (i) from harvesting source (h) to secondary processing unit (j)
$Ct_j^{Main-Sec}$	Transportation cost of the product from the main processing unit to a secondary location (j)
F_{Min}^{Main}	Minimum biomass flow rate required for the main processing unit
F_{Max}^{Main}	Maximum biomass flow rate allowed for the main processing unit
F_{Min}^{Sec}	Minimum biomass flow rate required for the secondary processing unit
F_{Max}^{Sec}	Maximum biomass flow rate allowed for the secondary processing unit
H_Y	Yearly working days
k_{Max}^{Main}	Maximum product flow rate allowed for the main processing unit
k_{Min}^{Main}	Minimum product flow rate allowed for the main processing unit
P_{Factor}	Large constant value for the cumulative penalty
$Z_{j,d}$	Product demand for user (d) at the secondary processing unit (j)
δ	Coefficient for the economy of scale

Determined parameters

τ_i^t	Biomass to the biofuel conversion factor for technology (t) corresponding to biomass type (i)
a_i^t	Fixed cost coefficient for installing t^{th} technology corresponding to i type biomass at secondary processing units
b_i^t	Variable cost coefficient for installing t^{th} technology corresponding to i type biomass at secondary processing units
BC^{Main}	Total biomass procurement cost for the main processing unit
BC_j^{Sec}	Total biomass procurement cost for the j^{th} secondary processing unit
C^{Main}	Total capital cost for the main processing unit
C_j^{Sec}	Total capital cost for the j^{th} secondary processing unit
f	Fitness value of the potential solution
k_j^{Main}	Total product flow rate from main processing unit to j^{th} secondary processing unit
k_j^{Sec}	Total product flow rate from j^{th} secondary processing unit to corresponding demand locations
K^{Main}	Total product produced at the main processing unit
MCp_i^t	Processing cost of biomass (i) from technology (t) at the main processing unit
P_{Domain}^{Main}	Penalty for domain violation of biomass flow rate in the main processing unit
$P_{CAP}^{Main-min}$	Penalty for minimum capacity limit violation in the main processing unit
$P_{CAP}^{Main-max}$	Penalty for maximum capacity limit violation in the main processing unit
$P_{Upper}^{Product}$	Penalty for upper bound violation in the product flow rate from the main processing unit
$P_{Lower}^{Product}$	Penalty for domain violation in the product flow rate from the main processing unit
P_{Domain}^{Sec}	Penalty for the domain violation in the biomass flow rate to the secondary processing units
P_{Domain}	Penalty for domain violation in upper bound of product flow rate
$P_{Resource}$	Penalty for violation of raw material availability constraint
P_{Demand}	Penalty for unsatisfied demand
PC^{Main}	Total processing cost in the main processing unit
PC_j^{Sec}	Total processing cost in the j^{th} secondary processing unit
SCp_i^t	Processing cost of biomass (i) from technology (t) at the secondary processing unit

$TC^{Bio-Main}$	Total biomass transportation cost for the main processing unit
$TC^{Product-Main}$	Total product transportation cost for the main processing unit
$TC_j^{Bio-Sec}$	Total biomass transportation cost for the j^{th} secondary processing unit
TAC	Total cost
$Vio_{h,i,j}^{Sec}$	Domain violation of the i^{th} biomass flow rate to the j^{th} secondary processing unit
$Vio_j^{Product}$	Domain violation in product flow rate to j^{th} secondary processing unit
Vio_j	Upper bound violation in the product flow rate in the j^{th} secondary processing unit
$V_{j,d}$	Unsatisfied demand for user d in the j^{th} secondary processing unit
$V_{h,i}$	Violation in biomass (i) availability at source (h)
w_i^t	Binary variable denoting the selection of (t) type technology corresponding to (i) type biomass
x_i^t	Fixed cost coefficient for installing technology (t) corresponding to (i) type biomass at the main processing unit
y_i^t	Variable cost coefficient for installing technology (t) corresponding to (i) type biomass at the main processing unit

Decision Variables

$F_{h,i}^{Main}$	Flow rate of biomass (i) from harvesting site (h) to the main processing unit
$F_{h,i,j}^{Sec}$	Flow rate of biomass (i) harvesting site (h) to the secondary location (j)
t	Selected technology $t \in T_i$
$US_{j,d}^{Main}$	Product share of the user (d) in the secondary processing unit (j) from the main processing unit.
$US_{j,d}^{sec}$	Product share of the user (d) from the secondary processing unit (j))
$U_{j,d}^{Main}$	Product delivered to user (d) in the secondary processing unit (j) from the main processing unit
$U_{j,d}^{Sec}$	Product delivered to the user (d) in the secondary processing unit (j).

2.3. General metaheuristic-based strategy for the superstructure

The model constitutes a set of bioresources or harvesting sites ($h \in H$) capable of supplying different types of biomass ($i \in I$) to the main processing unit and a group of secondary processing units ($j \in J$) for biofuel production (El-Halwagi et al. 2013). Each secondary processing location has a set of users ($d \in D_j$) with a specific demand ($Z_{j,d}$). The procured biomass can be processed using one of the appropriate technologies ($t \in T_i$) available for processing. The model requires three significant decisions: (i) the raw material flow rate from the harvesting sites to the main processing unit ($F_{h,i}^{Main}$) and the secondary processing units ($F_{h,i,j}^{Sec}$), (ii) the product flow rate from the main processing unit ($U_{j,d}^{Main}$) and the secondary processing units ($U_{j,d}^{Sec}$) to the demand locations, and (iii) the conversion factor of the technology determined using a determined variable (τ_i^t) for processing the biomass at each of the processing units. The choice of the conversion factor depends on the integer decision variable $t \in T_i$. The model explained below relies on the penalty approach to avoid infeasible solutions and is termed the standard model for further discussions. The proposed strategy, explained in the later section, utilizes domain corrections and repair schemes to satisfy some of the constraints and thus reduces the number of constraints. The metaheuristic strategy inherently does not require binary variables; however, to depict the constraints mathematically, a binary variable (w_i^t) is used in certain constraints. The variable represents the technology (t) used to process the appropriate biomass (i) at any processing facility. The detailed solution strategy and the selection of technologies in the proposed technique are explained in the later sections.

2.3.1. Balances at the harvesting locations

The total amount of biomass (i) supplied from a source (h) to the main processing unit ($F_{h,i}^{Main}$) as well as to the secondary processing units ($F_{h,i,j}^{Sec}$) cannot exceed the available feedstock ($A_{h,i}$), as given in Equation (2.1) (El-Halwagi et al. 2013).

$$F_{h,i}^{Main} + \sum_{j \in J} F_{h,i,j}^{Sec} \leq A_{h,i} \qquad \forall h \in H, \forall i \in I \tag{2.1}$$

The above constraint is realized by associating a penalty value ($P_{Resource}$), which is a function of the constraint violations ($Vio_{h,i}$) that occurred at the harvesting sites. The violation ($Vio_{h,i}$) in the constraint associated with biomass flow at any harvesting location exists only when the total biomass transported from a harvesting site is higher than the actual availability and is determined using Equation (2.2).

$$Vio_{h,i} = \begin{cases} \left(F_{h,i}^{Main} + \sum_{j \in J} F_{h,i,j}^{Sec} \right) - A_{h,i}, & if \;\; F_{h,i}^{Main} + \sum_{j \in J} F_{h,i,j}^{Sec} > A_{h,i} \\ 0 & else \end{cases} \qquad \forall i \in I, h \in H$$

$$P_{Resource} = \sum_{h \in H} \sum_{i \in I} Vio_{h,i} \tag{2.2}$$

2.3.2. Balances at the main processing unit

The processing of biofuel in the main processing unit involves biofuel production from various available biomass using appropriate technologies. The associated costs include the capital cost for implementing the technology and the operating cost of the processing unit. The capital cost of the main processing unit depends on the technology selected for the feedstock conversion and the processing capacity of the unit, whereas the operating cost of the unit is dependent on the transportation, procurement, and processing costs of the feedstock.

The biomass (i) received from each source (h) is processed using an appropriate technology ($t \in T_i$) selected from a set of available technologies. The selection of different technologies also changes the product yield, as the yield depends on a technology-dependent conversion factor (τ_i^t). Each of the secondary processing units (j) can receive biofuel (k_j^{Main}) from the main processing unit to satisfy the available user demands ($U_{j,d}^{Main}$). The Equations (2.3) and (2.4) represent the mass balance for biomass and the processed biofuel distribution to end-users at the main processing unit. In order to represent the technology selection mathematically, a binary variable is introduced in the Equation (2.3). The binary variable (w_i^t) represents the selection of technology (t) from the set of available technologies (T_i) suitable for the selected biomass (i).

$$K^{Main} = \sum_{i \in I} \sum_{t \in T_i} \tau_i^t w_i^t \left(\sum_{h \in H} F_{h,i}^{Main} \right) \tag{2.3}$$

$$K^{Main} = \sum_{j \in J} k_j^{Main} \quad and \quad k_j^{Main} = \sum_{d \in D_j} U_{j,d}^{Main}, \quad \forall\, j \in J \tag{2.4}$$

Unlike the mixed integer linear programming (MILP) model, binary variables are not required for the model that can be solved using metaheuristic techniques. However, a binary variable is used for the mathematical representation of the technology selection, and it is not considered while implementing Equation (2.3) in the objective function. The value of the conversion factor (τ_i^t) for a technology is a known constant; however, the technology selection is a decision variable. In the Equation (2.3), the term ($\tau_i^t w_i^t$) confirms that the conversion factor of the selected technology for a specific biomass is multiplied by the total flow of the same biomass. In order to illustrate the selection of technologies for biomass at the processing units, consider

the example given in Fig 2.2. In the example, three different sets of technologies are available for processing biomass types 1, 2, and 3. Each set can constitute one or more technologies for processing appropriate biomass. Based on the example given in Fig 2.2, the second technology is selected for biomass 1 among the three types of technologies available; accordingly, the conversion factor corresponding to the second technology of biomass 1 (τ_1^2) is selected at the processing facility.

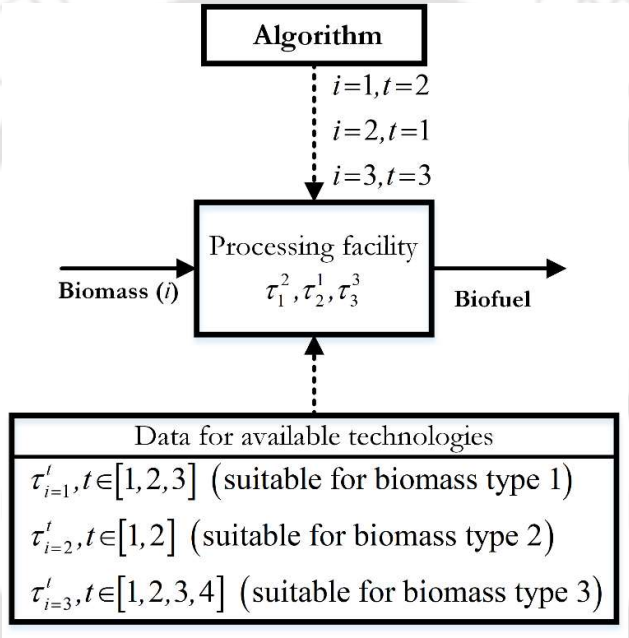

Fig 2.2 Selection of technology for biomass processing

Similarly, the conversion factors (τ_2^1 and τ_3^3) are selected for biomass types 2 and 3. As per this model, an integer variable for selecting the appropriate technology (t) corresponding to the biomass (i) is considered, which in turn selects the value of the conversion factor (τ_i^t) used in the Equation (2.3). The bounds of the integer variable are dependent on the number of technologies available for biomass. The solution modeling given in Section 5 further demonstrates the selection of technologies and corresponding valuable parameters. The total product produced at the main processing unit is determined by first accumulating the individual

biomass received from each harvesting site and is calculated as in Equation (2.4). Each type of biomass (i) is processed using a chosen technology appropriate for the selected biomass (τ_i^t), and the total biofuel is determined by summing all the produce. The biomass processing facilities at the main processing unit can operate under a maximum ($CAP_i^{Main-Max}$) and a minimum ($CAP_i^{Main-Min}$) processing capacity. The processing capacity of zero for any biomass indicates the absence of the corresponding processing facility at the main processing unit (Santibañez-Aguilar et al. 2014; El-Halwagi et al. 2013).

$$\left(\sum_{h\in H} F_{h,i}^{Main} = 0\right) \vee \left(CAP_i^{Main-Min} \le \sum_{h\in H} F_{h,i}^{Main} \le CAP_i^{Main-Max}\right), \quad i \in I \tag{2.5}$$

Any violation in the lower or upper bound of the processing capacity is penalized using Equations (2.6) and (2.7). The violation in the lower bound is realized using a hard penalty (M), as the lower capacity limit has dual boundaries of approach; a proper dynamic penalty function is difficult to decide. The penalty for violating the lower bound is determined using Equation (2.6). The violation in the upper bound is penalized with respect to the magnitude of violation from the maximum processing unit capacity as Equation (2.7).

$$Vio_i = \begin{cases} M & if\ 0 < \sum_{h\in H} F_{h,i}^{Main} < CAP_i^{Main-Min} \\ 0 & else \end{cases}, \quad \forall i \in I$$
$$P_{CAP}^{Main-min} = \sum_{i\in I} Vio_i \tag{2.6}$$

$$Vio_i = \begin{cases} \sum_{h\in H} F_{h,i}^{Main} - CAP_i^{Main-Max} & if \sum_{h\in H} F_{h,i}^{Main} > CAP_i^{Main-Max} \\ 0 & else \end{cases}, \quad \forall i \in I$$
$$P_{CAP}^{Main-Max} = \sum_{i\in I} Vio_i \tag{2.7}$$

The transportation of biomass and biofuel from various sources requires a minimum flow rate and is restrained by an upper limit for the flow rate. This domain restriction on the flow rate is important as it avoids any unrealistic flow rates. For example, a flow rate of 0.001kg/day of biomass may be practically undesirable. The flow domain of the biomass and the biofuel in the main processing unit is provided in Equations (2.8) and (2.9). Any nonzero biomass and biofuel flow rates in the main processing unit are valid only in the appropriate flow interval (El-Halwagi et al., 2013).

$$\left(F_{h,i}^{Main}=0\right) \vee \left(F_{Min}^{Main} \le F_{h,i}^{Main} \le F_{Max}^{Main}\right) \quad \forall i \in I, h \in H \tag{2.8}$$

$$\left(k_{j}^{Main}=0\right) \vee \left(k_{Min}^{Main} \le k_{j}^{Main} \le k_{Max}^{Main}\right) \quad \forall j \in J \tag{2.9}$$

The standard approach introduces penalties (M) for violating the flow domains as given in the Equation (2.10). The upper bound of the decision variables directly addresses the violation in the upper flow rate of biomass. The presence of discontinuity at the minimum required flow rate forbids using bounds alone to realize constraints provided in Equations (2.8) and (2.9).

$$\begin{aligned} Vio_{h,i} &= \begin{cases} M & if\ 0 < F_{h,i}^{Main} < F_{Min}^{Main} \\ 0 & else \end{cases} \quad \forall i \in I, h \in H \\ P_{Domain}^{Main} &= \sum_{i \in I} \sum_{h \in H} Vio_{h,i} \end{aligned} \tag{2.10}$$

Similarly, the penalty corresponding to the violation in the bounds of the biofuel flow rate is provided in the Equation (2.11).

$$\begin{aligned} Vio_{j} &= \begin{cases} M & if\ 0 < k_{j}^{Main} < k_{Min}^{Main} \\ 0 & else \end{cases} \quad \forall j \in J \\ P_{Lower}^{Product} &= \sum_{j \in J} Vio_{j} \end{aligned} \tag{2.11}$$

Any violation in the upper bound of the product flow rate from the main processing unit to the secondary processing unit is penalized. The assigned penalty value ($P_{Upper}^{Product}$) is a function of flow rate violation occurring in the main processing unit and is calculated using the Equation (2.12). Unlike the hard penalty assigned for domain violation of biomass flow rate, an adaptive penalty is considered to penalize the solution that violates the biofuel flow rate.

$$Vio_j = \begin{cases} k_j^{Main} - k_{Max}^{Main}, & if\ k_j^{Main} > k_{Max}^{Main} \\ 0 & else \end{cases} \quad \forall j \in J$$
$$P_{Upper}^{Product} = \sum_{j \in J} Vio_j, \quad \forall j \in J \tag{2.12}$$

The cost associated with biofuel production and supply includes the biomass procurement cost (BC^{Main}), the capital cost of the processing unit (C^{Main}), the processing cost for the biomass obtained from different harvesting sites (PC^{Main}), and the transportation costs for transferring biomass from harvesting sites to the main processing unit ($TC^{Bio-Main}$) and biofuel to secondary locations ($TC^{Product-Main}$). The procurement and processing cost of the biomass are given in Equations (2.13) and (2.14). In Equations (2.13) and (2.14), the term $B_{h,i}$ represents the unit cost of biomass (i) procured from the harvesting site (h), whereas the term MCp_i^t represents the unit processing cost of biomass (i) using the selected technology (t) (El-Halwagi et al. 2013).

$$BC^{Main} = \sum_{h \in H} \sum_{i \in I} F_{h,i}^{Main} B_{h,i} \tag{2.13}$$

$$PC^{Main} = \sum_{i \in I} \sum_{t \in T_i} MCp_i^t w_i^t \left(\sum_{h \in H} F_{h,i}^{Main} \right) \tag{2.14}$$

In Equation 2.14, the binary variable (w_i^t) is used to mathematically represent the determination of processing cost with respect to the technology (t) chosen for the biomass (i). The transportation costs related to biomass feed to the main processing unit and biofuel to the secondary locations are given in Equations (2.15) and (2.16) , respectively (El-Halwagi et al. 2013).

$$TC^{Bio-Main} = \sum_{i \in I} \sum_{h \in H} F_{h,i}^{Main} Ct_{h,i}^{Bio-Main} \tag{2.15}$$

$$TC^{Product-Main} = \sum_{j \in J} k_j^{Main} Ct_j^{Main-Sec} \tag{2.16}$$

The capital cost is a technology-dependent parameter, and the cost coefficients are taken as per the selected technology with a nonlinear relationship between processing unit capacity and capital cost, as depicted in Fig 2.3.

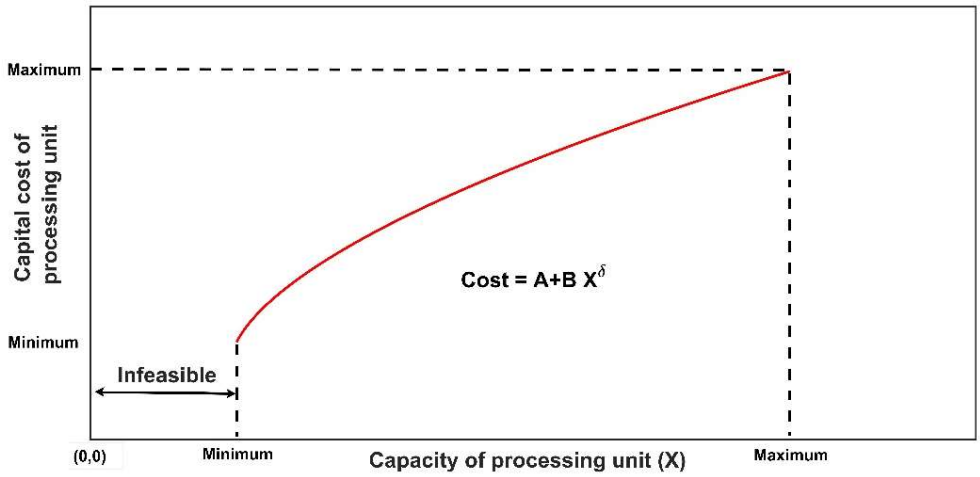

Fig 2.3 Nonlinear relation between plant capacity and its capital cost

For any biomass ($i \in I$), the capital cost for the processing unit with a chosen technology ($t \in T_i$)with the selected processing unit capacity is determined using Equation (2.17), where

the cost coefficients (x_i^t) and (y_i^t) are technology-dependent, and the exponent (δ) is used to account for economic scaling (Bowling, Ponce-Ortega, and El-Halwagi 2011). The values of cost coefficients (x_i^t and y_i^t) in the Equation (2.17) are chosen depending on the selected technology (t) for the biomass (i).

$$C^{Main} = \sum_{i \in I} \sum_{t \in T_i} w_i^t \left(x_i^t + y_i^t \left(\sum_{h \in H} F_{h,i}^{Main} \right)^{\delta} \right) \tag{2.17}$$

2.3.3. Balances at the secondary processing units

The model considers the users at the secondary locations, and biofuel produced at the secondary processing units is distributed directly to the users, neglecting any fuel transportation cost.

Each of the secondary processing units receives different biomass ($i \in I$) from each source ($h \in H$) and processes them using an appropriate technology selected from the set of available technologies ($t \in T_i$). Each secondary processing unit distributes biofuel (k_j^{Sec}) among the users located in that region ($U_{j,d}^{Sec}$). In Equation (2.18), the value of the conversion factor (τ_i^t) is selected appropriately for processing the biomass (i) using the selected technology (t) at the secondary processing unit (j).

$$k_j^{Sec} = \sum_{i \in I} \sum_{t \in T_i} \tau_i^t w_i^t \left(\sum_{h \in H} F_{h,i,j}^{Sec} \right), \quad \forall j \in J \tag{2.18}$$

$$\sum_{d \in D_j} U_{j,d}^{Sec} = k_j^{Sec} \quad \forall\, j \in J \tag{2.19}$$

The distribution of biofuel to various end users from a secondary processing unit is mathematically represented in the Equation (2.19). Analogous to the biomass processing facilities at the main processing unit, the processing at secondary facilities can operate under a maximum and minimum processing domain as given in Equation (2.20) (El-Halwagi et al. 2013).

$$\left(\sum_{h\in H} F_{h,i,j}^{Sec}=0\right)\vee\left(CAP_i^{Sec-Min}\le\sum_{h\in H} F_{h,i,j}^{Sec}\le CAP_i^{Sec-Max}\right),\quad i\in I, j\in J \tag{2.20}$$

The occurrence of a violation at the lower or upper bound of the processing capacity is penalized using Equations (2.21) and (2.22).

$$Vio_{i,j}=\begin{cases} M & if\ 0<\sum_{h\in H} F_{h,i,j}^{Sec}<CAP_i^{Sec-Min} \\ 0 & else \end{cases},\quad \forall i\in I, j\in J$$
$$P_{CAP}^{Sec-Min}=\sum_{j\in J}\sum_{i\in I} Vio_{i,j} \tag{2.21}$$

$$Vio_{i,j}=\begin{cases} \sum_{h\in H} F_{h,i,j}^{Sec}-CAP_i^{Sec-Max} & if\ \sum_{h\in H} F_{h,i,j}^{Sec}>CAP_i^{Sec-Max} \\ 0 & else \end{cases},\quad \forall i\in I, j\in J$$
$$P_{CAP}^{Sec-Max}=\sum_{j\in J}\sum_{i\in I} Vio_{i,j} \tag{2.22}$$

The flow rate of biomass from various harvesting sites to secondary processing units follows a domain constraint as in Equation (2.23) that restricts the minimum (F_{Min}^{Sec}) and maximum (F_{Max}^{Sec}) possible flow rate required for a feasible transportation link. Unlike the main processing unit, the users and secondary processing units are located at a common location and avoid any fuel flow limit (El-Halwagi et al. 2013).

$$\left(F_{h,i,j}^{Sec}=0\right)\vee\left(F_{Min}^{Sec}\le F_{h,i,j}^{Sec}\le F_{Max}^{Sec}\right)\quad \forall h\in H, i\in I, j\in J \tag{2.23}$$

The above constraints are handled similarly to the domain constraints discussed for the main processing unit. Any biomass flow in the restricted domain is penalized as provided in the Equation (2.24).

$$Vio_{h,i,j} = \begin{cases} M & if\ 0 < F_{h,i,j}^{Sec} < F_{Sec}^{Min} \\ 0 & else \end{cases} \quad \forall h \in H, i \in I, j \in J$$
$$P_{Domain}^{Sec} = \sum_{i \in I} \sum_{h \in H} \sum_{j \in J} Vio_{h,i,j} \tag{2.24}$$

The operating cost of secondary processing units includes the cost associated with the procurement (BC_j^{Sec}), transportation ($TC_j^{Bio-Sec}$), and processing (PC_j^{Sec}) of the raw materials, which is determined using Equations (2.25) − (2.26), respectively. The cost of biomass and its transportation to the secondary processing unit depends on the location of the source. The processing cost depends on the type of technology selected and the quantity of biomass to be processed (El-Halwagi et al. 2013).

$$BC_j^{Sec} = \sum_{h \in H} \sum_{i \in I} F_{h,i,j}^{Sec} B_{h,i}, \quad \forall j \in J \tag{2.25}$$

$$TC_j^{Bio-Sec} = \sum_{h \in H} \sum_{i \in I} F_{h,i,j}^{Sec} Ct_{h,i,j}^{Bio-Sec}, \quad \forall j \in J \tag{2.26}$$

$$PC_j^{Sec} = \sum_{i \in I} \sum_{t \in T_i} SCp_i^t w_i^t \left(\sum_{h \in H} F_{h,i,j}^{Sec} \right), \quad \forall j \in J \tag{2.27}$$

In the Equation (2.27), the value (SCp_i^t) represents the processing cost of biomass (i) using the selected technology (t) at the secondary processing unit (j). The capital cost for each secondary processing unit (C_j^{Sec}) is determined using a procedure similar to that followed in the main processing unit. The cost depends on the processing unit capacity and the type of technology selected to process the biomass, as given in the Equation (2.28). The values of the

cost coefficients (a_i^t and b_i^t) are chosen depending on the selected technology (t) for the biomass (i) at the secondary processing unit (j).

$$C_j^{Sec} = \sum_{i \in I} \sum_{t \in T_i} w_i^t \left(a_i^t + b_i^t \left(\sum_{h \in H} F_{h,i,j}^{Sec} \right)^{\delta} \right), \quad \forall j \in J \tag{2.28}$$

The demand of users is cumulatively satisfied by both main and secondary processing units as in Equation (2.29). Each of the processing units has the choice to provide biofuel to a particular user. Moreover, when the fuel flow from any processing unit to the user is null, that flow route is not considered. The violation of the user demand constraint assigns a penalty (P_{Demand}) if the total product delivered at the demand locations is less than the actual demand. The assigned penalty is a function of the violations ($V_{j,d}$) occurring at all the demand locations and is determined using Equation (2.30).

$$U_{j,d}^{Main} + U_{j,d}^{Sec} \geq Z_{j,d} \quad \forall j \in J, d \in D_j \tag{2.29}$$

$$V_{j,d} = \begin{cases} Z_{j,d} - \left(U_{j,d}^{Main} + U_{j,d}^{Sec} \right), & if\ Z_{j,d} > \left(U_{j,d}^{Main} + U_{j,d}^{Sec} \right) \\ 0 & else \end{cases}, \quad \forall j \in J, d \in D_j$$
$$P_{Demand} = \sum_{j \in J} \sum_{d \in D_j} V_{j,d} \tag{2.30}$$

2.3.4. Objective: Minimize total cost

The objective is to minimize the total cost of the model while satisfying the periodic fuel demand among the users over the entire operational life of the processing units. The total running cost of a processing unit is calculated by multiplying its periodic operating cost with the operational life period (H_Y) (El-Halwagi et al. 2013). The capital cost is determined only once and directly added to the operational cost to obtain the total cost of the processing unit. The total cost of the processing unit is determined using Equation (2.31).

$$TLC = H_Y \left(\underbrace{BC^{Main} + \sum_{j \in J} BC_j^{Sec}}_{Total\ biomass\ cost} + \underbrace{TC^{Bio-Main} + TC^{Product-Main} + \sum_{j \in J} TC_j^{Bio-Sec}}_{Total\ transportation\ cost} + \underbrace{PC^{Main} + \sum_{j \in J} PC_j^{Sec}}_{Total\ processing\ cost} \right) + \underbrace{C^{Main} + \sum_{j \in J} C_j^{Sec}}_{Total\ capital\ cost}$$

(2.31)

$$Violation_{Total}(\lambda) = P_{Resource} + P_{Domain}^{Main} + P_{Domain}^{Sec} + P_{CAP}^{Main-Min} + P_{CAP}^{Main-Max} + P_{CAP}^{Sec-Min} + P_{CAP}^{Sec-Max} + P_{Lower}^{Product} + P_{Upper}^{Product} + P_{Demand}$$

$$f = TLC + \lambda P_{Factor}$$

(2.32)

The fitness value (f) of a potential solution is determined by including all the applicable penalty values corresponding to each constraint. A large value as a penalty factor (P_{Factor}) is also accommodated with the total violations to isolate infeasible solutions from the feasible ones. The fitness value is determined using Equation (2.32).

2.4. Proposed solution framework

Metaheuristic techniques imitate the optimization strategies followed by nature into mathematical equations and attempt to solve real-world problems through an iterative process. Most of these techniques begin their search by initializing a random population within the search domain. Each member of the population denotes a possible solution, and the objective function value determines its quality. The algorithms explore the available search space iteratively to determine better solutions using the mathematical formulation of its inspiration. Most of the classical optimization techniques are problem-dependent and require certain problem information a priori. However, for metaheuristic techniques, such information is not

mandatory, and usually, the optimization problem is treated as a black box. The solution approach using these techniques does not require the model to be in canonical form; hence, the model is free from binary variables. This feature primarily helps in reducing the problem dimension, which is otherwise increased exponentially.

Although classical approaches are popular in solving supply chain problems, they often use approximations with model nonlinearities. Such models use heuristic techniques for solving problems with increased complexity. In this context, we propose an efficient way to optimize the supply chain model by using metaheuristic techniques. We also demonstrate the flexibility of incorporating nonlinearity into the model. In recent years, many nature-inspired algorithms have been proposed; however, according to the no-free lunch theorem (Wolpert and Macready 1997), a specific algorithm cannot perform well in all types of optimization problems. Hence, it is unfair to test the effectiveness of the proposed strategy using a single algorithm. Due to these reasons, this chapter has employed some popular metaheuristic techniques, variants of better-performing techniques, and recently proposed techniques for analysis. This study solves a test case of the supply chain model using eight metaheuristic techniques: Differential Evolution (DE) (Storn and Price 1997), Grey Wolf Optimizer (GWO) (Mirjalili, Mirjalili, and Lewis 2014), Dynamic Yin-Yang pair Optimization (DYYPO) (Maharana et al., 2017), Single Phase Multi-Group Teaching Learning Optimization (SPMGTLO) (Kommadath, Sivadurgaprasad, and Kotecha 2016), Simultaneous Heat Transfer Search (SHTS) (Maharana & Kotecha, 2016), Particle Swarm Optimization (PSO) (Kennedy and Eberhart 1995), Coyote Optimization Algorithm (COA) (Pierezan & Dos Santos Coelho, 2018) and Genetic Algorithm (GA) (Goldberg 1989). The salient features of these selected metaheuristic techniques are provided in Table A1 of Appendix A.

The supply chain model needs to be appropriately modeled for metaheuristic techniques, as these techniques lack inherent constraint-handling strategies. Most of the constraint-handling techniques incorporate various penalty approaches to avoid the infeasible search space. The current study utilizes a repairing strategy for handling the equality and domain constraints, thus reducing the number of constraint penalties and aiding the techniques in determining feasible solutions. The decision variables for the proposed model provide information regarding (i) the flow of biomass to processing units from each source, (ii) the distribution of biofuel to the demand locations, and (iii) the type of processing technology used at each processing unit. The general decision structure is given in Fig 2.4. The structure is categorized into three sets. The first set represents the amount of biomass transported to various processing units. The second set determines the product flow from processing units to different demand locations, and the last set indicates the technologies installed in the processing unit corresponding to the different types of biomass received.

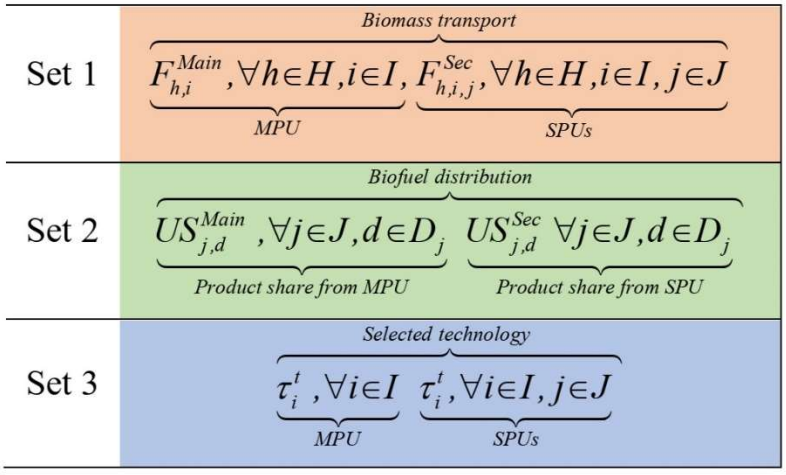

Fig 2.4 Proposed decision structure for the main processing unit (MPU) and secondary processing units (SPUs)

The decision variables representing technologies are integer variables, and the number of such variables depends upon the types of biomass available and the number of processing units

installed. In the current study, each biomass is assumed to be processed by utilizing one of the available technologies and can be represented mathematically as Equation (2.33).

$$\sum_{t\in T_i} w_i^t = 1, \quad \forall i \in I \tag{2.33}$$

The proposed decision structure satisfies the above constraint directly and does not require a binary variable to solve the problem using metaheuristic strategies. The standard approach uses the biofuel flow rates as the decision variables for set 2 of the decision structure, requiring balancing constraints for the Equation (2.18). Instead of directly considering the product flow rates, the proposed solution model uses the ratios of fuel transported to each demand location as the decision variables that have to be normalized for each processing unit. Thus, equations representing mass balance at main and secondary processing units in Equation (2.4) and (2.19), respectively, are remodelled and provided in Equations (2.34) and (2.35). The mass balance for the main processing unit and the secondary processing units is given in Equations (2.34) and (2.35).

$$\begin{aligned} K^{Main} &= \sum_{i\in I}\sum_{t\in T_i} w_i^t \tau_i^t \left(\sum_{h\in H} F_{h,i}^{Main} \right) \\ U_{j,d}^{Main} &= \widehat{US}_{j,d}^{Main} \; K^{Main}, \forall j \in J, d \in D_j \end{aligned} \tag{2.34}$$

$$\begin{aligned} k_j^{Sec} &= \sum_{i\in I}\sum_{t\in T_i} w_i^t \tau_i^t \left(\sum_{h\in H} F_{h,i,j}^{Sec} \right) \quad \forall j \in J \\ U_{j,d}^{Sec} &= \widehat{US}_{j,d}^{Sec} k_j^{Sec} \quad \forall j \in J, d \in D_j \end{aligned} \tag{2.35}$$

Equation (2.36) determines the product distribution profile among the demand locations from the main processing unit and the secondary processing units. The variables ($\widehat{US}_{j,d}^{Main}$) and ($\widehat{US}_{j,d}^{Sec}$) represent the sharing ratio of the total product produced at the main and secondary

processing units, respectively, among the users ($d \in D_j$). As illustrated in the Equation (2.36), the sharing ratios corresponding to each processing unit are normalized to ensure the total distribution of produced products.

$$\begin{aligned} &\sum_{j=1}^{J}\sum_{d=1}^{D_j}\widehat{US}_{j,d}^{Main}=1 \\ &\sum_{d=1}^{D_j}\widehat{US}_{j,d}^{Sec}=1,\ \forall j\in J \end{aligned} \tag{2.36}$$

A correction approach is adopted for domain violations in the biomass flow rates from the source to the processing unit, as given in Equations (2.37) and (2.38). Any nonzero flow rate lesser than the minimum required is assigned a null value.

$$F_{h,i}^{Main}=\begin{cases}0 & if\ 0<F_{h,i}^{Main}<F_{Min}^{Main}\\ F_{h,i}^{Main} & else\end{cases} \qquad \forall i\in I, h\in H \tag{2.37}$$

$$F_{h,i,j}^{Sec}=\begin{cases}0 & if\ 0<F_{h,i,j}^{Sec}<F_{Min}^{Sec}\\ F_{h,i,j}^{Sec} & else\end{cases} \qquad \forall i\in I, j\in J, h\in H \tag{2.38}$$

The domain constraint for fuel flow is handled using two approaches. Any nonzero fuel flow from the main processing unit is analyzed for the required flow domain and is either penalized or corrected depending upon the violated limit. The flow is corrected if it falls below the minimum rate of flow needed, as given in the Equation (2.39). The violation of the upper flow limit is handled as per the standard approach Equation (2.12).

$$\begin{aligned} k_j^{Main}&=\begin{cases}0, & if\ 0<k_j^{Main}<k_{Min}^{Main}\\ k_j^{Main} & else\end{cases} && \forall j\in J \\ U_{j,d}^{Main}&=\begin{cases}0 & if\ k_j^{Main}=0\\ U_{j,d}^{Main} & else\end{cases} && \forall j\in J, d\in D_j \end{aligned} \tag{2.39}$$

The domain correction strategy employed for the product flow also probes the instance when there is no product flow from the main processing unit to any of the secondary locations and then assigns null values to the biomass flow rates coming to the main processing unit from all the harvesting sites as in the Equation (2.40). In this case, none of the secondary locations receives the product from the main processing unit; hence, the main processing unit becomes insignificant in the model.

$$F_{h,i}^{Main} = \begin{cases} 0, & if \sum_{j=1}^{J} k_j^{Main} = 0 \\ F_{h,i}^{Main} & else \end{cases} \quad \forall i \in I, h \in H \tag{2.40}$$

The domain constraints representing the capacity restrictions in the main and the secondary processing units are handled as shown in the Equation (2.41). The lower capacity violation is corrected by assigning null values for the corresponding biomass flows, and the processing unit is not installed. However, any violation over the maximum capacity is penalized with respect to the amount of violation given in Equations (2.7) and (2.22).

$$\begin{aligned} F_{h,i}^{Main} &= \begin{cases} 0 & if\ 0 < \sum_{h \in H} F_{h,i}^{Main} < CAP_i^{Main-Min} \\ F_{h,i}^{Main} & else \end{cases} && ,\forall h \in H, i \in I \\ F_{h,i,j}^{Sec} &= \begin{cases} 0 & if\ 0 < \sum_{h \in H} F_{h,i,j}^{Sec} < CAP_i^{Sec-Min} \\ F_{h,i,j}^{Sec} & else \end{cases} && ,\forall h \in H, i \in I, j \in J \end{aligned} \tag{2.41}$$

The violations in the resource and demand constraints are determined using similar calculations followed in the standard approach. The fitness value of the solution is determined by considering all the involved costs and the penalties associated with the constraint violation.

$$\begin{aligned} Violation_{Total}(\lambda) &= P_{Resource} + P_{CAP}^{Main-Max} + P_{CAP}^{Sec-Max} + P_{Upper}^{Product} + P_{Demand} \\ f &= TLC + \lambda P_{Factor} \end{aligned} \tag{2.42}$$

A comparison of the objective function between the standard approach (Equation (2.32)) and the proposed approach (Equation (2.42)) shows the absence of domain and equality constraints in the latter formulation due to the incorporation of new constraint-handling strategies.

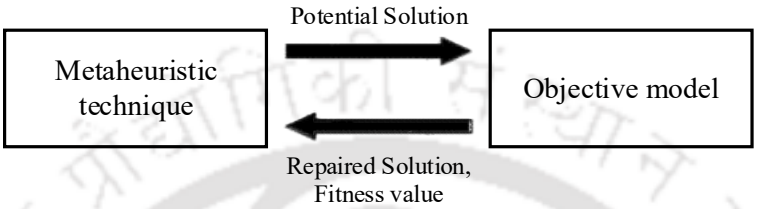

Fig 2.5 Relation between model and metaheuristic technique

The proposed solution strategy provides a potential solution to the objective model, which repairs the solution if necessary and evaluates its fitness. After the fitness value is determined, the repaired solution and its fitness value are returned to the metaheuristic techniques, as shown in Fig 2.5. A sample decision structure is shown in Fig 2.6, based on the supply chain example provided in Fig 2.1.

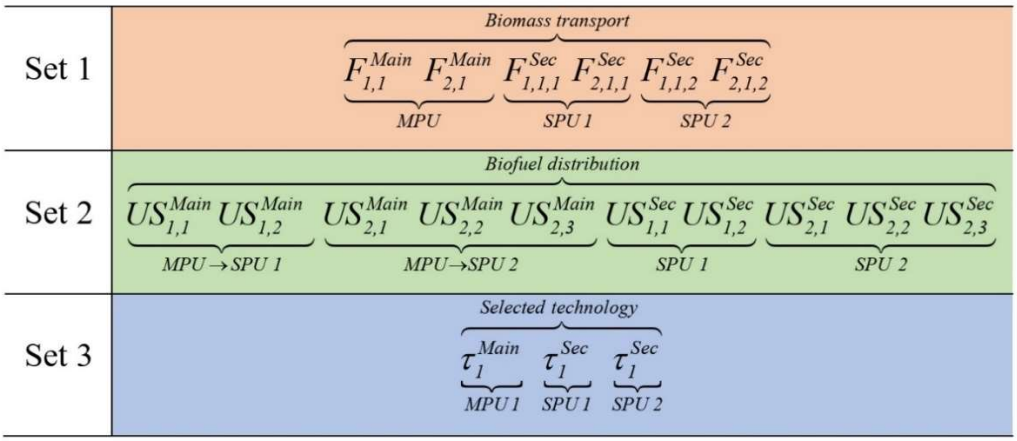

Fig 2.6 Decision structure for a distributed biorefineries case for the main processing unit (MPU) and secondary processing units (SPUs)

The example is assumed to have a single type of biomass that can be received from two different bio-source locations and two options for the technology to convert the raw material into products. The decision structure consists of nineteen variables, where the set one variables

decide the flow rate of biomass from the source to the processing units. Similarly, the product produced at the first secondary location is shared between two users, whereas there are three shares of products for the second secondary location. It should be noted that all the ratios corresponding to individual processing units are to be normalized. Since only one type of biomass is available, the solution structure has three variables representing the processing technologies used at each processing unit. Each of the Set 3 variables represents integer values with the upper bound as the number of available technologies. The main processing unit utilizes the first technology, whereas the first secondary processing unit has chosen the second technology, and the second secondary processing unit has chosen the first technology for processing the biomass. A summarized flowchart of the solution process is in Fig 2.7.

2.5. Case study of distributed biorefineries

The effectiveness of the proposed model is validated using a distributed biofuel supply chain problem in Mexico. The biomass is available at six different harvesting locations and can be processed using one main and two secondary processing units. The case study requires the satisfaction of the demand at four user locations shared among the secondary locations evenly. The data related to raw material availability, the cost of implementing the processing units, processing cost for the biomass using various available technologies, the transportation cost, and demand at users are available in the literature (Santibañez-Aguilar et al. 2014; Santibañez-Aguilar et al. 2011; Ponce-Ortega and Santibañez-Aguilar 2019) and also provided in the Appendix C. The case considers monthly demand and total plant life of 20 years.

The penalty value (M) assigned for the domain violation is taken as 10^5, while the penalty factor (P_{Factor}) required to penalize an infeasible solution is 10^{15}. In view of the stochastic nature of metaheuristic techniques, twenty-five independent runs are performed to analyze the results.

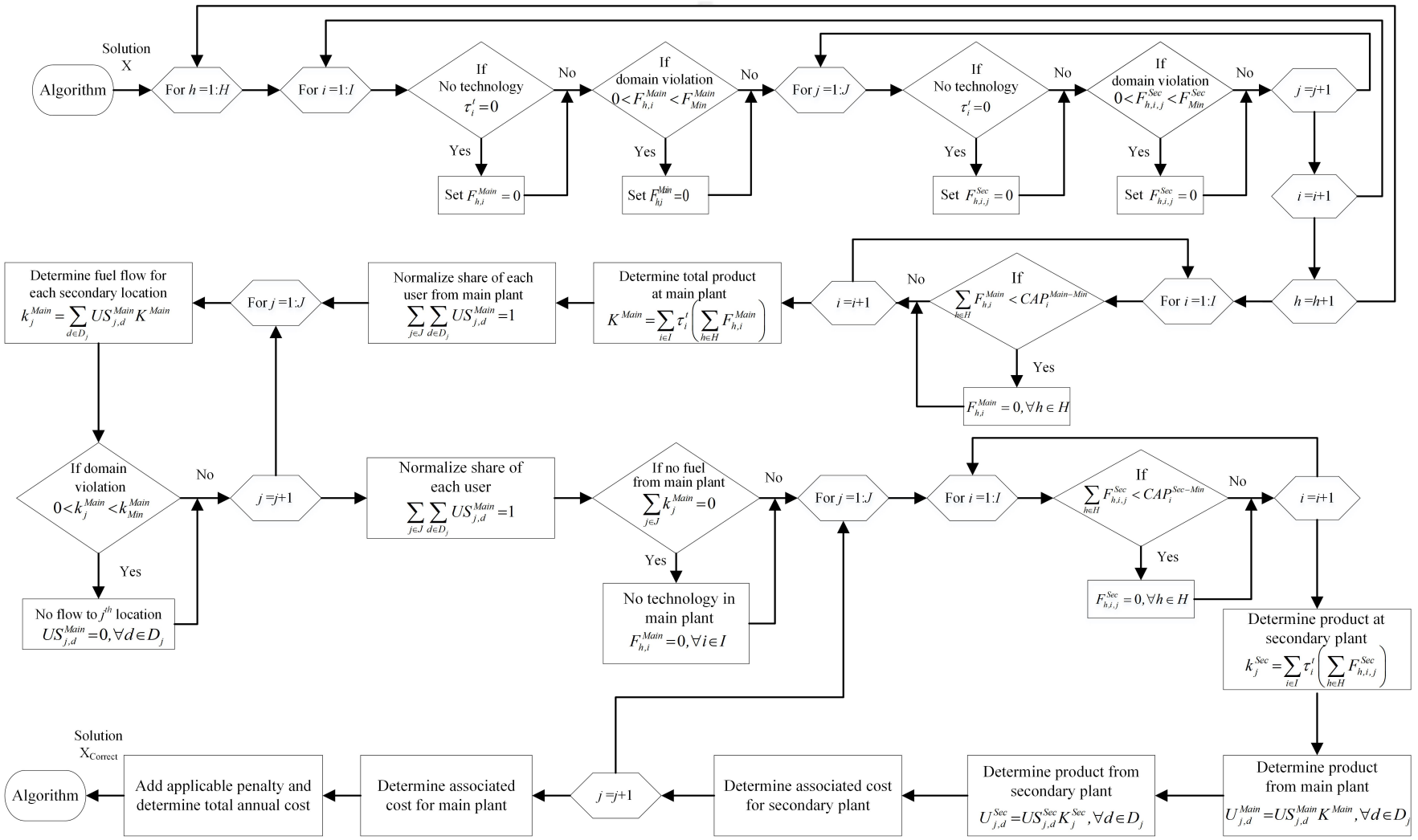

Fig 2.7 Flowchart of the objective evaluation

The optimization was performed on a computer with an Intel i7 @4.2 GHz processor and 32 GB of RAM using a MATLAB simulation environment. The population size is fixed at 250 for all algorithms except DYYPO, where it works with only two solutions. The termination criterion for all the algorithms is selected as the maximum function evaluation set at 50,000 to perform a fair comparison. Some metaheuristic algorithms utilize algorithm-specific parameters other than population size and termination condition, which the users must define. The values of the algorithmic parameters used in this chapter are provided in Appendix C.

2.6. Results and discussion

The proposed strategy is evaluated against the standard penalty-based model discussed in Section 2.3. This chapter has adopted similar experimental conditions (as provided in the Section 2.5 case study) for both strategies for solving the test case using the eight metaheuristic techniques. The discussions broadly focus on two aspects of the results. In the first part, the benefits of the proposed model in determining better solutions are demonstrated. The second investigation provides a detailed solution analysis for superstructure design insights. Solution analysis is an important aspect of models involving case studies, as it helps researchers better understand the significance of each optimal decision variable and provides confidence in the factual correctness of the study.

2.6.1. Statistical analysis

The fitness values corresponding to the best, worst, mean, median, and standard deviation (SD) for all the algorithms with both approaches are given in Table 2.1. The best value among each of the statistics is highlighted using bold typeface font. The total violations in the best solution determined by each algorithm using both approaches are also provided in Table 2.1. The techniques that have solved the biorefinery case study with the proposed strategy have

identified feasible solutions in all of their runs. On the contrary, the violation reported in the best solution of the metaheuristic techniques along with the standard approach indicates that this approach has determined infeasible solutions in all the runs. The proposed strategy reports the objective value with no violation, whereas the standard approach reports the fitness value with violation. A detailed analysis of the solution determined by each algorithm using the conventional approach has identified that the primary reason for the infeasibility of solutions is the violation due to the equality constraints. Considering the best statistics of all techniques with the proposed method, SPMGTLO determined the best solution with the lowest total cost, whereas DYYPO found the solution with the highest total cost.

Table 2.1 Statistical analysis of the techniques

	Algorithm	Best	Worst	Mean	Median	SD	*Violation
Proposed Strategy	GWO	1.224E+09	1.419E+09	1.293E+09	1.281E+09	4.470E+07	-
	DE	1.376E+09	1.493E+09	1.440E+09	1.446E+09	2.648E+07	-
	SPMGTLO	**1.131E+09**	**1.247E+09**	**1.193E+09**	**1.191E+09**	**2.499E+07**	-
	GA	1.367E+09	1.614E+09	1.475E+09	1.463E+09	7.426E+07	-
	PSO	1.221E+09	1.562E+09	1.324E+09	1.312E+09	8.564E+07	-
	DYYPO	1.658E+09	2.598E+09	2.095E+09	2.065E+09	2.589E+08	-
	SHTS	1.318E+09	1.437E+09	1.372E+09	1.363E+09	3.668E+07	-
	COA	1.232E+09	1.399E+09	1.299E+09	1.297E+09	3.979E+07	-
Standard penalty approach	GWO	4.364E+17	5.090E+18	2.587E+18	2.500E+18	9.998E+17	4.36E+02
	DE	2.910E+17	8.611E+17	6.086E+17	6.390E+17	1.511E+17	2.91E+02
	SPMGTLO	1.432E+16	3.262E+18	1.730E+18	1.574E+18	8.041E+17	5.34E+02
	GA	8.238E+16	2.185E+18	9.200E+17	7.341E+17	6.663E+17	8.24E+01
	PSO	8.325E+14	1.458E+19	4.544E+18	3.896E+18	3.570E+18	8.33E-01
	DYYPO	6.166E+17	5.307E+18	3.120E+18	2.967E+18	1.343E+18	6.17E+02
	SHTS	1.727E+17	4.847E+18	2.172E+18	1.895E+18	1.143E+18	1.73E+02
	COA	1.205E+16	3.937E+17	1.194E+17	7.689E+16	9.058E+16	1.20E+01

*Violations are observed in the best solution

The second-best solution among all techniques is determined by PSO and is followed by GWO. In most runs, GWO has determined better solutions than all techniques except SPMGTLO. The violation in PSO and COA in the best solution reported using the standard approach is low. However, the mean fitness value reported by PSO and DYYPO suggests higher violations in multiple runs. Considering the statistical analysis of the standard penalty-based approach, PSO is observed to determine the least violated solution followed by COA.

2.6.2. Convergence analysis

The convergence of the fitness function value of feasible solutions with respect to the maximum allowed function evaluations for the proposed approach and the corresponding violations are given in Fig 2.8 (c) and (d), respectively. GA has provided a quick convergence among all the techniques by identifying the final value using minimum function evaluations. Even after utilizing the maximum function evaluations, SPMGTLO, GWO, DYYPO, and DE are unable to converge and suggest the need for relaxation in the termination criterion. Even though SPMGTLO was unable to converge to its final value before the maximum function evaluation, it has reported the best solution followed by PSO. The convergence of violations for the proposed approach identifies PSO as the first technique in determining the feasible solution among all, whereas DYYPO was able to determine the initial feasible solution only after utilizing approximately 10 % of the allowed function evaluations.

The violations occurring in solutions are due to the constraints in the Equations (2.1), (2.9), and (2.29). Each of the techniques was able to determine feasible solutions within the termination criterion. Fig 2.8 (a) and (b) indicate the convergence of the fitness function value of all solutions determined with respect to allowed function evaluation for the conventional approach and the corresponding violation values by each technique.

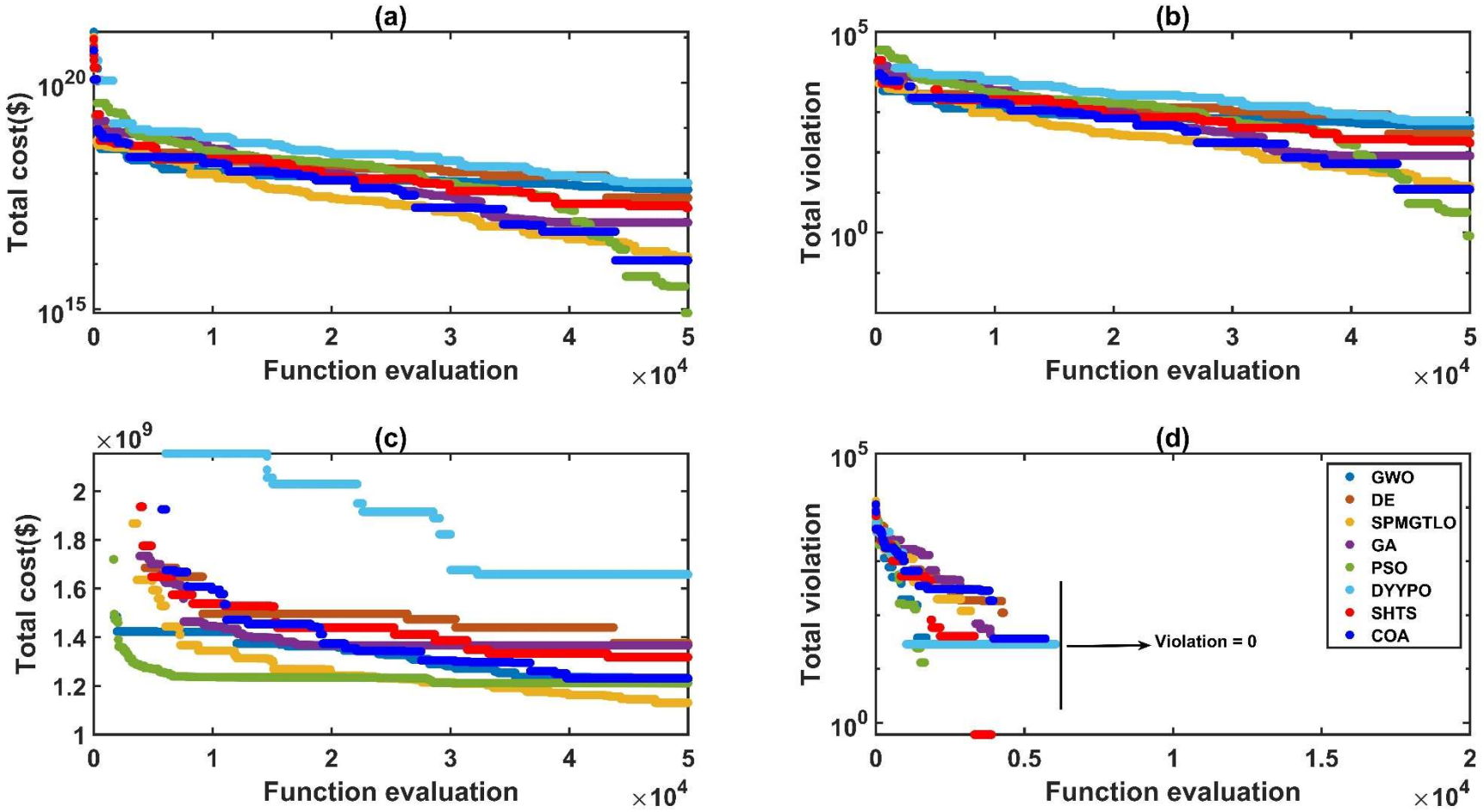

Fig 2.8 Convergence of total cost and constraint violation with standard approach (a and b) and proposed approach (c and d) in the best run

Due to the absence of any correction approach for domain constraints (Equations (2.8) and (2.23)) and the presence of equality constraints (Equations (2.3) and (2.18)) in the standard model, the algorithms could not determine a feasible solution in any of the runs within the specified termination criterion. The analysis highlights the effectiveness of the proposed approach against the conventional formulation and provides evidence for aiding the metaheuristic technique in moving toward a feasible search space.

The details of constraint violations representing the demand constraint (DMC), resource constraint (RC), domain constraint (DC), capacity constraint (CC), and mass balance constraint (MBC) obtained in the proposed approach, and the standard model is shown in Fig 2.9 and Fig 2.10 respectively. In the proposed approach, the constraints are violated up to the initial 10 % function evaluations in all the techniques. In the initial phases of the search, the violation of the resource constraint is higher for all the techniques, whereas satisfying the demand constraint takes the majority of the elapsed function evaluation for determining feasible solutions. Determining a feasible solution in the earlier stages helps the metaheuristic technique improve the solutions and report better optimal solutions against the standard model. The higher violations in the standard model are due to a large number of constraints and the absence of any repairing strategy. The presence of equality constraints in the biomass-to-biofuel conversion process is dominant at the termination criterion.

The violation value is significant in the majority of the techniques except for PSO. The absence of domain correction also contributes largely to the increased violations and proves it is difficult for the metaheuristic techniques to determine a feasible solution. This determination of an initial feasible solution helps significantly improve the further search process and is justified by the solutions determined by both approaches.

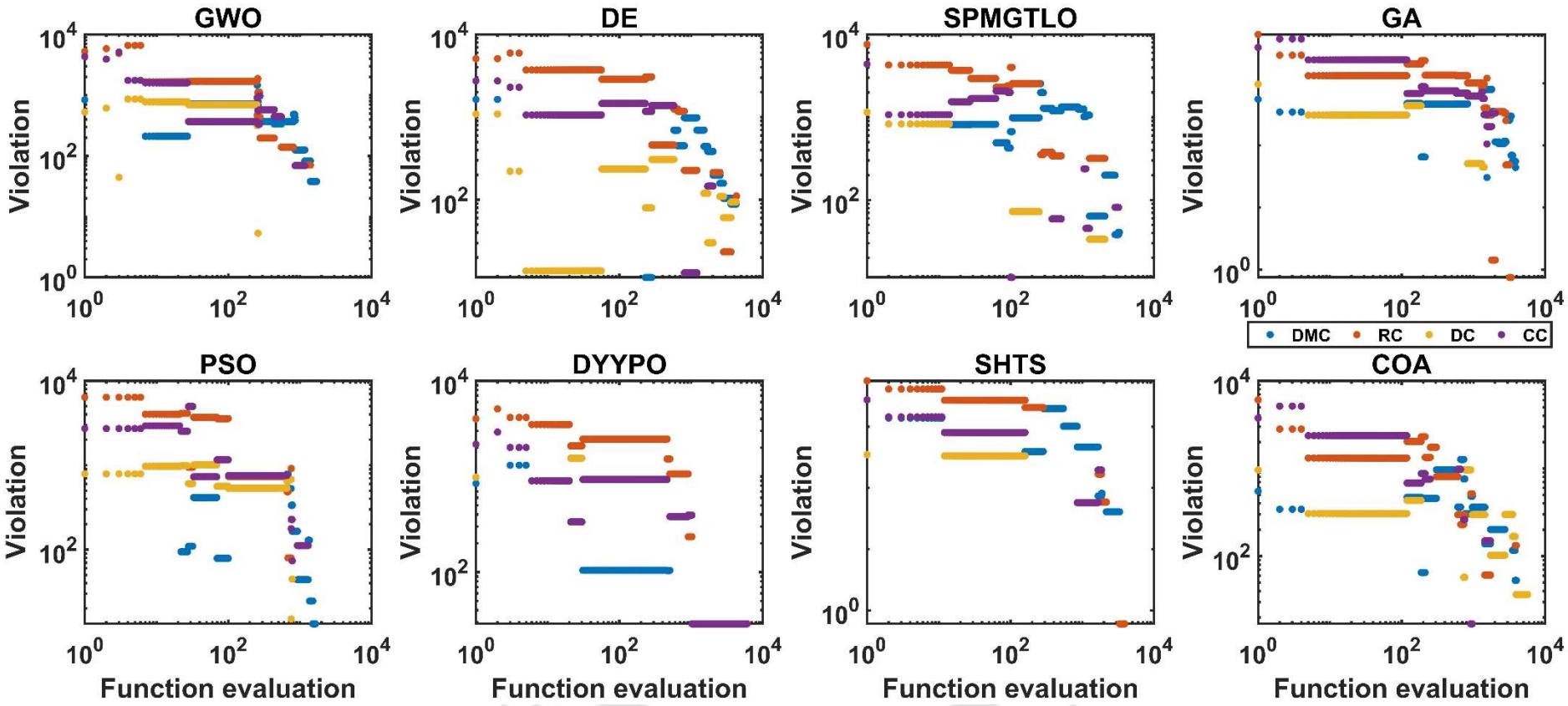

Fig 2.9 Violations in various constraints for the best solution determined using the proposed approach

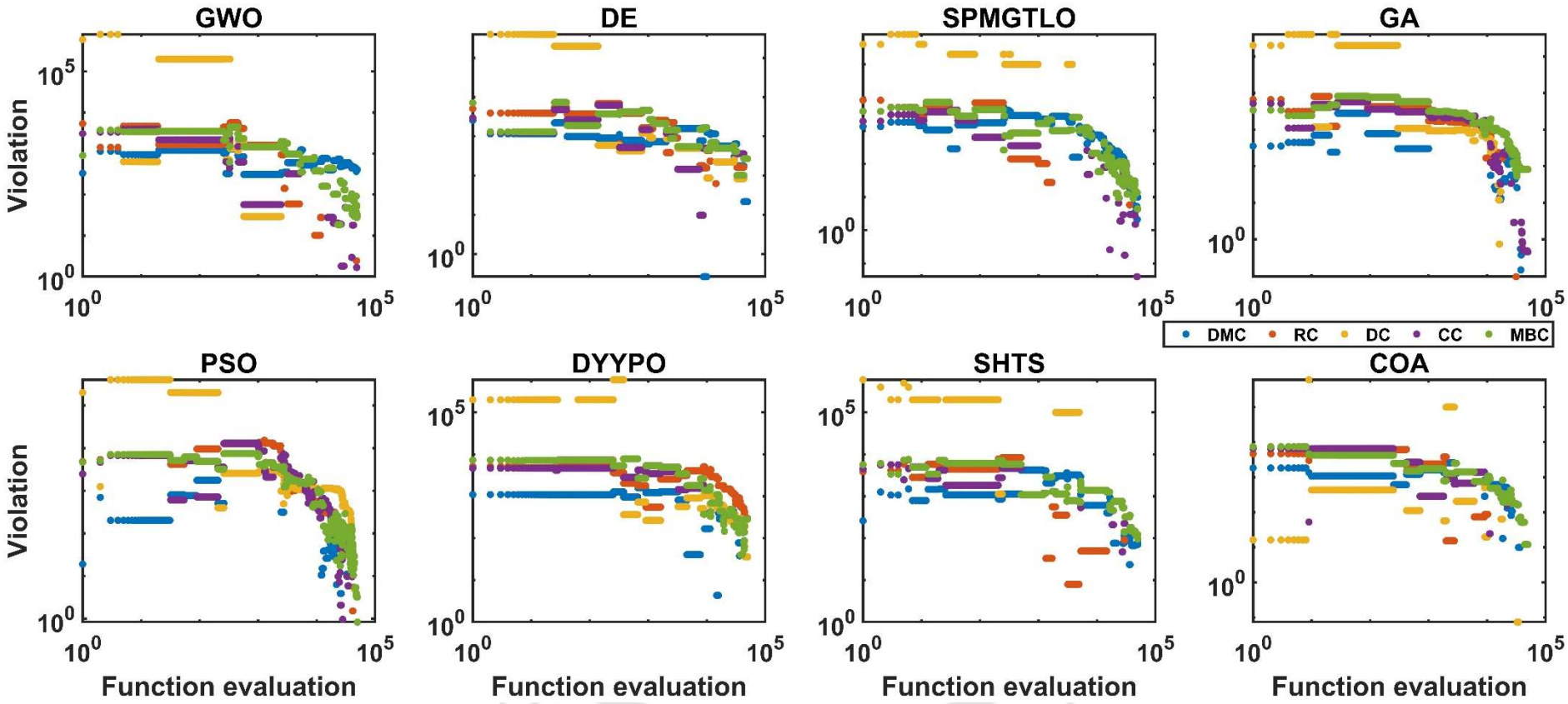

Fig 2.10 Violations in various constraints for the best solution determined using the standard approach

Considering the violation in PSO in the standard model as acceptable and comparing the cost reported with the proposed approach, it is observed to achieve a reduction of 45 % in the total cost. Similarly, the performance of each technique has improved while using the proposed approach, as observed in Fig 2.8. It has to be noted that the constraint violations are not monotonic with respect to the function evaluations, as the fitness value of the solution considers the cumulative violations, which are monotonic in the convergence profile of each technique.

The statistical analysis and the convergence profile of the violations reveal the superiority of the proposed model in determining feasible solutions and helping the metaheuristic techniques in improving the objective function value. Additionally, the use of repairing strategies for the domain constraints reduces the complexity of the proposed model by efficiently handling multiple constraints given in Equations (2.6), (2.8), (2.9), (2.21) and (2.23). The proposed model also reduces the problem dimension by avoiding using binary variables, commonly used in mathematical modeling for selecting technologies and determining active flow channels between the supply chain hubs.

2.6.3. Optimal solution analysis

The optimal biofuel production plan aims to produce products equivalent to demand and avoid excess production. The excess product increases the production cost as the users discard any quantity above the demand. The product delivered to the demand sites by each algorithm is shown in Fig 2.11. The analysis of product delivery schedules to different demand locations determined by each metaheuristic technique will help identify the reason for total annual cost variations. The production plan determined by DYYPO has provided the maximum quantity of excess products, followed by DE. PSO has produced the least excess products for most demand locations among all the algorithms, followed by GWO. Even though the excess

products delivered by PSO for various demand locations are less than those delivered by SPMGTLO, the total cost for the production plan determined by PSO is observed to be higher. This ambiguity requires a detailed investigation of the technology implemented at each processing unit and optimal site selection.

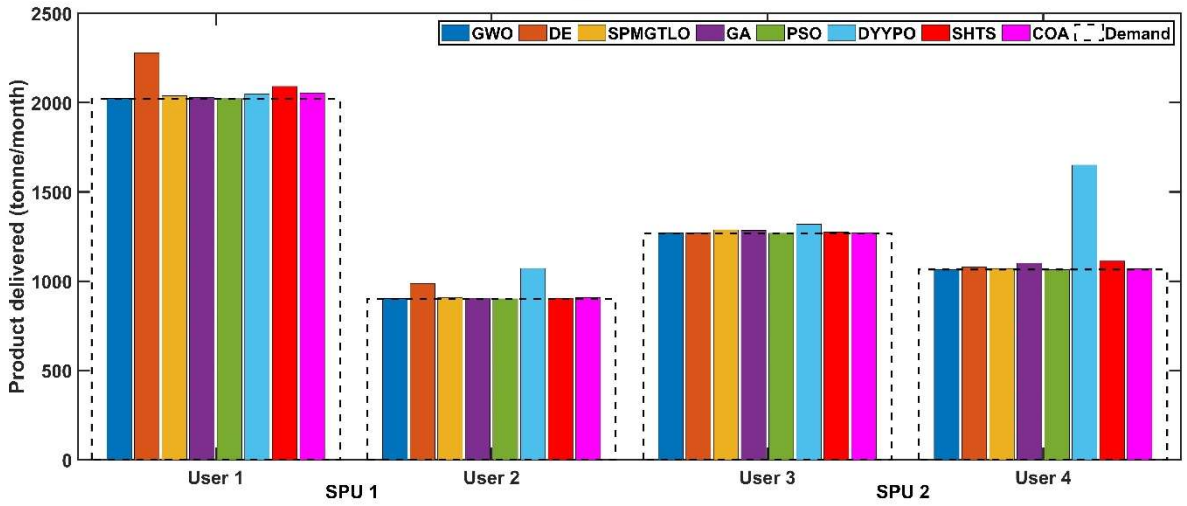

Fig 2.11 Product delivery at each demand location by all techniques

The analysis of product delivery schedules to different demand locations determined by each metaheuristic technique will help identify the reason for total annual cost variations. The production plan determined by DYYPO has provided the maximum quantity of excess products, followed by DE. PSO has produced the least excess products for most demand locations among all the algorithms, followed by GWO. Even though the excess products delivered by PSO for various demand locations are less than those delivered by SPMGTLO, the total cost for the production plan determined by PSO is observed to be higher. This ambiguity requires a detailed investigation of the technology implemented at each processing unit and optimal site selection. The details regarding the implemented technologies and the corresponding amount of biomass processed at various processing units are given in Fig 2.12.

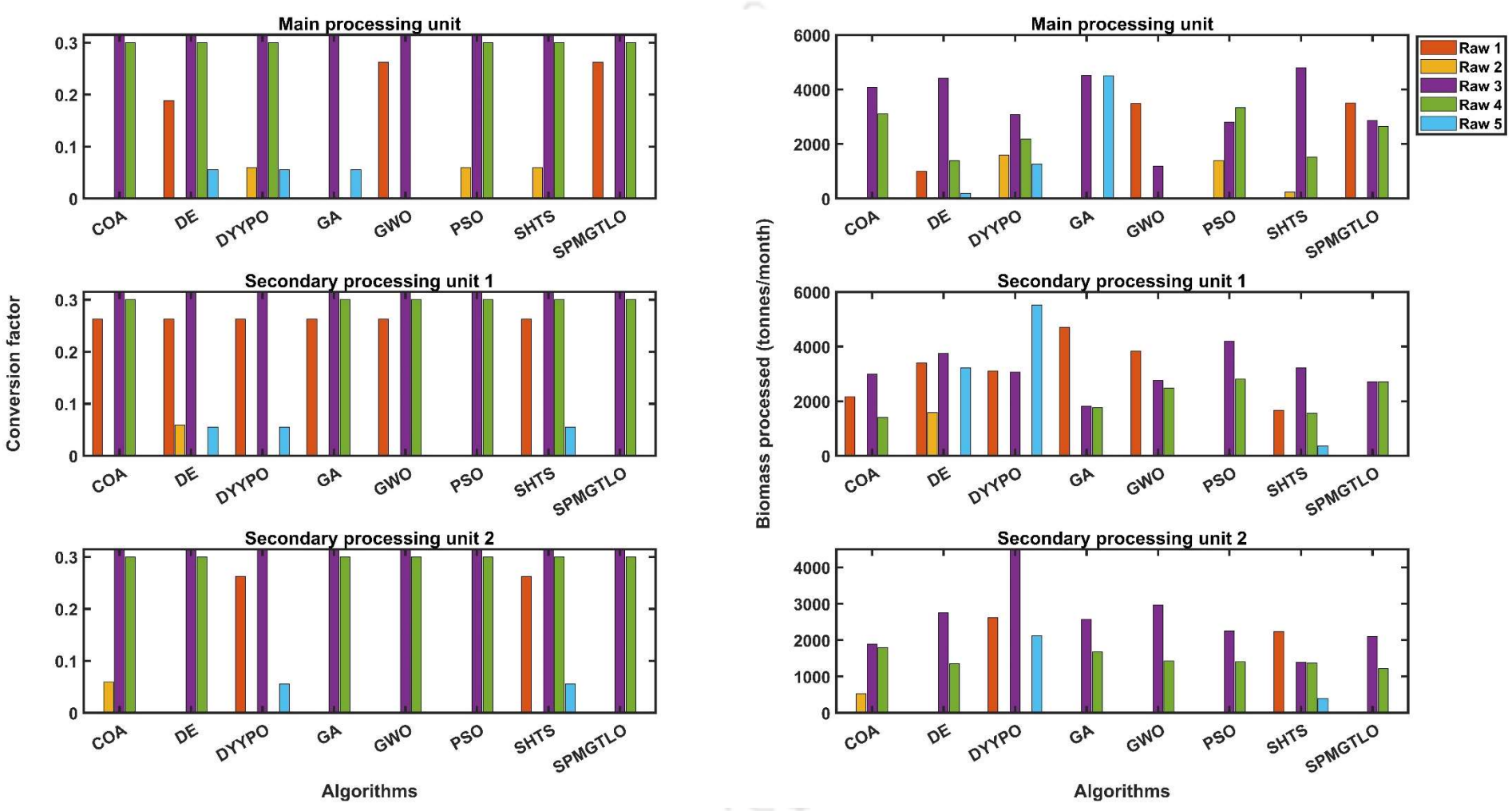

Fig 2.12 Technology utilized and quantity of biomass processed at the processing facilities

Among all techniques, DE and DYYPO utilize the highest number of technologies across all the processing units to satisfy the demand. In all the available processing units, the techniques have selected the third and fourth raw materials to be processed in a higher amount, as the yield obtained by the third raw material is the highest, followed by the fourth raw material. Since the total production cost for products produced from the fourth raw material is significantly lesser than those manufactured using the third raw material, the majority of the techniques have chosen to process the maximum allowed quantity of the fourth raw material at the main and the secondary processing units. Most processing units avoid using the second and fifth raw materials, as the total production cost of biofuel from these raw materials two is higher than the product yield. The choice of inferior technology and biomass selection has resulted in costly production plans determined by DE and DYYPO. The economics of scale helps the processing at the main processing unit be economical for all the production plans.

The production plan determined by SPMGTLO has processed the maximum amount of raw materials and more types of raw materials at the main processing unit, resulting in reduced production costs. In this case, regional demand also plays an important role in determining the total cost. The higher demand of users at the first secondary location forces the corresponding implemented technologies to process a large quantity of the available biomass. The lower demand at the second secondary location relaxes the production strategy, and thus, the total amount and type of biomass processed at the second secondary processing location are less than those processed at other secondary processing locations. The operating cost largely depends upon the selection of harvesting sites, the quantity of raw material procurement, and the type and capacity of the processing units. The breakdown for the total cost constituting the installation cost of various technologies and operating cost (feed cost, transportation cost for feed and biofuel, biomass-processing cost) for all the algorithms are given in Table 2.2.

Table 2.2. Costs associated with the processing facilities

Algorithm	Plant	Raw material cost ($)					Transport cost ($)						Installation Cost($)	Processing cost ($)	Fuel transport Cost ($)
		Raw 1	Raw 2	Raw 3	Raw 4	Raw 5	H 1	H 2	H 3	H 4	H 5	H 6			
GWO	MPU	7.23E+07	-	5.90E+07	-	-	3.04E+07	-	1.02E+07	7.40E+06	-	-	1.21E+07	8.33E+07	1.03E-02
	SPU 1	7.95E+07	-	1.37E+08	9.98E+07	-	1.77E+07	2.87E+07	1.38E+07	9.67E+06	5.39E+06	1.13E+07	2.30E+07	1.74E+08	-
	SPU 2	-	-	1.48E+08	5.72E+07	-	2.23E+07	-	-	7.79E+06	1.00E+07	2.02E+07	1.30E+07	7.11E+07	-
DE	MPU	2.07E+07	-	2.19E+08	5.60E+07	1.39E+06	2.31E+07	1.31E+07	1.01E+07	3.14E+06	1.10E+07	3.33E+06	1.75E+07	9.65E+07	1.33E-02
	SPU 1	7.05E+07	1.10E+07	1.87E+08	-	2.41E+07	-	2.41E+07	1.85E+07	3.82E+07	9.14E+06	8.14E+06	2.32E+07	1.77E+08	-
	SPU 2	-	-	1.37E+08	5.42E+07	-	-	-	1.06E+07	9.22E+06	1.07E+07	9.14E+06	1.30E+07	6.63E+07	-
SPMGTLO	MPU	7.27E+07	-	1.43E+08	1.06E+08	-	-	-	2.61E+07	7.21E+06	4.38E+06	5.66E+06	1.61E+07	1.36E+08	1.69E-02
	SPU 1	-	-	1.35E+08	1.09E+08	-	-	-	3.78E+06	-	8.65E+06	1.04E+07	1.30E+07	8.42E+07	-
	SPU 2	-	-	1.04E+08	4.90E+07	-	-	-	1.26E+07	7.19E+06	1.05E+07	-	1.30E+07	5.31E+07	-
GA	MPU	-	-	2.24E+08	-	3.36E+07	3.81E+07	2.82E+07	1.13E+07	4.47E+06	8.40E+06	5.86E+06	6.50E+06	8.04E+07	1.22E-02
	SPU 1	9.79E+07	-	9.03E+07	7.11E+07	-	3.13E+07	4.54E+07	7.43E+06	3.21E+07	2.75E+06	7.01E+06	2.30E+07	1.69E+08	-
	SPU 2	-	-	1.28E+08	6.73E+07	-	2.25E+07	1.57E+07	2.14E+07	-	1.29E+07	-	1.30E+07	6.76E+07	-
PSO	MPU	-	9.74E+06	1.39E+08	1.34E+08	-	-	-	-	4.03E+06	2.11E+07	5.09E+06	1.18E+07	8.61E+07	1.39E-02
	SPU 1	-	-	2.09E+08	1.13E+08	-	-	3.98E+07	1.17E+07	2.25E+07	4.50E+06	-	1.30E+07	1.11E+08	-
	SPU 2	-	-	1.12E+08	5.64E+07	-	-	-	1.89E+07	9.22E+06	6.98E+06	-	1.30E+07	5.84E+07	-
DYYPO	MPU	-	1.11E+07	1.53E+08	8.79E+07	9.38E+06	2.19E+07	8.59E+06	1.06E+07	5.41E+06	1.18E+07	4.16E+06	1.33E+07	8.36E+07	1.06E-02
	SPU 1	6.46E+07	-	1.52E+08	-	4.12E+07	9.83E+07	3.52E+07	9.49E+06	3.12E+07	4.67E+06	1.24E+07	1.93E+07	1.55E+08	-
	SPU 2	5.44E+07	-	2.24E+08	-	1.58E+07	2.87E+07	4.76E+07	2.10E+07	1.25E+07	1.93E+07	2.03E+07	1.93E+07	1.51E+08	-
SHTS	MPU	-	1.65E+06	2.39E+08	6.13E+07	-	3.74E+07	1.12E+07	3.00E+06	1.20E+06	9.70E+06	6.48E+06	1.18E+07	8.54E+07	1.24E-02
	SPU1	3.47E+07	-	1.61E+08	6.31E+07	2.68E+06	1.13E+07	-	3.27E+06	3.90E+07	8.07E+06	4.56E+06	2.50E+07	1.19E+08	-
	SPU2	4.64E+07	-	6.91E+07	5.51E+07	2.96E+06	1.69E+07	1.96E+07	2.89E+07	8.99E+06	7.09E+06	-	2.50E+07	9.84E+07	-
COA	MPU	-	-	2.03E+08	1.25E+08	-	-	-	1.05E+07	3.65E+06	1.40E+07	4.51E+06	9.07E+06	9.06E+07	1.46E-02
	SPU1	4.49E+07	-	1.49E+08	5.64E+07	-	2.16E+07	3.98E+07	1.61E+07	-	1.69E+06	1.08E+06	2.30E+07	1.23E+08	-
	SPU2	-	3.70E+06	9.40E+07	7.20E+07	-	-	9.80E+06	1.89E+07	1.18E+07	6.23E+06	-	1.69E+07	6.24E+07	-

All null values are represented by '-'; MPU: Main processing unit, SPU 1: Secondary processing unit 1, SPU 2: Secondary processing unit 2; Raw 1: Wood Chips, Raw 2: Sugar cane, Raw 3: Grain corn, Raw 4: Grain sorghum, Raw 5: Sweet sorghum; H 1: Northwest region, H 2: South region, H 3: Center west region, H 4: Northeast region, H 5: East region, H 6: Center region

The biomass and processing costs contribute up to 55% and 25% of the total cost. The decisions related to the selection of optimal biomass type and processing technology are major contributors to the superstructure design. The best supply chain network is determined by SPMGTLO and is depicted in Fig 2.13. The interactions between harvesting sites, processing units, and demand locations are shown in the optimal network. None of the harvesting sites have supplied the second and fifth raw materials to any of the processing units, which are among the available raw materials. Harvesting sites three and five have contributed the highest number of network connections to all the processing units for supplying different types of biomass. The processing units do not prefer the first and second harvesting sites among all the available biomass sources. In all the demand locations, the demand is satisfied using both the main and secondary processing unit.

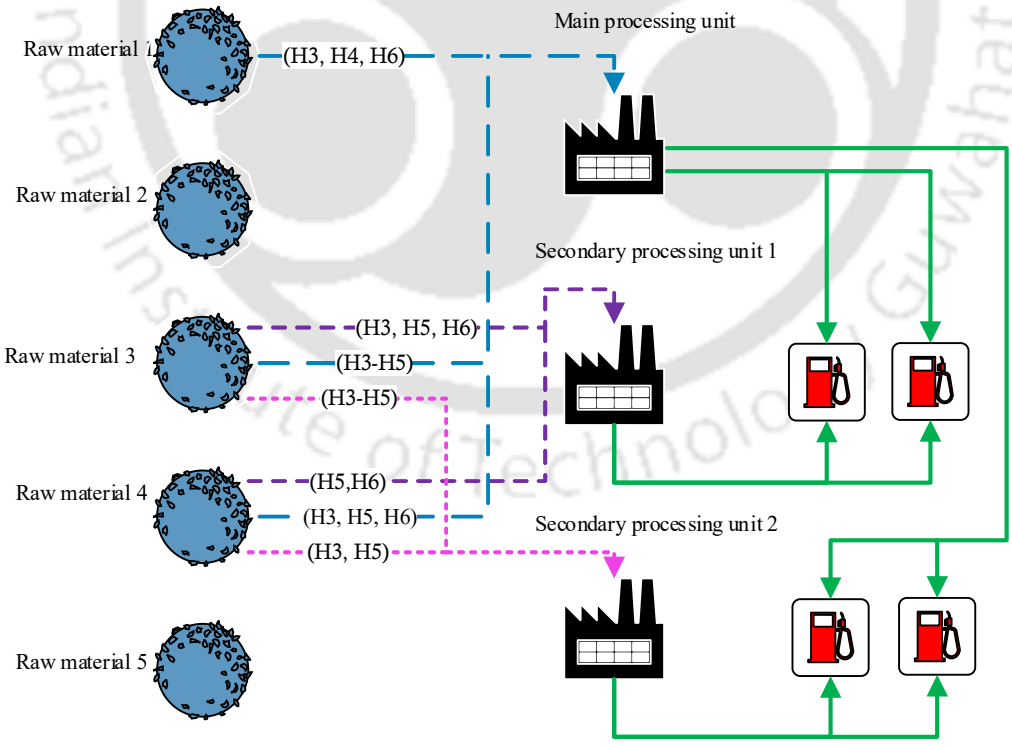

Fig 2.13 Supply chain network for the best solution

2.7. Conclusion

This chapter proposes a novel modeling approach for solving the biomass-biofuel supply chain problem using metaheuristic techniques. The newly introduced strategy aids the metaheuristic technique in searching for the optimal solution by removing the hard equality constraints. Moreover, it also integrates a repairing strategy for handling the domain hole constraints arising in the feed and product transportation stages. The efficacy of the proposed model is tested on a case study using six metaheuristic techniques to minimize the total cost. The studied algorithms were able to determine optimal solutions for all the independent runs, representing the robustness of the proposed strategy. The use of the standard approach for solving the case study resulted in reporting infeasible solutions using metaheuristic techniques. This chapter also discusses the importance of optimal decisions in various biofuel production stages, such as selecting feed sources, transportation routes, technology selection, etc., with the help of a diversified case study. Among all the selected techniques, SPMGTLO was able to satisfy the product demand with minimum cost, followed by PSO. The proposed solution strategy will guide the researchers in employing metaheuristic techniques to optimize the supply chain in biorefineries as well as in other domains involving mass balances. The chapter discussed in this chapter also provides insights regarding the effectiveness of efficient constraint-handling strategies with metaheuristic techniques.

Chapter 3

A multi-unit strategy based framework using metaheuristics for biorefinery supply chain network

This chapter discusses a novel heuristic-based multi-unit supply chain framework that can implement multiple units of a beneficial process to overcome plant capacity limitations. The proposed framework is suitable for metaheuristic techniques and uses novel repairing operators discussed in the previous chapter to handle the constraints and aid metaheuristic techniques in determining quick, feasible solutions. The efficacy of the proposed formulation and strategies used are demonstrated in a biorefinery case study solved using multiple metaheuristic techniques, and the results are compared with the single-unit strategy.

This chapter is structured as follows: Section 3.1 provides the literature review related to this chapter. Section 3.2 describes the problem statement used in this chapter. Section 3.3 details the multi-unit framework for the biorefinery supply chain and the heuristic mechanism employed for capacity planning. Section 3.4 discusses the proposed strategy for the multi-unit framework, which is well-suited to the metaheuristic techniques. This is followed by Section 3.5, which details the various experimental settings employed in this chapter. Section 3.6 provides the results, a detailed discussion, and inferences from the results. The last section discusses the major findings and benefits of the proposed multi-unit framework.

3.1. Background

The commercialization of biofuel needs optimal distribution and planning of the biorefinery supply chain. Both terrestrial and aquatic categories of biofeed possess a large number of biomass types. The selection of biomass would require information related to its availability, choice of technology, and energy content (Aboytes-Ojeda et al., 2022). Approximately 40 –

60% of the total operating cost of a biorefinery is used according to the feedstock selection, which enforces the optimal choice of feedstocks based on their economic and environmental loadings (Parajuli et al., 2015). In addition to the selection, quantity, and location of the feedstocks, the strategic planning in the biorefinery supply chain involves the quantity of feedstock to be processed, the site of the processing plant, the choice and capacity of technology unit, and the selection of markets (Espinoza Pérez et al., 2017).

Among the decisions to be made in the supply chain network, locating the facilities at different tiers is the most critical (Farahani et al., 2014). Ng & Maravelias (2017) solved the cellulosic biofuel supply chain model by considering biomass selection and allocation, technology selection, and capacity planning at the depots and biorefineries as the decisions. Santibañez-Aguilar et al. (2014) studied the sustainable planning of biorefineries by considering multiple biomass feedstocks at various harvesting sites, different processing plants that produce multiple products, economies of scale for the production technologies, product demand at markets, location of storage facilities, and the transportation mode between each facility. A two-stage biorefinery network involving stochasticity in the quality of biomass in terms of moisture and ash content is solved for the large-scale production and distribution of bioethanol (Aboytes-Ojeda et al., 2020).

There has been extensive research to propose various network design models for biorefinery supply chains (Aboytes-Ojeda et al., 2022). These models often consider harvesting, collecting, and processing biomass, storage, and transporting biomass and biofuel in the designing and planning stages of the supply chains (Atashbar et al., 2016). Similarly, a widespread study in the literature provides simulation-based models for exploring new technologies or optimizing the existing biofuel generation methodologies. Giarola et al. (2012) observed that integrating

first and second-generation technologies is more profitable and sustainable for bioethanol production than standalone first and second-generation technologies. Shahbaz et al. (2020) reviewed biomass processing and conversion technologies based on their merits, demerits, process parameters, types, and routes of all processes for biohydrogen production. A biorefinery superstructure guiding its technical, economic, and environmental aspects considered 39 processing alternatives to produce bio-succinic acid (Dickson et al., 2021). Although multiple studies have been performed on various biomass conversion technologies and the supply chain management of biorefineries involving multiple technologies, the capacity planning of the processing unit with a processing technology has been studied the least.

The capacity selection of a processing technology plays a crucial role in selecting profitable biomass and corresponding processing routes. The restriction on the processing capacity of an economical technology will lead to the selection of suboptimal technologies to satisfy the energy demand. Various supply chain studies have used capacity selection as a decision variable but did not analyze the effect of capacity planning (F. Zhang et al., 2017; J. Zhang et al., 2013). The processed quantity of profitable biomass should only be constrained by raw material availability for any biorefinery. However, the capacity constraints arising due to design limitations of the processing units recommend operating the biorefineries using suboptimal production plans. In case the economical processing technologies are unable to process additional biomass, the production plan uses other lesser economic processing technologies to satisfy the user demands. Although such constraints restrict the biorefineries from reaching their optimal operating conditions, they play a significant role in avoiding unrealistic plant configurations. Further, capacity constraints in distributed biorefineries limit the use of economy of scale, where processing units with larger processing capacity are often cheaper to produce biofuel (Santibañez-Aguilar et al., 2014).

The requirement of optimal decisions towards the selection of harvesting locations, choice and quantity of biomass transportation, selection of processing locations, processing technologies and their capacities, the quantity of biomass processed, and a detailed distribution profile of the biofuel makes the superstructure a complex combinatorial optimization problem. The choice of processing technology and the quantity of biomass processed are the two decision variables in the mass balance equations that cause nonlinearity. In order to use linear solvers for biorefinery supply chain problems requires additional binary variables to model such nonlinearities. Additionally, these solvers use binary variables for the domain constraints related to biomass and biofuel flow rates, processing capacities, etc. The use of such variables often leads to an exponential increase in the problem dimension. These difficulties can be handled using metaheuristic techniques, which are nature-inspired intelligent algorithms. However, due to the lack of specific constraint-handling approaches, it is challenging for these techniques to fulfill several constraints and find feasible solutions, which limits the volume of research in this area (Ba et al., 2016).

In view of the above research gaps, the present study proposes a heuristic-based multi-unit supply chain for biorefinery superstructures, which is suitable for metaheuristic techniques. The framework uses a heuristic technique that helps in capacity planning at the biorefineries without introducing additional binary variables. The framework optimally allocates multiple process units for a profitable technology at any of the processing facilities. The repairing operators proposed in Chapter 2 are integrated with the framework to help the metaheuristic techniques quickly determine feasible solutions for the multi-unit strategy.

3.2. Problem statement

The biorefinery supply-chain network studied in this chapter is adapted from Chapter 2 (El-Halwagi et al. 2013), and it constitutes three echelons: harvesting sites as source nodes, biorefineries as production nodes, and consumers as demand nodes. The harvesting sites can supply multiple types of biomass to the production units, which are responsible for converting the received biomass into biofuel using appropriate technology. They are categorized as the main processing unit (MPU) and secondary processing units (SPUs). The MPU can process larger volumes of biomass and is cheaper due to the economies of scale. The SPUs are small-scale production units and are closer to the consumers. The MPU and SPUs use one of the available technologies for each biomass to produce biofuel. The constraints involved in the network include resource constraints, transportation domain constraints on biomass and biofuel flow rates, capacity domain constraints at the production units, and demand constraints at consumers. Biorefineries are allowed to install multiple process units of a selected technology within their capacity domain. The generic network structure is shown in Fig. 3.1.

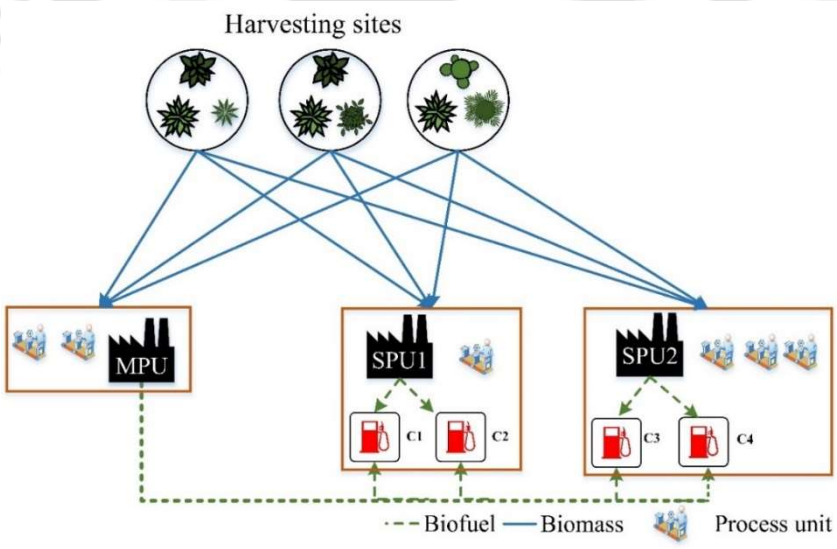

Fig. 3.1 Generic superstructure of the multi-unit biomass-biofuel supply chain

Nomenclature

Sets

H	Set representing the harvesting sites
I	Set representing the type of biomass
J	Set representing the secondary processing unit (SPU)
D_j	Set representing the consumer at SPU j
T_i	Set representing the available conversion technologies for biomass (i)

Indexes

i	Index of biomass source $i \in I$
j	Index of SPU $j \in J$
d	Index of consumer corresponding to j^{th} SPU, $d \in D_j$
t	Index of conversion technologies for i^{th} raw material type, $t \in T_i$

Parameters

δ	Coefficient for the economy of scale
$B_{h,i}^{Cost}$	Unit cost of biomass (i) from harvesting source (h)
B_{min}^{MPU}	Minimum biomass flow rate required for the MPU
B_{max}^{MPU}	Maximum biomass flow rate allowed for the MPU
B_{min}^{SPU}	Minimum biomass flow rate required for the SPU
B_{max}^{SPU}	Maximum biomass flow rate allowed for the SPU
H_Y	Yearly working periods
LPC_i^{MPU}	Minimum processing capacity at the MPU for i^{th} biomass
LPC_i^{SPU}	Minimum processing capacity at the SPU for i^{th} biomass
p_{min}^{MPU}	Minimum product flow rate required for the MPU
p_{max}^{MPU}	Maximum product flow rate allowed for the MPU
P_{Factor}	Large constant value for the cumulative penalty
$R_{h,i}$	Total biomass (i) available at harvesting site (h)
UPC_i^{MPU}	Maximum processing capacity at the MPU for i^{th} biomass

UPC_i^{SPU}	Maximum processing capacity at the SPU for i^{th} biomass
$Z_{j,d}$	Product demand for consumer (d) at the SPU (j)

Determined parameters

τ_i^t	Biomass to the biofuel conversion factor for technology (t) corresponding to biomass type (i)
a_i^t	Fixed cost coefficient for installing t^{th} technology corresponding to i type biomass at main processing unit (MPU)
b_i^t	Variable cost coefficient for installing t^{th} technology corresponding to i type biomass at MPU
$BTC_{h,i}^{MPU}$	Transportation cost of biomass (i) from harvesting source (h) to the MPU
$BTC_{h,i,j}^{SPU}$	Transportation cost of biomass (i) from harvesting source (h) to SPU (j)
BC^{MPU}	Total biomass procurement cost for the MPU
BC_j^{Sec}	Total biomass procurement cost for the j^{th} SPU
c_i^t	Fixed cost coefficient for installing t^{th} technology corresponding to i type biomass at SPU
d_i^t	Variable cost coefficient for installing t^{th} technology corresponding to i type biomass at SPU
f	Fitness value of the potential solution
I^{MPU}	Total capital cost for the MPU
I_j^{SPU}	Total capital cost for the j^{th} SPU
MC_i^t	Processing cost of biomass (i) from technology (t) at the MPU
MTC^P	Total product transportation cost for the MPU
MTC^B	Total biomass transportation cost for the MPU
$PTC_j^{MPU \to SPU}$	Transportation cost of the product from the MPU to a SPU (j)
p_j^{MPU}	Total product flow rate from MPU to j^{th} SPU
p_j^{SPU}	Total product flow rate from j^{th} SPU to corresponding demand locations
P^{MPU}	Total product produced at the MPU
PC^{MPU}	Total processing cost in the MPU

PC_j^{SPU}	Total processing cost in the j^{th} SPU
Pen_P	Penalty for upper bound violation in the product flow rate from the MPU
Pen_H	Penalty for violation of raw material availability constraint
Pen_D	Penalty for unsatisfied demand
SC_i^t	Processing cost of biomass (i) from technology (t) at the SPU
STC_j^B	Total biomass transportation cost for the j^{th} SPU
V_j	Upper bound violation in the product flow rate in the j^{th} SPU
$V_{j,d}$	Unsatisfied demand for consumer d in the j^{th} SPU
$V_{h,i}$	Violation in biomass (i) availability at source (h)

Variables

$B_{h,i}^{MPU}$	Flow rate of biomass (i) from harvesting site (h) to the MPU
$BP_{n,i}^{MPU}$	Biomass (i) processed at the n^{th} process unit of the MPU
$B_{h,i,j}^{Sec}$	Flow rate of biomass (i) harvesting site (h) to the SPU (j)
$BP_{n,i,j}^{SPU}$	Biomass (i) processed at the n^{th} process unit of the j^{th} SPU
$C_{j,d}^{MPU}$	Product delivered to consumer (d) in the SPU (j) from the MPU
$C_{j,d}^{SPU}$	Product delivered to the consumer (d) in the SPU (j).
$S_{j,d}^{MPU}$	Product share of the consumer (d) in the SPU (j) from the MPU
$S_{j,d}^{SPU}$	Product share of the consumer (d) from the SPU (j))
y_i^t	Binary variable denoting the selection of (t) type technology corresponding to (i) type biomass
t	Selected technology

3.3. Multi-unit framework for biorefinery supply chain

The framework uses certain repair mechanisms and a heuristic-based capacity-planning technique for the supply chain. The framework constitutes a set of H harvesting sites, which provide I type of biomass to the MPU, and a set of SPUs denoted by J. Each of the j^{th} SPU locations has D_j consumer demands. These demands are satisfied using the biofuel produced from the MPU and the corresponding SPU. Each production center can use biomass-based conversion technology τ_i^t from a set of available technologies T_i. The biorefinery network is modeled using three sets of decision variables, as depicted in Fig. 3.2. These sets represent (i) the biomass flow rate from the harvesting sites to the production units ($B_{h,i}^{MPU}$ and $B_{h,i,j}^{SPU}$), (ii) the biofuel sharing percentage of the production units ($S_{j,d}^{MPU}$ and $S_{j,d}^{SPU}$) for the consumers and (iii) the choice of technologies (τ_i^t) at the production units.

Biomass transport		*Biofuel distribution*		*Selected technology*	
$\underbrace{B_{h,i}^{MPU}}_{\forall h \in H, i \in I}$	$\underbrace{B_{h,i,j}^{SPU}}_{\forall h \in H, i \in I, j \in J}$	$\underbrace{S_{j,d}^{MPU}}_{\forall j \in J, d \in D_j}$	$\underbrace{S_{j,d}^{SPU}}_{\forall j \in J, d \in D_j}$	$\underbrace{\tau_i^t}_{\forall i \in I, t \in T_i}$	$\underbrace{\tau_{i,j}^t}_{\forall i \in I, j \in J, t \in T_i}$
MPU	*SPUs*	*MPU share*	*SPUs share*	*MPU*	*SPUs*

Fig. 3.2 Decision structure for the multi-unit framework

Instead of the product flow rates, the proposed strategy utilizes the product sharing percentages as the decision variable, which implicitly handles the equality constraints arising from the mass balance between raw materials and products. The detailed formulation for the framework is provided below.

3.3.1. Balances at the harvesting locations

Each harvesting site can provide biomass to the production centers as per the available produce ($R_{h,i}$), which acts as a resource constraint at the source as in Equation (3.1) (El-Halwagi et al. 2013). In the event of any resource constraint violation, where the total biomass transported from any harvesting site exceeds the actual availability, a penalty value is determined depending upon the violation as given in Equation (3.2).

$$B_{h,i}^{MPU} + \sum_{j \in J} B_{h,i,j}^{SPU} \leq R_{h,i} \qquad \forall h \in H, \forall i \in I \tag{3.1}$$

$$V_{h,i} = \begin{cases} \left(B_{h,i}^{MPU} + \sum_{j \in J} B_{h,i,j}^{SPU} \right) - R_{h,i}, & if \;\; B_{h,i}^{MPU} + \sum_{j \in J} B_{h,i,j}^{SPU} > R_{h,i} \\ 0 & else \end{cases} \qquad \forall i \in I, h \in H$$

$$Pen_H = \sum_{h \in H} \sum_{i \in I} V_{h,i} \tag{3.2}$$

The biomass transportation from the harvesting sites to the MPU and SPUs follows a flow domain where any nonzero flow rate should be within a minimum and maximum limit. This constraint helps in avoiding any impractical flow channels between the nodes. The maximum flow limit of the biomass is the upper bound of the decision variables. In the case of violation in the lower limit of the flow where a nonzero flow lesser than the minimum flow limit occurs, a repair mechanism is employed, as shown in Equations (3.3) , and (3.4) that assigns zero value to the flow rate.

$$B_{h,i}^{MPU} = \begin{cases} 0 & if \; 0 < B_{h,i}^{MPU} < B_{min}^{MPU} \\ B_{h,i}^{MPU} & else \end{cases} \qquad \forall i \in I, h \in H \tag{3.3}$$

$$B_{h,i,j}^{SPU} = \begin{cases} 0 & if \;\; 0 < B_{h,i,j}^{SPU} < B_{min}^{SPU} \\ B_{h,i,j}^{SPU} & else \end{cases} \qquad \forall i \in I, j \in J, h \in H \tag{3.4}$$

3.3.2. Balances at the main processing unit

The main processing unit is capable of large-scale biomass processing and is away from the consumer locations. Each of the received biomass is processed using one of the suitable technologies. The production of biofuel from biomass is shown in Equation (3.5). The metaheuristic framework does not require binary variables to implement the technology selection. However, a boolean variable y_i^t is used in Equation (3.5), which assumes a value of 1 if the technology t is selected for i^{th} biomass to mathematically represent the biofuel production at the MPU.

$$P^{MPU} = \sum_{i \in I} \tau_i^t y_i^t \left(\sum_{h \in H} B_{h,i}^{MPU} \right), \quad t \in T_i \tag{3.5}$$

As given in Equation (3.6), the biofuel produced at the MPU is distributed among consumers at different SPU locations using sharing percentages. The sharing among the consumers is normalized as per the Equation (3.7) , ensuring the entire distribution of biofuel produced at the MPU.

$$C_{j,d}^{MPU} = \hat{S}_{j,d}^{MPU} P^{MPU}, \forall d \in D_j, j \in J \tag{3.6}$$

$$\sum_{j=1}^{J} \sum_{d=1}^{D_j} \hat{S}_{j,d}^{MPU} = 1 \tag{3.7}$$

The biofuel produced at the MPU is distributed among the consumers through the corresponding SPUs. The biofuel transportation from the MPU follows a flow domain in which nonzero biofuel flow to any SPU location should be within a minimum and maximum flow limit. The biofuel flow to each SPU is determined using Equation (3.8). The upper flow limit violation to the SPUs is penalized as per Equation (3.9), whereas any nonzero value for the

biofuel flow lesser than the allowed minimum flow limit is assumed to be zero, as in Equation (3.10).

$$p_j^{MPU} = \sum_{d \in D_j} C_{j,d}^{MPU}, \quad \forall\, j \in J \tag{3.8}$$

$$\begin{aligned} V_j &= \begin{cases} p_j^{MPU} - p_{max}^{MPU}, & if\ p_j^{MPU} > p_{max}^{MPU} \\ 0 & else \end{cases} \\ Pen_P &= \sum_{j \in J} V_j, \quad \forall j \in J \end{aligned} \tag{3.9}$$

$$p_j^{MPU} = \begin{cases} 0, & if\ 0 < p_j^{MPU} < p_{min}^{MPU} \\ p_j^{MPU} & else \end{cases} \qquad \forall j \in J \tag{3.10}$$

The correction approach in Equation (3.10) for the MPU is implemented for two cases where the first represents the absence of one or more fuel flow channels to the SPUs, and the second resembles the absence of any flow channel to the SPUs. In the first case, the corresponding sharing percentages also assume zero value, as shown in Equation (3.11). The second case implies zero biofuel flow to all consumers, indicating no production at the MPU and no requirement for biomass at the MPU. The correction approach for the second case provides zero value to all the biomass flow channels from the harvesting sites to the MPU, as in Equation (3.11).

$$\begin{aligned} \hat{S}_{j,d}^{MPU} &= \begin{cases} 0 & if\ p_j^{MPU} = 0 \\ \hat{S}_{j,d}^{Main} & else \end{cases} \qquad \forall d \in D_j \\ B_{h,i}^{MPU} &= \begin{cases} 0, & if\ \sum_{j=1}^{J} p_j^{MPU} = 0 \\ B_{h,i}^{Main} & else \end{cases} \qquad \forall i \in I, h \in H \end{aligned} \tag{3.11}$$

The biomass at the MPU is processed within the capacity domain of the selected technology. The processing below the minimum limit is not permissible and is corrected by assigning zero values to the corresponding biomass flow channels as in Equation (3.12) .

$$\left(B_{h,i}^{MPU}=0,\forall h\in H\right)\vee\left(0<\sum_{h\in H}B_{h,i}^{MPU}<LPC_{i}^{MPU}\right),\qquad\forall i\in I \tag{3.12}$$

The requirement of biomass processing above the maximum permissible capacity limit is accommodated using the multi-unit capacity planning heuristic mechanism and is discussed in the later section. The operational costs of the MPU consist of the biomass cost, the processing cost, and the transportation cost of biomass and biofuel to the required nodes and are given in Equations (3.13) to (3.16) (El-Halwagi et al. 2013).

$$BC^{MPU}=\sum_{h\in H}\sum_{i\in I}B_{h,i}^{MPU}B_{h,i}^{Cost} \tag{3.13}$$

$$PC^{MPU}=\sum_{i\in I}MC_{i}^{t}y_{i}^{t}\left(\sum_{h\in H}B_{h,i}^{MPU}\right),\quad t\in T_{i} \tag{3.14}$$

$$MTC^{B}=\sum_{i\in I}\sum_{h\in H}B_{h,i}^{MPU}BTC_{h,i}^{MPU} \tag{3.15}$$

$$MTC^{P}=\sum_{j\in J}p_{j}^{MPU}PTC_{j}^{MPU\rightarrow SPU} \tag{3.16}$$

The investment cost of the MPU constitutes the cost required for installing multiple units of the implemented technologies and follows a nonlinear relationship. The cost estimation comprises fixed investment cost and capacity-dependent variable component, as shown in Equation (3.17).

$$I^{MPU}=\sum_{i\in I}\sum_{n\in N_{MPU}}y_{i}^{t}\left(a_{i}^{t}+b_{i}^{t}\left(BP_{n,i}^{MPU}\right)^{\delta}\right),\quad t\in T_{i} \tag{3.17}$$

3.3.3. Balances at the secondary processing units

The SPUs are small-scale processing units and are located near consumer locations. Similar to the production at the MPU, technologies suitable for the available biomass are used for biofuel production as given in Equation (3.18).

$$p_j^{SPU} = \sum_{i \in I} \tau_{i,j}^t y_{i,j}^t \left(\sum_{h \in H} B_{h,i,j}^{SPU} \right), \quad t \in T_i, \forall j \in J \tag{3.18}$$

The total biofuel production is distributed among the consumers using the sharing ratios and is given in Equation (3.19). The sharing ratios for the consumers related to each SPU are normalized using Equation (3.20) , ensuring the total distribution of the produce.

$$C_{j,d}^{SPU} = \hat{S}_{j,d}^{SPU} \, p_j^{SPU} \quad \forall d \in D_j, j \in J \tag{3.19}$$

$$\sum_{d=1}^{D_j} \hat{S}_{j,d}^{SPU} = 1, \forall j \in J \tag{3.20}$$

Analogous to the capacity constraints at the MPU, the processing capacity of SPUs follows a processing domain for each of the selected technologies. The processing of any biomass below the minimum capacity limit is not allowed, and the corresponding biomass flow rate is assigned a value of zero, as shown in the Equation (3.21) (El-Halwagi et al. 2013). The upper capacity limit (UPC_i^{SPU}) for any processing technology is relaxed by accommodating multiple processing units of the selected technology using the capacity planning heuristic mechanism.

$$\left(B_{h,i,j}^{SPU} = 0, \forall h \in H \right) \vee \left(0 < \sum_{h \in H} B_{h,i,j}^{SPU} < LPC_i^{SPU} \right), \quad \forall i \in I, j \in J \tag{3.21}$$

The costs associated with the SPUs are determined to be similar to the MPU and are given in Equations (3.22) - (3.25), where the Equations (3.22) - (3.24) represent the operational costs, whereas Equation (3.25) represents investment cost (El-Halwagi et al. 2013).

$$BC_j^{SPU} = \sum_{h \in H} \sum_{i \in I} B_{h,i,j}^{SPU} B_{h,i}^{Cost}, \quad \forall j \in J \tag{3.22}$$

$$STC_j^B = \sum_{h \in H} \sum_{i \in I} B_{h,i,j}^{SPU} BTC_{h,i,j}^{SPU}, \quad \forall j \in J \tag{3.23}$$

$$PC_j^{SPU} = \sum_{i \in I} SC_{i,j}^t y_{i,j}^t \left(\sum_{h \in H} B_{h,i,j}^{SPU} \right), \quad t \in T_i, \forall j \in J \tag{3.24}$$

$$I_j^{SPU} = \sum_{i \in I} \sum_{n \in N_{SPU}} y_{i,j}^t \left(c_{i,j}^t + d_{i,j}^t \left(BP_{n,i,j}^{SPU} \right)^{\delta} \right), \quad t \in T_i, \forall j \in J \tag{3.25}$$

The demand at the consumer locations needs to be satisfied by utilizing the biofuel produced at the processing centers, which is provided in Equation (3.26) (El-Halwagi et al. 2013). The shortage in fulfilling the demand is penalized using Equations (3.26) and (3.27).

$$C_{j,d}^{MPU} + C_{j,d}^{SPU} \geq Z_{j,d} \quad \forall d \in D_j, j \in J \tag{3.26}$$

$$V_{j,d} = \begin{cases} Z_{j,d} - \left(C_{j,d}^{MPU} + C_{j,d}^{SPU} \right), & Z_{j,d} > \left(C_{j,d}^{MPU} + C_{j,d}^{SPU} \right) \\ 0 \end{cases}, \quad \forall d \in D_j, \forall j \in J$$
$$Pen_D = \sum_{j \in J} \sum_{d \in D_j} V_{j,d} \tag{3.27}$$

3.3.4. Objective: Minimize total cost

The biorefinery network aims to minimize the total cost while satisfying the applicable constraints. The total cost is determined by adding the total operational cost of the plant and the investment cost. The total operational cost is determined by multiplying the total plant operational period by the periodic operational cost. However, the investment cost is determined only once.

$$TLC = H_Y \left(\underbrace{BC^{MPU} + \sum_{j \in J} BC_j^{SPU}}_{\text{Total biomass cost}} + \underbrace{MTC^B + MTC^P + \sum_{j \in J} STC_j^B}_{\text{Total transportation cost}} + \underbrace{PC^{MPU} + \sum_{j \in J} PC_j^{SPU}}_{\text{Total processing cost}} \right) +$$
$$\underbrace{I^{MPU} + \sum_{j \in J} I_j^{SPU}}_{\text{Total investment cost}} \tag{3.28}$$
$$f = TLC + \left(Pen_H + Pen_P + Pen_D \right) P_{Factor}$$

A fitness value (*f*) is assigned to each potential solution by including all the applicable penalty values. The fitness value of a potential solution is identified by including all the applicable penalty values corresponding to each constraint. A large penalty factor (P_{Factor}) is multiplied by the total violations to help the metaheuristic techniques prefer feasible solutions over infeasible solutions as in Equation (3.28).

3.4. Proposed heuristic mechanism-based framework

The heuristic mechanism helps in the capacity planning of the MPU and SPUs where the biomass availability exceeds the processing capacity of a single processing unit of the selected technology. A direct allocation of excess biomass to a second processing unit might violate the domain constraints related to the processing capacity, as the extra biomass is not assured to be within the processing capacity domain. The heuristic mechanism initially checks for domain violation in the capacity limits of the selected technologies. Any violation in the lower capacity limit is corrected, and the solution is returned to the objective function to determine the associated costs. Then, the violations in the upper capacity limit of the selected technologies are checked, and the technology units are based on two criteria. A single technology unit is designated if the total biomass processing falls within the upper capacity limit. In case the total biomass available for processing exceeds the capacity limit, multiple full-capacity units are assigned appropriately until the total biomass is allocated for processing. The assignment always checks the biomass allocation for lower domain violations and uses a repair mechanism to avoid such a scenario. The repair mechanism determines the shortage of biomass required to satisfy the lower production capacity and adjusts the quantity from the previously allotted full-capacity unit.

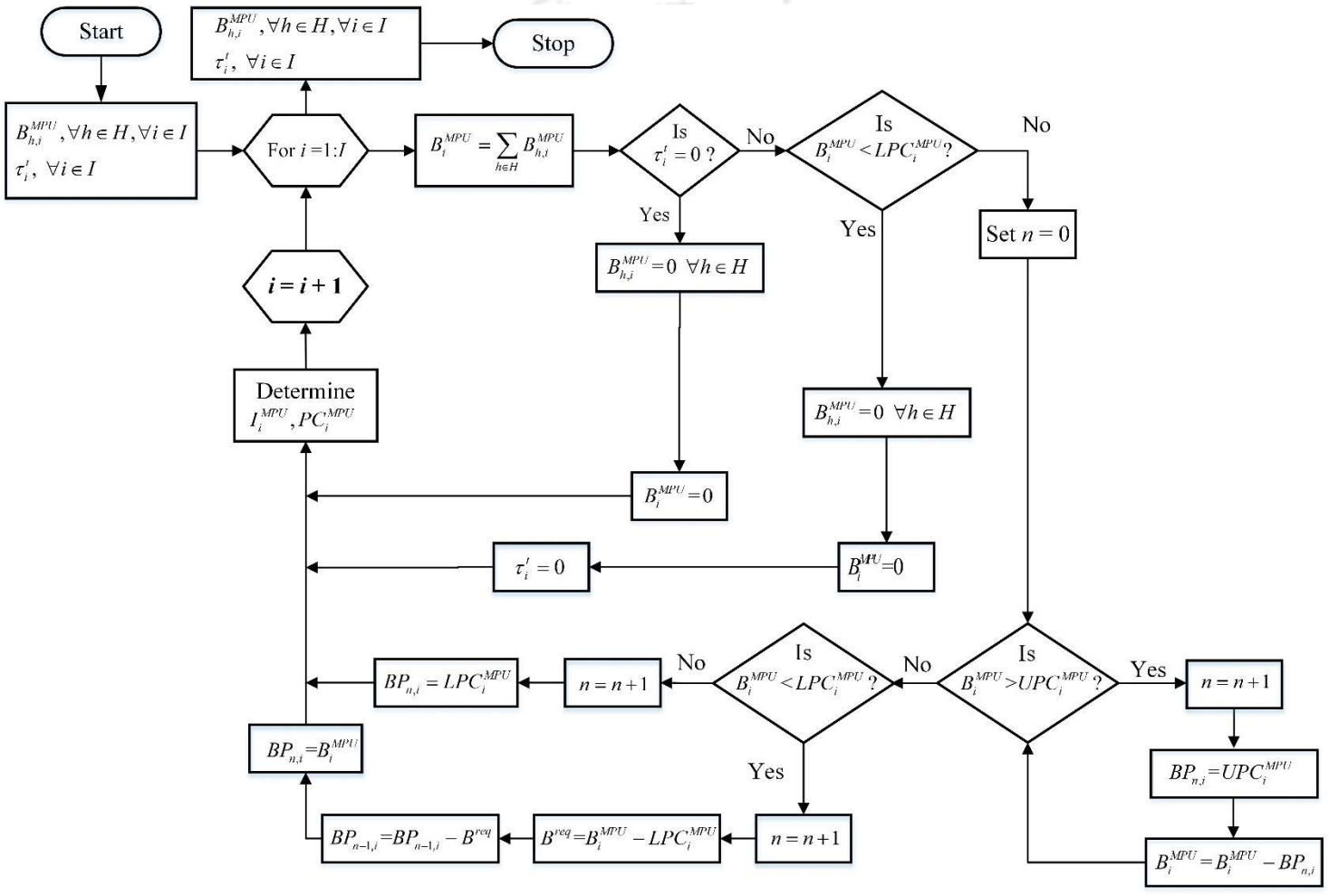

Fig. 3.3 Flowchart of the heuristic mechanism for capacity planning of MPU

For a better understanding of the mechanism, a detailed flowchart for the heuristic capacity planning of MPU is provided in Fig. 3.3. For the illustration of the heuristic mechanism, consider an example in which a biomass (i=1) can be procured from two harvesting source (h={1,2}). Assume that $B^{Main}_{h=1,i=1}=100$ and $B^{Main}_{h=2,i=1}=250$. The total availability of the biomass $B_{i=1}=400$. The lower processing capacity and the upper processing capacity for the biomass in the MPU is provided as $LPC^{Main}_{i=1}=150$ and $UPC^{Main}_{i=1}=250$. The various steps involved in the heuristic mechanism to determine the number and capacity of processing units for the given biomass quantity are provided below.

On analyzing the bounds, it is observed that $B_{i=1}\geq LPC^{Main}_{i=1}$ and $B_{i=1}\geq UPC^{Main}_{i=1}$. Hence, the required number of full capacity processing units is set as 1 and its capacity as $BP_{n=1,i=1}=250$ .The remaining quantity of biomass to be processed is $B_{i=1}=400-250=150$. To assign the unallocated biomass, the bound checking is performed and observed that $B_{i=1}\geq LPC^{Main}_{i=1}$ and $B_{i=1}<UPC^{Main}_{i=1}$. Hence, the required number of full capacity processing units is increased to 2, and the capacity of the second unit is set as $BP_{n=2,i=1}=150$.

In some instances, the remaining quantity of biomass to be allocated might be lesser than the lower capacity of a processing unit. To illustrate such a scenario, assume that $LPC^{Main}_{i=1}=200$ and $UPC^{Main}_{i=1}=250$. The first unit with a full capacity is allocated for processing the biomass. However, the remaining quantiy $\left(B_{i=1}=150\right)$, violates the lower capacity bound $B_{i=1}<LPC^{Main}_{i=1}$. Hence, the quantity of biomass lesser than $LPC^{Main}_{i=1}$ is identified as $B_{i=1}-LPC^{Main}_{i=1}=50$. The total amount of biomass is redistributed among two processing units as below

for $n=1$, $BP_{n=1,i=1}=250-50=200$ *and for* $n=2$, $BP_{n=2,i=1}=150+50=200$

Metaheuristic techniques try to improve the solutions in an iterative way using a set of equations. These techniques usually consider the problem as a black box and require suitable transformations of the mathematical model where each potential solution from the techniques can be measured for its goodness using the model equations. The general steps involved in the techniques can be summarized as (i) initialization of a random population within the variable bounds and determining their objective value, (ii) generation of new solutions using the variation operators of the metaheuristic technique, and evaluation of their objective value, (iii) determine the population for the next iteration using the selection strategy of the technique. Steps (ii) and (iii) are performed iteratively until the termination criterion is satisfied. Real-life optimization problems comprise multiple constraints, and the lack of dedicated constraint handling techniques often creates difficulties for the metaheuristic techniques in determining feasible solutions. There have been many approaches for handling constraint optimization problems using metaheuristics (Coello Coello, 2002). However, most techniques are observed to rely on penalty-based approaches (Mezura-Montes & Coello Coello, 2011)

The penalty-based approach uses penalty functions to penalize the objective function value of an infeasible solution. In that case, the objective function value is termed as the fitness of the solution. Using the fitness value as a measuring criterion helps the metaheuristic techniques identify feasible solutions among a pool of solutions. The determination of better solutions by depending only on penalty-based approaches often leads to poor performance of the metaheuristic techniques (Maharana et al., 2022), which can be improved by repairing infeasible solutions and communicating them to the techniques, as shown in Fig. 3.4.

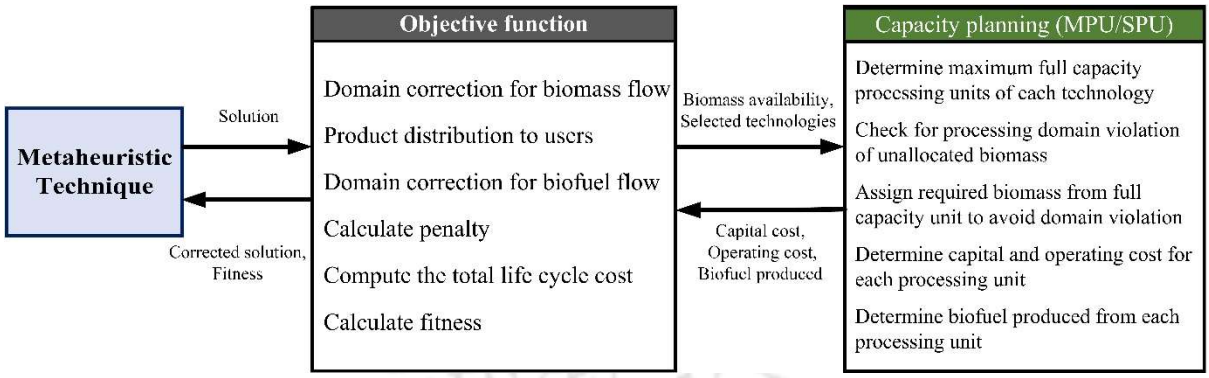

Fig. 3.4 Interaction between the objective function and metaheuristic technique

This chapter uses the same metaheuristic techniques used in Chapter 2 for analyzing the efficacy of the proposed multi-unit framework.

3.5. Case study for the multi-unit strategy

The proposed multi-unit framework is applied to address a case study of a distributed biofuel supply chain involving six harvesting sites, one main processing unit (MPU), and two secondary processing units (SPUs). The case study, previously introduced in Chapter 2, is revisited in this chapter. Detailed data on biomass costs, monthly availability, processing technologies, and both investment and operating costs for the case study are provided in the Appendix. This analysis uses 25 independent runs for the metaheuristic techniques using a desktop computer with an Intel i7 @4.2 GHz processor and 32 GB of RAM on the MATLAB 2019a simulation environment. The presented analysis uses a population size of 250 for all the metaheuristic techniques except DYYPO, as the population size for DYYPO is 2. A common termination criterion of maximum function evaluation is applied to all the techniques, and the value is set at 100000 function evaluations. The other user-defined parameters for the techniques are considered as suggested by the inventors of the algorithm without performing any tuning. The considered case study requires 98 continuous and 15 integer decision variables and 241 constraints.

3.6. Results and discussion

This section discusses the performance of the proposed multi-unit framework in determining solutions with better total cost than the solutions of the single-unit framework. Subsequently, a detailed solution analysis is performed to highlight the benefits of the multi-unit framework in various strategic and operational level decisions of the biorefinery superstructure.

3.6.1. Statistical analysis

The statistical measures for all the techniques are provided in Table 3.1, where the minimum value across each statistical measure is highlighted in boldface font. Each technique could determine better solutions using the multi-unit framework as against the single-unit framework. The maximum benefit of using the multi-unit framework is observed in the case of DE followed by GA, where these techniques are able to decrease the total cost by 8.3 % and 7.38 %, respectively, compared to a single-unit framework. In comparison to all other metaheuristic techniques, the best solution determined by SPMGTLO showed less improvement from the respective single-unit solution. However, SPMGTLO is able to determine the best solution with the least total cost, as observed in Table 3.1. For the best, worst, mean, and median statistics, SPMGTLO showed better performance compared to all the techniques, whereas the performance of DYYPO is worse in all the statistic measures. In all the performed runs, the metaheuristic techniques were able to determine feasible solutions, which can be observed from the mean fitness value in Table 3.1. The mean and median values of each metaheuristic technique with the multi-unit framework are close, indicating the consistency of these techniques in identifying similar solutions in the majority of runs.

Table 3.1 Statistical analysis using single and multi-unit strategies

Technique	Total cost of single-unit framework ($\$10^9$)					Total cost of multi-unit framework ($\$ 10^9$)					Improve unit fra
	Best	**Worst**	**Mean**	**Median**	**SD**	**Best**	**Worst**	**Mean**	**Median**	**SD**	
GWO	1.20	1.36	1.28	1.27	0.04	1.17	1.31	1.23	1.21	0.04	
DE	1.33	1.44	1.38	1.38	0.02	1.22	1.29	1.25	1.26	0.02	
SPMGTLO	1.13	1.21	1.17	1.17	0.02	**1.11**	**1.22**	**1.15**	**1.14**	**0.02**	
GA	1.34	1.57	1.45	1.46	0.06	1.24	1.63	1.39	1.37	0.08	
PSO	1.22	1.57	1.33	1.32	0.08	1.17	1.41	1.28	1.27	0.05	
DYYPO	1.52	2.33	1.85	1.84	0.22	1.42	2.06	1.69	1.66	0.15	
SHTS	1.24	1.39	1.32	1.32	0.03	1.18	1.33	1.27	1.29	0.04	
COA	1.18	1.33	1.26	1.25	0.04	1.13	1.29	1.20	1.20	0.04	

The deviation of the best value from the mean value is lower for DE compared to other metaheuristic techniques, specifying its potential to determine better solutions in most runs. Even though the best value determined by GWO and PSO is approximately equal, the better mean and median value of GWO indicates its superior performance compared to PSO. It is observed that DE with the multi-unit framework is able to obtain approximately a 9.15 % improvement in the mean value compared to the single-unit framework, followed by DYYPO with 8.53 %. The total cost determined at the end of each independent run corresponding to each algorithm is considered a sample for the Wilcoxon signed-rank test, which is performed to analyze whether the results obtained from the two algorithms (samples) are statistically different. The p-value obtained in each pair-wise comparison of algorithms is less than the significance level of 0.05, indicating the results provided by all algorithms are statistically different from each other. Such an inference is not observed when comparing the p-value of DE with SHTS and PSO. The results of the test are provided in Table B1 of Appendix B.

3.6.2. Convergence analysis

This section analyses the performance of the metaheuristic techniques based on convergence to the final solution within the termination criterion of maximum function evaluations. The convergence of the best objective value and the total constraint violations with the function evaluations are depicted in Fig. 3.5. All the techniques are able to determine a feasible solution within fewer functional evaluations by using the multi-unit framework, compared to the single-unit framework as observed from Fig. 3.5 (b) and (d). It should be noted that the presence of more constraints in the model leads to the usage of more function evaluations to determine better solutions. In this regard, the multi-unit framework uses a heuristic mechanism that provides flexibility in capacity planning at the MPU and SPUs by allowing multiple process units for the economical processing technologies.

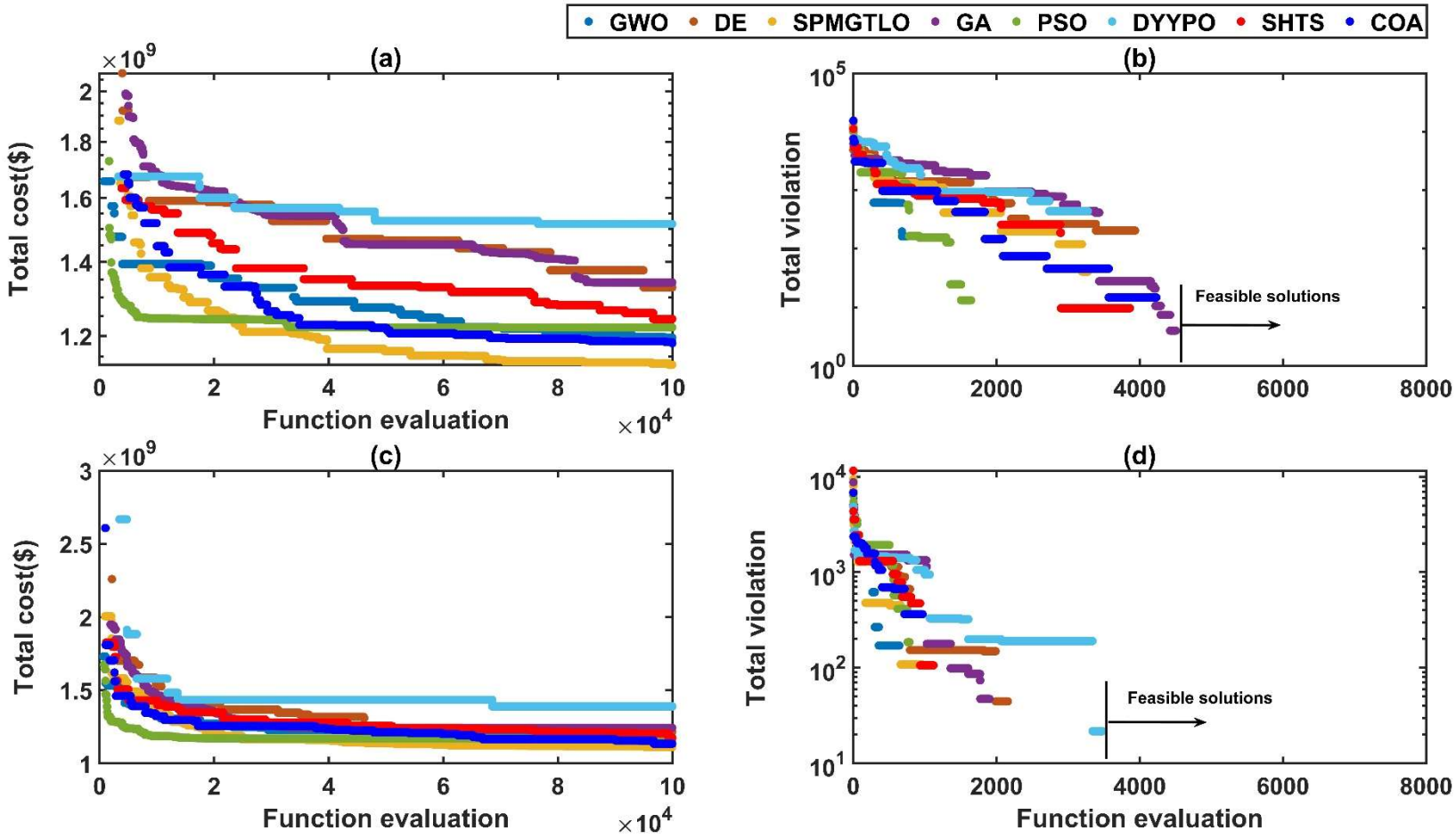

Fig. 3.5 Convergence of all techniques in the single-unit framework (a) total cost (b) violation of the constraints and the multi-unit framework (c) total cost (d) violation of the constraints

The proposed heuristic mechanism repairs the solutions that violate the capacity constraints of any process unit and thus helps the metaheuristic techniques determine feasible solutions in the earlier iterations. In both strategies, PSO was the first to determine the initial feasible solution and thus showed a faster convergence profile in the initial functional evaluations. However, in both the single and multi-unit framework, PSO is unable to improve the objective value further after utilizing approximately half of the maximum function evaluations. DYYPO and PSO converged more quickly to the final objective value for the multi-unit framework than the single-unit framework. For the multi-unit framework, DYYPO, PSO, and GA were able to converge to the final objective value within the maximum functional evaluations.

However, the convergence profiles of DE, SPMGTLO, GWO, COA, and SHTS indicate the possibility of improvement in the final objective value by providing more function evaluation. The final population analysis helps get a set of converged solutions that show a trade-off in their fitness value. These solutions can be used when the optimal solution is limited by any additional operational constraints. The fitness value (total cost) of the converged feasible population after utilizing the maximum allowed function evaluations is provided in Fig. B1 of Appendix B.

3.6.3. Optimal solution analysis

A detailed solution analysis helps identify key contributions of the multi-unit framework in reducing the total cost of the supply chain network. The biomass distribution at the processing units using the single and the multi-unit framework determined by SPMGTLO are shown in Fig. 3.6. Due to the capacity restriction in the single unit framework where only one unit of each processing technology is allowed, the MPU and SPU2 used a costlier production plan and

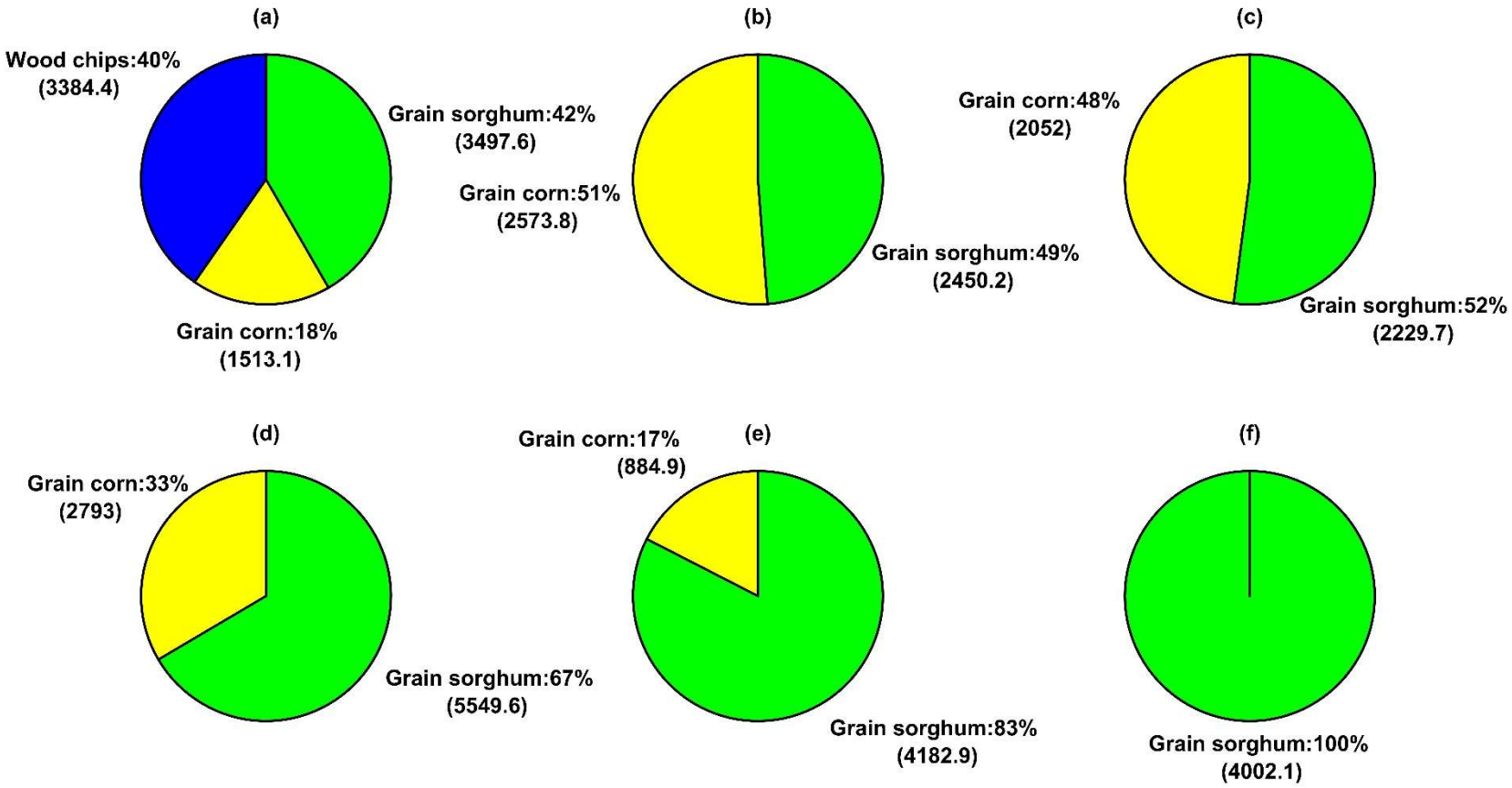

Fig. 3.6 Biomass distribution (in tonne/month) for single-unit framework (a) MPU, (b) SPU1, (c) SPU2 and multi-unit framework (d) MPU, (e) SPU1, (f) SPU2

additionally used wood chips and grain corn, respectively, to satisfy the demand. In contrast, the relaxation to process the additional quantity of biomass using multiple technology units helped the multi-unit framework satisfy the demand with only two types of biomass. In addition, due to the economies of scale, processing at the MPU is cheaper, and the multi-unit framework helps in processing a higher quantity of biomass at the MPU. The processing of biomass grain corn and grain sorghum has increased by 85% and 59%, respectively, at the MPU using the multi-unit framework. Similarly, the processing quantity of biomass grain corn decreased by 65%, and the processing of grain sorghum increased by 71% at SPU1.

In the case of SPU2, only one type of biomass is observed, and the unit completely avoids the use of biomass grain corn. It should be noted that the requirement to satisfy higher demand at the SPU2 necessitates the processing of a higher quantity of biomass. Hence, the multi-unit framework allows the processing of an additional quantity of biomass grain sorghum and removing biomass grain corn from the production plan of SPU2. The need to satisfy the demand of each customer can lead to excess production at each of the processing units. In such a scenario, producing additional biofuel causes a financial burden on the overall system and is directly related to a higher total cost. The biofuel supplied to each consumer using the single-unit strategy and the multi-unit framework are shown in Fig. 3.7. The consumer product distribution profile using the single-unit framework shows a higher product supply, exceeding the consumer demand. DYYPO and DE were observed to produce and distribute a higher quantity of products among the majority of the consumers. A similar trend is also witnessed while using the multi-unit framework; however, the additional quantity of biofuel produced and distributed among the consumers has been reduced significantly, leading to lower total cost.

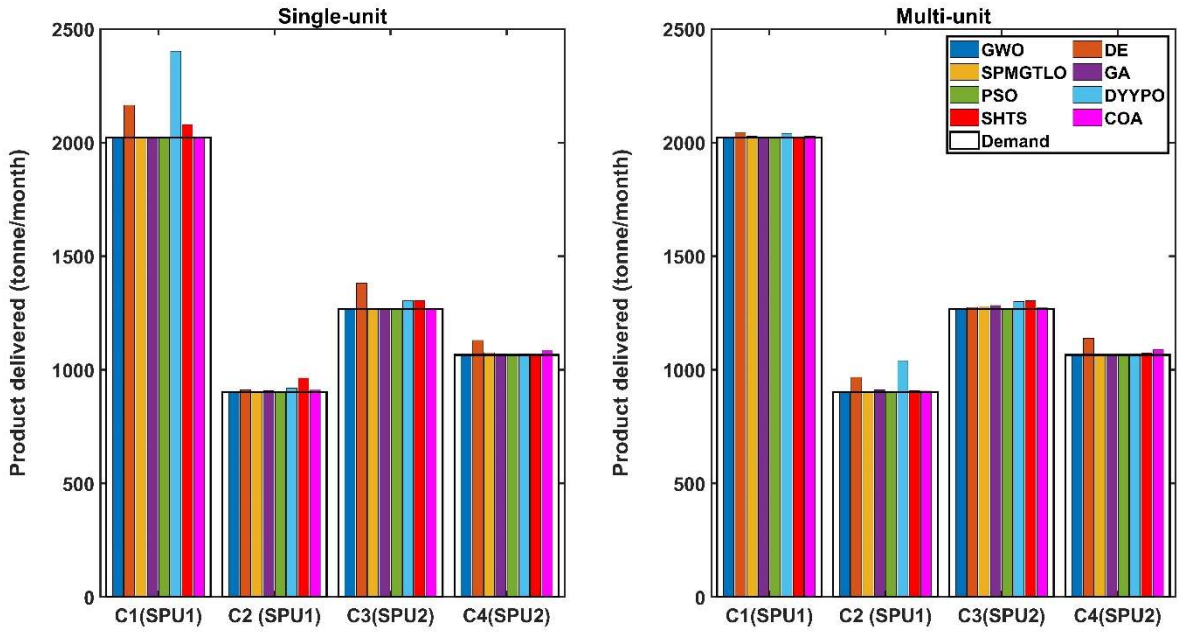

Fig. 3.7 Demand distribution for single-unit and multi-unit strategies

The production plan demonstrating the choice of harvesting location, the quantity of biomass procurement and processing at MPU and SPUs, and their associated costs are given in *Table 3.2*. In the single unit case, the capacity restriction led to the use of three types of biomass in the MPU and two types of biomass at each of the SPUs. However, the multi-unit strategy could use multiple process units at the MPU and SPUs, thereby avoiding the use of wood chips. Although the use of multiple process units increases the initial investment costs, it appears to be beneficial in long-term operations and can significantly reduce the total technology costs over the life of the processing units. Similarly, the use of economies of scale makes it cheaper to produce at the MPU, and hence, the total biomass processed for grain corn across the MPU is increased, whereas the total biomass processed across the SPUs for grain corn is reduced. The production of biofuel from grain sorghum is economical, and hence, the processing units have increased the processing share of the grain sorghum in the multi-unit strategy. It is noted that a large quantity of grain sorghum is also processed at the SPU2 due to the higher demand at the SPU2.

Table 3.2 Biomass procured, processed, and the cost associated with biomass conversion for single-unit and multi-unit frameworks

Single-unit framework								
		MPU			**SPU1**		**SPU2**	
Biomass type		**B1**	**B3**	**B4**	**B3**	**B4**	**B3**	**B4**
Biomass procured (tonne/month)	**H3**	1400	1341	1395	-	-	246	389
	H4	1317	172	-	-	-	760	712
	H5	-	-	703	1386	1383	1046	1128
	H6	667	-	1400	1187	1067	-	-
Technology		Gasification and Biosynthesis	Pretreatment, acid hydrolysis and fermentation		Pretreatment, acid hydrolysis and fermentation		Pretreatment, acid hydrolysis and fermentation	
Processing capacity of unit 1 (tonne/month)		3384	1513	3498	2574	2450	2052	2230
Biomass Cost ($ million/month)		0.29	0.31	0.59	0.53	0.41	0.43	0.37
Operating cost ($ million/month)		0.27	0.09	0.16	0.19	0.14	0.15	0.13
Investment Cost ($ million)		12.00	8.71	6.83	7.26	5.69	7.26	5.69
Total technology cost ($ million/20 yrs)		77.00	29.80	45.10	52.10	39.20	43.00	36.10
Multi-unit framework								
		MPU			**SPU1**		**SPU2**	
Biomass type		**B1**	**B3**	**B4**	**B3**	**B4**	**B3**	**B4**
Biomass procured (tonne/month)	**H3**	-	-	1399	306	1399	-	-
	H4	-	1393	1352	-	-	-	1359
	H5	-	-	1400	-	1384	-	1294
	H6	-	1400	1399	578	1400	-	1349
Technology		-	Pretreatment, acid hydrolysis, and fermentation		Pretreatment, acid hydrolysis, and fermentation		Pretreatment, acid hydrolysis, and fermentation	
Processing capacity of unit 1 (tonne/month)		-	2793	3551	885	2841	-	2841
Processing capacity of unit 2 (tonne/month)		-	-	1999	-	1342	-	1161
Biomass cost ($million /month)		-	0.58	0.93	0.18	0.70	-	0.67
Operating cost ($ million /month)		-	0.16	0.25	0.06	0.24	-	0.23
Investment Cost ($ million)		-	8.71	13.70	7.26	11.40	-	11.40
Total technology cost ($ million/20 yrs)		-	47.70	74.30	22.70	68.50	-	66.10

H3-H6: Harvesting locations, B1: Wood chips, B3: Grain corn, B4: Grain sorghum

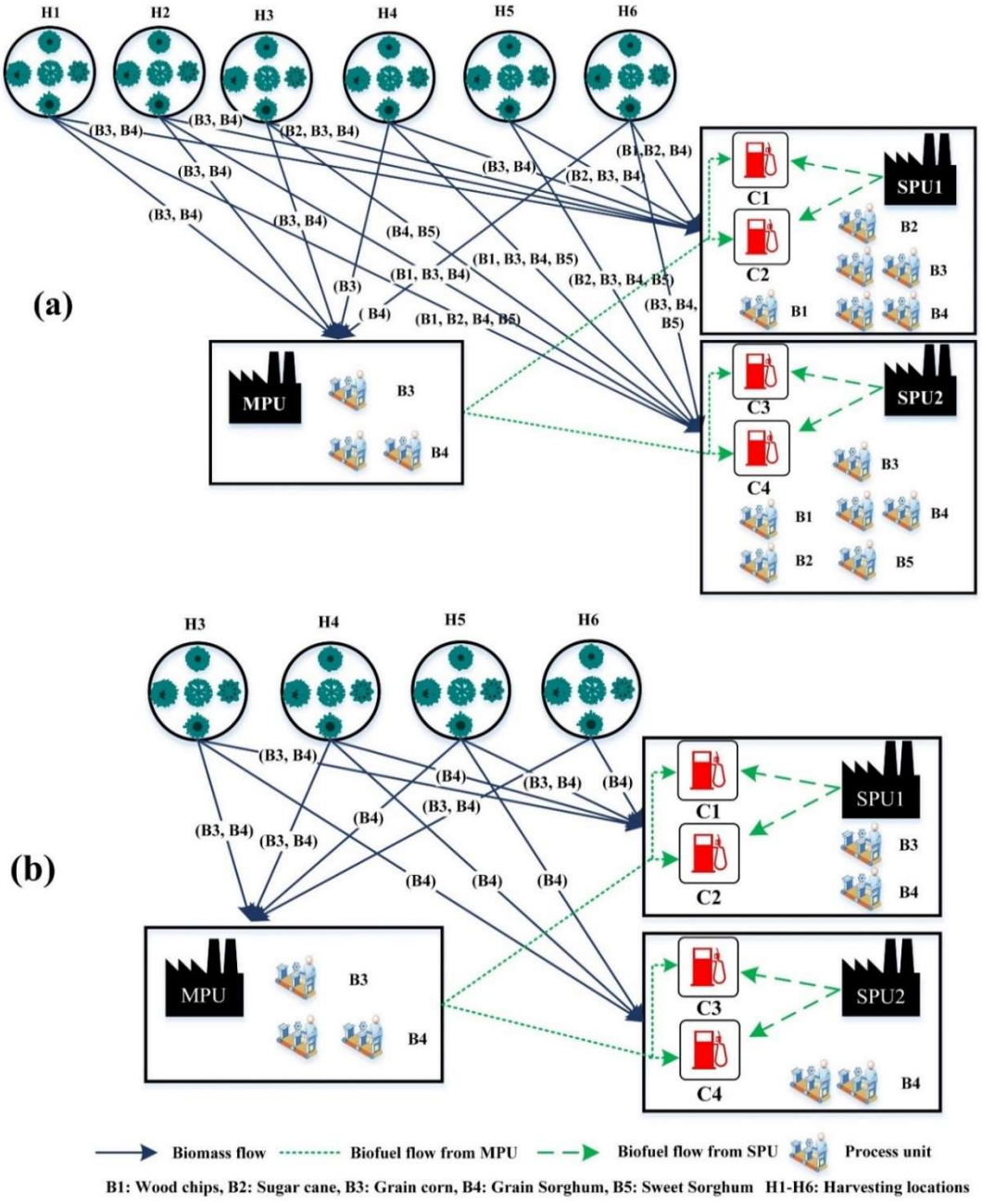

Fig. 3.8 Multi-unit network structure for the (a) initial feasible solution and (b) final solution determined by SPMGTLO

The network representation for the initial feasible solution and the final solution determined by SPMGTLO is shown in Fig. 3.8. The initial feasible solution uses all the harvesting locations, whereas the final solution uses only four harvesting locations for the supply of biomass to the processing units. The initial feasible solution for the multi-unit strategy uses two process units for biomass B4 at all the processing locations and two process units for biomass B3 at SPU1. The solution also uses single process units of the biomass at various processing locations. However, the final multi-unit framework implemented two process units, each for the MPU and SPUs for biomass B4. Biomass B3 is processed at the MPU and SPU1, whereas only biomass B4 is processed at the SPU2. The use of costlier biomass and additional process units for biomass B3 has resulted in a costlier production plan for the initial feasible solution.

3.7. Conclusion

The choice and production capacity of the processing technologies are critical in harnessing maximum economic benefits in the biorefinery supply chain. The restrictions on the capacity of processing technologies often result in a suboptimal production plan that uses less economical technologies to satisfy the demand. This study presented in this chapter has overcome the capacity restriction of processing technologies by proposing an efficient heuristic multi-unit supply chain framework that enables the installation of multiple beneficial process units at the biorefineries. The proposed framework is suitable for solving using metaheuristic techniques and uses novel repair operators to satisfy the domain constraints, mass balance constraints, and capacity constraints.

The effectiveness of the proposed framework is analyzed by solving a case study of distributed biorefinery involving nonlinear cost functions using eight metaheuristic techniques. All the techniques were able to determine feasible solutions for the multi-unit supply chain case study

in every independent run. The approach uses multiple units of processing technologies at the main and secondary processing facilities, increasing the economic gains over the single-unit supply chain. This chapter also studied the relevance of decisions in selecting the best choices at many stages of the biofuel production process, including the selection of feed sources, transportation routes, and technologies. SPMGTLO was able to satisfy the product demand with a minimum total cost, followed by COA with the multi-unit framework. The proposed framework is expected to aid researchers in addressing capacity planning in the supply-chain network of biorefineries and optimizing the model using metaheuristic techniques.

Chapter 4

Multi-unit strategy based mixed-integer linear programming model for biorefinery supply chain network

This chapter proposes a distributed multi-unit MILP supply chain model for biorefineries, which can utilize multiple technological units for each biomass. Firstly, a single-unit superstructure from the literature is improved to accommodate multiple technological choices for different biomass and constraints related to processing capacity and fuel transportation. The single-unit model is extended to a multi-unit model by providing provisions for installing more than one process unit of the selected technology. The proposed model incorporates the investment and operational costs for a biorefinery, and the efficacy of the model is demonstrated in a distributed biorefinery case study.

This chapter is structured as follows: Section 4.1 provides a detailed literature review highlighting the requirement of capacity planning in biorefineries. Section 4.2 details the proposed multi-unit mathematical model for the biorefinery supply chain. Section 4.3 provides the details of the case study employed to analyze the benefits of the multi-unit model of the biorefinery. Section 4.4 analyzes the obtained results and discusses the various inferences. The last section concludes the chapter by summarising the benefits of the proposed multi-unit model.

4.1. Background

The selection of optimal processing technologies is essential in determining the economic sustainability of biorefinery superstructures (Mitkidis et al., 2018; Shahbaz et al., 2020). Biomass processing requires several complex stages that differ depending on the type of biomass and the selected technologies (Mutenure et al., 2018). The efficiency of biomass supply can be improved by using pre-processing, as observed by Shastri et al. (2012). A MILP

model proposed by Potrč et al., (2020) incorporates multiple technologies to synthesize a large-scale biorefinery supply chain network while balancing economic, social, and environmental aspects. The quantity of biofuel produced also depends on the processing capacity of the technology employed and immediately impacts profitability (Ge et al., 2021).

In recent years, the exploration of numerous new technologies and the advancement in the procedures for generating biofuels have gathered more attention than the choice of processing capacity. Biomass to biofuel conversion is carried out using complex technologies, which are often capacity-restricted. Although these restrictions are used to satisfy the design limitations of processing technologies, they often lead to the selection of suboptimal technologies to fulfill the demand. A large capacity biorefinery might possess economics of benefit for the processing cost. However, such refineries are usually located away from the demand locations. The requirements at the demand locations might necessitate the installation of smaller processing units, considering the initial investment cost and periodic transportation cost. Similarly, the inability to process additional biomass using a cheaper technology will lead to the use of other costlier processing options for various demand points of the supply chain. Additionally, the use of processing domains on the chosen technologies often makes it a suboptimal choice to assign multiple process units directly based on the processing requirement.

Many works in the literature use the processing capacity as a decision variable (F. Zhang et al., 2017; J. Zhang et al., 2013); however, the capacity selection is restricted within the feasible range of a single processing unit. Processing technologies are usually associated with a considerable investment cost, and a long-term economic analysis is essential to determine their effect on the operational life of a plant. A profitable biorefinery should ideally be restricted only by resource constraints such as the available technologies, investment budget, or raw materials. However, the restriction on the processing capacity of a selected technology

artificially confines the biorefinery from reaching the true optimal processing capability. Each installed processing technology follows a processing domain to avoid unrealistic plant design, which is proportional to capital and operational costs (El-Halwagi et al., 2013). Such domain restrictions on the biorefineries often lead to suboptimal solutions where the processing of biomass at costlier facilities is selected to fulfill the user demand. In the case of distributed biorefineries, the domain of the processing capacity restricts the maximum utilization of economies of scale (Santibañez-Aguilar et al., 2014). In such scenarios, the superstructure selects processing units with lesser capacity, which are costlier.

This study proposes a multi-unit model for the distributed biorefinery superstructure to address the research gap in capacity planning and its effect on the economy. This chapter has adopted the single unit superstructure from the literature (El-Halwagi et al., 2013) and improved the model to accommodate decisions related to multiple technological choices for different biomass. The single-unit model is extended to a multi-unit model by allowing the installation of multiple processing units of the selected technology. The use of multi-unit strategies in process industries (Chauhan & Kotecha, 2018; Maharana et al., 2022b) is observed to be beneficial; however, these studies lack an analysis approach involving the investment and operational cost of the plant. This study incorporates investment and operational costs for a biorefinery and demonstrates the benefits of the multi-unit model on a distributed biorefinery superstructure.

Nomenclature

Sets

H	Set representing the harvesting sites
T	Set representing the processing technologies available for all processing units
J	Set representing the secondary processing unit
D_j	Set representing the users at secondary location j
I	Set representing the type of biomass
UM	Set of process units available at MPU
US	Set of process units available at SPUs

Indices

d	Index of users corresponding to jth secondary location, $d \in D_j$
h	Index of harvesting sites $h \in H$
i	Index of biomass source $i \in I$
j	Index of secondary location $j \in J$
t	Index of processing technologies $t \in T$
um	Index of process units in MPU $um \in UM$
us	Index of process units in SPUs $us \in US$

Parameters

$\alpha_{i,t}$	Conversion factor for biomass i using technology t
$A_{h,i}$	Total availability of biomass i at the harvesting site h
BFT_{Cost}	Biofuel transportation cost
BM_{Cost}	Biomass purchase cost
BMP_{Cost}	Biomass processing cost
BMT_{Cost}	Biomass transportation cost
HY	Total operational life of the biorefinery superstructure
I_{Cost}^{MPU}	Investment cost at MPU
I_{Cost}^{SPU}	Investment cost at SPU
$IC_{i,t}^{Main\_Fix}$	Fixed cost component of investment cost to process biomass i using technology t at MPU
$IC_{i,t}^{Main\_Var}$	Variable cost component of investment cost to process biomass i using technology t at MPU

$IC_{i,t}^{Sec\_Fix}$	Fixed cost component of investment cost to process biomass *i* using technology *t* at SPU
$IC_{i,t}^{Sec\_Var}$	Variable cost component of investment cost to process biomass *t* using technology *t* at SPU
$MPL_{i,t}^{Main \to Proc}$	Lower capacity limit for processing biomass *i* using technology *t* at MPU
$MPU_{i,t}^{Main \to Proc}$	Upper capacity limit for processing biomass *i* using technology *t* at MPU
$MPL_{i,t}^{Sec \to Proc}$	Lower capacity limit for processing biomass *i* using technology *t* at SPU
$MPU_{i,t}^{Sec \to Proc}$	Upper capacity limit for processing biomass *i* using technology *t* at SPU
$PC_{i,t}^{Main}$	Unit operational cost for biomass *i* using technology *t* at the MPU
$PC_{i,t}^{Sec}$	Unit operational cost for biomass *i* using technology *t* at the SPU
PTC_{j}^{Main}	Unit transportation cost of biofuel from MPU to SPU *j*
$PTL_{Min}^{Main \to Sec}$	Minimum flow domain of biofuel transported from MPU to SPUs
$PTL_{Max}^{Main \to Sec}$	Maximum flow domain of biofuel transported from MPU to SPUs
RC_{i}^{Main}	Unit purchase cost of biomass *i* at the MPU
RC_{i}^{Sec}	Unit purchase cost of biomass *i* at SPUs
$RTC_{h,i}^{Main}$	Unit transportation cost of biomass *i* from harvesting site *h* to MPU
$RTC_{h,i,j}^{Sec}$	Unit transportation cost of biomass *i* from harvesting site *h* to SPU *j*
$RTL_{h,i}^{Harv \to Main}$	Lower transportation limit of biomass *i* from harvesting site *h* to MPU
$RTL_{h,i,j}^{Harv \to Sec}$	Lower transportation limit of biomass *i* from harvesting site *h* to SPU *j*
$RTU_{h,i}^{Harv \to Main}$	Upper transportation limit of biomass *i* from harvesting site *h* to MPU
$RTU_{h,i,j}^{Harv \to Sec}$	Upper transportation limit of biomass *i* from harvesting site *h* to SPU *j*
TLC	Total lifecycle cost
$Z_{j,d}$	Demand of the user *d* located at SPU *j*

Decision variables

$F_{h,i}^{Harv \to Main}$	Flow rate of biomass *i* from the harvesting site *h* to the MPU
$F_{h,i,j}^{Harv \to Sec}$	Flow rate of biomass *i* from the harvesting site *h* to the SPU *j*
$F_{i,t}^{Main \to Proc}$	Flow rate of biomass *i* sent for processing at MPU using technology *t*
$F_{um,i,t}^{Main \to Proc}$	Flow rate of biomass *i* sent for processing at MPU using technology *t* at process unit *um*
$F_{i,j,t}^{Sec \to Proc}$	Flow rate of biomass *i* sent for processing at SPU *j* using technology *t*

$F^{Sec\rightarrow Proc}_{us,i,t,j}$	Flow rate of biomass *i* sent for processing at SPU *j* using technology *I* at process unit *us*
$Y^{Harv\rightarrow Main}_{h,i}$	Binary variable whose value is 1, if the biomass *i* transported from harvesting site *h* to MPU
$Y^{Harv\rightarrow Sec}_{h,i,j}$	Binary variable whose value is 1, if the biomass *i* transported from harvesting site *h* to SPU *j*
$Y^{Main\rightarrow Proc}_{i,t}$	Binary variable whose value is 1, if the biomass *i* is processed in MPU using a process unit with technology *t*
$Y^{Main\rightarrow Proc}_{um,i,t}$	Binary variable whose value is 1, if the biomass *i* is processed in MPU using the process unit *um* with technology *t*
$Y^{Main\rightarrow Tec}_{i,t}$	Binary variable whose value is one if the biomass *i* is processed using technology *t* in MPU
$Y^{Sec\rightarrow Proc}_{i,j,t}$	Binary variable whose value is 1, if the biomass *i* is processed in SPU *j* using a process unit with technology *t*
$Y^{Sec\rightarrow Proc}_{us,i,j,t}$	Binary variable whose value is 1, if the biomass *i* is processed in SPU *j* using the process unit *us* with technology *t*
$YF^{Main\rightarrow Sec}_{j}$	Binary variable whose value is 1 if biofuel is transported from the MPU to SPU *j*
$U^{Main}_{j,d}$	Biofuel provided by MPU to satisfy demand *d* of user located at SPU *j*
$U^{Sec}_{j,d}$	Biofuel provided by SPU *j* to satisfy the demand *d* of user

4.2. Proposed mathematical formulation of the multi-unit model

The problem statement for the biorefinery supply-chain network is adapted from Chapter 2 with linear approximations for the investment cost calculations for the MPU and SPUs (El-Halwagi et al., 2013). The model constitutes a set of *H* harvesting sites that supply *I* types of biomass to the processing units using various means of transport. The processing units comprise one MPU and a set of *J* SPUs distributed across various locations. Each SPU has D_j nearby users whose demands have to be satisfied using the biofuel from MPU and the j^{th} SPU. A set of *T* processing technologies is available for all processing units to convert the raw materials into the final product. *UM* and *US* units are available for each processing technology in the MPU and SPUs, respectively. The details of balances and applicable constraints are provided as follows. The system structure of the multi-unit biorefinery model can inferred from Fig 3.1 given in Chapter 3.

4.2.1. Balances at the harvesting locations

The availability of biomass at harvesting sites depends on various factors such as geographical location, seasonality, farm size, etc. The resource limitation at the harvesting sites restricts the total biomass supplied to the processing hubs. Hence, the supply of biomass (*i*) from the harvesting site (*h*) to the MPU ($F_{h,i}^{Harv\to Main}$) and the j^{th} SPU ($F_{h,i,j}^{Harv\to Sec}$) should not exceed the total availability ($A_{h,i}$) as in Equation (4.1) (El-Halwagi et al., 2013).

$$F_{h,i}^{Harv\to Main}+\sum_{j\in J}F_{h,i,j}^{Harv\to Sec}\le A_{h,i},\qquad \forall h\in H, i\in I \tag{4.1}$$

The upper and lower flow limits on the flow rate restrict the transportation of biomass from the harvesting sites to the processing hubs within a finite domain. The domain constraints on the

flow rate for the MPU and SPUs are given in Equation (4.2) and Equation (4.3) , respectively (El-Halwagi et al., 2013). Here, the terms $RTL_{h,i}^{Harv\rightarrow Main}$ and $RTU_{h,i}^{Harv\rightarrow Main}$ represent the lower and upper transportation limits of biomass (i) from the harvesting sites (h). Similarly, the terms $RTL_{h,i,j}^{Harv\rightarrow Sec}$ and $RTU_{h,i,j}^{Harv\rightarrow Sec}$ indicate the lower and upper limits of biomass flow from harvesting sites to the SPUs.

$$Y_{h,i}^{Harv\rightarrow Main} RTL_{h,i}^{Harv\rightarrow Main} \le F_{h,i}^{Harv\rightarrow Main} \le Y_{h,i}^{Harv\rightarrow Main} RTU_{h,i}^{Harv\rightarrow Main}, \forall\ i\in I, h\in H \qquad (4.2)$$

$$Y_{h,i,j}^{Harv\rightarrow Sec} RTL_{h,i,j}^{Harv\rightarrow Sec} \le F_{h,i,j}^{Harv\rightarrow Sec} \le Y_{h,i,j}^{Harv\rightarrow Sec} RTU_{h,i,j}^{Harv\rightarrow Sec}, \forall h\in H, i\in I, j\in J \qquad (4.3)$$

Here $Y_{h,i}^{Harv\rightarrow Main}$ is the binary variable whose value is one if the biomass i is transported from harvesting site h to MPU; otherwise, it takes a value of zero. Similarly, the binary variable $Y_{h,i,j}^{Harv\rightarrow Sec}$ takes a value of one when the biomass i is transported from the harvesting site h to the secondary processing unit j.

4.2.2. Balances at the main processing unit

The total biomass received at the MPU from different harvesting sites is sent for processing and is given in Equation (4.4).

$$\sum_{t\in T_i} F_{i,t}^{Main\rightarrow Proc} = \sum_{h\in H} F_{h,i}^{Harv\rightarrow Main}, \quad \forall i\in I \qquad (4.4)$$

The biomass (i) is converted into biofuel using one of the suitable technologies (t), as shown in Equation (4.5). The term $\alpha_{i,t}$ represents the conversion factor for i^{th} biomass using t^{th} technology. The available biomass is processed by using any one of the available technologies. The corresponding unique process constraint is represented using the Equation (4.6) .

$$\sum_{i\in I}\sum_{t\in T_i} F_{i,t}^{Main\to Proc}\alpha_{i,t} = \sum_{j\in J}\sum_{d\in D_j} U_{j,d}^{Main} \tag{4.5}$$

$$\sum_{t\in T_i} Y_{i,t}^{Main\to Proc} \le 1,\ \forall i\in I \tag{4.6}$$

The variable $U_{j,d}^{Main}$ indicates the biofuel provided by MPU to satisfy the demand d of a user located at SPU j. The value of the binary variable becomes one if the biomass i is processed in MPU uses a process unit of technology. Each selected technology at the MPU has a capacity restriction, where biomass processing can only be performed between the lower and upper processing capacities, as in Equation (4.7) (El-Halwagi et al., 2013).

$$Y_{i,t}^{Main\to Proc} MPL_{i,t}^{Main\to Proc} \le F_{i,t}^{Main\to Proc} \le Y_{i,t}^{Main\to Proc} MPU_{i,t}^{Main\to Proc},\ \forall t\in T_i, i\in I \tag{4.7}$$

The Equations (4.4) – (4.6) represent the constraints at the MPU for the single-unit model where only one process unit of the selected technologies is implemented. The multi-unit model allows for the implementation of additional process units to increase the economical processing of biomass, which is given in Equations (4.8) – (4.10). Here, each selected technology can use multiple process units from the available *UM* units, where the upper and lower processing capacity limits the processing at each *um* unit. The variable $F_{um,i,t}^{Main\to Proc}$ represents the flow rate of biomass *i* sent for processing at MPU using technology *t* at process unit *um*. $Y_{um,i,t}^{Main\to Proc}$ is the binary decision variable that takes a value of one when the biomass *i* is processed in MPU using the process unit *um* with technology *t*.

$$\sum_{um\in UM}\sum_{t\in T_i} F_{um,i,t}^{Main\to Proc} = \sum_{h\in H} F_{h,i}^{Harv\to Main},\quad \forall i\in I \tag{4.8}$$

$$\sum_{um\in UM}\sum_{i\in I}\sum_{t\in T_i} F_{um,i,t}^{Main\to Proc}\alpha_{i,t} = \sum_{j\in J}\sum_{d\in D_j} U_{j,d}^{Main} \tag{4.9}$$

$$Y_{um,i,t}^{Main\to Proc} MPL_{i,t}^{Main\to Proc} \le F_{um,i,t}^{Main\to Proc} \le Y_{um,i,t}^{Main\to Proc} MPU_{i,t}^{Main\to Proc}, \forall t\in T_i, i\in I, um\in UM \tag{4.10}$$

In the multi-unit model, the unique process constraint for the MPU is realized using Equations (4.11) – (4.13). In Equations (4.11) and (4.12), the variable $Y_{i,t}^{Main\to Tec}$ assumes a value of 1 if any of the process units corresponding to the t^{th} technology and i^{th} biomass is selected. The variable $Y_{i,t}^{Main\to Tec}$ uses Equation (4.13) to restrict the process selection variable $Y_{um,i,t}^{Main\to Proc}$ to satisfy the unique process constraint.

$$Y_{um,i,t}^{Main\to Proc} \le Y_{i,t}^{Main\to Tec} \quad \forall um\in UM, i\in I, t\in T_i \tag{4.11}$$

$$Y_{i,t}^{Main\to Tec} \le \sum_{um\in UM} Y_{um,i,t}^{Main\to Proc}, \forall i\in I, t\in T_i \tag{4.12}$$

$$\sum_{t\in T_i} Y_{i,t}^{Main\to Tec} \le 1, \ \forall i\in I \tag{4.13}$$

4.2.3. Balances at the secondary processing units

Similar to the MPU, the total biomass received at the SPUs is sent for processing using the available technologies and is given in Equation (4.14) where the term $F_{i,j,t}^{Sec\to Proc}$ represents the flow rate of biomass *i* sent for processing at SPU *j* using technology *t*.

$$\sum_{t\in T_i} F_{i,j,t}^{Sec\to Proc} = \sum_{h\in H} F_{h,i,j}^{Harv\to Sec}, \quad \forall i\in I, j\in J \tag{4.14}$$

SPUs use an appropriate technology to process the biomass, and the corresponding quantity of biofuel produced is determined using a technology-dependent conversion factor $\alpha_{i,t}$. The biomass (*i*) is converted into biofuel using one of the suitable technologies (*t*) in the secondary processing unit (*j*), as shown in Equation (4.15). SPUs are also restricted by the unique process constraint where each biomass can be processed using only one of the available technologies as given in Equation (4.16) where the binary variable $Y_{i,j,t}^{Sec\to Proc}$ takes a value of one, if the biomass *i* is processed in SPU *j* using a process unit with technology *t* .

$$\sum_{i\in I}\sum_{t\in T_i} F_{i,j,t}^{Sec\to Proc}\alpha_{i,t} = \sum_{d\in D_j} U_{j,d}^{Sec}, \quad \forall j\in J \tag{4.15}$$

$$\sum_{t\in T_i} Y_{i,j,t}^{Sec\to Proc} \le 1, \ \forall i\in I, j\in J \tag{4.16}$$

The processing of biomass at the SPUs is limited by the capacity domain of the selected technology, which permits the process units to be operational between lower and upper capacity. The processing capacity constraint applicable to all SPUs is given in the Equation (4.17), where $MPU_{i,t}^{Sec\to Proc}$ and $MPL_{i,t}^{Sec\to Proc}$ represent the upper and lower capacity limit of the t^{th} technology of i^{th} biomass at j^{th} SPU (El-Halwagi et al., 2013).

$$Y_{i,t}^{Sec\to Proc} MPL_{i,t}^{Sec\to Proc} \le F_{i,j,t}^{Sec\to Proc} \le Y_{i,t}^{Sec\to Proc} MPU_{i,t}^{Sec\to Proc}, \ \forall t\in T_i, i\in I, j\in J \tag{4.17}$$

In the multi-unit model, SPUs implement multiple process units of the selected technologies. The constraints given in the Equations (4.14) – (4.17) represent the associated constraints in the single-unit model. The use of *us* process units in the SPUs changes the balance equations for biomass processing, which are represented in Equations (4.18) and (4.19). The term $F_{us,i,tj}^{Sec\to Proc}$ represents the flow rate of biomass *i* sent for processing at SPU *j* using technology *t* at process unit *us*.

$$\sum_{h\in H} F_{h,i,j}^{Harv\to Sec} = \sum_{us\in US}\sum_{t\in T_i} F_{i,j,t}^{Sec\to Proc}, \quad \forall i\in I, j\in J \tag{4.18}$$

$$\sum_{us\in US}\sum_{i\in I}\sum_{t\in T_i} F_{us,i,t,j}^{Sec\to Proc}\alpha_{i,t} = \sum_{d\in D_j} U_{j,d}^{Sec}, \quad \forall j\in J \tag{4.19}$$

In the multi-unit model, the domain constraints on the capacity corresponding to each installed process unit of the technology are given in Equation (4.20). The binary variable $Y_{us,i,t}^{Sec\to Proc}$ whose value is 1, if the biomass *i* is processed in SPU *j* using the process unit *us* with technology *t*.

$$Y_{us,i,t}^{Sec\to Proc} MPL_{i,t}^{Sec\to Proc} \le F_{us,i,j,t}^{Sec\to Proc} \le Y_{us,i,t}^{Sec\to Proc} MPU_{i,t}^{Sec\to Proc}, \ \forall us \in US, i \in I, t \in T_i \quad (4.20)$$

The unique process constraints for the SPUs in the multi-unit model are realized using Equations (4.21) – (4.23). Here, the variable $Y_{us,i,j,t}^{Sec\to Proc}$ takes a value of 1, if the process unit *us*, corresponding to i^{th} biomass at the j^{th} SPU installs the t^{th} technology. The binary variable $Y_{i,j,t}^{Sec\to Tec}$ whose value is one if the biomass *i* is processed in SPU *j* using technology *t*.

$$Y_{us,i,j,t}^{Sec\to Proc} \le Y_{i,j,t}^{Sec\to Tec} \quad \forall us \in US, i \in I, j \in J, t \in T_i \quad (4.21)$$

$$Y_{i,j,t}^{Sec\to Tec} \le \sum_{us \in US} Y_{us,i,j,t}^{Sec\to Proc}, \forall i \in I, j \in J, t \in T_i \quad (4.22)$$

$$\sum_{t \in T_i} Y_{i,j,t}^{Sec\to Tec} \le 1, \ \forall j \in J, i \in I \quad (4.23)$$

The demand of the users ($Z_{j,d}$) is satisfied by using the biofuel produced by the MPU ($U_{j,d}^{Main}$) and the corresponding SPU ($U_{j,d}^{Sec}$). Each SPU can provide biofuel to the nearby users, whereas all the users can receive the biofuel from the MPU. The demand constraints of the superstructure are required to satisfy the demand of each user and is represented in Equation (4.24).

$$U_{j,d}^{Main} + U_{j,d}^{Sec} \ge Z_{j,d} \quad \forall d \in D_j, j \in J \quad (4.24)$$

Users are assumed to be near the SPUs and thus do not have any domain constraint on their flow rate. However, the biofuel transported from the MPU to each SPU is restricted by the flow domain, represented by a minimum ($PTL_{Min}^{Main\to Sec}$) and maximum ($PTL_{Max}^{Main\to Sec}$) biofuel flow rate, which is given in the Equation (4.25). The variable $YF_j^{Main\to Sec}$ is a binary variable and assumes a value of 1 if the biofuel is transported from the MPU to the j^{th} SPU.

$$YF_j^{Main\to Sec} PTL_{Min}^{Main\to Sec} \le \sum_{d \in D_j} U_{j,d}^{Main} \le YF_j^{Main\to Sec} PTL_{Max}^{Main\to Sec}, \quad \forall j \in J \quad (4.25)$$

4.2.4. Objective: Minimize total cost

The objective of the model is to identify an optimal solution with minimum total cost while satisfying the user demands. The objective function constitutes various cost components related to the harvesting sites, processing units, and user locations. The purchase cost of biomass is determined by multiplying its per unit cost (RC_i^{Main} and RC_i^{Sec}) with the amount procured from the harvesting site, which is given in the Equation (4.26) (El-Halwagi et al., 2013).

$$BM_{Cost} = \sum_{h\in H}\sum_{i\in I} F_{h,i}^{Harv\rightarrow Main} RC_i^{Main} + \sum_{h\in H}\sum_{i\in I}\sum_{j\in J} F_{h,i,j}^{Harv\rightarrow Sec} RC_i^{Sec} \tag{4.26}$$

The various costs associated with the MPU and SPUs constitute the periodic operational cost and a one-time investment cost. The processing cost of biomass is directly proportional to the quantity of biomass processed using multiple process units of the technologies at the MPU and SPUs, as in the Equation (4.27). The terms $PC_{i,t}^{Main}$ and $PC_{i,t}^{Sec}$ represent the unit operational cost for i^{th} biomass using t^{th} technology at the MPU and SPU, respectively.

$$BMP_{Cost} = \sum_{um\in UM}\sum_{i\in I}\sum_{t\in T_i} F_{um,i,t}^{Main\rightarrow Proc} PC_{i,t}^{Main} + \sum_{us\in US}\sum_{i\in I}\sum_{j\in J}\sum_{t\in T_i} F_{us,i,j,t}^{Sec\rightarrow Proc} PC_{i,t}^{Sec} \tag{4.27}$$

The investment cost at MPU (I_{Cost}^{MPU}) and SPUs (I_{Cost}^{SPU}) is determined based on the installed capacity of the process unit and is given in the Equation (4.28) and Equation (4.29), respectively. Here, the investment cost consists of a fixed cost component ($IC_{i,t}^{Sec\_Fix}$ and $IC_{i,t}^{Main\_Fix}$) and a capacity-based variable component ($IC_{i,t}^{Sec\_Var}$ and $IC_{i,t}^{Main\_Var}$). In the Equation (4.28) and Equation (4.29), the binary variables $Y_{us,i,j,t}^{Sec\rightarrow Proc}$ and $Y_{um,i,t}^{Main\rightarrow Proc}$ ensure the consideration of the investment cost for the implemented process units in the MPU and SPUs, respectively. In the absence of a process unit (*us* or *um*), the corresponding variable

representing its implementation takes a value of zero, and thus the investment cost of that process unit is not considered.

$$I_{Cost}^{MPU} = \sum_{um \in UM} \sum_{i \in I} \sum_{t \in T_i} \left(Y_{um,i,t}^{Main \rightarrow Proc} IC_{i,t}^{Main\_Fix} + F_{um,i,t}^{Main \rightarrow Proc} IC_{i,t}^{Main\_Var} \right) \tag{4.28}$$

$$I_{Cost}^{SPU} = \sum_{us \in US} \sum_{i \in I} \sum_{j \in J} \sum_{t \in T_i} \left(Y_{us,i,j,t}^{Sec \rightarrow Proc} IC_{i,t}^{Sec\_Fix} + F_{us,i,j,t}^{Sec \rightarrow Proc} IC_{i,t}^{Sec\_Var} \right) \tag{4.29}$$

The cost corresponding to the transportation of biomass and biofuel is given in Equation (4.30) and Equation (4.31) (El-Halwagi et al., 2013). The biomass transportation cost is directly proportional to the quantity of biomass transported to the MPU and SPU, where the unit transportation cost ($RTC_{h,i,j}^{Sec}$ and $RTC_{h,i}^{Main}$) depends on the type of biomass and the distance between the harvesting site and the processing unit.

$$BMT_{Cost} = \sum_{h \in H} \sum_{i \in I} F_{h,i}^{Harv \rightarrow Main} RTC_{h,i}^{Main} + \sum_{h \in H} \sum_{i \in I} \sum_{j \in J} F_{h,i,j}^{Harv \rightarrow Sec} RTC_{h,i,j}^{Sec} \tag{4.30}$$

$$BFT_{Cost} = \sum_{j \in J} \sum_{d \in D_j} U_{j,d}^{Main} PTC_{j}^{Main} \tag{4.31}$$

The biofuel transportation cost is determined only for the biofuel supplied from the MPU to the users available at the SPUs. It is determined using the quantity of biofuel transported and per unit transportation cost (PTC_{j}^{Main}) between the MPU and the SPUs. The users are located near the SPUs and can directly access the biofuel from the SPUs. Hence, there is no fuel transportation cost for the SPUs. The total cost constitutes the biomass procurement cost, investment and operational cost of the process units, and the transportation cost of the biomass and the biofuel to the required hubs. The objective function is given in Equation (4.32). The parameter *HY* represents the total operational life of the superstructure, which is multiplied by the periodic operational costs, whereas the cost related to the installation of the required process

units of the technology in both MPU and SPUs constitute the investment cost that is considered only once.

$$TLC = HY\left(BM_{Cost} + BMP_{Cost} + BMT_{Cost} + BFT_{Cost}\right) + I_{Cost}^{MPU} + I_{Cost}^{SPU} \quad (4.32)$$

4.3. Case study

The proposed multi-unit model is demonstrated in a case study of biofuel production in Mexico, adapted from the literature (Maharana et al., 2022a; Ponce-Ortega & Santibañez-Aguilar, 2019). The case study is similar to the case study discussed in Chapter 2 and Chapter 3 with linear approximations for the investment cost calculation. The details related to various parameters, such as conversion factors, biomass procurement cost, transportation cost, processing cost, investment cost, and product demand, are provided in Appendix C. The model was implemented using IBM ILOG CPLEX optimization studio software and solved using the CPLEX solver. The single-unit model has 701 constraints, 137 binary variables, and 143 continuous variables, whereas the multi-unit model has 1061 constraints, 272 binary variables, and 233 continuous variables, considering the availability of three process units per technology.

4.4. Results and discussion

This section analyzes the results obtained on optimizing the single and multi-unit models. The discussion focuses on the benefits of the proposed multi-unit model over the single-unit model using a rigorous solution analysis approach.

4.4.1. Optimal solution analysis

The detailed production planning for the single and multi-unit models highlighting the procurement and processing schemes are given in Table 4.1. In the single-unit model, MPU and SPU 1 have used the maximum possible processing of the grain sorghum using one process

unit each. In the multi-unit model, the processing of grain sorghum at the MPU and SPU 1 has increased by implementing two process units of the technology. The availability of cheaper biofuel at the SPU 1 using grain sorghum led to less of a requirement for woodchips, which are transferred to the MPU. It has to be noted that the availability of wood chips at the harvesting site H5 is limited, and it was selected to be processed only at SPU 1 in the single-unit model.

In the multi-unit model, a reduction in the processing of biomass in SPU 2 is observed as the demand is majorly satisfied by the MPU, considering the economies of scale. In the multi-unit model, the total processing of woodchips and grain sorghum in MPU increased, helping to satisfy user demands without using grain corn, which was considered a raw material in the single-unit model. The superstructures representing the optimal solution determined using the single and multi-unit models are shown in Fig. 4.1. In both the models, MPU and SPU 1 have used four harvesting locations to procure biomass, whereas, in SPU 2, the biomass has been procured only from two harvesting locations. The restriction in the capacity of process units of the technologies in the single-unit model led to the procurement of biomass from three harvesting locations.

Also, the capacity restriction requires the MPU to process a costlier production route using corn to satisfy the user demand. In the multi-unit model, the MPU used multiple units to process large volumes of biomass. On considering the biofuel production from grain sorghum, MPU has procured additional biomass from H3 apart from the harvesting sites selected in the single unit model and employed two process units. The use of multiple process units is also observed to change the optimal processing routes for producing biofuel using wood chips. In the single-unit model, SPU 1 procured woodchips from H3, H4, and H5, whereas the multi-unit model selected only the harvesting site H3 for the procurement. The multi-unit model also changes the optimal distribution profile of the single-unit model.

Table 4.1 Biomass procurement and processing schemes for the single unit and multi-unit model (tonne/month)

		Single unit model						Multi-unit model						
		H3	H4	H5	H6	Process unit 1 capacity	Technology	H3	H4	H5	H6	Process unit 1 capacity	Process unit 2 capacity	Technology
MPU	Wood chips	1400	1400	-	779	3579	Gasification and Biosynthesis	1400	1400	779	779	4358		Gasification and Biosynthesis
	Grain corn	-	257	-	1400	1657	Pretreatment, acid hydrolysis and fermentation	-	-	-	-	-	-	-
	Grain sorghum	-	1400	751	1400	3551	Pretreatment, acid hydrolysis and fermentation	1322	1400	1400	1400	3551	1971	Pretreatment, acid hydrolysis and fermentation
SPU 1	Wood chips	1400	377	779	-	2556	Gasification and Biosynthesis	1400	-	-	-	1400	-	Gasification and Biosynthesis
	Grain sorghum	1301	-	1400	140	2841	Pretreatment, acid hydrolysis and fermentation	1400	-	1400	1052	2841	1012	Pretreatment, acid hydrolysis and fermentation
SPU 2	Wood chips	-	1400	-	-	1400	Gasification and Biosynthesis	-	1400	-	-	1400	-	Gasification and Biosynthesis
	Grain sorghum	-	1400	1400	-	2800	Pretreatment, acid hydrolysis and fermentation	-	1400	486.96	-	1886.96	-	Pretreatment, acid hydrolysis and fermentation

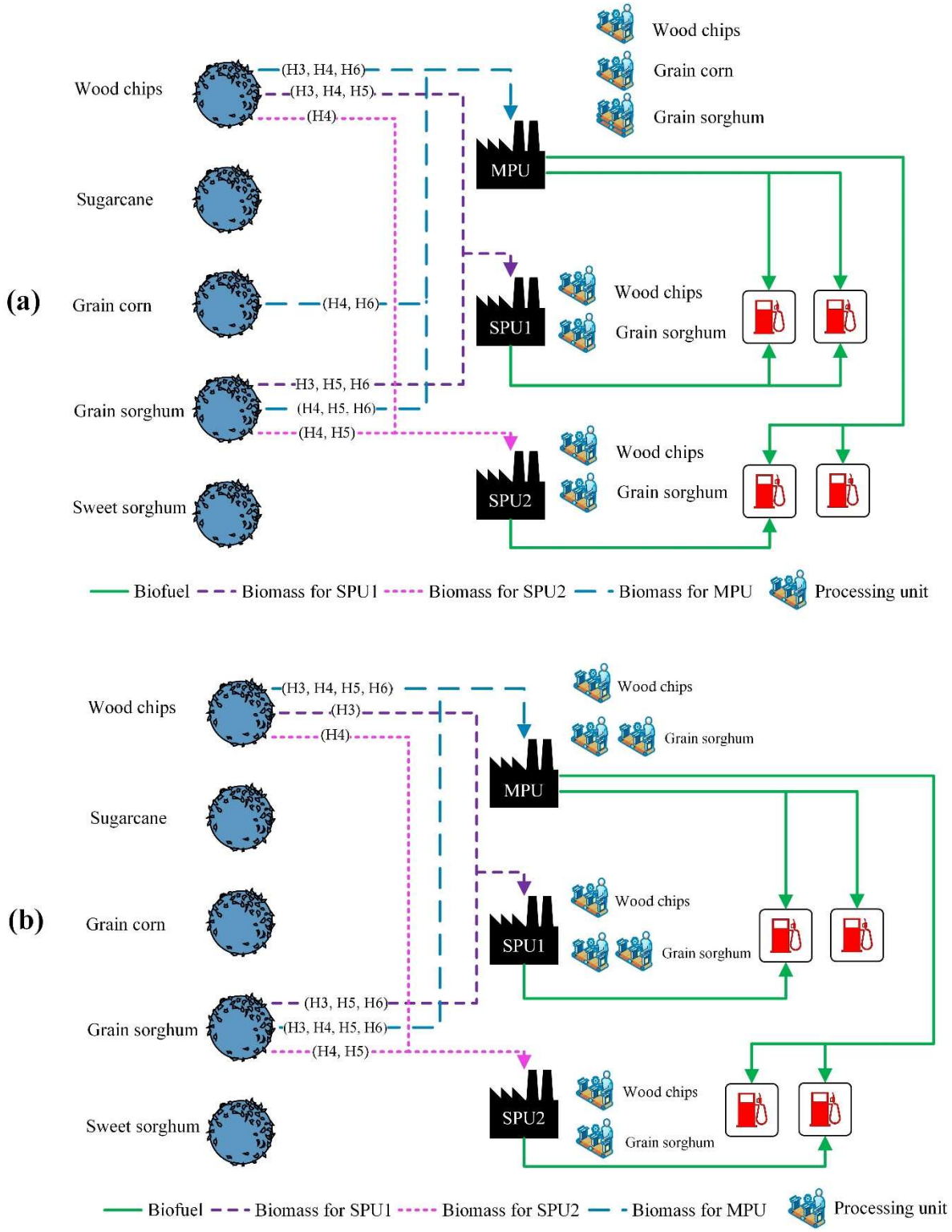

Fig. 4.1 Optimal solution of (a) single unit model and (b) proposed multi-unit model

In the single-unit model, the limited production at the MPU was mainly used to satisfy the demand of users at SPU 2. However, in the multi-unit model, the MPU provided biofuel to all the users at SPU 1 and SPU 2. In the multi-unit model, SPU 1 provided biofuel to user 1, and SPU2 to user 2 instead of user 1, as in the case of the single-unit model.

4.4.2. Impact of the multi-unit model on the operation of processing hubs

The multi-unit model provided benefits in making economic operational decisions at various processing hubs. Fig. 4.2 shows the contribution of processing hubs to the supply chain in terms of processing capacity, investment cost, and operational cost for single and multi-unit models. The single-unit model uses the MPU to process maximum biomass and gain economies of scale. Thus, the investment and operational costs of the MPU are higher compared to the SPUs. The restriction of allowing single process units led to similar investment costs at both SPUs. However, the quantity of biomass processed and the corresponding operational cost at SPU 1 is higher, inferring the processing at the SPU 2 is costlier to satisfy the demand.

The multi-unit model helped to increase the processing at the MPUs and enabled the maximum utilization of economies of scale, as the processing of biomass at the MPU is cheaper due to their capability to process high volumes of biomass. The solution obtained using the multi-unit model reduced the investment cost from 27% to 25% and the operational cost from 24% to 19% of SPU 2 towards the complete supply chain. These benefits validated the effectiveness of the multi-unit model in providing better decisions in selecting and processing biomass with appropriate technology units. Although MPU processed a higher biomass quantity, the investment cost contribution has been reduced. The solution obtained using the multi-unit model reduced the investment cost from 27% to 25% and the operational cost from 24% to 19% of SPU 2 towards the complete supply chain.

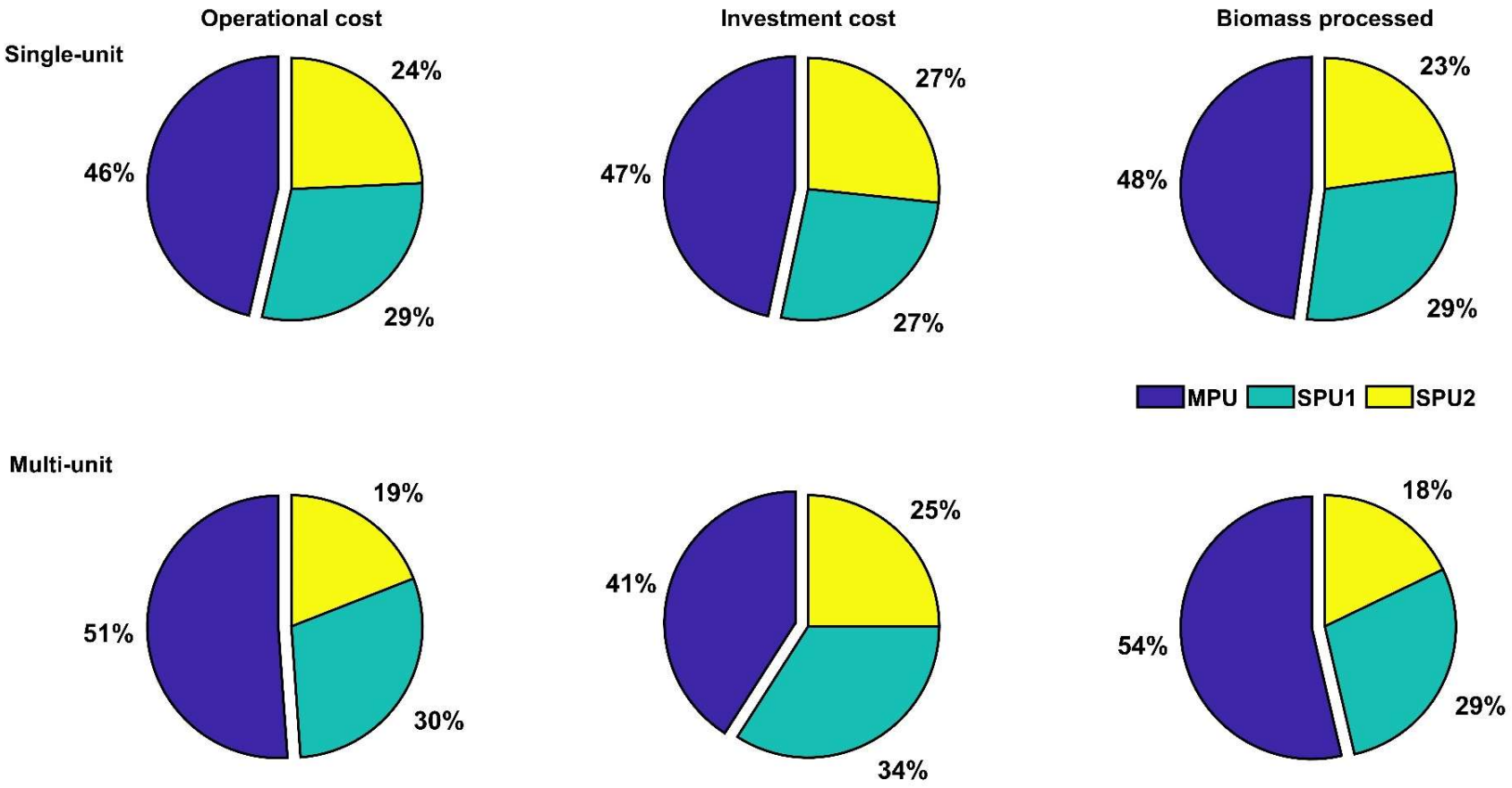

Fig. 4.2 Distribution of costs and biomass processing for the single and multi-unit models

These benefits validated the effectiveness of the multi-unit model in providing better decisions in selecting and processing biomass with appropriate technology units. Although MPU processed a higher biomass quantity, the investment cost contribution has been reduced. Such a scenario requires further investigation in the decisions of process unit selection and is given in the next section.

The single-unit model allows only single process units of the selected technology at the MPU and SPUs. The processing of biomass at the hubs and the product delivery from each hub to the users are shown in Fig. 4.3. Each processing hub used full-capacity units for sorghum grain. The MPU processes wood chips, corn, and sorghum grain, whereas each SPU processes sorghum grain and wood chips to produce ethanol. The demand at the SPUs is satisfied by the ethanol produced from MPU and the corresponding SPU. Among the users, the demand of the second user is satisfied using only the nearby SPU, whereas, for the fourth user, the total demand is satisfied with the ethanol delivered from the MPU.

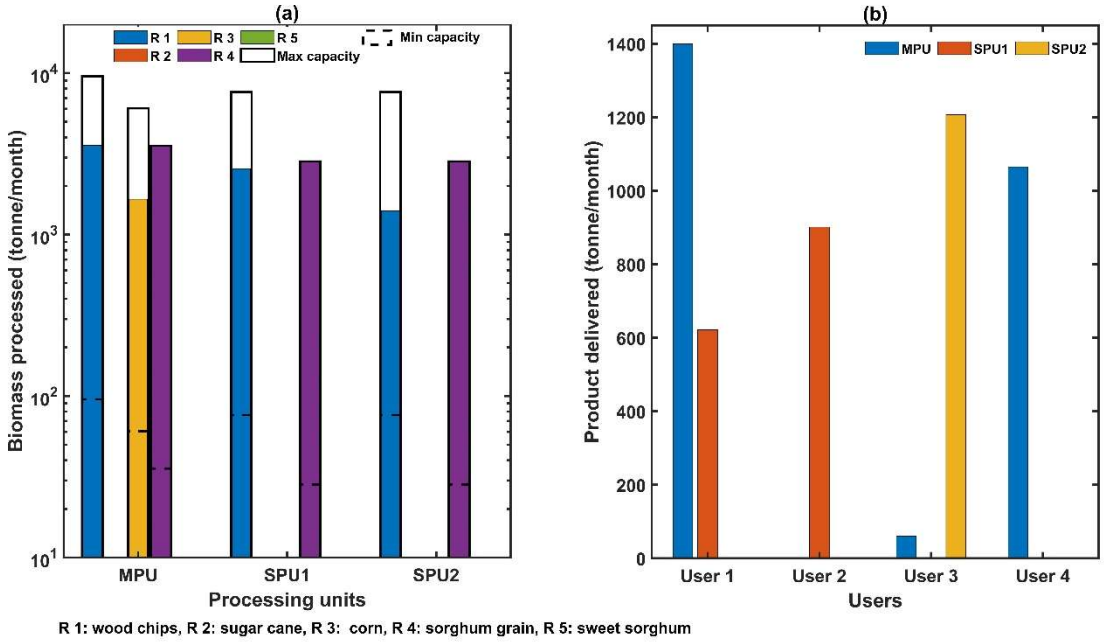

Fig. 4.3 Optimal decisions of single-unit model corresponding to the processing hubs for (a) biomass processed and (b) product delivery to each user

The biomass processed at each processing hub based on the optimal solution of the multi-unit model is provided in Fig. 4.4. The capacity restriction for the single-unit model led to the implementation of a single full-capacity process unit at the MPU and SPUs for sorghum grain (Fig. 4.3). However, as per the optimal solution of the multi-unit model, two process units are installed for the sorghum grain at the MPU and SPU1.

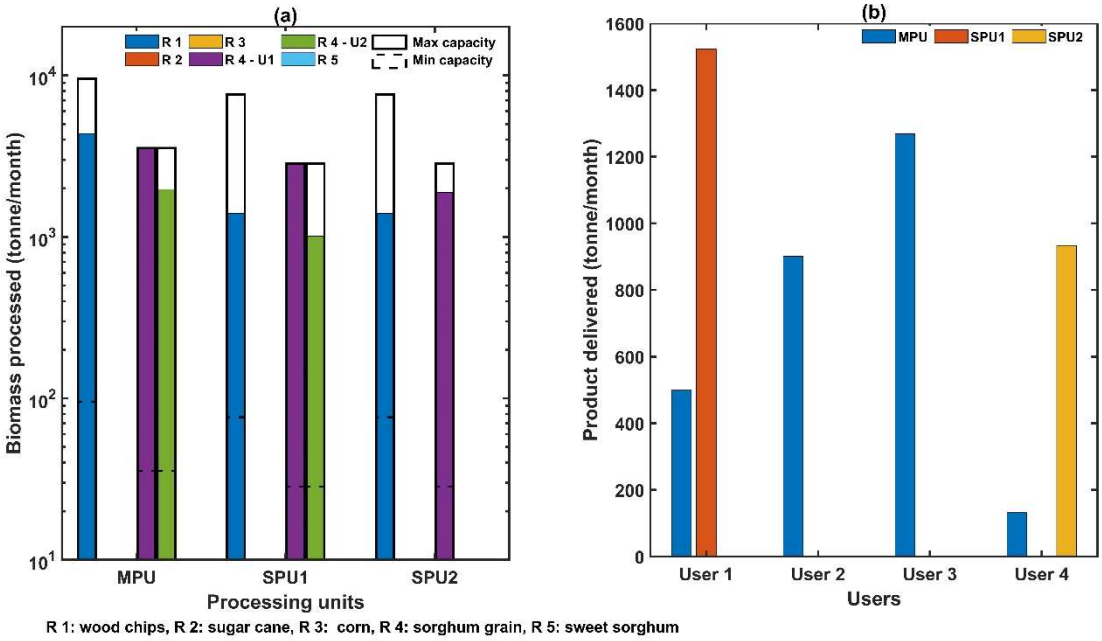

Fig. 4.4 Multi-unit optimization results corresponding to the processing hubs for (a) biomass processed and (b) product delivery to each user

The optimal decision for the multi-unit model is to select wood chips and sorghum grain as the only two types of biomass in the entire supply chain. Subsequently, it avoids corn, which has been selected in the single-unit model. In the single-unit model, full-capacity process units for sorghum grain are used at all the processing hubs. Hence, the solution obtained in the single-unit model can be inferred as a suboptimal operational decision due to capacity restrictions. The use of multiple process units at the MPU and SPU 1 for sorghum could reduce the processing at the SPU 2, which in turn is a costlier option to satisfy the demand. It should be

noted that the lower operational limit of the process unit restricts the use of arbitrary capacity allocation schemes. The high investment cost for installing an additional process unit of the technology necessitates an analysis of the total cost of a plant before implementing them as per the multi-unit model.

4.4.3. Economic benefits of the multi-unit model

The multi-unit model uses multiple economic process units to satisfy the user demands and thus reduces the total cost of the bio-refinery supply chain. A detailed cost analysis of the single unit and the multi-unit model is given in Table 4.2. The investment cost of the MPU in the multi-unit model is lesser than in the single-unit model, even after implementing multiple process units. In contrast, implementing additional process units of the technologies increased biomass procurement, processing, and transportation costs. The investment cost for SPU 1 has increased along with the total biomass cost, whereas the total processing cost and transportation cost have been reduced. This implies that multiple economic process units installed at the SPU 1 use cheaper biomass to satisfy user demand.

Table 4.2 Cost analysis of the single-unit and multi-unit models

Categories	Single unit model			Multi-unit model		
	MPU	SPU 1	SPU 2	MPU	SPU 1	SPU 2
Investment cost ($ 10 million)	2.75	1.57	1.57	2.57	2.14	1.57
Processing cost ($ 10 million)	13.10	10.00	7.18	14.40	8.62	5.94
Biomass transportation cost ($ 10 million)	3.25	2.51	2.99	4.52	2.22	2.24
Biomass cost ($ 10 million)	30.00	16.70	14.20	31.30	18.40	10.50
Total cost ($ 100 million)		10.60			**10.40**	

The investment cost for SPU 2 in the multi-unit model is similar to the single-unit model; however, the biomass cost, processing cost, and transportation cost are less compared to the single-unit model. In this multi-unit model, SPU 2 utilized cheaper biofuel from external

sources (MPU) and reduced the in-house production, which is otherwise costlier in satisfying the demand. Implementing cheaper process units reduced the total cost for the multi-unit model by 1.31 %.

4.5. Conclusion

This chapter primarily explored the benefits of capacity planning in a distributed biorefinery, which lacked much attention from the research community. In this direction, a multi-unit model for the biorefinery superstructure that allows the implementation of multiple economic process units of the selected technology while satisfying the individual capacity domains is proposed. This chapter first considered a single-unit model of a distributed biorefinery superstructure available in the literature and improved it to accommodate the decisions for multiple technologies. The improved single-unit model is extended to a multi-unit model that can implement multiple process units of selected technologies. The efficacy of the proposed model is demonstrated in a distributed biorefinery case study. The objective is to obtain an optimal production plan by minimizing the total cost while satisfying the demands of all users and other resource constraints. The optimal solution of the multi-unit model has a reduced total cost of 1.31% compared to the single-unit model. As per the optimal solution obtained in the multi-unit model, more than one process unit of the selected technology is installed to process the most beneficial biomass compared to the single-unit model. The multi-unit model also helped identify the beneficial biomass over the total plant operational time. Among all five types of biomass, the demand satisfaction using Grain sorghum is the most economical, followed by woodchips. The use of corn to produce biofuel is observed in the single-unit case; however, better planning using the multi-unit model helped avoid the use of corn and reduced the total cost.

Chapter 5

Multi-objective MILP model using the multi-unit strategy for periodic distributed biorefineries with economic and social benefits

This chapter proposes a multi-unit, multi-period supply chain model to overcome the restriction in plant capacity by establishing multiple units of a profitable process. The proposed model considers the periodic assessment of a biorefinery supply chain and evaluates the performance of the multi-unit strategy using economic and social objectives. The economic objective evaluates the profit of the supply chain, whereas the social objective is based on the number of jobs generated. The multi-objective optimization study of the proposed model has been demonstrated in a case study from the literature that requires the design of a supply chain for bioenergy.

The literature review for the study is discussed in Section 5.1, revealing different bioenergy models and their challenges. The problem description is given in Section 5.2, followed by the multi-unit model in Section 5.3. The case study and solution settings are provided in Section 5.4. The results for single and multi-objective cases are discussed in Section 5.5. The chapter concludes in Section 5.6 by summarising the benefits of the proposed model.

5.1. Background

The various technologies used to process biomass into biofuel are among the crucial steps that significantly contribute to deciding the optimal superstructure design and operations. The transformation of biomass to biofuel requires complex processes in the bio-refineries using multiple stages (Mutenure et al. 2018). The model presented by Potrč et al. (2020) provides a broad idea regarding the use of technologies in biomass pre-processing and converting into multiple products. Apart from the chosen technology, the quantity of biofuel production

depends on the installed capacity of the technology at the processing plant, and it directly impacts the revenue of the model (Ge et al. 2021). The model by Li and Ge (2017) showed the relationship between process characteristics and economic performance. The selection of technology solely based on biomass species restricts the processing of other types of biomass. Lim and Lam (2016) have suggested the element classification of the biomasses, thereby integrating the underutilized biomass into the existing system, which improved the supply chain model.

Design limitations in capacity modeling often restrict the processing capacities of real-life refineries. The use of domain constraints on the capacity level limits reaching the true optimality but is vital in avoiding unrealistic plant capacities. The restriction on processing capacities might compel the distributed biorefineries to process the biomass at less profitable plant locations. There have been models incorporating multiple distributed processing facilities with varying capacities (Santibañez-Aguilar et al. 2014). In such cases, the capacity constraint restricts the economics of scale for higher-capacity plants. The majority of the biorefinery superstructures are designed for periodic assessment, including storage systems. The selection of a single unit of a higher capacity facility might become redundant in a period of low biomass availability and market demand. Similarly, the limitation on the production capacity corresponding to a selected technology restricts the maximum production from the most profitable process. In order to satisfy the demand, the production plan chooses other less profitable processes, resulting in a sub-optimal solution. The proposed strategy aims to address the research gap in the literature for the capacity planning of biorefineries, where the units related to the processing technologies are capacity-constrained, limiting the bioenergy superstructures in achieving greater benefits in the design stage. In this chapter, a multi-unit strategy is proposed to overcome the limitations by implementing multiple units of profitable

processes, subject to various resource and operational constraints, at the biorefineries. The strategy is incorporated into a biorefinery superstructure model available in the literature (Santibañez-Aguilar et al. 2014). The new model provides flexibility in installing multiple process units for each technology at the processing centers. The competency of the model is compared with the literature case study (Santibañez-Aguilar et al. 2014). This chapter also justifies the concept with rigorous analysis of the decision structure using two objectives: maximization of total annual profit and maximization of social impact in terms of the number of jobs generated. The proposed mathematical model is generic and can be used for various geographies, and it has been successfully demonstrated in a case study to maximize economic and social objectives.

5.2. Problem statement

The problem explores the long-term planning of a supply chain involving distributed biorefineries that aim to determine the strategic and operational level decisions. The model constitutes a group of harvesting locations capable of providing various types of biomass, a list of geographical areas available for installing the processing plants, and a set of markets to sell the products (Santibañez-Aguilar et al. 2014). Strategic planning of the supply chain requires the identification of beneficial locations corresponding to the harvesting sites, installing biomass processing plants, and selecting markets for demand satisfaction among the available choices. The operational level decisions determine the periodic biomass to be harvested, flow rates to be maintained, and inventory requirements at various supply chain hubs. The generic problem model is defined below.

A set of *R* raw materials can be obtained from *H* harvesting locations supplied to the processing units using various transportation methods. The processing units are classified as the main processing unit (*C*) and secondary processing units (*SP*) with different processing capacities. The main processing unit can process a higher amount of raw materials than the secondary processing units. A set of *I* processing technologies is available for all processing units to convert the raw materials into *P* products. The model uses storage facilities (*S*) at various production and distribution hubs to store unprocessed raw materials and unsold products. The superstructure is analyzed for *T* time periods over which *P* products can be sold in *MK* markets (Fig. 5.1). The time period for the model is not restricted to a particular range. The selection of a shorter or longer time period does not require any conceptual change to the proposed model. Apart from resource availability and product demand, the production capacity of the processing plant is also a crucial factor that restricts the processing amount of a process.

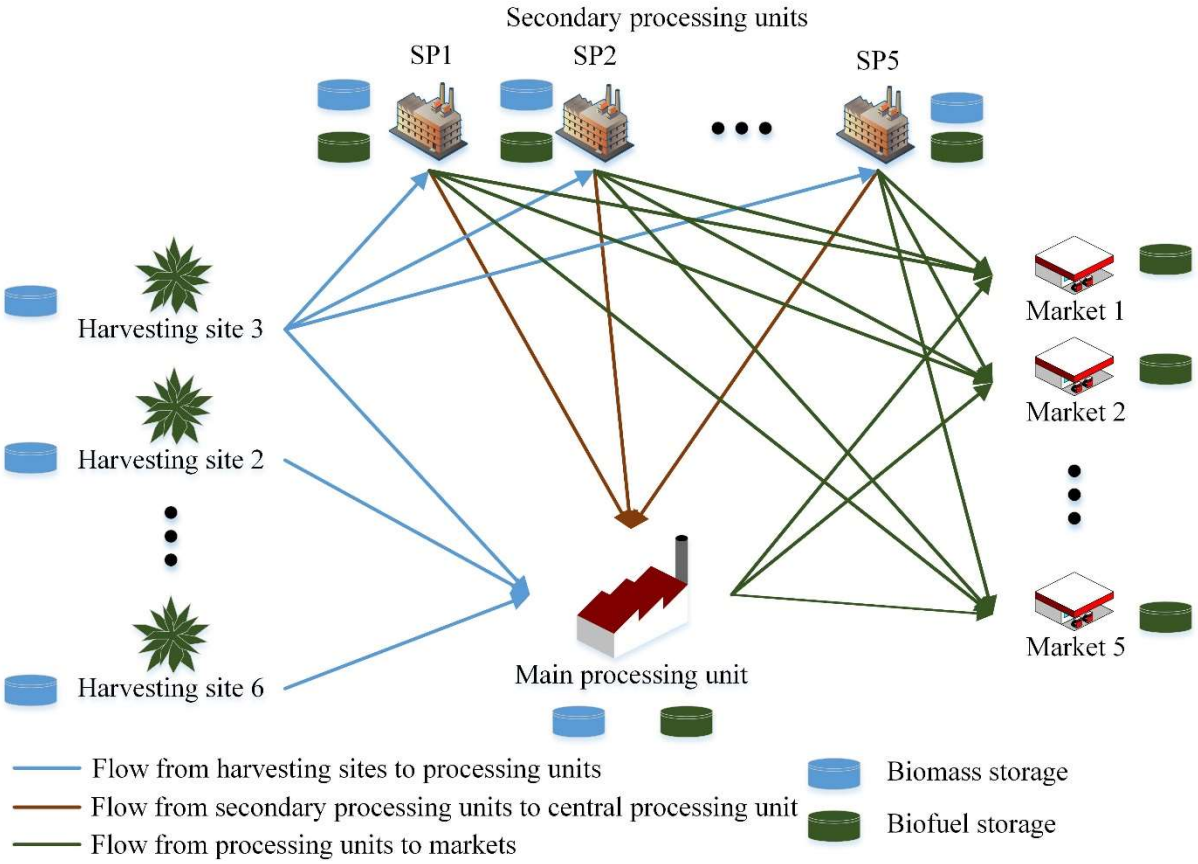

Fig. 5.1 Superstructure of the biofuel supply chain

This restriction can be overcome by accommodating multiple process units of the selected technology within the economic barrier. The maximum production is enhanced by incorporating the ability to include products from multiple units of each selected technology, which aids in the maximum production of the most profitable product and leads to higher profit. The single-unit bio-refinery model is extended to a multi-unit model by integrating multiple process units of the technologies in the plants. The model incorporates a maximum of *UC* and *USP* number of units available for each processing technology in the main and secondary processing units. The proposed formulation enables the selection of multiple secondary processing units as well as the establishment of multiple units of the same technology at a selected secondary processing unit.

Nomenclature

Sets

C	Main processing unit
I_R	Technologies suitable for processing raw material R
P_R	Products produced from raw material R
R	Raw material
H	Harvesting site
T	Time period
SP	Secondary processing plant
UC	Process units for main processing unit
USP	Process units for secondary processing units

Continuous variables

$r^{P}_{r,h,t}$	Biomass (r) produced at harvesting location (h) at the end of the time period (t) (tonne/month)
$r^{H}_{r,h,t}$	Biomass (r) available at harvesting location (h) at the end of the time period (t) (tonne/month)
$r^{C}_{r,t}$	Biomass (r) available at the main processing unit at the end of the time period (t) (tonne/month)
$r^{SP}_{r,sp,t}$	Biomass (r) available at the secondary processing unit (sp) at the end of the time period (t) (tonne/month)
$r^{H\to SP}_{r,h,sp,t}$	Biomass (r) transported to secondary processing unit (sp) from harvesting location (h) at the end of the time period (t) (tonne/month)
$r^{H\to C}_{r,h,t}$	Biomass (r) transported to main processing unit from harvesting location (h) at the end of the time period (t) (tonne/month)
$r^{SP\to C}_{r,sp,t}$	Biomass (r) transported to main processing unit from secondary processing unit (sp) at the end of the time period (t) (tonne/month)
$ra^{H\to SP}_{r,h,sp,t}$	Biomass (r) received at secondary processing unit (sp) from harvesting location (h) at the end of the time period (t) (tonne/month)
$ra^{H\to C}_{r,h,t}$	Biomass (r) received at the main processing unit from harvesting location (h) at the end of the time period (t) (tonne/month)
$ra^{SP\to C}_{r,sp,t}$	Biomass (r) received at the main processing unit from the secondary processing unit (sp) at the end of the time period (t) (tonne/month)

$rp^{C}_{uc,r,p,i,t}$	Biomass (r) processed at processing unit (uc) of the main processing unit using technology (i) for the product (p) at the end of the time period (t) (tonne/month)
$rp^{SP}_{usp,r,p,i,sp,t}$	Biomass (r) processed at processing unit (usp) of the secondary processing unit (sp) using technology (i) for the product (p) at the end of the time period (t) (tonne/month)
$pd^{C}_{uc,r,p,i,t}$	Product (p) produced at processing unit (uc) of the main processing unit using technology (i) from biomass (r) at the end of the time period (t) (tonne/month)
$pd^{SP}_{usp,r,p,i,sp,t}$	Product (p) produced at processing unit (usp) of the secondary processing unit (sp) using technology (i) from biomass (r) at the end of the time period (t) (tonne/month)
$p^{C}_{p,t}$	Product (p) available at the main processing unit at the end of the time period (t) (tonne/month)
$p^{SP}_{p,sp,t}$	Product (p) available at the secondary processing unit (sp) at the end of the time period (t) (tonne/month)
$p^{C\rightarrow MK}_{p,mk,t}$	Product (p) transported to market (mk) from the main processing unit at the end of the time period (t) (tonne/month)
$pa^{C\rightarrow MK}_{p,mk,t}$	Product (p) received at the market (mk) from the main processing unit at the end of the time period (t) (tonne/month)
$p^{SP\rightarrow C}_{p,sp,t}$	Product (p) transported to main processing unit from secondary processing unit (sp) at the end of the time period (t) (tonne/month)
$pa^{SP\rightarrow C}_{p,sp,t}$	Product (p) received at the main processing unit from the secondary processing unit (sp) at the end of the time period (t) (tonne/month)
$p^{SP\rightarrow MK}_{p,sp,mk,t}$	Product (p) transported to market (mk) from the secondary processing unit (sp) at the end of the time period (t) (tonne/month)
$pa^{SP\rightarrow MK}_{p,sp,mk,t}$	Product (p) received at the market (mk) from the secondary processing unit (sp) at the end of the time period (t) (tonne/month)
$p^{MK}_{p,mk,t}$	Product (p) available at the market (mk) at the end of the time period (t) (tonne/month)
$p^{Sold}_{p,mk,t}$	Product (p) sold at market (mk) at the end of the time period (t) (tonne/month)
$x_{a,b,t_{end}}$	Inventory at ending of the time period for the material (a) at location (b) (tonne/month)
$x_{a,b,0}$	Inventory at starting of the time period for the material (a) at location (b) (tonne/month)

Boolean variables

$YR^{H\to SP}_{r,h,sp,t}$	Assumes the value 1 if biomass (r) is transported to secondary processing unit (sp) from harvesting location (h) at the end of the time period (t)
$YR^{H\to C}_{r,h,t}$	Assumes the value 1 if biomass (r) is transported to main processing unit from harvesting location (h) at the end of the time period (t)
$YS^{H}_{r,h,t}$	Assumes the value 1 if biomass (r) is stored at harvesting location (h) for the time period (t)
$YP^{C}_{uc,r,p,i,t}$	Assumes the value 1 if biomass (r) is processed at processing unit (uc) of the main processing unit using technology (i) for the product (p) at the end of the time period (t)
$YS^{C}_{r,t}$	Assumes the value 1 if biomass (r) is stored at the main processing unit for the time period (t)
$YSP^{C}_{p,t}$	Assumes the value 1 if the product (p) is stored at the main processing unit for the time period (t)
$YP^{SP}_{usp,r,p,i,sp,t}$	Assumes the value 1 if biomass (r) is processed at processing unit (usp) of the secondary processing unit (sp) using technology (i) for the product (p) at the end of the time period (t)
$YS^{SP}_{r,sp,t}$	Assumes the value 1 if biomass (r) is stored at the secondary processing unit (sp) for the time period (t)
$YSP^{SP}_{p,sp,t}$	Assumes the value 1 if the product (p) is stored at the secondary processing unit (sp) for the time period (t)
$YSP^{MK}_{p,mk,t}$	Assumes the value 1 if the product (p) is stored at the market (mk) for the time period (t)
$YRT^{SP\to C}_{r,sp,t}$	Assumes the value 1 if biomass (r) is transported to main processing unit from secondary processing unit (sp) at the end of the time period (t)
$YPT^{SP\to C}_{p,sp,t}$	Assumes the value 1 if the product (p) is transported to main processing unit from secondary processing unit (sp) at the end of the time period (t)
$YPT^{SP\to MK}_{p,sp,mk,t}$	Assumes the value 1 if the product (p) is transported to market (mk) from the secondary processing unit (sp) at the end of the time period (t)
$YPT^{C\to MK}_{p,mk,t}$	Assumes the value 1 if the product (p) is transported to market (mk) from the main processing unit at the end of the time period (t)

Parameters

$\alpha_{r,p,i}$	Unit mass conversion ratio for biomass (r) into the product (p) using technology (i) (unit product /unit raw material)
$csr^{H}_{r,h,t}$	Storage cost for biomass (r) at harvesting site (h) in the time period (t) ($/tonne)
$csr^{C}_{r,t}$	Storage cost for biomass (r) at main processing unit in the time period (t) ($/tonne)
$csr^{SP}_{r,sp,t}$	Storage cost for biomass (r) at secondary processing unit (sp) in the time period (t) ($/tonne)
$csp^{C}_{p,t}$	Storage cost for product (p) at main processing unit in the time period (t) ($/tonne)
$csp^{SP}_{p,sp,t}$	Storage cost for product (p) at secondary processing unit (sp) in the time period (t) ($/tonne)
$csp^{MK}_{p,mk,t}$	Storage cost for product (p) at market (mk) in the time period (t) ($/tonne)
$ctr^{H\rightarrow SP}_{r,h,sp,t}$	Transportation cost of biomass (r) from harvesting location (h) to secondary processing unit (sp) in the time period (t) ($/tonne)
$ctr^{H\rightarrow C}_{r,h,t}$	Transportation cost of biomass (r) from harvesting location (h) to main processing unit in the time period (t) ($/tonne)
$ctr^{SP\rightarrow C}_{r,sp,t}$	Transportation cost of biomass (r) from secondary processing unit (sp) to main processing unit in the time period (t) ($/tonne)
$ctp^{SP\rightarrow MK}_{p,sp,mk,t}$	Transportation cost of product (p) from secondary processing unit (sp) to market (mk) in the time period (t) ($/tonne)
$ctp^{SP\rightarrow C}_{p,sp,t}$	Transportation cost of product (p) from secondary processing unit (sp) to main processing unit in the time period (t) ($/tonne)
$ctp^{C\rightarrow MK}_{p,mk,t}$	Transportation cost of product (p) from main processing unit to market (mk) in the time period (t) ($/tonne)
$e^{R}_{r,h}$	Employment index for biomass(r) produced at harvesting location (h) (jobs/ tonne)
$e^{H\rightarrow SP}_{r,h,sp}$	Employment index for biomass (r) transported from harvesting location (h) to secondary processing unit (sp) (jobs/ tonne)
$e^{H\rightarrow C}_{r,h}$	Employment index for biomass (r) transported from harvesting location (h) to main processing unit (jobs/ tonne)
$e^{C\rightarrow MK}_{p,mk}$	Employment index for product (p) transported from main processing unit to market (mk) (jobs/ tonne)
$e^{C}_{r,p,i,t}$	Employment index for biomass (r) processed at main processing unit using technology (i) for product (p) in the time period (t) (jobs/ tonne)

$e_{r,sp}^{SP\rightarrow C}$	Employment index for biomass (r) transported from secondary processing unit (sp) to main processing unit (jobs/ tonne)
$e_{p,sp,mk}^{SP\rightarrow MK}$	Employment index for product (p) transported from secondary processing unit (sp) to market (mk) (jobs/ tonne)
$e_{p,sp}^{SP\rightarrow C}$	Employment index for product (p) transported from secondary processing unit (sp) to main processing unit (jobs/ tonne)
$e_{r,sp,p,i,t}^{SP}$	Employment index for biomass (r) processed at secondary processing unit (sp) using technology (i) for product (p) in the time period (t) (jobs/ tonne)
$mpl_{r,p,i,sp,t}^{SP}$	Lower limit for biomass (r) processed at secondary processing unit (sp) using technology (i) for product (p) in the time period (t) (tonne/ month)
$mpl_{r,p,i,t}^{C}$	Lower limit for biomass (r) processed at main processing unit using technology (i) for product (p) in the time period (t) (tonne/ month)
$mpu_{r,p,i,t}^{C}$	Upper limit for biomass (r) processed at main processing unit using technology (i) for product (p) in the time period (t) (tonne/ month)
$mpu_{r,sp,p,i,t}^{SP}$	Upper limit for biomass (r) processed at secondary processing unit (sp) using technology (i) for product (p) in the time period (t) (tonne/ month)
$p_{p,mk,t}^{demand}$	Demand of Product (p) at market (mk) for the time period (t) (tonne/ month)
$ptl_{p,sp}^{SP\rightarrow C}$	Lower limit for transportation of product (p) from secondary processing unit (sp) to main processing unit (tonne/ month)
$ptu_{p,sp}^{SP\rightarrow C}$	Upper limit for transportation of product (p) from secondary processing unit (sp) to main processing unit (tonne/ month)
$ptl_{p,sp,mk}^{SP\rightarrow MK}$	Lower limit for transportation of product (p) from secondary processing unit (sp) to market (mk) (tonne/ month)
$ptu_{p,sp,mk}^{SP\rightarrow MK}$	Upper limit for transportation of product (p) from secondary processing unit (sp) to market (mk) (tonne/ month)
$ptl_{p,mk}^{C\rightarrow MK}$	Lower limit for transportation of product (p) from main processing unit to market (mk) (tonne/ month)
$ptu_{p,mk}^{C\rightarrow MK}$	Upper limit for transportation of product (p) from main processing unit to market (mk) (tonne/ month)
$pcr_{r,h,t}^{P}$	Production cost of biomass (r) at harvesting site (h) for the time period (t) ($/tonne)
$pc_{r,sp,p,i,t}^{SP}$	Processing cost for biomass (r) at secondary processing unit (sp) using technology (i) for product (p) in the time period (t) ($/tonne)
$pc_{r,p,i,t}^{C}$	Processing cost for biomass (r) at main processing unit using technology (i) for product (p) in the time period (t) ($/tonne)
$rp_{r,h,t}^{Max}$	Maximum production capacity of biomass (r) at harvesting location (h) for time period (t) (tonne/ month)

$rtu_{r,sp}^{SP\rightarrow C}$	Upper limit for transportation of biomass (r) from secondary processing unit (sp) to main processing unit (tonne/ month)
$rtl_{r,sp}^{SP\rightarrow C}$	Lower limit for transportation of biomass (r) from secondary processing unit (sp) to main processing unit (tonne/ month)
$rtl_{r,h,sp,t}^{H\rightarrow SP}$	Lower limit for transportation of biomass (r) from harvesting location (h) to secondary processing unit (sp) for the time period (t) (tonne/ month)
$rtu_{r,h,sp,t}^{H\rightarrow SP}$	Upper limit for transportation of biomass (r) from harvesting location (h) to secondary processing unit (sp) for the time period (t) (tonne/ month)
$rtl_{r,h,t}^{H\rightarrow C}$	Lower limit for transportation of biomass (r) from harvesting location (h) to main processing unit for the time period (t) (tonne/ month)
$rtu_{r,h,t}^{H\rightarrow C}$	Upper limit for transportation of biomass (r) from harvesting location (h) to main processing unit for the time period (t) (tonne/ month)
$slcr_{r,h}^{H}$	Lower limit for storage of biomass (r) at harvesting location (h) (tonne/ month)
$sucr_{r,h}^{H}$	Upper limit for storage of biomass (r) at harvesting location (h) (tonne/ month)
$slcr_{r}^{C}$	Lower limit for storage of biomass (r) at main processing unit (tonne/ month)
$sucr_{r}^{C}$	Upper limit for storage of biomass (r) at main processing unit (tonne/ month)
$slcp_{p}^{C}$	Lower limit for storage of product (p) at main processing unit (tonne/ month)
$sucp_{p}^{C}$	Upper limit for storage of product (p) at main processing unit (tonne/ month)
$slcr_{r,sp}^{SP}$	Lower limit for storage of biomass (r) at secondary processing unit (sp) (tonne/ month)
$sucr_{r,sp}^{SP}$	Upper limit for storage of biomass (r) at secondary processing unit (sp) (tonne/ month)
$slcp_{p,sp}^{SP}$	Lower limit for storage of product (p) at secondary processing unit (sp) (tonne/ month)
$sucp_{p,sp}^{SP}$	Upper limit for storage of product (p) at secondary processing unit (sp) (tonne/ month)
$slcp_{p,mk}^{MK}$	Lower limit for storage of product (p) at market (mk) (tonne/ month)
$sucp_{p,mk}^{MK}$	Upper limit for storage of product (p) at market (mk) (tonne/ month)
$sp_{p,mk,t}^{sold}$	Selling price of product (p) at market (mk) for the time period (t) ($/tonne)

5.3. Proposed mathematical model for the multi-unit bio-refinery superstructure

The superstructure constitutes various constraints at multiple nodes of the model, starting from the harvesting locations to the end-user supply centers. The individual constraints are detailed in the following sections.

5.3.1. Balances at the harvesting locations

The biomass production capacity at the harvesting locations usually depends on climatic conditions, land size, equipment, labor availability, demand at processing units, etc. The biomass production at the harvesting location ($r^{P}_{r,h,t}$) cannot exceed the maximum production capacity ($rp^{Max}_{r,h,t}$) of the harvesting site for any time instant as given in Equation (5.1) (Santibañez-Aguilar et al. 2014).

$$r^{P}_{r,h,t} \le rp^{Max}_{r,h,t} \quad ,\forall r \in R, h \in H, t \in T \tag{5.1}$$

The biomass at the harvesting location at any time instant ($r^{H}_{r,h,t}$) depends on multiple factors such as the amount of biomass available from the previous time instant ($r^{H}_{r,h,t-1}$), production of biomass ($r^{P}_{r,h,t}$), and distribution of available biomass to processing facilities ($r^{H\to SP}_{r,h,sp,t}$ and $r^{H\to C}_{r,h,t}$) at the current time instant which is provided in Equation (5.2) (Santibañez-Aguilar et al. 2014).

$$r^{H}_{r,h,t} = r^{H}_{r,h,t-1} + r^{P}_{r,h,t} - r^{H\to C}_{r,h,t} - \sum_{sp} r^{H\to SP}_{r,h,sp,t} \quad ,\forall r \in R, h \in H, t \in T \tag{5.2}$$

Biomass transportation from the harvesting location

The biomass available at the harvesting locations is transported to various processing locations using different modes of transport. Each transport link between the harvesting locations and the various processing units can operate within a domain of maximum ($rtu^{H\to SP}_{r,h,sp,t}$ and $rtu^{H\to C}_{r,h,t}$)

and minimum ($rtl^{H\to SP}_{r,h,sp,t}$ and $rtl^{H\to C}_{r,h,t}$) transportation capacity. The domain constraints for the transportation of biomass to main and secondary processing units are given in Equations (5.3) and (5.4) respectively (Santibañez-Aguilar et al. 2014).

$$YR^{H\to SP}_{r,h,sp,t} rtl^{H\to SP}_{r,h,sp,t} \le r^{H\to SP}_{r,h,sp,t} \le YR^{H\to SP}_{r,h,sp,t} rtu^{H\to SP}_{r,h,sp,t} \quad ,\forall r\in R, h\in H, sp\in SP, t\in T \tag{5.3}$$

$$YR^{H\to C}_{r,h,t} rtl^{H\to C}_{r,h,t} \le r^{H\to C}_{r,h,t} \le YR^{H\to C}_{r,h,t} rtu^{H\to C}_{r,h,t} \quad ,\forall r\in R, h\in H, t\in T \tag{5.4}$$

The above constraints are realized using binary variables ($YR^{H\to SP}_{r,h,sp,t}$ and $YR^{H\to C}_{r,h,t}$), which ensure a feasible transport link between the harvesting locations and the corresponding processing unit.

Time constraints on transportation from harvesting locations

The biomass transported from the harvesting locations is delivered ($ra^{H\to SP}_{r,h,sp,t}$ and $ra^{H\to C}_{r,h,t}$) to the processing units after a finite transportation time ($t+trans$). This transportation time usually depends on the medium and distance of the transportation link. The use of transportation time in the supply from the harvesting locations and reception at the processing units is realized using Equations (5.5) and (5.6) (Santibañez-Aguilar et al. 2014).

$$r^{H\to SP}_{r,h,sp,t} = ra^{H\to SP}_{r,h,sp,t+trans}, \quad \forall r\in R, h\in H, sp\in SP, t\in T \tag{5.5}$$

$$r^{H\to C}_{r,h,t} = ra^{H\to C}_{r,h,t+trans}, \quad \forall r\in R, h\in H, t\in T \tag{5.6}$$

Biomass storage at harvesting locations

The harvesting locations utilize storage facilities to store the surplus amount of biomass produced at any time instant, which can be used in the next instant. The storage facilities are decided in advance depending upon the anticipations and can only be stored at the designed capacity. Apart from the restrictions on the maximum storage ($sucr^{H}_{r,h}$), the storage facilities

should be feasible considering the workable size and need to be designed above a minimum level ($slcr_{r,h}^{H}$). The domain of storage capacity is given in Equation (5.7) (Santibañez-Aguilar et al. 2014).

$$YS_{r,h,t}^{H} slcr_{r,h}^{H} \le r_{r,h,t}^{H} \le YS_{r,h,t}^{H} sucr_{r,h}^{H} \quad ,\forall r \in R, h \in H, t \in T \tag{5.7}$$

Biomass availability at the main processing unit

The main processing unit can receive biomass from the harvesting locations ($ra_{r,h,t}^{H \to C}$) as well as from any of the secondary processing units ($ra_{r,sp,t}^{SP \to C}$) (Santibañez-Aguilar et al. 2014). The biomass available at the main processing unit at any time instant ($r_{r,t}^{C}$) depends on the amount of stored, procured, and processed biomass as provided in Equation (5.8) .

$$r_{r,t}^{C} = r_{r,t-1}^{C} + \sum_{h} ra_{r,h,t}^{H \to C} + \sum_{sp} ra_{r,sp,t}^{SP \to C} - \sum_{uc} \sum_{p} \sum_{i} rp_{uc,r,p,i,t}^{C} \quad ,\forall r \in R, t \in T \tag{5.8}$$

5.3.2. Balances at the main processing unit

The biomass at the main processing unit utilizes multiple available technologies suitable for the received biomass and produces multiple products. The amount of product produced depends on a technology-dependent conversion factor ($\alpha_{r,p,i,t}$). Each biomass requires a finite processing time (tp) to produce the related product. The amount of product produced at a time instance ($t+tp$) can be determined using Equation (5.9).

$$pd_{uc,r,p,i,t+tp}^{C} = \alpha_{r,p,i} rp_{uc,r,p,i,t}^{C} \quad ,\forall uc \in UC, r \in R, p \in P_R, i \in I_R, t \in T \tag{5.9}$$

The total processing capacity of each unit in the main processing unit possesses a processing domain, with an upper limit equal to the maximum processing capacity ($mpu_{r,p,i,t}^{C}$) of the unit, and the lower limit is the minimum biomass required ($mpl_{r,p,i,t}^{C}$) to commence the unit operation as given in Equation (5.10).

$$YP^{C}_{uc,r,p,i,t} mpl^{C}_{r,p,i,t} \le rp^{C}_{uc,r,p,i,t} \le YP^{C}_{uc,r,p,i,t} mpu^{C}_{r,p,i,t} \quad \forall uc \in UC, r \in R, p \in P_R, i \in I_R, t \in T \text{ (5.10)}$$

The processing capacity of the units in the main processing unit is regulated using a binary variable ($YP^{C}_{uc,r,p,i,t}$), which gets activated if the selected biomass is processed within the appropriate processing domain.

Product balance at the main processing unit

The products available at t^{th} time instant ($p^{C}_{p,t}$) depend on the product stored from the previous time instant, the product produced at the current time ($pd^{C}_{uc,r,p,i,t}$), the product received from the secondary processing unit ($pa^{SP \to C}_{p,sp,t}$), and the total products dispatched to the markets ($p^{C \to MK}_{p,mk,t}$) which can be determined using Equation (5.11).

$$p^{C}_{p,t} = p^{C}_{p,t-1} + \sum_{uc}\sum_{r}\sum_{i} pd^{C}_{uc,r,p,i,t} + \sum_{sp} pa^{SP \to C}_{p,sp,t} - \sum_{mk} p^{C \to MK}_{p,mk,t} \quad , \forall p \in P_R, t \in T \qquad (5.11)$$

Storage at the main processing unit

The main processing unit stores the excess available biomass and products in two types of storage. The storage constraints present in the main processing unit are similar to the storage constraints of the harvesting locations and are followed when designing the storage at the main processing unit. The domain corresponding to the storage facility of the products and different biomass types are given in Equations (5.12) and (5.13) (Santibañez-Aguilar et al. 2014).

$$YS^{C}_{r,t} slcr^{C}_{r} \le r^{C}_{r,t} \le YS^{C}_{r,t} sucr^{C}_{r} \quad , \forall r \in R, t \in T \qquad (5.12)$$

$$YSP^{C}_{p,t} slcp^{C}_{p} \le p^{C}_{p,t} \le YSP^{C}_{p,t} sucp^{C}_{p} \quad , \forall p \in P, t \in T \qquad (5.13)$$

5.3.3. Balances at the secondary processing units

The secondary processing units can only receive the biomass from the harvesting locations. The total biomass available at any time instant ($r^{SP}_{r,sp,t}$) depends on the stored biomass from the

previous time instant ($r^{SP}_{r,sp,t-1}$), the biomass received from harvesting locations ($ra^{H\to SP}_{r,h,sp,t}$), the biomass transported to the units of the main processing unit ($r^{SP\to C}_{r,sp,t}$), and the amount of biomass processed at the secondary processing unit for the current time instant ($rp^{SP}_{usp,r,sp,p,i,t}$) as given in Equation (5.14).

$$r^{SP}_{r,sp,t} = r^{SP}_{r,sp,t-1} + \sum_{h} ra^{H\to SP}_{r,h,sp,t} - \sum_{usp}\sum_{p}\sum_{i} rp^{SP}_{usp,r,sp,p,i,t} - r^{SP\to C}_{r,sp,t} \quad ,\forall r\in R, sp\in SP, t\in T \qquad (5.14)$$

The time difference between the origin and the terminating station of the transport is denoted as the transportation time, and it is crucial in analyzing the effect of transportation links on the model. The relation between the raw material sent from the secondary processing unit to the main processing unit is given in the Equation (5.15) (Santibañez-Aguilar et al. 2014).

$$r^{SP\to C}_{r,sp,t} = ra^{SP\to C}_{r,sp,t+trans} \quad ,\forall r\in R, sp\in SP, t\in T \qquad (5.15)$$

Biomass processing at the secondary processing units

The biomass processing at the secondary processing unit utilizes an appropriate technology with respect to the biomass for producing the products. The production is realized mathematically using a conversion factor that determines the final mass of the product made from the biomass as provided in Equation (5.16).

$$pd^{SP}_{usp,r,sp,p,i,t+tp} = \alpha_{r,p,i} rp^{SP}_{usp,r,sp,p,i,t} \quad ,\forall usp\in USP, r\in R, p\in P_R, i\in I_R, sp\in SP, t\in T \qquad (5.16)$$

Similar to the main processing unit, the processing in the secondary processing units follows a processing domain, as given in Equation (5.17) , that allows the biomass to be processed within a finite processing limit.

$$YP^{SP}_{usp,r,sp,p,i,t} mpl^{SP}_{r,sp,p,i,t} \le rp^{SP}_{usp,r,sp,p,i,t} \le YP^{SP}_{usp,r,sp,p,i,t} mpu^{SP}_{r,sp,p,i,t}, \quad \forall usp\in USP, r\in R, p\in P_R, i\in I_R, sp\in SP, t\in T \qquad (5.17)$$

Product balance at secondary processing units

Similar to the raw material balance, the product at the secondary processing unit for any time instance ($p^{SP}_{p,sp,t}$) is dependent on the product available at the previous time instance ($p^{SP}_{p,sp,t-1}$), the amount of product produced ($pd^{SP}_{usp,r,sp,p,i,t}$) using biomass through different processing routes, the amount of product transported to the main plant ($p^{SP\to C}_{p,sp,t}$), and the market ($p^{SP\to MK}_{p,sp,mk,t}$) for the corresponding time instant as Equation (5.18).

$$p^{SP}_{p,sp,t} = p^{SP}_{p,sp,t-1} + \sum_{usp}\sum_{r}\sum_{i} pd^{SP}_{usp,r,sp,p,i,t} - p^{SP\to C}_{p,sp,t} - \sum_{mk} p^{SP\to MK}_{p,sp,mk,t} \quad ,\forall p\in P, sp\in SP, t\in T \tag{5.18}$$

The transportation of product from a secondary processing unit to the main processing unit requires a finite time and is given in the Equation (5.19) (Santibañez-Aguilar et al. 2014).

$$p^{SP\to C}_{p,sp,t} = pa^{SP\to C}_{p,sp,t+trans} \quad ,\forall p\in P, sp\in SP, t\in T \tag{5.19}$$

Storage at the secondary processing unit

Analogous to the main processing unit, the excess biomass and product are stored in two different storage facilities in the secondary processing unit. The storage facilities follow a storage domain for the products and different biomass types as in Equations (5.20) and (5.21) (Santibañez-Aguilar et al. 2014).

$$YS^{SP}_{r,sp,t} slcr^{SP}_{r,sp} \le r^{SP}_{r,sp,t} \le YS^{C}_{r,sp,t} sucr^{C}_{r,sp} \quad ,\forall r\in R, sp\in SP, t\in T \tag{5.20}$$

$$YSP^{sp}_{p,sp,t} slcp^{SP}_{p,sp} \le p^{SP}_{p,sp,t} \le YSP^{SP}_{p,sp,t} sucp^{SP}_{p,sp} \quad ,\forall p\in P, sp\in SP, t\in T \tag{5.21}$$

Domain constraints on transportation

The transportation of biomass and products among the processing units is constrained by a domain constraint, which ensures a realistic flow rate. This constraint helps avoid unrealistic flow rates, such as a biomass flow rate of 0.0001 tons/month. The secondary processing units

are allowed to transfer the products and biomass with the main processing unit, and the transportation follows the relation in the Equations (5.22) and (5.23) (Santibañez-Aguilar et al. 2014).

$$YRT_{r,sp,t}^{SP\to C} rtl_{r,sp}^{SP\to C} \le r_{r,sp,t}^{SP\to C} \le YRT_{r,sp,t}^{SP\to C} rtu_{r,sp}^{SP\to C} \quad ,\forall r\in R, sp\in SP, t\in T \tag{5.22}$$

$$YPT_{p,sp,t}^{SP\to C} ptl_{p,sp}^{SP\to C} \le p_{p,sp,t}^{SP\to C} \le YPT_{p,sp,t}^{SP\to C} ptu_{p,sp}^{SP\to C} \quad ,\forall p\in P, sp\in SP, t\in T \tag{5.23}$$

The products produced from the main and secondary processing units are sent to the market, and the transportation domain follows the Equation (5.24) and (5.25) (Santibañez-Aguilar et al. 2014).

$$YPT_{p,sp,mk,t}^{SP\to MK} ptl_{p,sp,mk}^{SP\to MK} \le p_{p,sp,mk,t}^{SP\to MK} \le YPT_{p,sp,mk,t}^{SP\to MK} ptu_{p,sp,mk}^{SP\to MK}, \quad \forall p\in P, sp\in SP, mk\in MK, t\in T \tag{5.24}$$

$$YPT_{p,mk,t}^{C\to MK} ptl_{p,mk}^{C\to MK} \le p_{p,mk,t}^{C\to MK} \le YPT_{p,mk,t}^{C\to MK} ptu_{p,mk}^{C\to MK} \quad ,\forall p\in P, mk\in MK, t\in T \tag{5.25}$$

Time constraints on product transportation from processing plants

The delivery of products from each processing plant to the markets requires a finite transportation time. Each of the shipments reaches the market after the elapsed transportation time as given in Equations (5.26) and (5.27) (Santibañez-Aguilar et al. 2014).

$$p_{p,mk,t}^{C\to MK} = pa_{p,mk,t+trans}^{C\to MK}, \quad \forall p\in P, mk\in MK, t\in T \tag{5.26}$$

$$p_{p,sp,mk,t}^{SP\to MK} = pa_{p,sp,mk,t+trans}^{SP\to MK}, \quad \forall p\in P, sp\in SP, mk\in MK, t\in T \tag{5.27}$$

5.3.4. Balances at the markets

The products from the main and secondary processing units are sent to the markets to fulfill the demands. Any excess product is kept at the storage facility available at the markets. The product available at the market for any time instant ($p_{p,mk,t}^{MK}$) depends on the product available from the

previous time ($p^{MK}_{k,mk,t-1}$), the total product received from the main ($pa^{C\to MK}_{p,mk,t}$) and secondary processing units ($pa^{SP\to MK}_{p,sp,mk,t}$), and the total products sold to consumers ($p^{Sold}_{p,mk,t}$) as provided in Equation (5.28) (Santibañez-Aguilar et al. 2014).

$$p^{MK}_{p,mk,t} = p^{MK}_{k,mk,t-1} + \sum_{sp} pa^{SP\to MK}_{p,sp,mk,t} + pa^{C\to MK}_{p,mk,t} - p^{Sold}_{p,mk,t} \quad ,\forall p\in P, mk\in MK, t\in T \tag{5.28}$$

The model allows the selling of the products only up to the demand as in the Equation (5.29).

$$p^{sold}_{p,mk,t} \le p^{demand}_{p,mk,t} \quad ,\forall p\in P, mk\in MK, t\in T \tag{5.29}$$

Storage at the markets

The excess products delivered from the main and the secondary processing units above the current demand are stored at the respective markets. The surplus products are used for subsequent time periods. The domain constraints of the storage facilities are given in Equation (5.30).

$$YSP^{MK}_{p,mk,t} slcp^{MK}_{p,mk} \le p^{MK}_{p,mk,t} \le YSP^{MK}_{p,mk,t} sucp^{MK}_{p,mk} \quad ,\forall p\in P, mk\in MK, t\in T \tag{5.30}$$

Model constraints at the starting and ending of time periods

The model is equipped to solve for any period of time and thus needs to define a relation at the start and end of the time periods. This requirement is realized using a realistic time frame approach where for each time horizon, the inventory at the end of a time horizon ($x_{a,b,t_{end}}$) is considered equal to the inventory at the start of the next time horizon ($x_{a,b,0}$). This constraint is applied to the storage facilities and is generalized in the Equation (5.31) (Santibañez-Aguilar et al. 2014).

$$x_{a,b,t_{end}} = x_{a,b,0}, \quad \forall a\in\{R,P\}, b\in\{H,SP,C,MK\} \tag{5.31}$$

5.3.5. Objective: Maximize profit and social impact

The economic constraints define the associated operational cost of the superstructure and are present at various supply chain nodes. These costs include the cost associated with producing, transporting, and storing raw materials and products at various locations. The total production cost (J^P) consists of biomass production cost at different harvesting locations and the processing cost of the available biomass into valuable products at the processing plants, which is calculated using Equation (5.32).

$$J^P = \sum_r \sum_h \sum_t r^P_{r,h,t} pcr^P_{r,h,t} + \sum_{uc} \sum_r \sum_p \sum_i \sum_t rp^C_{uc,r,p,i,t} pc^C_{r,p,i,t} + \sum_{usp} \sum_r \sum_{sp} \sum_p \sum_i \sum_t rp^{SP}_{usp,r,sp,p,i,t} pc^{SP}_{r,sp,p,i,t} \tag{5.32}$$

The transportation cost (J^T) usually depends on the mode of transportation selected and the amount of material transported. The current model accounts for the cost due to the transportation of raw materials and products between various processing units, as given in the Equation (5.33) (Santibañez-Aguilar et al. 2014).

$$J^T = \sum_r \sum_h \sum_{sp} \sum_t ctr^{H\to SP}_{r,h,sp,t} r^{H\to SP}_{r,h,sp,t} + \sum_r \sum_h \sum_t ctr^{H\to C}_{r,h,t} r^{H\to C}_{r,h,t} + \sum_r \sum_{sp} \sum_t ctr^{SP\to C}_{r,sp,t} r^{SP\to C}_{r,sp,t} \sum_p \sum_{sp} \sum_{mk} \sum_t ctp^{SP\to MK}_{p,sp,mk,t} p^{SP\to MK}_{p,sp,mk,t} + \sum_p \sum_{sp} \sum_t ctp^{SP\to C}_{p,sp,t} p^{SP\to C}_{p,sp,t} + \sum_p \sum_{mk} \sum_t ctp^{C\to MK}_{p,mk,t} p^{C\to MK}_{p,mk,t} \tag{5.33}$$

The storage cost (J^S) is determined by using a variable operational cost for the storage of raw material or products at the production and distribution centers as given in Equation (5.34). The cost is proportional to the amount of storage required at any particular time period.

$$J^S = \sum_r \sum_h \sum_t csr^H_{r,h,t} r^H_{r,h,t} + \sum_r \sum_t csr^C_{r,t} r^C_{r,t} + \sum_r \sum_{sp} \sum_t csr^{SP}_{r,sp,t} r^{SP}_{r,sp,t} + \sum_p \sum_t csp^C_{p,t} p^C_{p,t} + \sum_p \sum_{sp} \sum_t csp^{SP}_{p,sp,t} p^{SP}_{p,sp,t} + \sum_p \sum_{mk} \sum_t csp^{MK}_{p,mk,t} p^{MK}_{p,mk,t} \tag{5.34}$$

The social impact (SI^H) of the model, determined using Equation (5.35), is quantified using the number of jobs generated from any particular process. The number of jobs generated at the harvesting location is mainly dependent on the amount of biomass produced and transported to various processing units.

$$SI^H = \sum_r \sum_h \sum_t e^R_{r,h} r^P_{r,h,t} + \sum_r \sum_h \sum_{sp} \sum_t e^{H\to SP}_{r,h,sp} r^{H\to SP}_{r,h,sp,t} + \sum_r \sum_h \sum_t e^{H\to C}_{r,h} r^{H\to C}_{r,h,t} \tag{5.35}$$

The number of jobs at the processing units is proportional to the quantity of raw material and product transported to various locations along with the quantity of raw material processed. The social impact at the main processing unit (SI^C) and the secondary processing unit (SI^{SP}) is determined using Equations (5.36) and (5.37) , respectively.

$$SI^C = \sum_p \sum_{mk} \sum_t e^{C\to MK}_{p,mk} p^{C\to MK}_{p,mk,t} + \sum_{uc} \sum_r \sum_p \sum_i \sum_t e^C_{r,p,i,t} rp^C_{uc,r,p,i,t} \tag{5.36}$$

$$\begin{aligned} SI^{SP} = & \sum_r \sum_{sp} \sum_t e^{SP\to C}_{r,sp} r^{SP\to C}_{r,sp,t} + \sum_p \sum_{sp} \sum_{mk} \sum_t e^{SP\to MK}_{p,sp,mk} p^{SP\to MK}_{p,sp,mk,t} \\ & + \sum_p \sum_{sp} \sum_t e^{SP\to C}_{p,sp} p^{SP\to C}_{p,sp,t} + \sum_{usp} \sum_r \sum_{sp} \sum_p \sum_i \sum_t e^{SP}_{r,sp,p,i,t} rp^{SP}_{usp,r,sp,p,i,t} \end{aligned} \tag{5.37}$$

The multi-unit biorefinery model is solved for optimal design and operational decisions corresponding to the selected objectives. The objectives demonstrate the economic and social benefits of the proposed strategy. The economic performance of the model is measured by determining the total profit over the available time period, which is the difference between the net revenue obtained from the products and the total involved cost. In this case, the total involved cost includes the cost of raw material, storage at various locations, transportation between various nodes, and the plant operational costs.

$$Profit = \sum_p \sum_{mk} \sum_t p^{sold}_{p,mk,t} sp^{sold}_{p,mk,t} - \left(J^P + J^T + J^S \right) \tag{5.38}$$

The model uses a second objective in terms of social impact by generating jobs and trying to deduce the relationship with economic performance. The cumulative effects at the harvesting (SI^H), main (SI^C) and secondary processing units (SI^{SP}) are maximized, which is understood to benefit the communities socially by generating higher employment.

$$SI = SI^H + SI^C + SI^{SP} \tag{5.39}$$

5.4. Case study of periodic distributed biorefineries

The proposed multi-unit strategy is tested on a case study of biofuel production in Mexico adapted from literature (Santibañez-Aguilar et al. 2014). The case study constitutes wood chips (r_1), sugar cane (r_2), corn (r_3), sorghum grain (r_4), sweet sorghum (r_5), African palm oil (r_6), jatropha (r_7), and safflower (r_8) as biomass. Six harvesting sites located at different geographical locations provide eight types of biomass. Biomass processing can be carried out using four processing technologies at one main processing unit and five secondary processing units. The main processing unit has a higher processing capacity with lower processing costs, considering the economics of scale.

The case study considers the production and distribution of ethanol and biodiesel among five markets over a 12-month time period. The details regarding the technologies and corresponding conversion factors for different products, bio-resource cost, transportation cost, processing cost, and product demand are available in Ponce-Ortega and Santibañez-Aguilar (2019 and are provided in Appendix D. The single objective multi-unit optimization model involves 20134 binary variables, 37928 continuous variables, and 59596 constraints considering three units per technology. The upper limit on maximum allowable processing units is decided using a sensitivity analysis and is given in later sections. The limits on various flow rates and processing capacities are considered as per the data available in the literature (Ponce-Ortega

and Santibañez-Aguilar 2019). The multi-objective model is solved using the ε-constraint method discussed in Mavrotas (2009). The multi-unit model is formulated using IBM ILOG CPLEX Optimization Studio V12.8.0 and solved using the CPLEX solver with default settings. Each determined Pareto point took an average of 2.01 seconds using a 4.20 GHz i7-7700K processor with 32 GB of RAM.

5.5. Results and discussion

This section analyses the benefits of the multi-unit strategy by first considering the objectives individually. The trade-off between profit and social impact is discussed in the multi-objective section. A sensitivity analysis corresponding to the effects of varying demand and number of processing units on the multi-unit model is also presented to demonstrate the features of the proposed model.

5.5.1. Single objective analysis

The production restriction can be improved by implementing multiple units, which significantly helps produce more profitable products. The total product sold and corresponding profit are given in Table 5.1. Using the proposed strategy has increased ethanol production and increased profit by 4.73 %. Biodiesel production remains similar to the single-unit strategy, indicating a saturation limit in the production and thus cannot provide any additional economic benefits.

The multi-unit strategy also helps in increasing the processing of additional biomass, such as woodchips, in the current case study. Even though the multi-unit strategy has the provision of processing a higher amount of biomass, the processing of the other types of biomass in Table 5.1 remains unchanged for both single and multi-unit strategies. This is mainly due to reaching the breakeven point of sorghum grain and African palm oil, where any further processing does not contribute to the profit and leads to losses. Such a scenario is due to the unavailability of

jatropha for further processing. A unit increase in the use of sorghum grain leads to a loss of $2/year; however, a loss of $7305/year is observed per unit increase in the use of African palm. This large deviation of losses per unit increase of raw materials is due to the change in the optimal solution structure, forcing the structure to reroute the processing. The higher breakeven point of woodchips could be identified using the multi-unit strategy and the assistance in the increment of profit.

Table 5.1 Annual raw material processed, product sold, and profit

		Single unit	Multi-Unit
Raw material processed (tonne/year)	Wood Chips (Gasification and Biosynthesis)	105684.5	**108995.3**
	Sorghum grain (Pre-treatment, acid hydrolysis, and fermentation)	2172738	2172738
	African Palm oil (Extraction and trans-esterification with methanol)	73548	73548
	Jatropha (Extraction and trans-esterification with methanol)	1059600	1059600
Product (tonne/year)	Ethanol	679346.4	**680215.4**
	Biodiesel	361457.6	361457.6
Profit ($/year)		60552782	**63417058**

The breakeven point for the current case study solely depends on the availability of jatropha. Any increase in its availability will change the solution structure and the maximum profitable quantities of the other raw materials. The benefits of economies of scale can be observed from Fig. 5.2, where the higher capacity main processing unit is supplied with the majority of the processing task. Although the maximum profitable use of the jatropha is achieved in the single unit case, the additional units in the main processing unit help restructure the transportation and processing strategy of the superstructure.

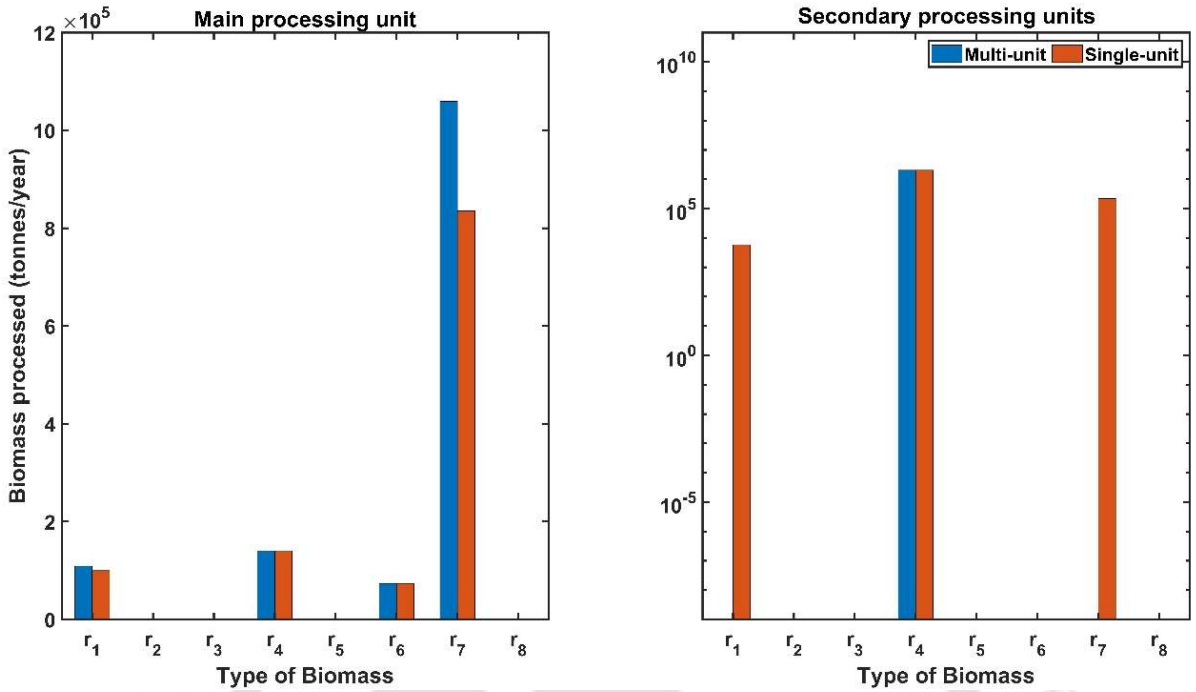

Fig. 5.2 Biomass processing contribution of the main and secondary processing units

The main processing unit is of higher capacity and can process the biomass with lower processing costs using economies of scale. Hence, the processing of jatropha and woodchips has been moved entirely to the main processing unit. The contribution of various processing plants towards the produced products using single-unit and multi-unit strategies is depicted in Fig. 5.3.

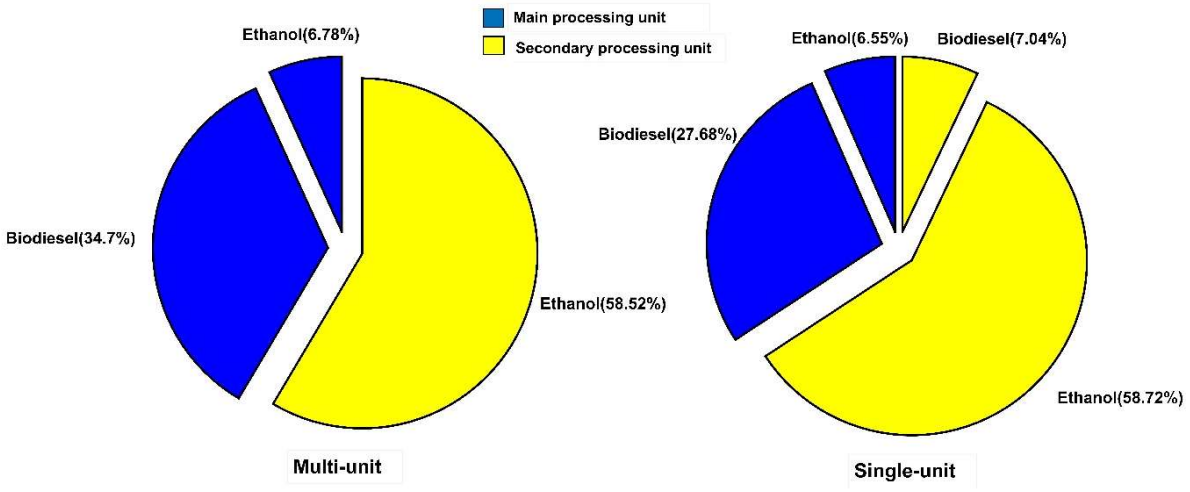

Fig. 5.3 Product contribution from the processing units

In the single-unit production strategy, each product was produced at both types of processing plants, whereas in the proposed strategy, only ethanol production is carried out at the secondary processing units. The total production share of the secondary processing unit is reduced to 58.52 % from 65.76 %. At the same time, the share of the main processing unit increased from 34.23 % to 41.48 %. The significant reduction is in biodiesel production in the secondary processing units, as the total biodiesel is sourced from the main processing unit using the multi-unit strategy.

A pictorial representation of the solution for maximum profit using the multi-unit strategy is given in Fig. 5.4 (a). The optimal solution utilizes four of six harvesting locations and one of five secondary processing units. Each selected harvesting location sends biomass to the main processing unit, whereas only the third harvesting location is responsible for the biomass at the secondary processing unit. The secondary processing unit and the main processing unit use multiple processing units to process the received biomass.

It has to be noted that the main plant received biomass from the secondary processing unit as the storage capacity of the main processing unit also restricts the maximum available raw material at any point in time. In order to use the cheaper processing facility, additional biomass is stored and procured from the secondary processing units. The transportation of a certain quantity of ethanol from the secondary processing units to the markets through the main processing unit is observed to benefit from cheaper transportation. The detailed solution obtained for the maximization of profit case is given in Appendix D. The social impact focuses on generating the maximum number of jobs distributed over various nodes of the superstructure. The maximization of this objective is highlighted using three observations, as given in Table 5.2.

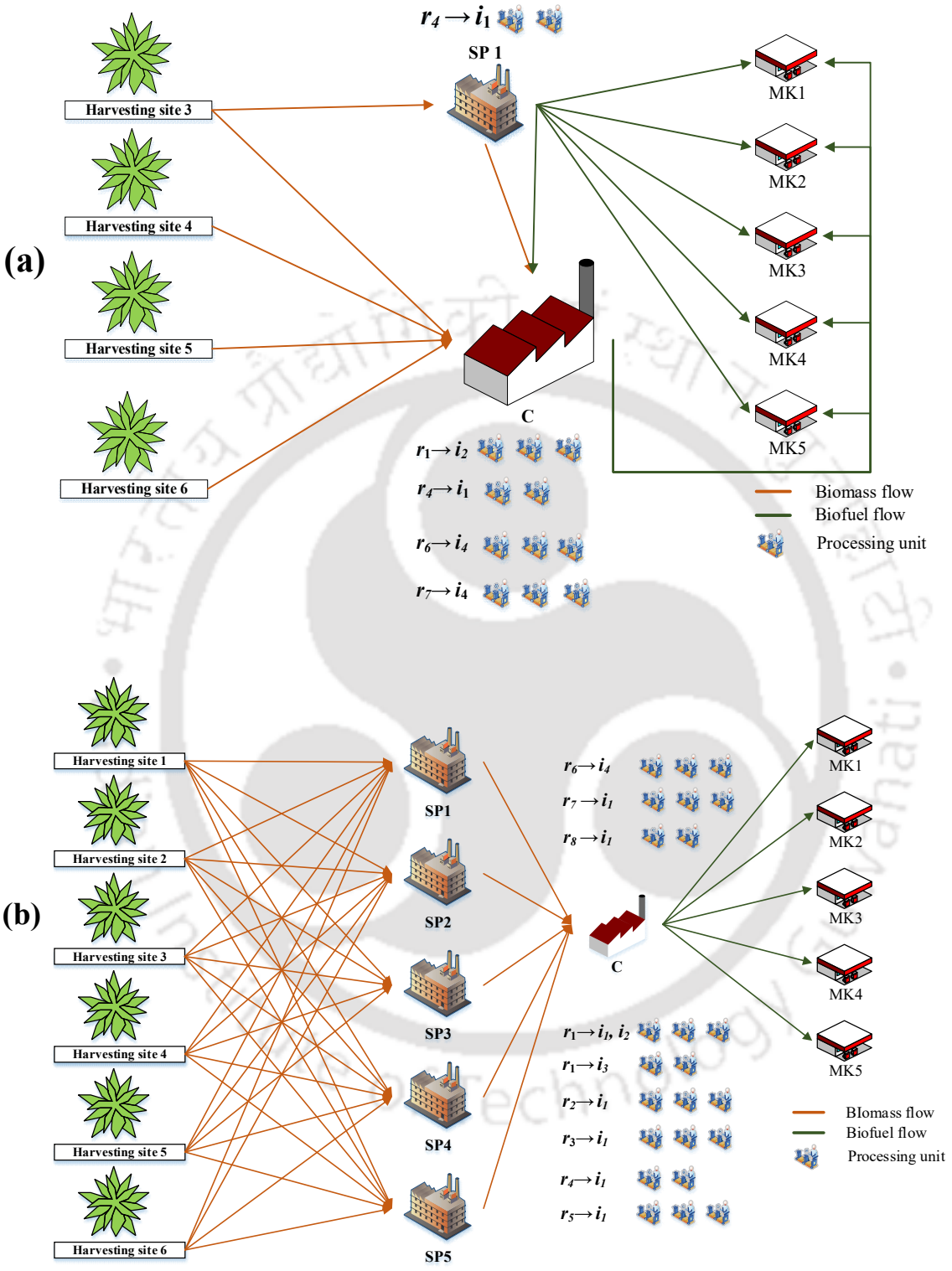

Fig. 5.4. Multi-unit solution for (a) Maximum profit (b) Maximum SI

The emphasis on only job creation leads to a negative profit as the solution tries to create maximum employability through producing and transporting biomass and biofuel, irrespective

of the profits. The solution structure for the maximize SI case is provided in Fig. 5.4 (b). The solution accepts the maximum available biomass from all the harvesting locations and processes at the main processing unit. Instead of accepting the biomass directly from the harvesting locations, procurement is done through the secondary processing unit, which helps provide additional storage capacity and job opportunities in the transportation sector.

Table 5.2. Number of jobs generated (jobs/year)

Objective		Biomass production	Transportation	Processing
Maximize SI	Single unit	391629	96257	39274
	Multi-unit	391629	**96632**	**39287**
Maximize Profit	Single unit	371	2035	2699
	Multi-unit	**372**	**2110**	**2701**
Maximize SI, nonnegative profit	Single-unit	17758	4159	4685
	Multi-unit	**18420**	**4324**	**4737**

The second observation demonstrates the number of jobs generated from the model for the maximum profit case while using the multi-unit strategy. The increase in biomass processing capacity also increases biomass production at the harvesting locations for the proposed approach. An additionally produced biomass generates additional jobs at all the important nodes capable of influencing the social impact. The last observation is based on the case where the model generates maximum jobs without incurring any losses. The total number of jobs generated using the nonnegative profit constraint is significantly higher than the maximum profit case. It is due to biasing the superstructure for only profitable production and distribution of both biomass and products, which in turn limits the number of jobs generated.

5.5.2. Multi-objective analysis

The association of social impact on the profit of the model using both the single-unit and multi-unit strategy is shown in Fig. 5.5. The behavior of the two objectives is summarized using two

relations. The initial generation of jobs varies directly with the profit, where the rate of change of profit with respect to the number of jobs generated is significantly higher.

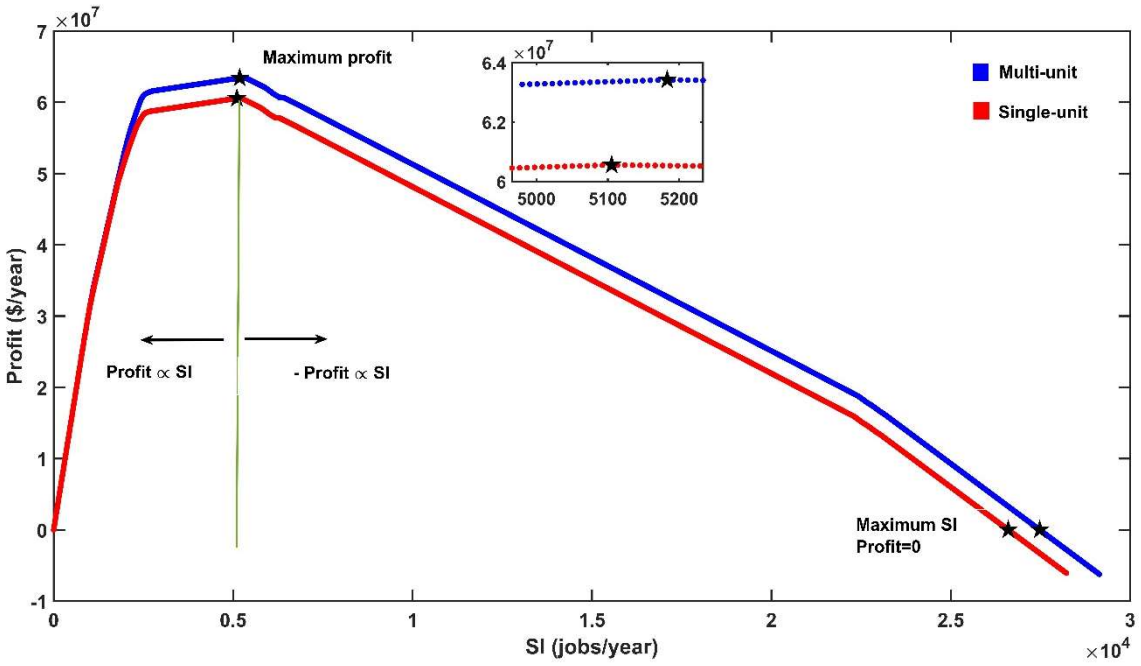

Fig. 5.5. Relation between profit and social impact

An inflection point in the curve can be observed at the maximum profit, where any further increase in the number of jobs decreases the profit. It validates the observation obtained in the single objective case considering the maximization of social impact. Implementing the multi-unit strategy helps achieve better profit and the number of generated jobs in each obtained solution. A notable difference can be observed once the multi-unit strategy surpasses the single-unit restrictions in the production and distribution of biomass and biofuel.

Table 5.3. Selected Pareto points for maximum profit vs maximum social impact

Maximize profit ($/year)	Maximize SI (jobs/year)
6.34E+07	5.18E+03
-2.85E+10	**5.27E+05**
0	2.74E+04

Table 5.3 provides three major Pareto points of the case study, where the first two points are the extreme objectives that correspond to each of the objectives. The third point unveils the decisive point of social impact on decision-makers when negotiating between employment and annual profit.

5.5.3. Effect of number of processing units and demand variation

The installation of multiple units can be restricted by the investment budget or by reaching the optimal processing capacity of the superstructure. Investors and government policies mainly influence the restriction on the budget. On the other hand, once the profit is stagnant, the addition of multiple units does not affect the optimal conditions of the superstructure unless any external disturbance is attributed. The effect of multiple processing units on the total annual profit is given in Table 5.4. The use of more than three processing units for the superstructure does not provide any economic benefit to the model, even with surplus raw material and unsatisfied total demand. Using multiple processing units across various processing centers increases their processing capacity and helps satisfy additional demand. The effect of demand variation on the multi-unit model is shown in Fig. 5.6.

Table 5.4. Effect of the number of processing units on profit and social impact

Maximum units	Profit ($/year)	SI (jobs/year)	% Improvement (profit)
1	60552782	5105	-
2	63415343	5189	4.727
3	63417058	5183	0.003
4	63417058	5183	-
5	63417058	5183	-

The actual product demand is varied between 50% to 150%, and the corresponding profit from the single and multi-unit models is analyzed. The increase in demand from 50% increases the profit in both the single-unit and the multi-unit model. However, any increase in demand above

the actual demand, i.e., 100%, does not benefit the single-unit model due to the restriction of the capacity constraints at various processing centers. The demand below the actual demand helps the multi-unit model due to the economics of scale, and the products are processed using cheaper processing costs at the main processing units. The profit increment by varying the demand from 50% to 150% of the actual demand is observed to be from 3.96% to 4.76%, respectively.

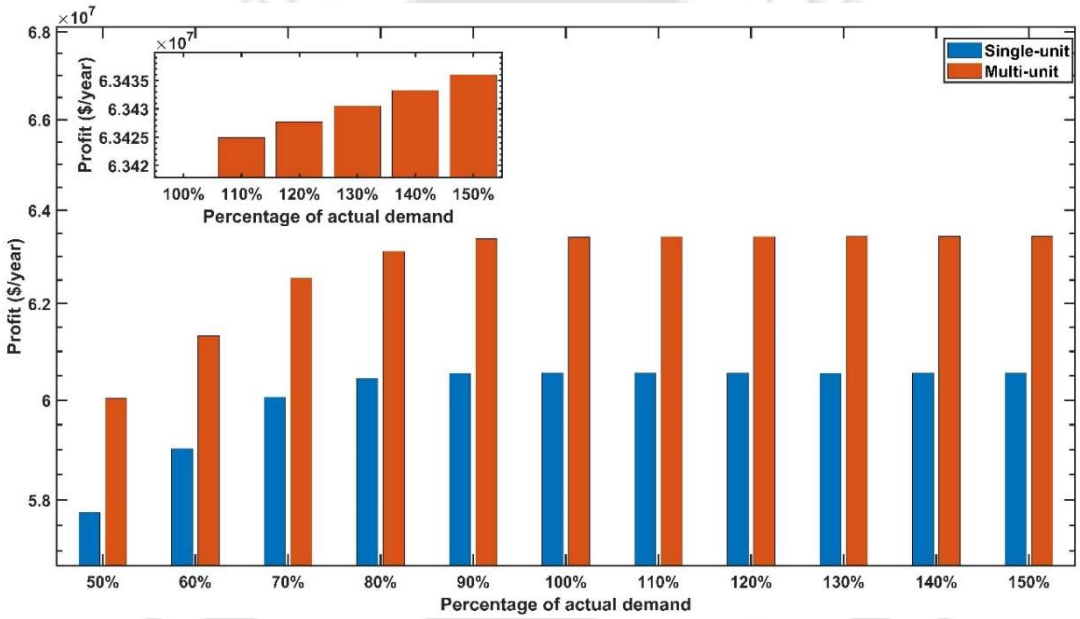

Fig. 5.6. Effect of demand variation on profit

5.6. Conclusion

The choice of processing technologies and their processing capacity plays a crucial role in achieving optimal benefits in the bioenergy supply chain. This chapter addresses the lacuna in the capacity planning of biorefineries by proposing a multi-unit model that allows the implementation of multiple profitable process units at the biorefineries. The efficacy of the model is demonstrated in a case study with economic and social objectives. The proposed multi-unit, multi-period biorefinery superstructure model determines optimal decisions related to the location of the harvesting sites and processing plants, selection of processing

technologies, capacity planning for processing plants, and material distribution for the supply chain network. The model is able to increase the economic and social benefits over the literature by employing multiple units of profitable processing technologies at the main and secondary processing units. The single objective studies of the model have provided valuable insights into the effect of plant capacity on superstructure design and breakeven analysis of the raw materials towards the economic performance of the overall network. The multi-objective study has identified multiple observations regarding the relationship between total profit and the number of jobs generated. The study also identified the regions where the profit exhibits a dual relationship with the number of jobs. The multi-unit model has improved the profit by 4.73% and has generated 78 additional jobs in the analysis performed over 12 months.

Chapter 6

An optimization framework using metaheuristic techniques for solar air collectors

This chapter proposes a framework using metaheuristic techniques for exergetic optimization of simple and finned flat plate solar air collectors that determines the optimal design and operational parameters for humid subtropical climatic conditions. A comprehensive optical, energy and exergy analysis is carried out to evaluate the performance, energy, and exergetic efficiency of simple and finned flat plate solar air collectors under humid subtropical climatic conditions. The proposed model is optimized using computational intelligence technique for maximum mean exergy efficiency in simple and finned solar air collectors.

The literature review for the study is discussed in Section 6.1, revealing the application of metaheuristics on solar energy models and their challenges. A detailed model of the solar air collectors considered in this chapter is provided in Section 6.2. Section 6.3 provides a detailed mathematical model and the general metaheuristic approach to optimize the model. Section 6.4 of this chapter explains the proposed solution strategy to improve the performance of metaheuristic techniques and briefly highlights the features of the selected algorithms. The problem description and the results are discussed in Sections 6.5 and 6.6, respectively. The chapter concludes by summarising the benefits of the proposed formulation.

6.1. Background

The performance of solar collectors is significantly dependent on their geometrical optical and operational parameters, and optimization is the only method to find the best controlling parameters that will yield the best-performing efficiency. Ajam et al., (2005) performed exergetic optimization of simple solar air heaters and compared it with the energy analysis and

concluded that exergy analysis has a larger impact when compared to energy analysis for optimization and design purposes. Luminosu & Fara, (2005) optimized operational conditions based on exergy analysis for a serpentine flat plate collector and presented optimal area and mass flow rate for maximum energy and exergy efficiency for the place of interest. Shojaeizadeh et al., (2015) performed exergy efficiency optimization for a nanofluid-based flat-plate solar collector. The optimization was performed using the interior point technique with mass flow rate, inlet fluid temperature, nanoparticle volume concentration, and solar radiation as independent parameters. Hedayatizadeh et al., (2016) performed exergy loss-based efficiency optimization for v-corrugated double-pass solar air heater. The maximum exergy efficiency was found by varying the distance between the two adjacent glazings, corrugation height, heater area, and mass flow rate. It was shown that the exergy loss due to the temperature difference between the sun and absorber plays the most important role, and the other terms remain insignificant. Debnath et al., (2019) used a fuzzy logic-based expert system (FLES) to determine the thermal performance of a corrugated plate solar air collector. The use of the FLES model was observed to provide high accuracy against the experimental data. The use of transparent insulation material for performance improvement was studied by Ammar et al., (2021). Reddy et al., (2021) used a sand-coated absorber to enhance the outlet temperature and thermal efficiency of solar collectors.

Designing solar collectors requires in-depth studies of governing concepts and parameters that affect the operational condition and assembly process. Advanced solution techniques for solving solar models are a common practice. Computational Intelligence (CI) techniques, which do not require any gradient information, are generally used for problems of complex nature. When compared to deterministic techniques, CI techniques are able to handle nonlinear

equations easily and are used extensively in solar collector models. Kim et al., (2016) solved an integrated solar thermal energy model with multiple objectives using the genetic algorithm. The multi-objective model optimized five objective functions using the type of storage, type of collectors, and slope of the collectors as decision variables. The model was constrained by the rooftop length and width along with budget and annual heat generation requirements. Yıldırım & Aydoğdu, (2017) optimized thermo-hydraulic efficiency based on channel depth and air mass flow rate as design and operational variables for single-pass and double-pass solar air heater under steady-state conditions.

Despite the performance and wide usage of solar collectors depending on the optimum design and operational parameters, there have been minimal insights available in the literature. For example, previous literature (Siddhartha et al., 2012; Varun et al., 2011; Varun & Siddhartha, 2010) considered various approximations in the heat transfer processes of the system, such as the side loss coefficient of the solar collector is negligible, the top loss coefficient depends on the constant wind convection coefficient, the efficiency factor does not account for radiation loss coefficient, and the collector removal factor refers to the outlet temperature, etc. Previous studies (Ajam et al., 2005) have mainly focused on identifying the objective function of the problem with its constraints, but they did not address the problem of the upper/lower bounds on decision variables. The lack of proper optimization problem formulation, details on decision variables, constraints parameters, optimization algorithms, defined parameters, etc., in previous literature have been addressed in this chapter. It is also to be noted that Jawaharlal Nehru National Solar Mission of the Ministry of New and Renewable Energy, Government of India, has identified Guwahati city (humid subtropical climatic conditions) as a solar city among 60 identified cities to be developed as a solar city under the mission. Due to the

favorable humid subtropical climate conditions, the possibility of implementing solar air heating collectors for conversion of solar energy into heat using actual hourly data over a year is also a subject of research effort in this chapter, exhibiting significant possibility for space heating, running irrigation, greenhouses, and grain drying in agricultural fields. In order to identify optimum design and operational parameters for the preliminary stages of design of simple conventional air collectors and finned air collectors for humid subtropical climatic conditions, maximizing exergetic efficiency was identified as the objective function for optimization without cost minimization. In this chapter, simple and finned solar air collectors (cases 1 and 2) are optimized using a CI technique by incorporating the shortcomings discussed in the previous literature and are analyzed for the effects of various design and operational parameters on their performance. The major objectives of the current study are summarized as follows: (i) Literature gap related to optimization problem formulation is presented by providing crucial details related to the bounds of the decision variables, constraints, optimization algorithm, and related parameters (ii) Simple and finned type solar air collector models for humid subtropical climatic conditions are proposed (iii) Feasibility of using solar air collectors for conversion of solar energy into heat for Guwahati, India (identified as a solar city by Ministry of New and Renewable Energy, Government of India) is analyzed and (iv) Optimization of proposed solar air collector models for maximum exergy efficiency using CI technique and determination of optimal design and operational parameters are addressed.

Nomenclature

a	Constant
a_1	Constant
A_p	Area of absorber plate (m^2)
A_{flow}	Fluid flow area (m^2)
b_1	Constant
b	Constant
C_1, C_2, C_3	Constraints on the optimization model
C_p	Specific heat of fluid (kJ/kg K)
c_{p-a}	Specific heat of air (kJ/kg K)
D_e	Equivalent diameter of the channel (m)
$\dot{E}_d$	Destroyed exergy rate (kJ)
$\dot{E}_{in}$	Inlet exergy rate (kJ)
$\dot{E}_l$	Leakage exergy rate (kJ)
E_l	Elevation of Guwahati, India (kms)
$\dot{E}_{out}$	Outlet exergy rate (kJ)
$\dot{E}_s$	Stored exergy rate (kJ)
$\dot{E}_{d,\Delta T_f}$	Exergy rate due to temperature difference between the plate and working fluid (kJ)
$\dot{E}_{d,\Delta P}$	Exergy rate due to pressure drop due to friction in the flow channel (kJ)
$\dot{E}_{d,\Delta T_s}$	Exergy rate due to temperature difference between the plate and the sun (kJ)
$\dot{E}_{in,Q}$	Absorbed solar radiation exergy rate by the heater (kJ)
$\dot{E}_{in,f}$	Inlet exergy rate with fluid flow (kJ)
$\dot{E}_{out,f}$	Outlet exergy rate with fluid flow (kJ)
F_R	Heat removal factor
F'	Collector efficiency factor
h_e	Effective heat transfer coefficient (W/m^2 K)
h_i	Convective heat transfer coefficient inside the channel(W/m^2 K)
h_r	Equivalent radiative heat transfer coefficient (W/m^2 K)
h_w	Heat transfer coefficient between first cover and surrounding air (W/m^2 K)

h_{fp}	Heat transfer coefficient between working fluid and absorber plate (W/m^2 K)
h_{fb}	Heat transfer coefficient between working fluid and bottom plate (W/m^2 K)
$h_{c_1-c_2}$	Heat transfer coefficient between first and second glass cover (W/m^2 K)
$h_{c_1-c_2}$	Heat transfer coefficient between first and second glass covers (W/m^2 K)
h_{p-c_1}	Heat transfer coefficient between absorber plate and first cover (W/m^2 K)
h_{f-fin}	Heat transfer coefficient between working fluid and fin(W/m^2 K)
$\overline{H}_o$	Monthly average of the daily extra-terrestrial on a horizontal surface radiation (W/m^2)
$\overline{H}_d$	Monthly average of the daily diffuse radiation (W/m^2)
$\overline{H}_g$	Monthly average of the daily global radiation on a horizontal surface (W/m^2)
I_T	Flux incident on the absorber plate (W/m^2)
$\overline{I}_b$	Monthly average of the hourly beam radiation (W/m^2)
$\overline{I}_d$	Monthly average of the hourly diffuse radiation on a horizontal surface (W/m^2)
$\overline{I}_g$	Monthly average of the hourly global radiation on a horizontal surface (W/m^2)
$\overline{I}_o$	Monthly average of the hourly extra-terrestrial radiation on a horizontal surface (W/m^2)
j	j factor
k_i	Thermal conductivity of the insulation (W/m K)
L	Depth of the channel (m)
L_1	Absorber plate length (m)
L_2	Absorber plate width (m)
L_3	Height of the collector (m)
L_a	Latitude of Guwahati, India (^{o})
L_{fin}	Fin height (m)
$\dot{m}$	Mass flow rate (kg/s)
Nu	Nusselt number
P_a	Atmospheric pressure (Pa)
P_{in}	Fluid inlet pressure (Pa)
P_{out}	Fluid outlet pressure (Pa)
ΔP	Pressure drop due to fluid friction (Pa)
Pr	Prandtl number

q_t	Heat loss from the top (W/ m^2)
q_L	Overall heat loss (W/ m^2)
Q_u	Useful heat gain (W)
r_b	Tilt factor for beam radiation
r_d	Tilt factor for diffuse radiation
r_r	Tilt factor for reflected radiation
R	Universal Gas constant (kJ/kg K)
Ra	Rayleigh number
Re	Reynolds number
S	Absorbed radiation flux by the absorber plate (W/m^2)
$\overline{SH}$	Monthly average of the sunshine hours per day (hr)
$\overline{SH}_{max}$	Monthly average of the maximum possible sunshine hours per day (hr)
T_a	Ambient temperature (K)
T_p	Temperature of absorber plate (K)
T_{fm}	Mean fluid temperature (K)
T_s	Temperature of Sun (K)
T_{C_1}	Temperature of first glass cover (K)
T_{C_2}	Temperature of second glass cover (K)
T_b	Temperature of bottom plate (K)
T_{out}	Outlet fluid temperature (K)
T_{in}	Inlet fluid temperature (K)
T_{av}	Average temperature (K)
T_{sky}	Temperature of sky (K)
U_b	Bottom heat loss coefficient (W/m^2 K)
U_s	Side heat loss coefficient (W/m^2 K)
U_l	Overall heat loss coefficient (W/m^2 K)
U_t	Top heat loss coefficient of (W/m^2 K)
V_{wind}	Wind velocity (m/s)
V_{av}	Average velocity of fluid (m/s)
W	Center to center distance between two fins (m)

α_p	Absorptivity of plate
β	Tilt angle (°)
δ_b	Thickness of the back insulation (m)
δ_s	Thickness of the side insulation (m)
δ_1	Distance between the absorber plate and the first glass cover (m)
δ_2	Distance between the first glass cover and the second glass cover (m)
ε_p	Emissivity of absorber plate
ε_c	Emissivity of the covers
ε_b	Emissivity of bottom plate
φ_{fin}	Fin effectiveness
η_o	Optical efficiency (%)
η_{th}	Thermal efficiency (%)
η_{ex}	Exergy efficiency (%)
μ	Fluid viscosity at the bulk fluid temperature (kg/ms)
μ_w	fluid viscosity at the heat-transfer boundary surface temperature (kg/ms)
ρ_d	Diffusive reflectivity of the cover system
ρ	Density of fluid (kg/m^3)
σ	Stefan–Boltzmann constant (W/m^2 K^4)
$\tau\alpha$	Transmissivity absorptivity factor
$(\tau\alpha)_b$	Transmissivity absorptivity factor based on beam radiation
$(\tau\alpha)_d$	Transmissivity absorptivity factor based on diffuse radiation
τ_a	Absorptivity losses
$(\tau\alpha)_p$	Transmissivity absorptivity factor of absorber plate
τ_r	Reflectivity losses
ω	Hour angle at sunrise or sunset (°)
ω_s	Hour angle at sunrise or sunset (°)

6.2. Mathematical modeling and simulation

The mathematical model presented in this chapter considers the optical, energy, and exergy analysis of solar air collectors. The schematic diagram detailing the energy flow in the solar air collectors is provided in Fig. 6.1.

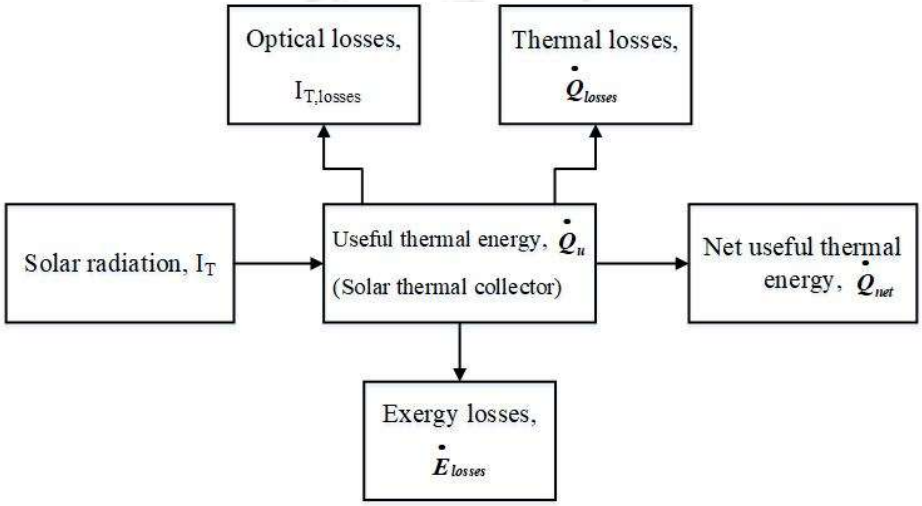

Fig. 6.1. Schematic diagram of the energy flow in the solar air collectors

6.2.1. Optical and energy analysis

The optical efficiency (η_o) of the system relates to the total falling flux on the system (I_T) and the total absorbed flux by the system (S) using the Equation (6.1) (Ajam et al., 2005):

$$S=\eta_o I_T \tag{6.1}$$

Energy analysis

An energy balance on the working fluid of the collectors at steady-state gives the useful heat gain of the system as provided in Equations (6.2) and (6.3),

$$Q_u=\dot{m}C_p\left(T_{out}-T_{in}\right) \tag{6.2}$$

$$\dot{m}=\rho V_{av}A_{flow} \tag{6.3}$$

The flow area for simple and finned air collectors is given in Equations (6.5).

$$A_{flow} = LL_2 \tag{6.4}$$

$$A_{flow} = LL_2 - \frac{L_2}{W} LFin_{fraction}\delta_f \tag{6.5}$$

The useful energy output of the collectors obtained by Equation (6.6) (Ajam et al., 2005),

$$Q_u = A_p S - U_l A_p \left(T_p - T_a\right) \tag{6.6}$$

The collector gains the maximum possible useful energy as a result of minimum possible losses at the surroundings if the whole collector is at the inlet fluid temperature. This maximum possible useful energy, when multiplied by the heat removal factor (F_R), gives the useful heat energy as given in Equation (6.7) (Ajam et al., 2005). The heat removal factor is calculated using Equation (6.8).

$$Q_u = A_p F_R \left[S - U_l \left(T_{in} - T_a\right)\right] \tag{6.7}$$

$$F_R = \frac{\dot{m}C_p}{U_l A_p}\left[1 - exp\left\{-\frac{F' U_l A_p}{\dot{m}C_p}\right\}\right] \tag{6.8}$$

Where F' is the collector efficiency factor and is given by Equation (6.9),

$$F' = \left(1 + \frac{U_l}{h_e}\right)^{-1} \tag{6.9}$$

For a simple air heater, h_e is given in Equation (6.10) (Sukhatme, 1984),

$$h_e = \left[h_{fp} + \frac{h_r h_{fb}}{\left(h_r + h_{fb}\right)}\right] \tag{6.10}$$

$$h_{fp} = h_{fb} = Nu\, k_f / D_e \tag{6.11}$$

When there are metallic fins inside the fluid flow path, the heat transfer coefficient between fins and fluid is also considered while calculating the heat transfer coefficient (Sukhatme, 1984), and it can be written as in Equation (6.12),

$$h_e = \left[h_{fp} \left(1 + \frac{2L_{fin}\varphi_{fin}h_{f-fin}}{Wh_{fp}} \right) + \frac{h_r h_{fb}}{\left(h_r + h_{fb}\right)} \right] \tag{6.12}$$

$$\varphi_{fin} = \frac{tanh\left(L_f \sqrt{2h_{f-fin} / \left(k_{fin}\delta_f\right)} \right)}{L_f \sqrt{2h_{f-fin} / \left(k_{fin}\delta_f\right)}} \tag{6.13}$$

$$h_{f-fin} = Nu\, k_f / D_e \tag{6.14}$$

Hence, the energy efficiency of the system can be written as,

$$\eta_{th} = \frac{Q_u}{I_T A_P} \tag{6.15}$$

6.2.2. Exergy Analysis:

As discussed above, the second law analysis can predict the performance of the collectors more accurately than the first law analysis. The analysis, which is carried out considering the inlet, outlet, stored, leaked, and destroyed exergy over solar air collectors and ambient as a reference, gives the exergy balance equation given in Equation (6.16) (Ajam et al., 2005):

$$\dot{E}_{in} + \dot{E}_{out} + \dot{E}_s + \dot{E}_l + \dot{E}_d = 0 \tag{6.16}$$

The term, rate of exergy inlet to the system, arises due to the fluid flow and the solar radiation absorbed by the collectors and are calculated as Equation (6.17) (Ajam et al., 2005):

$$\dot{E}_{in,f} = \dot{m}C_p \left(T_{in} - T_a - T_a\, ln\left(\frac{T_{in}}{T_a} \right) \right) + \dot{m}RT_a\, ln\left(\frac{P_{in}}{P_a} \right) \tag{6.17}$$

$$\dot{E}_{in,Q} = \eta_o I_T A_p \left(1 - \frac{T_a}{T_s} \right) \tag{6.18}$$

The next term, rate of exergy outlet, is caused by outlet fluid flow and is given as in Equation (6.19) (Ajam et al., 2005):

$$\dot{E}_{out,f} = -\dot{m}C_p\left(T_{out} - T_a - T_a\, ln\left(\frac{T_{out}}{T_a}\right)\right) - \dot{m}RT_a\, ln\left(\frac{P_{out}}{P_a}\right) \tag{6.19}$$

The term stored exergy rate vanishes during the steady-state analysis of the system as there is no accumulation of energy in the system. The leakage of exergy is due to the overall losses from the system because of convection and radiation and can be written as Equation (6.20) (Ajam et al., 2005):

$$\dot{E}_l = -U_l A_p \left(T_p - T_a\right)\left(1 - \frac{T_a}{T_p}\right) \tag{6.20}$$

Heat transfer arises due to temperature differences, and the pressure drop due to friction in the flow channel causes the destruction of exergy. The destroyed exergy term due to the temperature difference between the plate and sun is given as Equation (6.21) (Ajam et al., 2005),

$$\dot{E}_{d,\Delta T_s} = -\eta_o I_T A_p T_a \left(\frac{1}{T_p} - \frac{1}{T_s}\right) \tag{6.21}$$

The term due to temperature difference between the plate and the working fluid is given as Equation (6.22) (Ajam et al., 2005):

$$\dot{E}_{d,\Delta T_f} = -\eta_{th} I_T A_p T_a \left(\frac{1}{T_{fm}} - \frac{1}{T_p}\right) \tag{6.22}$$

The friction in the flow channel causes a pressure drop, and thus, the exergy destroyed is given as Equation (6.23) (Ajam et al., 2005; Sukhatme, 1984):

$$\begin{aligned} \dot{E}_{d,\Delta P} &= -\frac{\dot{m}\Delta P T_a}{\rho T_{fm}} \\ \Delta p &= \frac{4F_r \rho L_1 V_{av}^2}{2D_e} \end{aligned} \tag{6.23}$$

$$F_r = M\ Re^{-m}$$

$$m = \begin{cases} 0.075\left(3.4 - \dfrac{(L-L_f)}{L_f}\right)^{0.711} & if\ Re<15000 \\ 0.138\left(1.435 - \dfrac{(L-L_f)}{L_f}\right)^{0.773} & otherwise \end{cases} \qquad (6.24)$$

$$M = \begin{cases} 0.040\left(2.058 - \dfrac{(L-L_f)}{L_f}\right)^{0.313} & if\ Re<15000 \\ 0.033\left(1.394 - \dfrac{(L-L_f)}{L_f}\right)^{0.408} & otherwise \end{cases}$$

The exergetic efficiency of the whole system can be written as Equation (6.25) and can be found out based on the Equations (6.16) − (6.24) stated above.

$$\eta_{ex} = \frac{\dot{m}C_p\left(T_{out} - T_{in} - T_a\, ln\left(\frac{T_{out}}{T_{in}}\right)\right)}{I_T A_p\left(1-\frac{T_a}{T_s}\right)} - \frac{\dot{m}RT_a\, ln\left(\frac{P_{out}}{P_{in}}\right)}{I_T A_p\left(1-\frac{T_a}{T_s}\right)}$$

$$= 1 - \left\{(1-\eta_o) + \frac{\dot{m}\Delta P T_a}{\rho T_{fm} I_T A_p\left(1-\frac{T_a}{T_s}\right)} + \frac{\eta_o T_a}{\left(1-\frac{T_a}{T_s}\right)}\left(\frac{1}{T_p} - \frac{1}{T_s}\right) + \frac{U_l\left(T_p - T_a\right)}{I_T\left(1-\frac{T_a}{T_s}\right)}\left(1-\frac{T_a}{T_p}\right) + \eta_{th} T_a \frac{\left(\frac{1}{T_{fm}} - \frac{1}{T_p}\right)}{\left(1-\frac{T_a}{T_s}\right)}\right\} \qquad (6.25)$$

6.2.3. Calculation of overall heat loss coefficient and heat transfer coefficients

The overall heat loss coefficient (U_l), as mentioned in Equations (6.6) − (6.9) is the summation of top, bottom, and side loss coefficients and is given as Equation (6.26),

$$U_l = U_t + U_b + U_s \qquad (6.26)$$

The heat losses from the top are the radiation and convection losses from the glass covers and the absorber plate to the surrounding air and are given by the following equations (Sukhatme, 1984):

$$\frac{q_t}{A_p}=h_{p-c1}\left(T_p-T_{c1}\right)+\frac{\sigma\left(T_p^4-T_{c1}^4\right)}{\left(\frac{1}{\varepsilon_p}+\frac{1}{\varepsilon_c}-1\right)} \tag{6.27}$$

$$\frac{q_t}{A_p}=h_{c1-c2}\left(T_{c1}-T_{c2}\right)+\frac{\sigma\left(T_{c1}^4-T_{c2}^4\right)}{\left(\frac{1}{\varepsilon_c}+\frac{1}{\varepsilon_c}-1\right)} \tag{6.28}$$

$$\frac{q_t}{A_p}=h_w(T_{c_2}-T_a)+\sigma\varepsilon_c(T_{c_2}^4-T_{sky}^4) \tag{6.29}$$

$$h_{p-c1}=\frac{Nuk_a}{\delta_1} \tag{6.30}$$

$$h_{c1-c2}=\frac{Nuk_a}{\delta_2} \tag{6.31}$$

$$T_{sky}=T_a-6 \tag{6.32}$$

The series of resistances to heat losses from the top can be represented with a single term, U_t, known as the top loss coefficient and heat loss from the top can be written as Equation (6.33)

$$\frac{q_t}{A_p}=U_t(T_p-T_a) \tag{6.33}$$

The bottom loss and side loss coefficients can be calculated by following relations:

$$U_b=\frac{k_i}{\delta_b} \tag{6.34}$$

$$U_s=\frac{\left(L_1+L_2\right)L_3k_i}{L_1L_2\delta_s} \tag{6.35}$$

$$L_3 = \delta_1 + \delta_2 + L + \delta_b \tag{6.36}$$

The Equations (6.26) − (6.36) can be solved to find out Q_u, U_l, T_p, T_{c1} and T_{c2}.

Convection heat transfer during fluid flow

The heat transfer coefficient between the fluid and top and bottom plates can be calculated for simple air heater configuration from the following correlation (Sukhatme, 1984):

$$Nu = 0.0158\, Re^{0.8} \tag{6.37}$$

In the case of solar air heater with fins, the heat transfer coefficient can be calculated using the following correlations, based on Reynold's Number (Naphon, 2005)

(a) The Nusselt number correlation for the laminar region ($Re < 2300$) is given as follows

$$Nu = \frac{h_i D_e}{k_f} = 5.4 + \frac{0.00190(Re\, Pr(D_e / L_1))^{1.71}}{1 + 0.00563(Re\, Pr(D_e / L_1))^{1.17}} \tag{6.38}$$

$$D_e = \frac{4\left(cross\text{-}sectional\ area\ of\ a\ fin\ channel\right)}{Wetted\ \ perimeter\ of\ \ a\ \ fin\ channel} \tag{6.39}$$

(b) At the transition region ($2300 < Re < 6000$), the following correlation is used to predict the heat transfer coefficient.

$$Nu = 0.116\left(Re^{2/3} - 125\right) Pr^{1/3} \left(1 + \left(\frac{D_e}{L_1}\right)^{2/3}\right)\left(\frac{\mu}{\mu_w}\right)^{0.14} \tag{6.40}$$

(c) The heat transfer coefficient in the turbulent regime ($Re > 6000$) can be calculated using the following correlation:

$$Nu = 0.018\, Re^{0.8}\, Pr^{0.4} \tag{6.41}$$

The heat transfer coefficients from the top plate, bottom plate, and fins to fluid are considered equal.

Convective heat transfer across inclined air layers between plate and glass covers

The heat transfer coefficient between parallel plates is calculated using the following correlation (Hollands et al., 1976):

$$Nu = 1 + 1.44\left[1 - \frac{1708(\sin 1.8\beta)^{1.6}}{Ra\cos\beta}\right]\left[1 - \frac{1708}{Ra\cos\beta}\right]^{+} + \left[\left(\frac{Ra\cos\beta}{5830}\right)^{1/3} - 1\right]^{+} \quad (6.42)$$

The '+' sign represents that the term should be taken into account if and only if it is positive; otherwise, it should be taken as zero.

Convection heat transfer from glass cover to ambient

The convection heat transfer coefficient from the top glass cover to the ambient can be calculated from the following correlation (Sukhatme, 1984):

$$h_w = \frac{j}{Pr^{2/3}}\rho c_{p-a} V_{wind} \quad (6.43)$$

$$j = 0.86\, Re^{-0.5} \quad (6.44)$$

The wind velocity for the calculation of the Reynold's Number is taken as the monthly average for the humid subtropical region.

Radiation heat transfer between the absorber plate and bottom plate

The radiation heat transfer between the absorber plate and bottom plate of the collectors is,

$$h_r = \frac{4\sigma T_{av}^3}{\left(\frac{1}{\varepsilon_p} + \frac{1}{\varepsilon_b} - 1\right)} \quad (6.45)$$

$$T_{av} = \frac{T_p + T_b}{2} \quad (6.46)$$

The mean temperature of the absorber plate and the bottom plate (T_{av}) is assumed to be equal to the fluid mean temperature (T_{fm}), as the values of the terms ($T_{fm}-T_p$) and ($T_{fm}-T_b$) are considered to be negligible (Sukhatme, 1984).

6.2.4. Calculation of solar radiation

The heat flux falling on the tilted collectors can be represented by the following relation (Sukhatme, 1984):

$$I_T=\overline{I}_b r_b+\overline{I}_d r_d+\left(\overline{I}_b+\overline{I}_d\right)r_r \tag{6.47}$$

Calculation procedure for beam radiation and diffusive radiation:

The monthly average of the daily global radiation $\overline{H}_g$ and the monthly average of the daily extra-terrestrial radiation on a horizontal surface at a location $\overline{H}_o$ can be related as follows (Gopinathan, 1988)

$$\frac{\overline{H}_g}{\overline{H}_o}=a_1+b_1\left(\frac{\overline{SH}}{\overline{SH}_{max}}\right) \tag{6.48}$$

$$a_1=-0.309+0.539\cos L_a-0.0693E_l+0.290\left(\frac{\overline{SH}}{\overline{SH}_{max}}\right) \tag{6.49}$$

$$b_1=1.527-1.027\cos L_a+0.0926E_l-0.359\left(\frac{\overline{SH}}{\overline{SH}_{max}}\right) \tag{6.50}$$

$$\overline{SH}_{max}=\frac{2}{15}\omega_s \tag{6.51}$$

The monthly average of the sunshine hours per day is considered for the humid subtropical region. The monthly average of the daily diffuse radiation $\overline{H}_d$ can be calculated from $\overline{H}_g$ with the following relation (Garg & Garg, 1985):

$$\frac{\overline{H}_d}{\overline{H}_g}=0.8677-0.7365\left(\frac{\overline{SH}}{\overline{SH}_{max}}\right) \tag{6.52}$$

The monthly average of the hourly global radiation on a horizontal surface $\bar{I}_g$ and the monthly average of the hourly extra-terrestrial radiation on a horizontal surface $\bar{I}_0$ can be related to $\overline{H}_g$ and $\overline{H}_0$ with the following relation (Gueymard, 2000):

$$\frac{\bar{I}_g}{\overline{H}_g}=\frac{\bar{I}_o}{\overline{H}_o}\frac{(a+b\cos\omega)}{f_c} \tag{6.53}$$

$$f_c=a+0.5b\left(\frac{\omega_s-\sin\omega_s\cos\omega_s}{\sin\omega_s-\omega_s\cos\omega_s}\right) \tag{6.54}$$

The monthly average of the hourly diffuse radiation on a horizontal surface $\bar{I}_d$ can be calculated with the following relation (Sukhatme, 1984):

$$\frac{\bar{I}_d}{\overline{H}_d}=\frac{\bar{I}_o}{\overline{H}_o} \tag{6.55}$$

The monthly average of the hourly global radiation is the summation of the monthly average of the hourly beam and diffused radiation and is written as:

$$\bar{I}_g=\bar{I}_b+\bar{I}_d \tag{6.56}$$

The monthly average of the hourly beam and diffused radiation thus found is used for calculation of I_T. The radiation absorbed by the plate can be represented by the following Equation (Sukhatme, 1984):

$$S=\bar{I}_b r_b(\tau\alpha)_b+\left(\bar{I}_d r_d+\left(\bar{I}_b+\bar{I}_d\right)r_r\right)(\tau\alpha)_d \tag{6.57}$$

$$\tau\alpha=\frac{\tau\alpha_p}{1-\left(1-\alpha_p\right)\rho_d} \tag{6.58}$$

I_T and S is calculated by considering from 8:00 hrs (IST) in the morning to 16:00 hrs (IST) in the evening. The calculation of energy, exergy, and optical efficiency for each hour of each

day throughout the year will be tedious; hence I_T , and S are taken as a monthly average to predict the whole month data.

6.3. Optimization problem formulation and solution strategy

The air collector model discussed in the previous section has been transformed into an optimization problem that solves two air collector models, i.e., simple air collector and finned air collector. The finned air collector model is solved for two cases of different variable bounds. Maximizing exergy efficiency has been considered the objective of both models. The decision variables and their bounds for both models are given in Table 6.2. The optimization formulation for the problem can be defined as,

$$\begin{aligned} &\textit{Maximize } \eta_{ex} \\ &\textit{Subject to } \quad C_1 : T_{c1} > T_{c2} \\ &\qquad\qquad\quad C_2 : T_p > T_{c1} \\ &\qquad\qquad\quad C_3 : T_{c1}, T_{c2}, T_p > T_a \end{aligned} \tag{6.59}$$

The optimization is performed using Single Phase Multi-Group Teaching Learning Optimization (SPMGTLO) (Kommadath et al., 2016). The chosen algorithm is a recently proposed computational intelligence technique, which has shown better performance in computationally expensive problems.

Solution Procedure

In order to use CI techniques, the mathematical model discussed in the earlier section has been suitably arranged for calculating the exergy efficiency. A detailed flowchart of the objective evaluation process is given in Fig. 6.2. The model accepts a potential solution from the optimization algorithm and checks for any constraint violation for C_1 and C_2. The violation of constraints is handled by assigning new values to the corresponding decision variables as given in Equations (6.60) and (6.61).

$$T_{c1} = min\left(T_{c2} + r\left(T_{c1}^{ub} - T_{c1}\right), T_{c1}^{ub}\right), if\ T_{c2} > T_{c1} \tag{6.60}$$

$$T_p = min\left(T_{c1} + r\left(T_p^{ub} - T_p\right), T_p^{ub}\right), if\ T_{c1} > T_p \tag{6.61}$$

In the above equations, the value of r is chosen randomly between 0 and 1. For each month, the mean fluid temperature is initially assumed, and the specific heat of the fluid is calculated from the assumed temperature value. A new mean fluid temperature is estimated using Equations (6.2) and (6.3). This process is iteratively continued till the temperature difference is below 10^{-5} ºC. The values of Q_u, U_l, T_p, T_{cl} and T_{c2} are calculated by solving the Equations (6.27)-(6.29).

In order to have a thermodynamically feasible model, the Equations (6.6) and (6.7) are also solved simultaneously. The solution of these equations is checked for any constraint violation for $C_1 - C_3$ along with any negative values of U_l and Q_u. Any violation stops further evaluation of the objective, and the exergy efficiency for all the months are penalized by a penalty factor (100 in this case). In case there is no violation, the exergy efficiency is evaluated for all the months using the Equation (6.25). The corrected solution and the mean exergy efficiency are returned to the optimization algorithm. This process proceeds iteratively till the termination criteria of the optimization algorithm are met.

6.4. Problem Specifications and model validation

A schematic representation of simple and finned solar air collector is provided in Fig. 6.3. The place of interest for this study is Guwahati, India (26.18˚, 91.73˚), and the elevation is 53 m. The data for wind velocity, sunshine hours and Equation of time correction are taken in the year 2016. The ambient temperature (T_a) and the temperature of the sun (T_s) are taken as 300 K and 4350 K, respectively.

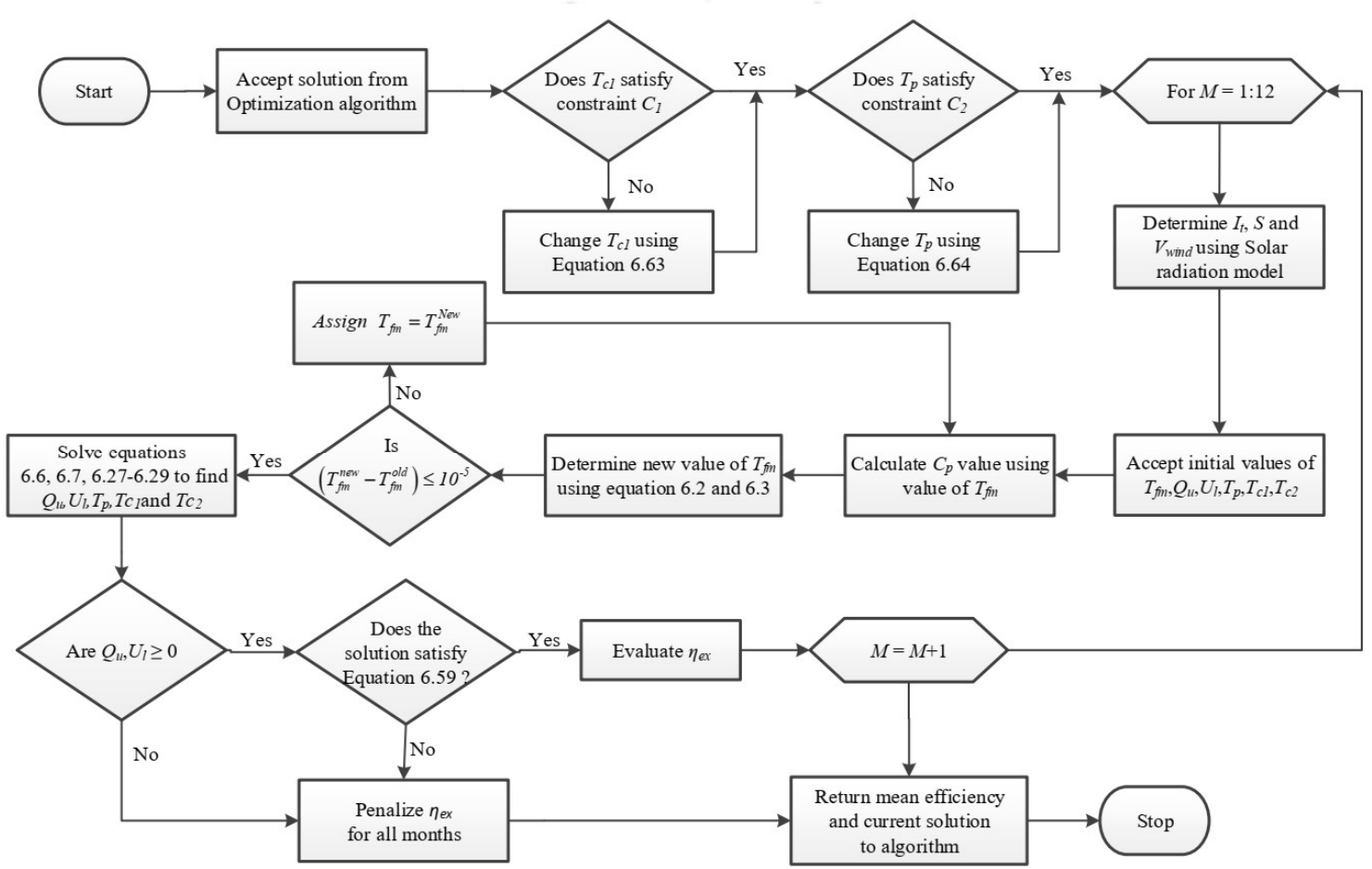

Fig. 6.2 Flow chart of the objective evaluation process

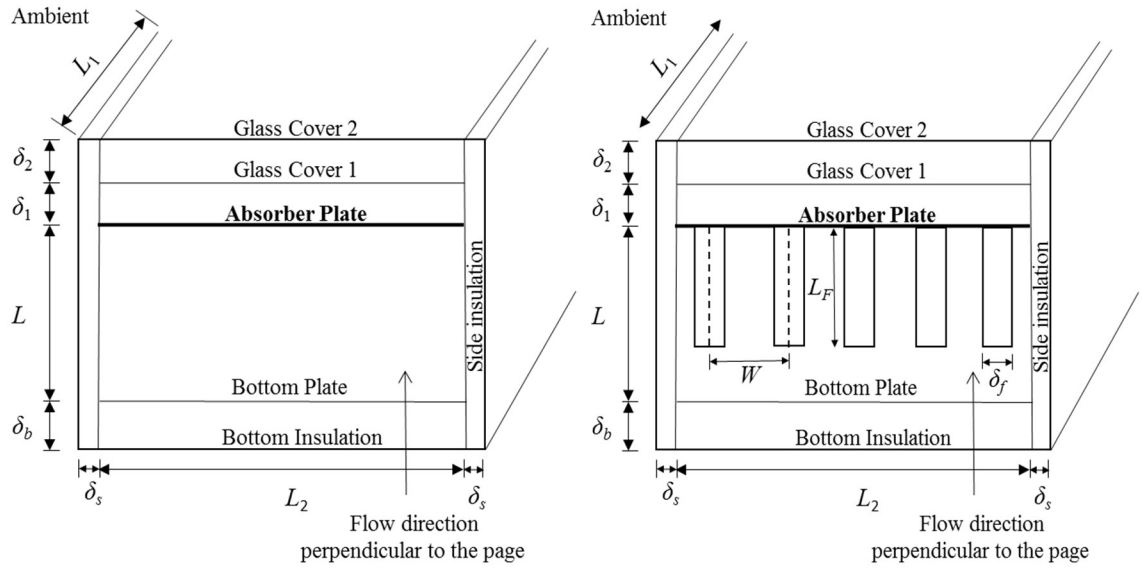

Fig. 6.3. Schematic diagram of (a) simple and (b) finned solar air collectors

The absorber plate (emissivity = 0.92) and fins are considered to be made of aluminum (thermal conductivity = 200 W/m K). The Glass covers (emissivity = 0.84) are made of Plexiglass material. Wool is considered the material of insulation (thermal conductivity = 0.05 W/m K). The collector is tilted to an angle of 20˚. The air gaps between the glass covers and the top plate are taken to be 25 mm. The thickness of insulation is considered to be 50 mm. The length of the collectors is considered to be constant (L_1 = 1 m), and the width of the collectors is fixed by the optimum area of the collectors. A schematic diagram representing the flow of heat energy in the solar air collectors is provided in Fig. 6.4.

All the fluid properties are calculated at mean fluid temperature, which is the average of inlet and outlet temperatures. The required correlations for fluid property calculations are taken from the literature (Holman, 2010). The performance and accuracy of the results obtained by solving the energy balance equations governing the performance of the simple solar air collector system were validated against Ajam et al. (2005) and are shown in Table 6.1.

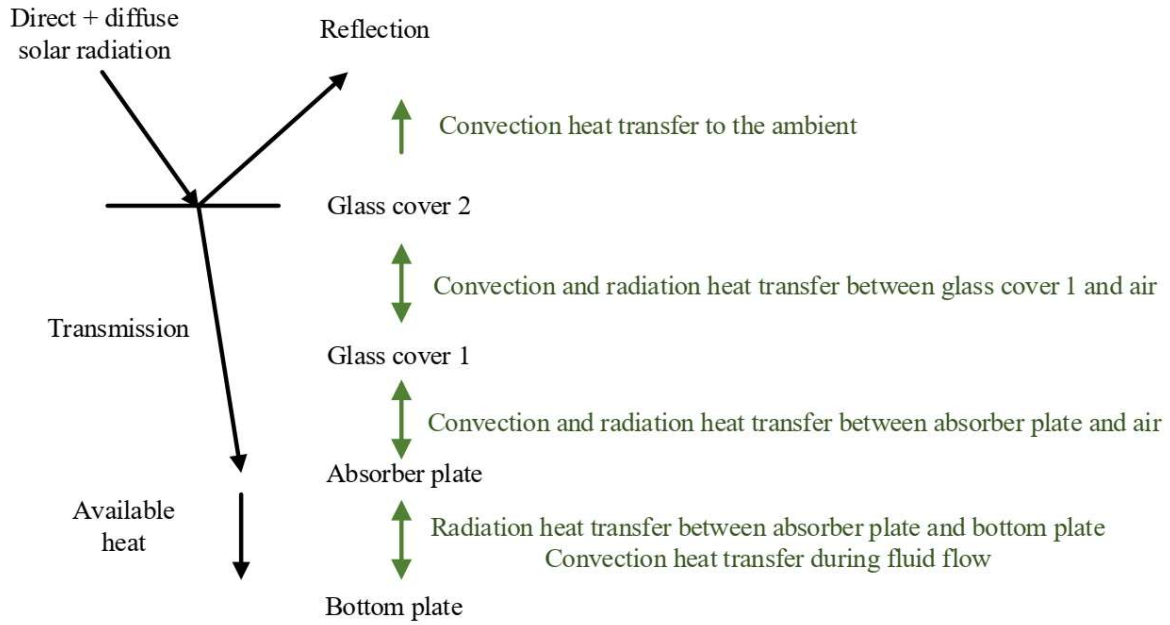

Fig. 6.4 Schematic diagram representing heat energy flow in solar air collectors

The simulation of the current model shows a better consistency between the present results and those reported by Ajam et al. (2005). The deviation of results in the present model is due to accurate calculation of U_l which is a function of parameters such as the temperature of the glass covers (1 and 2), the air properties in and out of the glass covers, the ambient temperature, the absorber plate temperature, the sky temperature, the wind speed, and the reflecting surface properties. However, the current simulation results are more accurate than Ajam et al. (2005) due to the fact that the useful heat gain calculated by Equations (6.2), (6.6) and (6.7) are similar, as in Table 6.1. On the other hand, useful heat gain calculated by Equations (6.2), (6.6) and (6.7) for parameters reported by Ajam et al. (2005) are 661.29 W, 663.35 W, and 665.21 W, respectively.

Table 6.1 Comparison between the current simulation and results of literature for simple air collectors

Parameters	Present Model	Ajam et al. (2005)
Overall heat loss coefficient ($Wm^{-2} K^{-1}$)	5.11	4.76
Outlet temperature (K)	359.84	364.40
Absorber plate temperature (K)	370.29	372.89
Glass Cover1 Temperature (K)	347.03	Not reported
Glass Cover 2 temperature (K)	319.09	Not reported
Heat transfer coefficient between working fluid and absorber plate ($Wm^{-2} K^{-1}$)	19.09	19.28
Collector Efficiency Factor, F'	0.83	0.84
Collector Heat Removal Factor	0.81	0.79
Mass flow rate ($kg\ s^{-1}$)	0.15	0.07
Useful Heat Gain (W) [using Equation (6.2)]	640.90	660.44
Useful Heat Gain (W) [using Equation (6.6)]	641.17	Not reported
Useful Heat Gain (W) [using Equation (6.7)]	641.16	Not reported
Pressure Drop (Pa)	14.21	Not reported
Energy Efficiency	0.40	0.41
Exergy Efficiency	0.068	0.074

6.5. Results and discussion

This section discusses the results obtained on optimizing the solar air collector. The optimal decision variables are analyzed for varying operational and environmental conditions. In addition, the performance of SPMGTLO on solving the solar collector model is also presented.

6.5.1. Optimal solution analysis

The optimized values of decision variables along with the maximum possible yearly average exergy and energy efficiencies determined by the SPMGTLO algorithm for both simple and finned air collector cases, are given in Table 6.2. The decision variables are categorized as

design and operational variables, and their corresponding bounds are provided in Table 6.2. The optimal values are highlighted in boldfaced font. The design variables remain constant for all the months, whereas the operational variables are dependent on solar radiation. In order to demonstrate the influence of upper and lower bounds over the choice of finned air collector parameters (design and operational variables), we have considered two cases (Case 1 and Case 2) for the finned air collectors in Table 6.2.

Table 6.2. Decision variables and their bounds for simple air collectors and finned air collectors (Case 1 and Case 2)

	Decision Variables	Simple air collectors			Finned air collectors					
					Case 1			Case 2		
		lb	ub	Optima	lb	ub	Optima	lb	ub	Optima
Design variables	A_p (m^2)	1	5	**5**	1	5	**5**	1	5	**5**
	L (m)	0.01	0.3	**0.01**	0.1	0.3	**0.1**	0.05	0.3	**0.05**
	W (m)	-	-	-	0.01	0.25	**0.01**	0.001	0.01	**0.0016**
	$Fin_{fraction}$	-	-	-	0.4	0.8	**0.8**	0.4	0.8	**0.4**
	δ_f (m)	-	-	-	0.002	0.005	**0.005**	0.002	0.005	**0.002**
Operational variables	V_{av} (ms^{-1})	1	10	**5.14**	1	10	**1**	0	7	**0.77**
	T_{in} (K)	300	400	**343.46**	300	400	**343.15**	300	375	**338.93**
	T_{fm} (m)	300	445	**345.62**	300	445	**345.31**	300	445	**345.94**
	Q_u (kJ)	0	3000	**1126.93**	0	3000	**1282.37**	0	3000	**1303.84**
	U_l ($Wm^{-2}K^{-1}$)	3	10	**4.51**	3	10	**4.55**	3	10	**4.49**
	T_p (K)	305	450	**353.87**	305	450	**346.55**	305	450	**346.24**
	T_{c1} (K)	303	448	**336.08**	303	448	**330.76**	303	448	**330.54**
	T_{c2} (K)	301	446	**315.39**	301	446	**312.62**	301	446	**312.51**
Average mass flow rate (Kgs^{-1})		0.26			0.30			0.095		
Average flow area (m^2)		0.05			0.3			0.125		
Average pressure drop (Pa)		25.08			1.96			5.84		
Average Energy efficiency (%)		37.12			42.25			43		
Average Exergy efficiency (%)		**5.06**			**5.93**			**6.10**		

It should be noted that in Table 6.2, the upper and lower bounds for channel depth (L), the fin spacing (W), average velocity (V_{av}), and inlet temperature (T_{in}) are different for both cases of finned air collectors. The quality of the upper and lower bounds concludes with optima values on the finned solar collectors and shows that probabilistic selection on bounds can affect the optima in many cases.

6.5.2. Effect of operational parameters on exergy efficiency

Effect of optimum plate area on collector efficiencies

As expected, heat input to the collectors increases with the collection (absorber plate) area, thereby increasing thermal efficiency. On the other hand, a rise in temperature is observed with heat input, which further leads to exergy destruction. Therefore, there is an optimum area beyond which there is no significant increase in exergy efficiency. By increasing the absorber plate area until the value of 5 m^2, the exergy efficiency increases significantly. Although energy efficiency increases with heat input, the increase in exergy efficiency is not significant beyond 5 m^2 for the given incident heat flux under humid subtropical climatic conditions. Hence, upper and lower bounds were chosen as 1 and 5 m^2, respectively, and the optimum collector area was found to be 5 m^2, irrespective of the type of collectors used (Table 6.2).

Effect of optimum flow area on collector efficiencies

A careful investigation into the optimized design variables reveals that simple air collectors require a lesser depth of the flow channel (L) than finned air collectors (cases 1 and 2) for the same optimum collector area (A_p) and optimum mean fluid temperature (T_{fm}) (Table 6.2). A lower flow channel depth would decrease flow area and mass flow rate, which are further due to dominant friction losses over buoyancy forces. Lower flow channel depth and mass flow

rate have further to be compensated by an increase in air velocity, which further increases the heat transfer coefficient. Hence, higher air velocity is required to achieve maximum average energy efficiency in simple air collectors, and hence, the pressure drop is significantly higher for simple air collectors as compared to the finned air collectors (Table 6.2). Also, an increase in heat transfer coefficient increases the heat transfer rate to the airflow, and consequently, the maximum possible average exergy efficiency in simple air collectors is almost comparable to finned air collectors (Table 6.2).

It is also noted that a higher optimum flow area and mass flow rate would have increased the outlet temperature of the air in the finned air collectors (cases 1 and 2) and, thereby, increased the mean temperature of the fluid for the same optimum collector area in both the cases. On the contrary, the mean fluid temperature of the fluid in finned collectors (case 1) is the same as that of simple collectors for the same inlet temperature of the fluid, and therefore, the pressure drop is significantly lower for finned collectors (case 1) when compared to simple collectors (Table 6.2). In finned air collectors (cases 1 and 2), fins would have resulted in an increase in heat transfer rate and mean fluid temperature. On the other hand, the addition of fins results in friction losses and a decrease in useful heat added to the fluid. Thus, the optimum flow depth of the channel to the height of the fin (fin fraction), fin thickness, and fin spacing (number of fins) is necessary to achieve higher heat transfer rates and low friction losses, which further results in maximum possible energy and exergy efficiencies in cases 1 and 2 (Table 6.2). Accordingly, a decrease in flow area increases fin spacing and decreases fin fraction and fin thickness for case 2 (Table 6.2). Also, case 2 shows higher optimum yearly average energy and exergy efficiencies compared to case 1 (Table 6.2).

Effect of optimum fluid velocity and temperature difference on collector efficiencies

It is also noted that heat transfer and pressure drop contribute to exergy destruction. Consequently, less temperature difference between the optimum inlet (simple air collectors: T_{in} = 343.46 K and finned air collectors: T_{in} = 343.15 K (case 1) and T_{in} = 338.93 K (case 2)) and outlet air temperatures (simple air collectors: T_{out} = 347.78 K and finned air collectors: T_{out} = 347.47 K (case 1) and T_{out} = 352.95K (case 2)) of the flow channel and higher optimum pressure drop (simple air collectors: ΔP = 25.08 kPa and finned air collectors: 1.96 kPa (case 1) and 5.84 kPa (case 2)) determines the maximum possible average exergy efficiency in air collectors via exergy destruction (Equation (6.23) and Table 6.2). However, with the optimum mass flow rate and mean fluid temperature, useful heat energy added into the fluid for simple air collectors is less than finned air collectors (cases 1 and 2), and thereby, lesser exergy efficiency is observed in simple air collectors (Table 6.2). It is noted that higher optimal flow area and mass flow rate have resulted in a decrease in air velocity in finned collectors (cases 1 and in Table 6.2), which is high enough to increase the heat transfer coefficient due to the presence of fins. Hence, lower air velocity is required to achieve maximum average exergy efficiency in finned air collectors (cases 1 and 2), and hence, the pressure drop is significantly lower for finned air collectors as compared to simple air collectors in spite of the fact that fins bring an additional pressure drop to the system (Table 6.2). As expected, a decrease in optimal flow area increases pressure drop in case 2 finned air collectors compared to case 1 finned air collectors (Table 6.2).

The total volume of fins beyond an optimum volume decreases the outlet temperature of the fluid due to the high specific heat of the fin material. Hence, there should be an optimum spacing between the fins, optimum fin fraction, and optimum fin thickness above which the

mean temperature of the fluid does not increase. It is noted that decreasing optimal flow area and number of fins (via spacing between the fins) decreases fin fraction and fin thickness, as shown in the difference between the cases in Table 6.2. It is observed that T_{in} = 343.15 K and T_{out} = 347.47 K for case 1 of finned collectors with the fin spacing of 0.01 m, whereas T_{in} = 338.93 K and T_{out} = 352.95K for case 2 finned collectors with the fin spacing of 0.0016 m. However, case 2 finned collectors do not show any significant improvement in exergy efficiency (6.1%) when compared to case 1 finned collector (5.93%) due to higher exergy destruction because of higher temperature differences and pressure drop (Table 6.2). The optimum absorber plate temperature for finned air collectors (cases 1 and 2) is lower compared to simple air collectors due to the higher optimal useful heat energy of air in the former case. To sum up, finned air collectors with higher optimal flow area and mass flow rate were able to achieve maximum possible optimum thermal and exergy efficiencies compared to simple air collectors for the same optimal collector area and mean fluid temperature due to the fact that higher amount of useful energy is being utilized by the fluid in finned air collectors (cases 1 and 2).

6.5.3. Effect of environmental conditions on exergy efficiency

Variations of the monthly average of the hourly incident heat flux and optical efficiency throughout the year are given in Fig. 6.5. The monthly average of the hourly incident heat flux (I_T) on the absorber plate is highest for March (668.7 W/m^2) while lowest during July (505.7 W/m^2) for humid subtropical climatic conditions (Fig. 6.5). This is confirmed as the rainy season reduces the sunshine hours during July in humid subtropical climatic conditions. It is also due to a comparatively lesser monthly average of the hourly diffuse radiation on a

horizontal surface ($\overline{I_d}$) than the monthly average of the hourly beam radiation ($\overline{I_b}$) during March, whereas ($\overline{I_d}$) is higher during the month of July. In March, the maximum I_T (821.5 W/m^2) was observed at 12.00 hrs (IST), whereas the minimum I_T (237.4 W/m^2) was observed at 16.00 hrs (IST). In this study, the I_T calculation (Equation (6.47)) is considered from 8:00 hrs (IST) in the morning to 16:00 hrs (IST) in the evening.

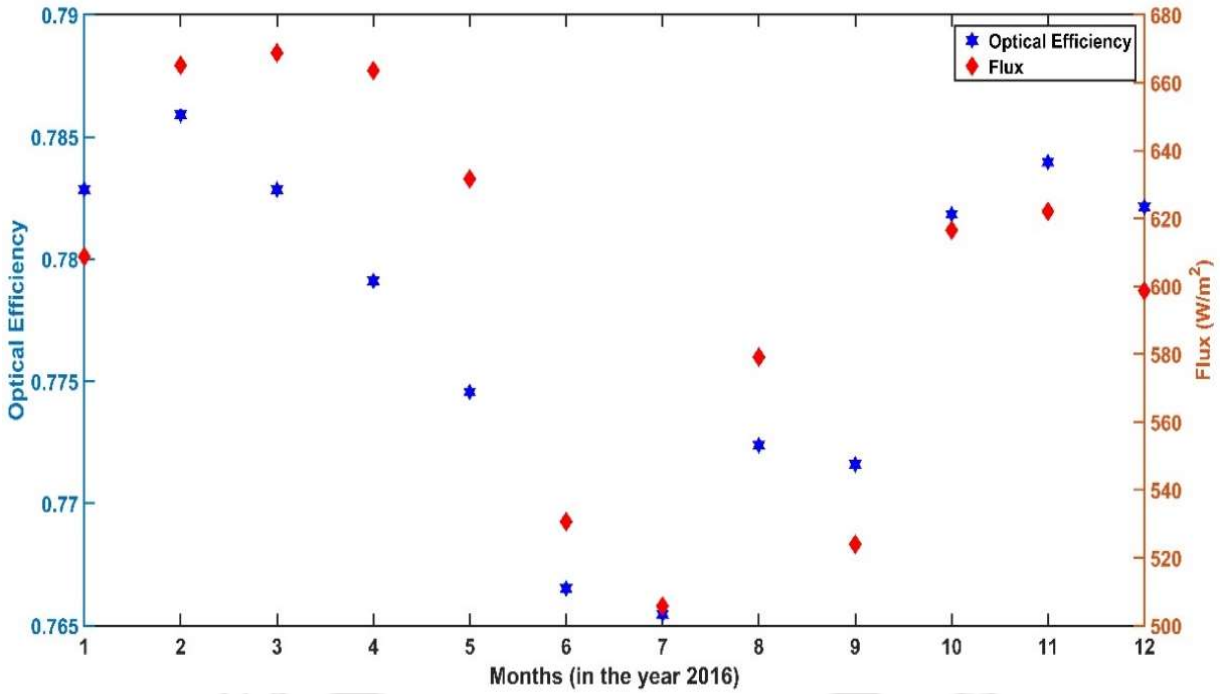

Fig. 6.5. Variations of monthly average of the hourly incident heat flux falling on the solar air collectors and optical efficiency of the collectors throughout the year for humid subtropical climatic conditions

Similarly, in the month of July, the maximum I_T (595.7 W/m^2) was observed at 11.00 hrs (IST), whereas the minimum I_T (206.6W/m^2) was observed at 16.00 hrs (IST). Similar to I_T, optical efficiency, which is the ratio of incident heat flux (I_T) and incident heat flux absorbed in the absorber plate (S), is highest during February (78.5%) while it is lowest for the month

of July (76.5%). Due to significant variations in the incident heat flux for humid subtropical climatic conditions, efficient use of solar air collectors necessitates the optimal design and operating parameters.

Effect of incident solar energy on collector efficiencies

Fig. 6.6 and Fig. 6.7 show the variations of monthly average energy and exergy efficiencies, respectively, throughout the year for both types of collectors. The monthly average energy and exergy efficiencies were calculated at optimal design and operational conditions mentioned in Table 6.2.

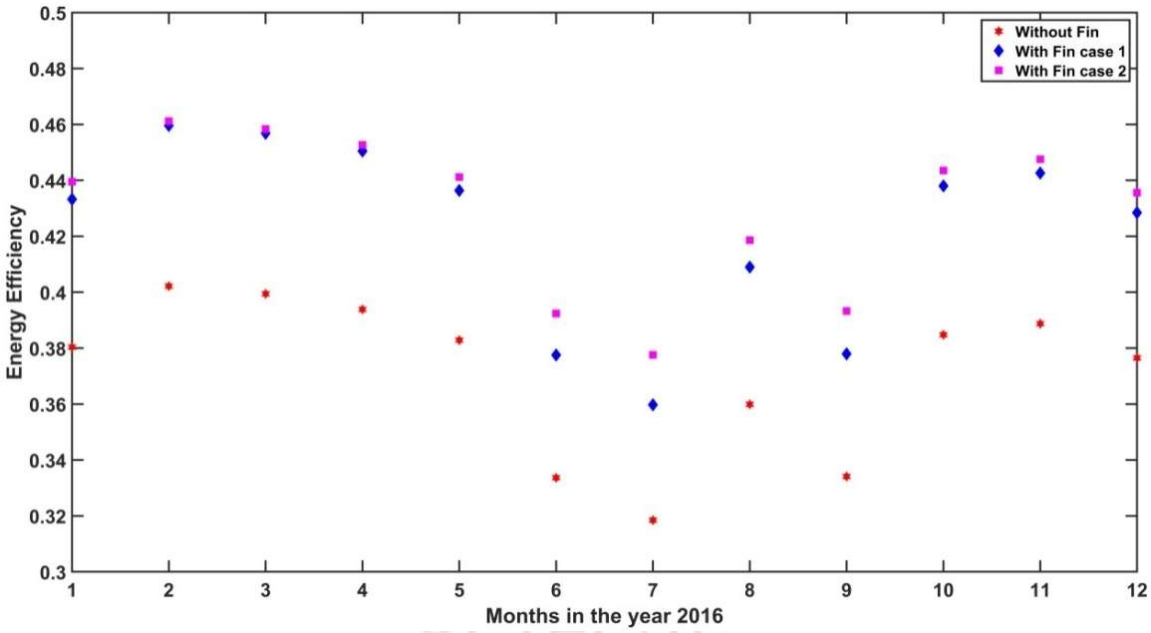

Fig. 6.6. The variations of energy efficiencies of the simple and finned (cases 1 and 2) solar air collectors throughout the year for humid subtropical climatic conditions

As expected, finned air collectors (cases 1 and 2) showed higher energy and exergy efficiencies than air collectors without fin case (Fig. 6.6 and Fig. 6.7). The maximum efficiency was observed in the month of February, whereas the least efficiency was observed in the month of

July (Fig. 6.6 and Fig. 6.7). addition of fins increased the heat transfer coefficient, which in turn showed higher monthly average energy efficiency for finned air collectors when compared to the case with simple air collectors (Fig. 6.6). The useful heat gain in the case of finned air collectors is higher due to higher heat removal from the absorber plate by fins. This further increases the monthly average exergy efficiency of finned air collectors over simple air collectors (Fig. 6.7).

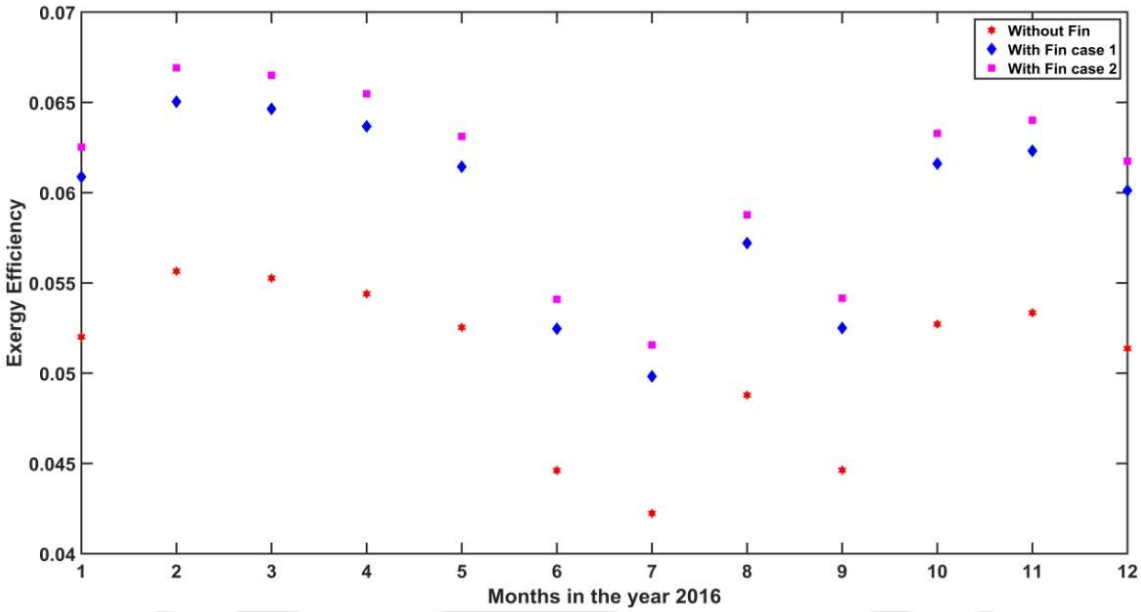

Fig. 6.7. The variations of exergy efficiencies of the simple and finned (cases 1 and 2) solar air collectors throughout the year for humid subtropical climatic conditions

Maximum energy and exergy efficiency is achieved in the case of finned air collectors. (Case 2) with a yearly optimal average energy and exergy efficiency of 43% and 6.10 %, respectively, for an optimal collector area of 5 m^2 and a yearly optimal average heat flux of 601 W/m^2 (Fig. 6.6, Fig. 6.7 and Table 6.2).

6.5.4. Convergence and statistical analysis

The solutions determined by SPMGTLO for 10 runs determine the mean exergy efficiency of 5.93 % and 6.1 % for finned air collector cases 1 and 2, respectively. The mean exergy efficiency for simple air collectors for 10 runs is determined to be 5.06 %. The standard deviation (SD) is found to be in the order of 10^{-10} for the above three cases. It is evident from the SD value that SPMGTLO is able to determine the optimal value consistently for all three cases of solar air collectors. The convergence curve corresponding to the best run for all the cases of air collectors is shown in Fig. 6.8.

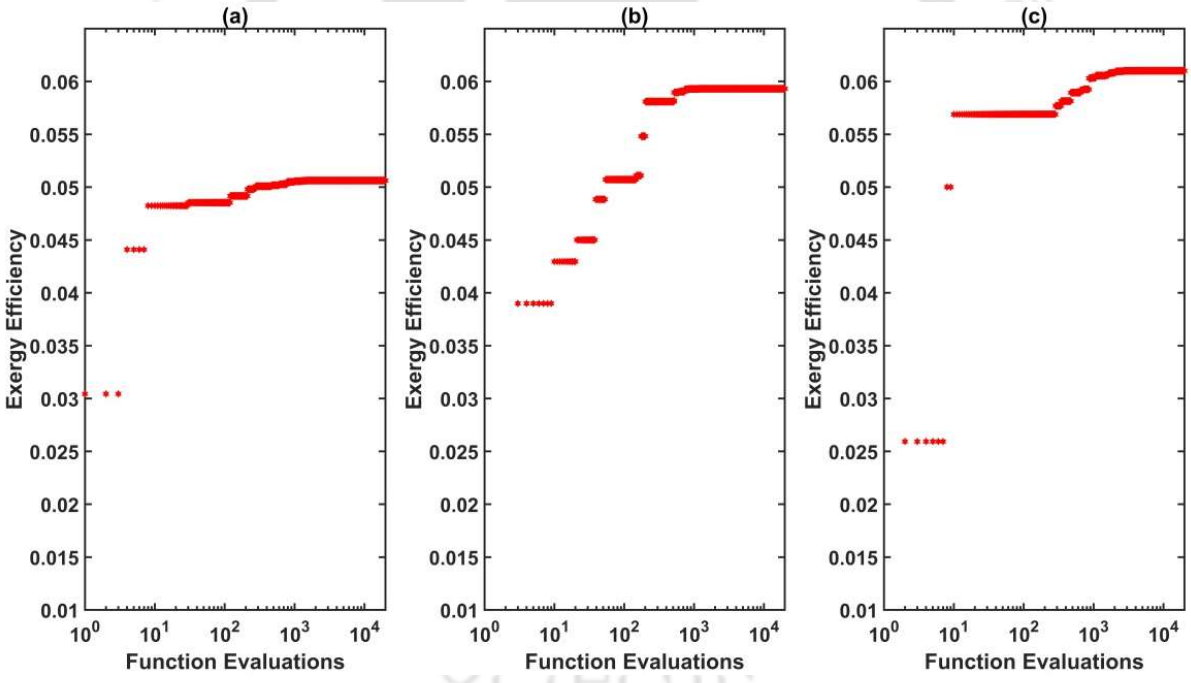

Fig. 6.8. Mean convergence profile for (a) Simple air collectors (b) Finned air collectors (Case 1) and (c) Finned air collectors (Case 2)

In all of the cases, quick convergence towards the final value is observed except for finned air collector case 2. The final solution has been obtained by utilizing only 18.4% and 18% of the total function evaluations in finned air collectors case 1 and simple air collectors, respectively,

while case 2 of the finned air collector used 70% of the total functional evaluations to reach the final value. The experiments with many other CI techniques such as Genetic Algorithm, Artificial Bee Colony, Grey Wolf Optimizer, and Yin Yang Pair Optimization, provided the same optima as reported by SPMGTLO. However, SPMGTLO has shown a quick convergence as compared to other CI algorithms, which led to the selection of SPMGTLO for the current study.

6.6. Conclusion

An integrated mathematical model for solar-thermal energy conversion, optical, thermal, and exergy efficiency analysis of simple and finned solar air collectors was derived for a case study of humid subtropical climatic conditions (Guwahati, India). Maximizing exergetic efficiency was identified as the objective function for optimization, and optimum design and operational parameters for the preliminary stages of design of simple conventional solar air collectors and finned air collectors for the case study were found out using a CI technique. Assumptions on constant incident solar heat flux, constant overall thermal loss coefficient, and other heat transfer coefficients of the collectors were relaxed in the mathematical model, and the optimization was aimed to achieve maximum yearly average exergy efficiency in the collectors in the case study. The proposed model was optimized using the SPMGTLO algorithm by considering its major design and operational variables as decision variables.

The optimization strategy eliminates all the infeasible solutions using constraints on operating conditions and making the system thermodynamically feasible. It was also shown that the probabilistic selection on upper and lower bounds of decision variables in the optimization procedure can affect the optima in finned air collectors (cases 1 and 2). The idea of reducing flow area via flow channel depth to a few mm considerably increases the pressure drop, which

was found to be even higher for simple air collectors than finned air collectors due to higher fluid velocity in order to achieve maximum average exergy efficiency. The finned solar collectors (cases 1 and 2) have the best exergy efficiency. However, the improvement is relatively small, even with higher temperature differences between the fluid inlet and outlet, due to the smaller flow area and higher pressure drop (case 2). The Maximum energy and exergy efficiency is achieved in the case of finned air collectors (case 2) with a yearly optimal average energy and exergy efficiency of 43% and 6.10 %, respectively, for an optimal collector area of 5 m^2 and yearly optimal average heat flux of 601 W/m^2 for humid subtropical climatic conditions.

Chapter 7

Multi-objective framework for solar water collectors using metaheuristic techniques

This chapter proposes a model to determine the optimal performance and design conditions for a flat plate solar water collector. The model uses hourly solar irradiation data over a year for humid subtropical climatic conditions to estimate thermal, optical, and exergy efficiency. The proposed model has been validated with the data in the literature. Six single objective metaheuristic techniques are used to determine the maximum exergy efficiency by optimizing the plate area of the absorber, mass flow rate, and inlet temperature of the working fluid. Six multi-objective metaheuristic techniques are used to evaluate the trade-off solutions between the conflicting objectives of maximizing exergy efficiency and minimizing the area of the absorber plate. A MATLAB-based GUI has also been provided to help determine the optimal values of the decision variables under various scenarios.

This chapter is structured as follows. Section 7.2 provides a detailed mathematical model for SWC. The single and multi-objective formulations and a brief comparison of selected metaheuristic techniques are presented in section 7.3. The model validation and optimization problem specifications are provided in section 7.4, followed by results and discussion in Section 7.5. The chapter concludes by summarizing the outcomes in section 7.6.

7.1. Background

The viability of a solar water heater depends on the type of collector, type of storage, capital cost, usage capacity, fuel cost, etc. The solar collector is the principal component of any solar domestic hot water system; therefore, optimal thermal performance is essential for the solar collector (Jadhav et al., 2020). Contrarily, the first law of thermodynamics alone does not

provide sources of thermodynamic inefficiencies in a thermal system, and accordingly, the first law of efficiency cannot provide the optimum thermal performance of a solar collector. Exergy analysis of solar collectors estimates the amount of available work in all energy streams by evaluating underlying sources of internal exergy destruction and external exergy losses to the surroundings. Exergy analysis also provides a systematic procedure to target the processes/components that are accountable for the deterioration of performance in the solar collector system. This information on optimum operating parameters, location, and magnitudes of energy inefficiencies is contributed by exergy analysis, which cannot be provided by energy analysis, and is very useful for augmenting the overall efficiency and cost-effectiveness of a system (Bejan et al., 1981).

Another critical issue in any solar-based energy system is to enhance the thermal performance of solar collectors. There are innumerable experimental analyses available to appraise and improve the performance of solar collectors. Nevertheless, these studies are time-consuming and costlier compared to numerical analysis. On the other hand, the design of experiments methods may not be sufficient enough to analyze and optimize the energy systems for their better performance. The modeling of solar collectors requires rigorous knowledge regarding both design and operational parameters, which play a significant role in system efficiency. These complex nonlinear models are often solved and optimized using some of the advanced optimization techniques. In this perspective, many optimization methods have been used in the literature to accomplish this objective. Sánchez-Bautista et al., (2015) used a mixed-integer nonlinear programming (MINLP) model to optimally design an integrated solar collector boiler system and minimize the total annual cost. The optimization of exergy efficiency for flat plate solar collectors using sequential quadratic programming (SQP) was reported in the literature (Farahat et al., 2009). Due to a high degree of nonlinearity, solar energy based system models

often use metaheuristic techniques (MT) to optimize various design parameters. Metaheuristic techniques are usually population-based stochastic algorithms and are highly efficient in solving many real-life nonlinear problems. In this context, Atia et al., (2012) employed the genetic algorithm (GA) for sizing a solar hot water system. Jalilian et al., (2016) used GA to enhance the thermal efficiency of a solar collector with heat pipes. The particle swarm optimization (PSO) technique was used by Cheng et al., (2015) to optimize the optical performance of a parabolic trough solar collector. Das, (2015) applied the simulated annealing (SA) technique to determine thermal and physical parameters of a single-glazed solar collector system to achieve a known thermal distribution. Another popular technique known as artificial bee colony (ABC) was implemented to improve the thermo-hydraulic efficiency of solar air heaters (Yıldırım & Aydoğdu, 2017).

Metaheuristic techniques are also popular in solving multi-objective models as their inherent capabilities ensure that multiple simulations are not required to determine the trade-off solutions. In the literature, a wide variety of metaheuristic techniques have been used to solve multi-objective optimization problems when designing or analyzing the performance of solar collector systems. Maximizing system efficiency and output power for solar dish Stirling systems were solved using a non-dominated sorting genetic algorithm (Carrillo Caballero et al., 2017) and multi-objective particle swarm optimization (Zayed et al., 2020). Rey & Zmeureanu, (2018) used micro time variant multi-objective particle swarm optimization (micro-TVMOPSO) for solar thermal combisystem considering three objectives: life cycle cost, life cycle energy use, and life cycle exergy destroyed. Metaheuristic techniques are stochastic algorithms and do not guarantee the global optima; hence, the use of multiple such techniques increases the chance of getting a better optimal solution compared to the optimal solution found by any individual metaheuristic technique. Earlier literature mostly used a single

metaheuristic technique for single and multi-objective optimization of solar energy-based systems.

To the best of the author's knowledge, multiple techniques to identify a better optimal solution in the context of the design of solar collector systems have not been reported in the literature. This chapter provides a detailed energy and exergy analysis of the thermal, optical, and exergetic performance of flat plate solar water collectors for determining the optimum absorber plate area and exergy efficiency for humid subtropical climatic conditions. The work by Farahat et al., (2009) reported optimal operating parameters of flat plate solar water collectors based on exergy analysis; however, there might be exergy errors due to (a) negligible adhesive resistance of the solar collector, (b) constant wind speed, (c) constant optical efficiency, (d) constant solar irradiation, (e) assumption of inlet water temperature is same as the environmental temperature. These shortcomings have been addressed in the present chapter. It is also to be noted that Guwahati City, India (humid subtropical climatic conditions) has been declared as a solar city among 60 identified cities to be developed as solar cities under the Jawaharlal Nehru National Solar Mission of the Ministry of New and Renewable Energy, Government of India. The probabilities of employing solar water heating collectors at Guwahati City, India (humid subtropical climatic conditions) to convert solar radiation into heat using actual hourly data over a year have also been discussed in this chapter.

This study also reports some of the popular and recently proposed single and multi-objective metaheuristic techniques to determine the optimal design and operational parameters for a flat plate solar water collector. Despite many research articles on this topic, there has been very little understanding of the optimization problem formulation, details on decision variables, details on constraints, optimization algorithm, etc., in the literature. This chapter addresses this

issue by providing a detailed description of the optimization steps of the model. Maximizing exergetic efficiency is identified as a single objective function to determine optimum operational parameters during humid subtropical climatic conditions for a flat plate solar water collector, whereas minimizing absorber plate area and maximizing exergy efficiency are identified as multi-objective functions. This chapter also demonstrates the performance of the metaheuristic techniques in determining the best solution. An optimization toolkit using MATLAB graphical user interface (GUI) is provided to optimize the model under different operational parameters. In short, a flat plate solar water collector is analyzed for the effects of various design and operating parameters on their performance and is optimized using multiple metaheuristic techniques by correcting the reported shortcomings in the literature.

Nomenclature

A_p	Area of absorber plate (m^2)
a_1	Constant
a	Constant
b_1	Constant
b	Constant
C_p	Specific heat of fluid (kJ/Kg K)
c_{p-a}	Specific heat of air (kJ/Kg K)
D_e	Equivalent diameter of the channel (m)
D_i	Inner diameter of the tube (m)
D_o	Outer diameter of the tube (m)
$\dot{E}_d$	Destroyed exergy rate (kJ)
$\dot{E}_{in}$	Inlet exergy rate (kJ)
$\dot{E}_l$	Leakage exergy rate (kJ)
E_l	Elevation of Guwahati (kms)
$\dot{E}_{out}$	Outlet exergy rate (kJ)
$\dot{E}_s$	Stored exergy rate (kJ)
$\dot{E}_{d,\Delta T_f}$	Exergy rate due to temperature difference between the plate and working fluid (kJ)
$\dot{E}_{d,\Delta P}$	Exergy rate due to pressure drop due to friction in the flow channel (kJ)
$\dot{E}_{d,\Delta T_s}$	Exergy rate due to temperature difference between the plate and the Sun (kJ)
$\dot{E}_{in,Q}$	Absorbed solar radiation exergy rate by the heater (kJ)
$\dot{E}_{in,f}$	Inlet exergy rate with fluid flow (kJ)
$\dot{E}_{out,f}$	Outlet exergy rate with fluid flow (kJ)
f_c	Normalizing factor

F_R	Heat removal factor
F'	Collector efficiency factor
$\overline{H}_d$	Monthly average of the daily diffuse radiation (W/m^2)
$\overline{H}_g$	Monthly average of the daily global radiation on a horizontal surface (W/m^2)
$\overline{H}_o$	Monthly average of the daily extraterrestrial on a horizontal surface radiation (W/m^2)
h_r	Equivalent radiative heat transfer coefficient (W/m^2 K)
h_w	Heat transfer coefficient between first cover and surrounding air (W/m^2 K)
h_f	Inside wall individual fluid convection heat transfer coefficient (W/ m^2 K)
$h_{c_1-c_2}$	Heat transfer coefficient between first and second glass cover (W/m^2 K)
h_{p-c_1}	Heat transfer coefficient between absorber plate and first cover (W/m^2 K)
I_T	Flux incident on the absorber plate (W/m^2)
$\overline{I}_b$	Monthly average of the hourly beam radiation (W/m^2)
$\overline{I}_d$	Monthly average of the hourly diffuse radiation on a horizontal surface (W/m^2)
$\overline{I}_g$	Monthly average of the hourly global radiation on a horizontal surface (W/m^2)
$\overline{I}_o$	Monthly average of the hourly extraterrestrial radiation on a horizontal surface (W/m^2)
j	j factor
k_a	Thermal conductivity of air (W/m K)
k_i	Thermal conductivity of the insulation (W/m K)
k_p	Thermal conductivity of the absorber plate (W/m K)
L	Depth of the channel (m)
L_1	Absorber plate length (m)
L_2	Absorber plate width (m)
L_3	Height of the collector (m)
L_a	Latitude of Guwahati (^{o})

$\dot{m}$	Mass flow rate (kg/s)
Nu	Nusselt number
ΔP	Pressure drop due to fluid friction (Pa)
ΔP_{in}	Pressure drop due to fluid friction (Pa)
ΔP_{out}	Pressure drop at the outlet (Pa)
Pr	Prandtl number
Q_u	Useful heat gain (W)
q_t	Heat loss from the top (W/ m^2)
Ra	Rayleigh number
Re	Reynolds number
r_b	Tilt factor for beam radiation
r_d	Tilt factor for diffuse radiation
r_r	Tilt factor for reflected radiation
S	Absorbed radiation flux by the absorber plate (W/m^2)
$\overline{SH}$	Monthly average of the sunshine hours per day (hr)
$\overline{SH}_{max}$	Monthly average of the maximum possible sunshine hours per day (hr)
T_a	Ambient temperature (K)
T_p	Temperature of absorber plate (K)
T_{fm}	Mean fluid temperature (K)
T_s	Temperature of Sun (K)
T_{C_1}	Temperature of first glass cover (K)
T_{C_2}	Temperature of second glass cover (K)
T_{out}	Outlet fluid temperature (K)
T_{in}	Inlet fluid temperature (K)
T_{av}	Average temperature (K)

T_{sky}	Temperature of sky (K)
U_b	Bottom heat loss coefficient (W/m^2 K)
U_s	Side heat loss coefficient (W/m^2 K)
U_l	Overall heat loss coefficient (W/m^2 K)
U_t	Top heat loss coefficient of (W/m^2 K)
V_f	Fluid velocity (m/s)
V_{wind}	Wind velocity (m/s)
W	Center to center distance between two tubes (m)
X	Solution from algorithm
α_p	Absorptivity of plate
β	Tilt angle (^{o})
δ_a	Thickness of adhesive
δ_b	Thickness of the back insulation (m)
δ_{c1-c2}	Distance between the first glass cover and the second glass cover (m)
δ_{p-c1}	Distance between the absorber plate and the first glass cover (m)
δ_s	Thickness of the side insulation (m)
δ_p	Thickness of the absorber plate (m)
ε_p	Emissivity of absorber plate
ε_c	Emissivity of the covers
ε_b	Emissivity of bottom plate
η_o	Optical efficiency (%)
η_{th}	Thermal efficiency (%)
η_{ex}	Exergy efficiency (%)
ρ_d	Diffusive reflectivity of the cover system
ρ	Density of fluid (kg/m^3)

σ	Stefan–Boltzmann constant (W/m^2 K^4)
$\tau\alpha$	Transmissivity absorptivity factor
$(\tau\alpha)_b$	Transmissivity absorptivity factor based on beam radiation
$(\tau\alpha)_d$	Transmissivity absorptivity factor based on diffuse radiation
$(\tau\alpha)_p$	Transmissivity absorptivity factor of absorber plate
μ_f	Viscosity of the fluid (kg/m s)
ω	Hour angle at sunrise or sunset (^{o})
ω_s	Hour angle at sunrise or sunset (^{o})

7.2. Mathematical modeling and simulation

In this section, a mathematical model is proposed to determine the optical, energy, and exergy efficiency of solar water collectors for the given solar radiation model of humid subtropical climatic conditions.

7.2.1. Optical and energy analysis

The total falling flux on the system (I_T) and the total absorbed flux by the system (S) can be related in terms of optical efficiency (η_o), which is otherwise known as the effective product of the transmittance - absorptance of the collector system (Farahat et al., 2009)

$$\eta_o = \frac{S}{I_T} = \tau\alpha \tag{7.1}$$

Energy analysis:

The useful heat gain of the system at a steady state can be calculated from the energy balance on the working fluid of the collectors using Equation (7.2),

$$Q_u = \dot{m} C_p \left(T_{out} - T_{in} \right) \tag{7.2}$$

The useful heat gain of the collectors can also be obtained from the difference between the solar energy absorbed by the absorber plate and the heat losses from the collector system using the following energy balance equation (Farahat et al., 2009)

$$Q_u = A_p S - U_l A_p \left(T_p - T_a \right) \tag{7.3}$$

Heat removal factor (F_R) is defined as the ratio of the actual useful heat gain to the useful heat gain if the entire collector was at the fluid inlet temperature.

$$F_R = \frac{Q_u}{A_p\left[S - U_l\left(T_{in} - T_a\right)\right]} \tag{7.4}$$

From the above Equation, the useful heat gain can be calculated as the product of the maximum possible useful heat gain and heat removal factor (Farahat et al., 2009)

$$Q_u = A_p F_R\left[S - U_l\left(T_{in} - T_a\right)\right] \tag{7.5}$$

where

$$F_R = \frac{\dot{m}C_p}{U_l A_p}\left[1 - exp\left\{-\frac{F' U_l A_p}{\dot{m}C_p}\right\}\right] \tag{7.6}$$

$$F' = \frac{1}{wU_l\left[\frac{1}{U_l\left[\left(w - D_o\right)\phi + D_o\right]} + \frac{\delta_a}{K_a D_o} + \frac{1}{\pi D_i h_f}\right]} \tag{7.7}$$

$$\phi = \frac{tanh\left(\frac{m\left(w - D_o\right)}{2}\right)}{\left(\frac{m\left(w - D_o\right)}{2}\right)} \quad where \quad m = \left(\frac{U_l}{K_p \delta_p}\right)^{0.5} \tag{7.8}$$

The energy efficiency of the system can be given by

$$\eta_{th} = \frac{Q_u}{I_T A_P} \tag{7.9}$$

7.2.2. Calculation of overall heat loss and heat transfer coefficient:

The heat loss from the top of the collector can be defined using the top loss coefficient (U_t)

$$\frac{q_t}{A_p} = U_t\left(T_p - T_a\right) \tag{7.10}$$

The overall heat loss coefficient (U_l), as given in Equation, (7.11) is the combined contribution of the top, bottom, and side loss coefficients.

$$U_l = U_t + U_b + U_s \tag{7.11}$$

The bottom loss and side loss coefficients can be determined using the following relations.

$$U_b = \frac{k_i}{\delta_b} \tag{7.12}$$

$$U_s = \frac{\left(L_1 + L_2\right) L_3 k_i}{L_1 L_2 \delta_s} \tag{7.13}$$

$$L_3 = \delta_{c1-c2} + \delta_{p-c1} + L + \delta_b \tag{7.14}$$

The radiation and convection losses from the glass cover and the absorber plate to the surrounding air contribute to heat losses from the top of the collector and are given by :

$$\frac{q_t}{A_p} = h_{p-c1}\left(T_p - T_{c1}\right) + \frac{\sigma\left(T_p^4 - T_{c1}^4\right)}{\left(\frac{1}{\varepsilon_p} + \frac{1}{\varepsilon_c} - 1\right)} \tag{7.15}$$

$$\frac{q_t}{A_p} = h_{c1-c2}\left(T_{c1} - T_{c2}\right) + \frac{\sigma\left(T_{c1}^4 - T_{c2}^4\right)}{\left(\frac{1}{\varepsilon_c} + \frac{1}{\varepsilon_c} - 1\right)} \tag{7.16}$$

$$\frac{q_t}{A_p} = h_w\left(T_{c_2} - T_a\right) + \sigma\varepsilon_c\left(T_{c_2}^4 - T_{sky}^4\right) \tag{7.17}$$

$$h_{p-c1} = \frac{Nuk_a}{\delta_{p-c1}} \tag{7.18}$$

$$h_{c1-c2} = \frac{Nuk_a}{\delta_{c1-c2}} \tag{7.19}$$

$$T_{sky} = T_a - 6 \tag{7.20}$$

The Equations (7.10) - (7.20) along with Equations. (7.2) - (7.3) can be solved to determine Q_u , U_l , T_p , T_{c1} and T_{c2}. The local heat transfer coefficients described in Equations (7.15)-(7.17) can be calculated using the following correlations

Convective heat transfer across inclined air layers in between plate and glass covers

The heat transfer coefficient between parallel plates is calculated using the following correlation (Hollands et al., 1976):

$$Nu = 1 + 1.44\left[1 - \frac{1708(sin1.8\beta)^{1.6}}{Ra\cos\beta}\right]\left[1 - \frac{1708}{Ra\cos\beta}\right]^{*} + \left[\left(\frac{Ra\cos\beta}{5830}\right)^{1/3} - 1\right]^{*} \quad (7.21)$$

The term indicated by '*' should be taken into account if and only if it is positive; otherwise, it should be taken as zero.

Convection heat transfer from glass cover to ambient

The following correlation (Sukhatme, 1984) can be used to calculate the convection heat transfer coefficient from the top glass cover to the surrounding

$$h_w = \frac{j}{Pr^{2/3}} \rho c_{p-a} V_{wind} \quad (7.22)$$

$$j = 0.86\, Re^{-0.5} \quad (7.23)$$

Reynolds Number is calculated using wind velocity as the monthly average wind velocity.

7.2.3 Exergy Analysis:

The exergetic efficiency of the solar collector based on the second law of thermodynamics can be given as

$$\eta_{ex}=1-\left\{\begin{array}{l}\left(1-\eta_o\right)+\dfrac{\dot{m}\Delta P}{\rho I_T A_p\left(1-\dfrac{T_a}{T_s}\right)}\dfrac{T_a\, ln\left(\dfrac{T_{out}}{T_a}\right)}{T_{out}-T_{in}}+\dfrac{\eta_o T_a}{\left(1-\dfrac{T_a}{T_s}\right)}\left(\dfrac{1}{T_p}-\dfrac{1}{T_s}\right)\\ +\dfrac{U_l\left(T_p-T_a\right)}{I_T\left(1-\dfrac{T_a}{T_s}\right)}\left(1-\dfrac{T_a}{T_p}\right)+\dfrac{\dot{m}C_p T_a}{I_T A_p}\left(\dfrac{ln\left(\dfrac{T_{out}}{T_{in}}\right)-\left(\dfrac{T_{out}-T_{in}}{T_p}\right)}{\left(1-\dfrac{T_a}{T_s}\right)}\right)\end{array}\right\} \tag{7.24}$$

The following exergy balance equation, which considers the inlet, outlet, stored, leaked, and destroyed exergy over solar water collectors and environment, serves as the basis for the determination of exergy efficiency as given by Equation (7.24) (Farahat et al., 2009)

$$\dot{E}_{in}+\dot{E}_{out}+\dot{E}_s+\dot{E}_l+\dot{E}_d=0 \tag{7.25}$$

The rate of exergy inlet to the system can be determined using the fluid flow ($\dot{E}_{in,f}$), and the absorbed solar radiation by the collectors ($\dot{E}_{in,Q}$)

$$\dot{E}_{in,f}=\dot{m}C_p\left(T_{in}-T_a-T_a\, ln\left(\frac{T_{in}}{T_a}\right)\right)+\frac{\dot{m}\Delta P_{in}}{\rho} \tag{7.26}$$

$$\dot{E}_{in,Q}=\eta_o I_T A_p\left(1-\frac{T_a}{T_s}\right) \tag{7.27}$$

The rate of exergy outlet ($\dot{E}_{out,f}$), can be calculated for the outlet of fluid flow using

$$\dot{E}_{out,f}=-\dot{m}C_p\left(T_{out}-T_a-T_a\, ln\left(\frac{T_{out}}{T_a}\right)\right)-\frac{\dot{m}\Delta P_{out}}{\rho} \tag{7.28}$$

As there is no accumulation of energy in the system at a steady state, the term stored exergy $\left(\dot{E}_s\right)$ rate becomes zero. The total losses due to convection and radiation components of the system can be accounted to the leakage rate of exergy ($\dot{E}_l$) and are given as:

$$\dot{E}_l = -U_l A_p \left(T_p - T_a\right)\left(1 - \frac{T_a}{T_p}\right) \tag{7.29}$$

Exergy destruction accounts for the heat transfer and the pressure drop due to temperature differences and friction in the flow channel. The destroyed exergy terms due to (i) temperature difference between the plate and the Sun and (ii) temperature difference between the plate and working fluid are given in Equation (7.30)-(7.31).

$$\dot{E}_{d,\Delta T_s} = -\eta_o I_T A_p T_a \left(\frac{1}{T_p} - \frac{1}{T_s}\right) \tag{7.30}$$

$$\dot{E}_{d,T_f} = -\dot{m} C_p T_a \left(ln\left(\frac{T_{out}}{T_{in}}\right) - \frac{\left(T_{out} - T_{in}\right)}{T_p}\right) \tag{7.31}$$

The exergy destroyed due to pressure drop caused by friction in the flow channel is given as:

$$\dot{E}_{d,\Delta P} = -\frac{\dot{m}\Delta P}{\rho}\left(\frac{T_a\, ln\left(\frac{T_{out}}{T_a}\right)}{T_{out} - T_{in}}\right) \tag{7.32}$$

$$\Delta P = \frac{128 \mu_f L_1 V_f}{\pi D_i^4} \tag{7.33}$$

7.3. Optimization problem formulation and solution strategy

In this section, the proposed model for the solar water collector has been transformed into an optimization formulation. Optimization formulation can be used to determine the optimal design and operational parameters for maximizing the exergy efficiency and studying the trade-offs between maximizing the exergy efficiency and minimizing the area of the absorber plate.

7.3.1. Single objective solution strategy

The single objective optimization problem for maximizing the exergy efficiency is defined as

$$\begin{aligned} &Maximize \quad \eta_{ex} \\ &s.t. \quad T_{c1} > T_{c2};\ T_p > T_{c1};\ T_{c1}, T_{c2}, T_p > T_a \\ &0.001 \le \dot{m} \le 0.02;\ 1 \le A_p \le 5;\ 300 \le T_{in} \le 350; \\ &0 \le Q_u \le 5000;\ 3 \le U_l \le 10;\ 305 \le T_p \le 450; \\ &303 \le T_{c1} \le 448;\ 301 \le T_{c2} \le 446;\ 4174 \le C_p \le 4250; \end{aligned} \tag{7.34}$$

In a typical solar water collector, the absorber plate has the highest temperature, followed by glass covers. The temperature of the topmost glass cover should be higher than the ambient temperature. These conditions are modeled as three constraints, which ensure that the thermodynamic constraints of the model are satisfied. The single objective formulation constitutes nine decision variables whose bounds and the associated constraints are given in Equation (7.34).

Single objective metaheuristic techniques

Metaheuristic techniques are stochastic population-based iterative optimization techniques that are inspired by natural or physical phenomena. Classical optimization algorithms are designed to solve specific types of problems, such as linear programming (LP), nonlinear programming (NLP), mixed-integer nonlinear programming (MINLP), etc., and require problem information before being used. This limitation can be overcome by the metaheuristic approach, where a group of solutions searches for the optima in the entire search space. Metaheuristic techniques start with a pool of potential solutions known as the population, and its objective function value indicates the quality of each solution. These techniques follow a set of rules to explore the search space and adopt some selection criteria to identify solutions with better objective function values to use for the next iteration. Most of the metaheuristic techniques are designed

to consider the optimization model as a black box, as shown in Fig. 7.1, and on that account, the user needs to model the system appropriately, considering all the phenomena involved in the system. In such a case, the objective function accepts the solution and returns only the objective value, which identifies the merit of the solution (Fig. 7.1 (a)). In many real-time problems, the objective function is designed to work within model boundaries and incorporate some internal corrections to the solutions. In such scenarios, the corrected solution and the objective value are to be reported to the metaheuristic techniques, as shown in Fig. 7.1 (b). The solution procedure used in this study is given in the following section.

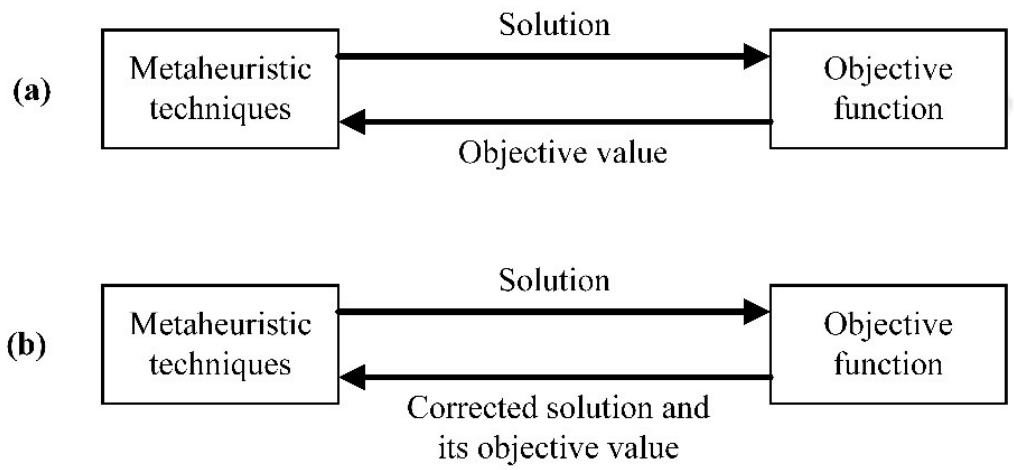

Fig. 7.1. Interaction between metaheuristic techniques and objective function
(a) without correction (b) with correction

Solution procedure for single objective metaheuristic techniques

In metaheuristic technique optimization formulation, the procedure for calculating the exergy efficiency is presented in an objective function. The optimization algorithm provides a potential solution to the objective function that constitutes all the decision variables. The solution is checked for any constraint violation in the temperature of the first glass cover (T_{c1}), and temperature of the absorber plate (T_p) as given in Equation (7.34).

Pseudocode for the solution procedure

Initialize all input parameters

Accept the values of $\dot{m}$, A_p , T_{in} , Q_u , U_l , T_P , T_{c1} , T_{c2} and C_P from the optimization algorithm

if T_{c1} violates constraint in Equation (7.34)

  Change T_{c1} using Equation (7.35)

end if

if T_P violates constraint in Equation (7.34)

  Change T_P using Equation (7.36)

end if

for month = 1 to 12

  Determine the monthly average I_T and S for the given wind velocity (V_{wind}) using solar radiation model

  Solve Equation (7.2), (7.3) and (7.15) - (7.17) to determine Q_u , U_l , T_P , T_{c1} , T_{c2} while satisfying fluid property calculations at an average fluid temperature

  if $(Q_u < 0) \vee (U_l < 0)$

    Assign least exergy efficiency for all months

    break

  else if T_P , T_{c1} , T_{c2} violate constraints in Equation (7.34)

    Assign least exergy efficiency for all months

    break

  end if

  Determine exergy efficiency using Equation (7.24)

end for

Determine mean exergy efficiency for all months

return mean exergy efficiency and values of $\dot{m}$, A_p , T_{in} , Q_u , U_l , T_P , T_{c1} , T_{c2} and C_P

Any violation of these constraints is corrected by assigning new values to the corresponding decision variables as given by equations Equation (7.35) and Equation (7.36).

$$T_{c1} = min\left(T_{c2} + r\left(T_{c1}^{ub} - T_{c1}\right), T_{c1}^{ub}\right), if\ T_{c2} > T_{c1} \tag{7.35}$$

$$T_p = min\left(T_{c1} + r\left(T_p^{ub} - T_p\right), T_p^{ub}\right), if\ T_{c1} > T_p \tag{7.36}$$

In these equations, *r* is a random number chosen between 0 and 1. The values of Q_u , U_l , T_P , T_{c1} and T_{c2} are calculated by solving the Equations (7.2), (7.3) and (7.15) - (7.17), while satisfying

fluid property calculations at an average fluid temperature. The obtained values are checked for any thermodynamic constraint violation as given in Equation (7.34). In case of any constraint violations in the model parameters, the exergy efficiency for all the months is penalized by assigning a small exergy efficiency value. In the absence of any constraint violation, the exergy efficiency is calculated for all the months using Equation (7.24). The values of all decision variables and the mean exergy efficiency are returned to the optimization algorithm. This process proceeds iteratively until the termination criterion of the optimization algorithm is satisfied. The pseudocode of the objective function evaluation process provided in this section details the solution procedure.

7.3.2. Multi-objective solution strategy

One of the desired objectives for a solar water collector is to reduce the absorber plate area for maximum exergy efficiency. In this chapter, a multi-objective solar collector model considering maximizing exergy efficiency (η_{ex}) and minimizing the absorber plate area $\left(A_p\right)$ are solved as two objectives. The optimization formulation is given below.

$$\begin{aligned} &Maximize \quad \eta_{ex} \\ &Minimize \quad A_p \\ &S.T \quad T_{c1} > T_{c2};\ T_p > T_{c1};\ T_{c1}, T_{c2}, T_p > T_a \end{aligned} \tag{7.37}$$

The decision variables and their operating ranges are the same as those of the single objective optimization formulation in the previous section.

Multi-objective computational intelligence techniques

Multi-objective optimization problems (MOOP) consist of two or more objective functions that are conflicting in nature. Instead of a single optimum solution, the solution of MOOP results

in a set of solutions that depicts the trade-off between the objective functions. These non-dominated solutions constitute the Pareto front, which are not dominated by any feasible point in the search space. Formally, a solution X_1 is said to dominate another solution X_2 only if (a) all objectives of X_1 are not worse than X_2, and (b) at least one objective function of X_1 is better than that of X_2. Metaheuristic techniques utilize several methods to determine the Pareto-optimal solutions such as non-dominated sorting and crowding distance(Deb et al., 2002), epsilon-domination (Deb et al., 2002), the weighted average of objectives (Deb, 2001), etc.

Solution procedure for multi-objective metaheuristic techniques

The solution procedure for multi-objective optimization is similar as discussed in the single-objective case. In this case, the optimization algorithm requires two objective function values from the objective model instead of one, as in a single objective model. A flowchart for the multi-objective evaluation is given in Fig. 7.2.

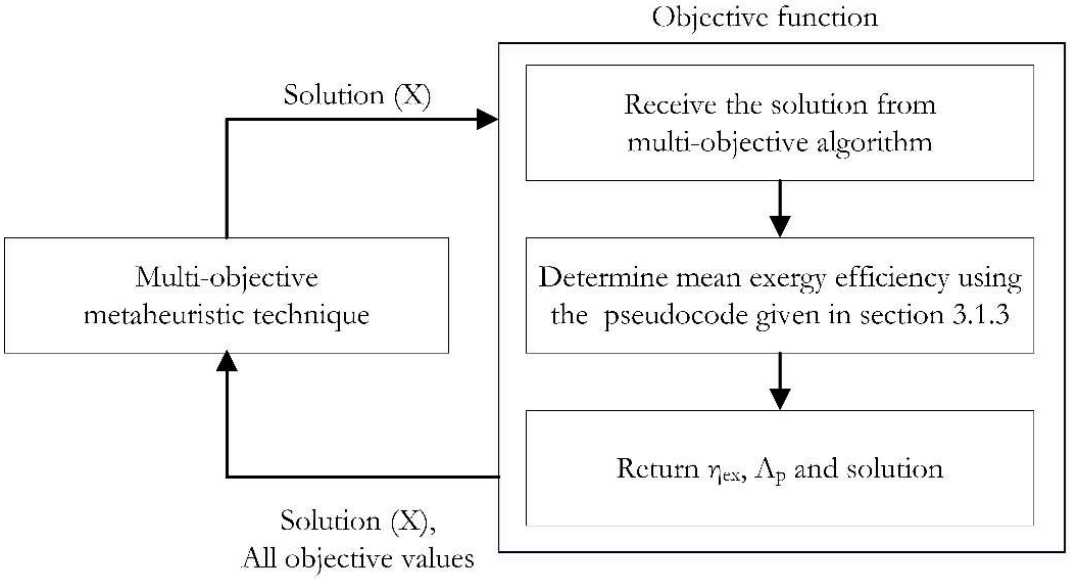

Fig. 7.2. Flow chart representing optimization of solar water collector model using multi-objective metaheuristic techniques

The initial step is to receive the solution provided by the multi-objective metaheuristic technique from the multi-objective solar collector model. The model determines the mean exergy efficiency as per the pseudocode given in Section 7.3.1. Unlike in the case of single-objective optimization, the model returns the solution values along with two objective function values η_{ex} and A_p to the multi-objective metaheuristic technique. The optimization process is continued until the termination criterion of the selected multi-objective metaheuristic techniques is satisfied.

7.4. Problem specifications and model validation

This study is conducted in humid subtropical climatic conditions. The longitude, latitude, and elevation of Guwahati are 26.18˚, 91.73˚, and 53 m. The Equation for time correction, wind velocity, and sunshine hours is considered for the year 2018. A double glass glazing flat plate solar collector is used in this study. The schematic of the solar water collector model is given in Fig. 7.3.

The ambient temperature (T_a) and the temperature of the Sun (T_s) are considered as 300 K, and 4350 K. The Absorber plate with an emissivity of 0.92 is made up of aluminium (thermal conductivity = 200 W/m K). The thickness of the absorber plate is considered to be 0.002 m. The Glass covers are made of Plexiglass material with an emissivity of 0.84. Bottom and side insulations are made up of wool with a thermal conductivity of 0.05 W/m K. The tilt angle of the collector is 20˚. The air gaps between the glass covers and the top plate are taken to be 0.04 m. The bottom and side insulation thickness is considered to be 0.08 and 0.04 m, respectively. The center-to-center tube distance and the inner diameter of the pipes were considered to be 0.15 m and 0.04 m. The length of the collectors is considered to be constant (L_1 =1 m), and the

width of the collectors is fixed by the optimum area of the collectors. The adhesive resistance of the solar collector is taken as 1.2 m^2 K/W. All the fluid properties are calculated at the average fluid temperature. The required data for fluid property calculations are taken from the literature (Holman 2010) and are given in Table 7.1.

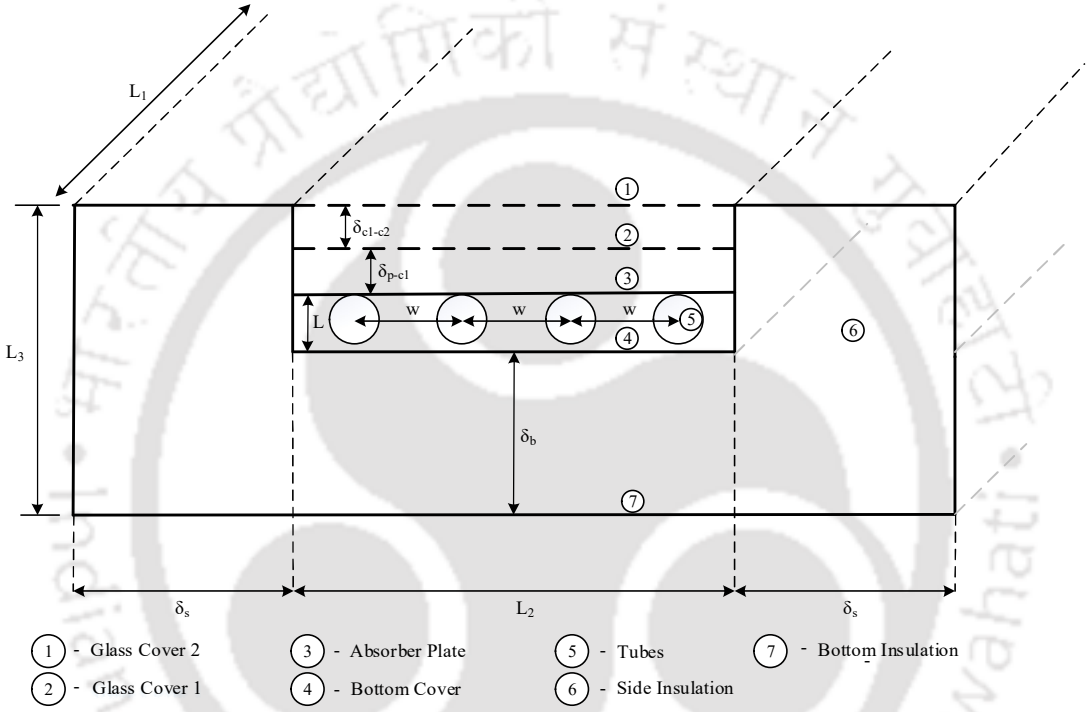

Fig. 7.3. Schematic diagram of solar water collector

The solar water collector model presented in this chapter is validated against (Farahat et al., 2009), and the results are in good agreement (Table 7.1.). The optimization model is nonlinear and consists of nine decision variables, six implicit constraints, and three explicit constraints. The current solar water collector model uses 32 equations to determine the mean exergy efficiency. It is implemented in MATLAB 2019a on a PC with an Intel i7@3.4GHz processor and 16 GB of RAM. The stochastic nature of metaheuristic techniques requires multiple runs under identical resource constraints for their performance evaluations. In this chapter, 25 independent runs are executed by utilizing the '*twister*' algorithm available in MATLAB and

varying its seed from 1 to 25. The population size and termination criterion for all the metaheuristic techniques are set as 30 and 200 functional evaluations, respectively. All other algorithmic parameters are used as provided in the codes given by respective authors. Apart from determining optimal parameters for maximum mean exergy efficiency, the model also investigates the effect of absorber plate area on exergy efficiency using a multi-objective optimization model.

Table 7.1. Comparison between the current simulation and results of literature for solar water collector

Parameters	Present Model	Literature Model (Farahat et al., 2009)
Fluid inlet temperature (K)	300	300
Incident solar energy per unit area of the absorber plate (W m^{-2})	500	500
Wind Speed (m s^{-1})	25	25
Overall heat loss coefficient (W m^{-2} K^{-1})	4.5660	4.6797
Outlet temperature (K)	359.47	358.8248
Absorber plate temperature (K)	340.17	339.4307
Glass Cover1 Temperature (K)	323.86	Not reported
Glass Cover 2 temperature (K)	304.85	Not reported
Absorber Plate Area (m^2)	9.14	9.14
Specific Heat Capacity (J/kg K)	4179.23	4180.4
Fluid Density (kg/m^3)	984.66	982.2709
Plate Effectiveness	0.9902	0.9943
Collector Efficiency Factor	0.9061	0.9114
Collector Heat Removal Factor	0.5633	0.5573
Mass flow rate (kg s^{-1})	0.0087	0.0087
Useful Heat Gain (W) [using Equation (7.2)]	2162.35	2139.4
Useful Heat Gain (W) [using Equation (7.3)]	2162.35	Not reported
Useful Heat Gain (W) [using Equation (7.5)]	2162.35	Not reported
Pressure Drop (Pa)	0.0010	0.0011
Energy Efficiency	0.4732	0.4681
Exergy Efficiency	0.0446	0.038

7.5. Results and discussion

This section discusses the single objective and multi-objective optimization solution for the solar water collector. A study is performed to test the effect of operational and environmental parameters on exergy efficiency. This section also analyses the performance of the algorithms in solving the optimization model.

7.5.1. Optimal solution analysis

The ambient and design conditions of the solar water collector required for the optimization analysis are mentioned in Section 7.4. The optimal values for maximum mean exergy efficiency are determined by the following algorithms using a single objective solar collector model: SHTS, SHO, WCA, DNLPSO, MPEDE and GA. The optimal values of independent and dependent optimization parameters, which are mentioned in Table 7.2, are determined using SHTS, SHO, WCA, DNLPSO, MPEDE, and GA for the given values of ambient and design conditions. As an example, WCA reports the following optimum values: η_{ex} = 5.926%, A_p = 5 m^2, $\dot{m}$ = 0.02 kg/s, T_{in} = 341.13 K, T_p = 354.07 K, T_{c1} = 336.12 K, T_{c2} = 314.92 K, U_l = 4.20 W/m^2 K, Q_u = 1205.81 W/m^2, C_p = 4189.75 J/kg K. The best solution is determined by WCA, DNLPSO, and MPEDE using the maximum available absorber plate area.

Since reducing the absorber plate area is a desirable choice in solar collectors, separate optimization simulations are carried out to investigate the exergy efficiency corresponding to the minimum absorber plate area. The results of the simulations considering minimizing plate area as the objective function are also given in Table 7.2. The optimal objective value determined by all the algorithms is highlighted using the boldfaced font. The results determined by SHTS and SHO suggest a decrease in exergy efficiency with minimum absorber plate area.

Table 7.2. Results of single objective optimization

	Objective: Maximize η_{ex}						**Objective: Minimize A_p**					
	SHTS	SHO	WCA	DNLPSO	MPEDE	GA	SHTS	SHO	WCA	DNLPSO	MPEDE	GA
$\dot{m}$	0.02	0.0166	0.02	0.02	0.02	0.0194	0.0114	0.0151	0.0179	0.0167	0.0085	0.0087
A_p	5	4.61	5	5	5	4.75	**1**	**1**	**1**	**1**	**1**	**1**
T_{in}	339.46	339.93	341.13	341.01	341.13	341.49	300	300	350	350	350	349.24
Q_u	1237.03	1115.63	1205.81	1207.90	1205.66	1142.16	409.35	413.15	213.95	213.48	207.01	210.53
U_l	4.19	4.20	4.20	4.20	4.20	4.20	4.31	4.34	4.52	4.52	4.53	4.52
T_P	352.74	353.78	354.07	353.98	354.08	354.22	313.64	312.70	356.30	356.39	357.65	356.96
T_{c1}	335.15	335.89	336.12	336.05	336.12	336.22	307.73	307.11	337.20	337.27	338.18	337.68
T_{c2}	314.43	314.78	314.92	314.89	314.93	314.96	301.26	301.01	314.50	314.54	314.97	314.74
C_P	4188.32	4189.38	4189.75	4189.65	4189.75	4189.93	4174.73	4175.74	4192.42	4192.49	4193.46	4192.93
η_{ex}	0.05921	0.05911	0.05926	0.05926	0.05926	0.05922	0.01023	0.00794	0.05528	0.05525	0.05479	0.05505
Mean CPU time (s)	37.25	21.73	31.96	29.32	28.13	35.80	35.99	23.02	26.48	24.8	27.37	30.88

Table 7.3. Corner Solutions of the Pareto fronts

	$\dot{m}$	A_p	T_{in}	Q_u	U_l	T_P	T_{c1}	T_{c2}	C_P	Max η_{ex}	Min A_p	Mean CPU time (s)
MOGA	0.0036	1	341.37	224.07	4.50	354.31	335.77	313.82	4190.28	0.05556	**1**	30.43
	0.0189	4.60	341.26	1109.26	4.21	354.02	336.06	314.87	4189.71	0.05919	4.60	
MODE	0.0198	1	344.23	239.98	4.46	351.14	333.50	312.73	4187.24	0.05611	**1**	27.9
	0.0176	4.31	340.66	1047.50	4.21	353.55	335.71	314.67	4189.21	0.05911	4.31	
FYYPO	0.0089	1.00	342.32	240.41	4.46	351.08	333.46	312.72	4187.14	0.05609	1.00	56.12
	0.0195	4.82	341.61	1155.20	4.20	354.38	336.34	315.03	4190.09	0.05923	4.82	
MSSA	0.0200	1	350	214.62	4.52	356.16	337.11	314.46	4192.31	0.05532	**1**	34.8
	0.0194	4.44	340.21	1094.56	4.20	352.77	335.15	314.40	4188.40	0.05914	4.44	
MALO	0.0141	1	343.19	241.93	4.46	350.75	333.22	312.60	4186.85	0.05611	**1**	30.98
	0.0194	4.44	340.21	1094.56	4.20	352.77	335.15	314.40	4188.40	0.05914	4.44	
MOWCA	0.0168	1	344.22	238.86	4.47	351.36	333.66	312.81	4187.46	0.05611	**1**	31.19
	0.0200	5	341.16	1205.08	4.20	354.10	336.14	314.94	4189.78	**0.05926**	5	

On the other hand, the solutions determined by WCA, DNLPSO, MPEDE, and GA suggest only 7 % decrease in best mean exergy efficiency by reducing 80% of the absorber plate area. Conducive to decide on the relation of mean exergy efficiency with the absorber plate area, a multi-objective optimization is performed, and the results are tabulated in Table 7.3. The corner points of a Pareto front represent the solutions that are best at one objective function and the worst at the other objective function. The corner points and the corresponding solutions determined by all the considered algorithms are provided in Table 7.3.

The corner point representing the minimum absorber plate area (best value) and minimum mean exergy efficiency (worst value) of MODE, MALO, and MOWCA are the same and dominates the corresponding corner point determined by MOGA, FYYPO, and MSSA. The corner point corresponding to maximum mean exergy efficiency and the maximum absorber plate area reported by all algorithms are non-dominating with each other. The corner points reported by MOWCA are either better or non-dominating to all other corner points, and it represents the best solution in accordance with the maximization of mean exergy efficiency.

7.5.2. Effect of operational parameters on exergy efficiency

Fig. 7.4 shows the trend of mean exergy efficiency (η_{ex}) as a function of design and operational conditions such as mass flow rate of fluid ($\dot{m}$), inlet fluid temperature (T_{in}), absorber plate area (A_p), absorber plate temperature (T_p) and glass cover temperatures (T_{c1} and T_{c2}) for other constant optimal values, as reported by the WCA algorithm. Variation of exergy efficiency (η_{ex}) is presented to a range of upper and lower bound values of design and operational conditions, within which η_{ex} reaches a maximum value. The calculated values for the maximum η_{ex} are: $A_p = 5$ m^2, $\dot{m} = 0.02$ kg/s, $T_{in} = 341.13$ K, as reported by the WCA algorithm.

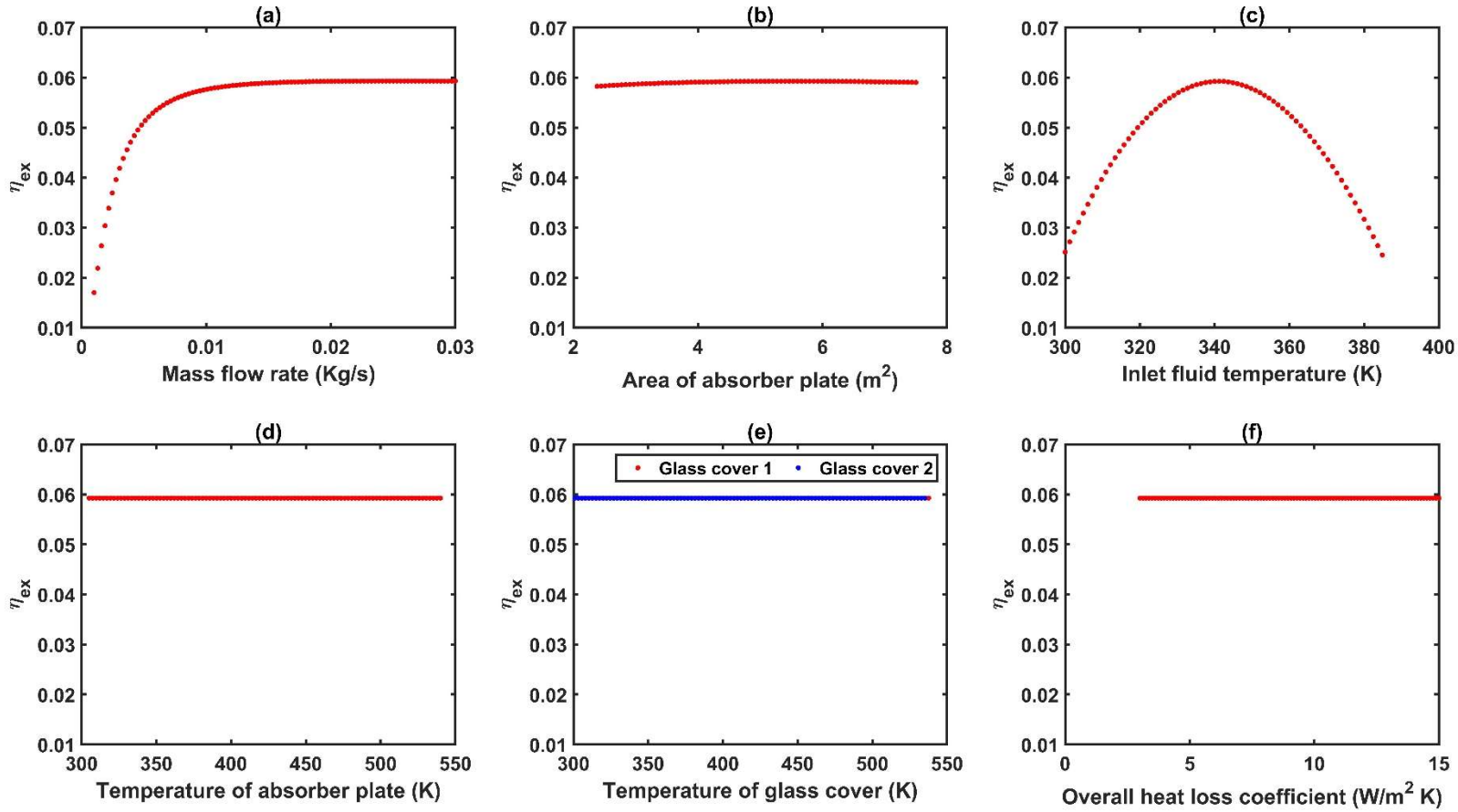

Fig. 7.4. Effect of operational parameters on exergy efficiency (a) mass flow rate, (b) area of absorber plate (c) fluid inlet temperature, (c) absorber plate temperature, (d) glass cover temperatures, and (f) total heat loss coefficient

It is observed that an increase in $\dot{m}$, A_p or T_{in} above, the optimal values reported by WCA does not improve η_{ex} while keeping other decision variables at the reported optima. It is noted that decreasing $\dot{m}$ below the value of 0.02 kg/s shows a very subtle decrease of η_{ex} until 0.006 kg/s. There is a sensible change of η_{ex} below 0.006 kg/s, and the value of η_{ex} approximately varies between 1.7 - 5.35 % for $\dot{m}$ = 0.001 - 0.006 kg/s (Fig. 7.4 (a)), which allows the user to optimize the solar water collector based on other design constraints and thermal applications.

Fig. 7.4 (b) shows the variations of η_{ex} versus A_p . An increase in A_p greater than 5 m^2 shows a slight increase in η_{ex} . Thereafter, η_{ex} starts decreasing with an increase in A_p . Fig. 7.4 (c) shows the effect of T_{in} on η_{ex} . It is observed that η_{ex} increases with T_{in} until the value of T_{in} = 341.13 K and then decreases abruptly (5.926% - 2.5%). This higher T_{in} can be achieved either by a waste heat recovery system or by increasing the storage water temperature for a particular time period in a closed circuit solar water collector system.Increasing T_{in} beyond 341.13 K decreases η_{ex} due to higher exergy destruction during inlet fluid flow. Fig. 7.4 (e-f) shows the effect of T_p , T_{c1} , T_{c2} and U_l on η_{ex} . As expected, an increase in these parameters leads to no observable change in η_{ex} for other constant optimal values.

7.5.3. Effect of environmental conditions on exergy efficiency

In this study, the calculation of I_T is considered from morning 8:00 hrs (IST) to 16:00 hrs (IST) in the evening. Variations of the monthly average of the hourly incident heat flux (I_T) and optical efficiency (η_o) throughout the year are calculated to determine mean exergy efficiency (η_{ex}). The month of March and July shows higher (668.7 W/m^2) and lower

(505.7W/m^2) monthly average of the hourly incident heat flux (I_T) on the absorber plate for humid subtropical climatic conditions. Lesser heat flux during the month of July is due to the rainy season, which reduces the sunshine hours and increases diffuse radiation ($\overline{I_d}$) in humid subtropical climatic conditions. Optical efficiency is the highest during February (78.5%) while it is the lowest for July (76.5%).

Fig. 7.5 shows the trend of mean exergy efficiency (η_{ex}) as a function of environmental conditions such as ambient temperature (T_a), wind velocity (V_{wind}), incident solar heat flux (I_T), and optical efficiency (η_o) for other constant optimal values as reported by WCA algorithm. An increase in T_a shows a sensible decrease (5.926% to 5.04%) in η_{ex} for other constant optimal values as reported by the WCA algorithm (Fig. 7.5 (a)). Increasing V_{wind} shows a marginal decrease of η_{ex} from 5.97 to 5.43% (Fig. 7.5 (b)). Fig. 7.5 (c) shows the variations of η_{ex} with respect to I_T. By increasing I_T from 500 to 1000 W/m^2, the exergy efficiency increases from 5.1% to 8.13%. Fig. 7.5 (d) shows the effect of η_o on η_{ex}. By increasing η_o from 50 to 100 %, η_{ex} increases from 2.45% to 9.05%.

7.5.4. Convergence and statistical analysis

The performance of metaheuristic techniques can be analyzed using the convergence profile and the statistical parameters in the case of single-objective optimization. The performance of multi-objective algorithms is evaluated by observing the spread and closeness of determined non-dominated solutions against global Pareto solutions. The following section discusses the results obtained by all metaheuristic techniques for both single and multi-objective optimization of the solar water collector model.

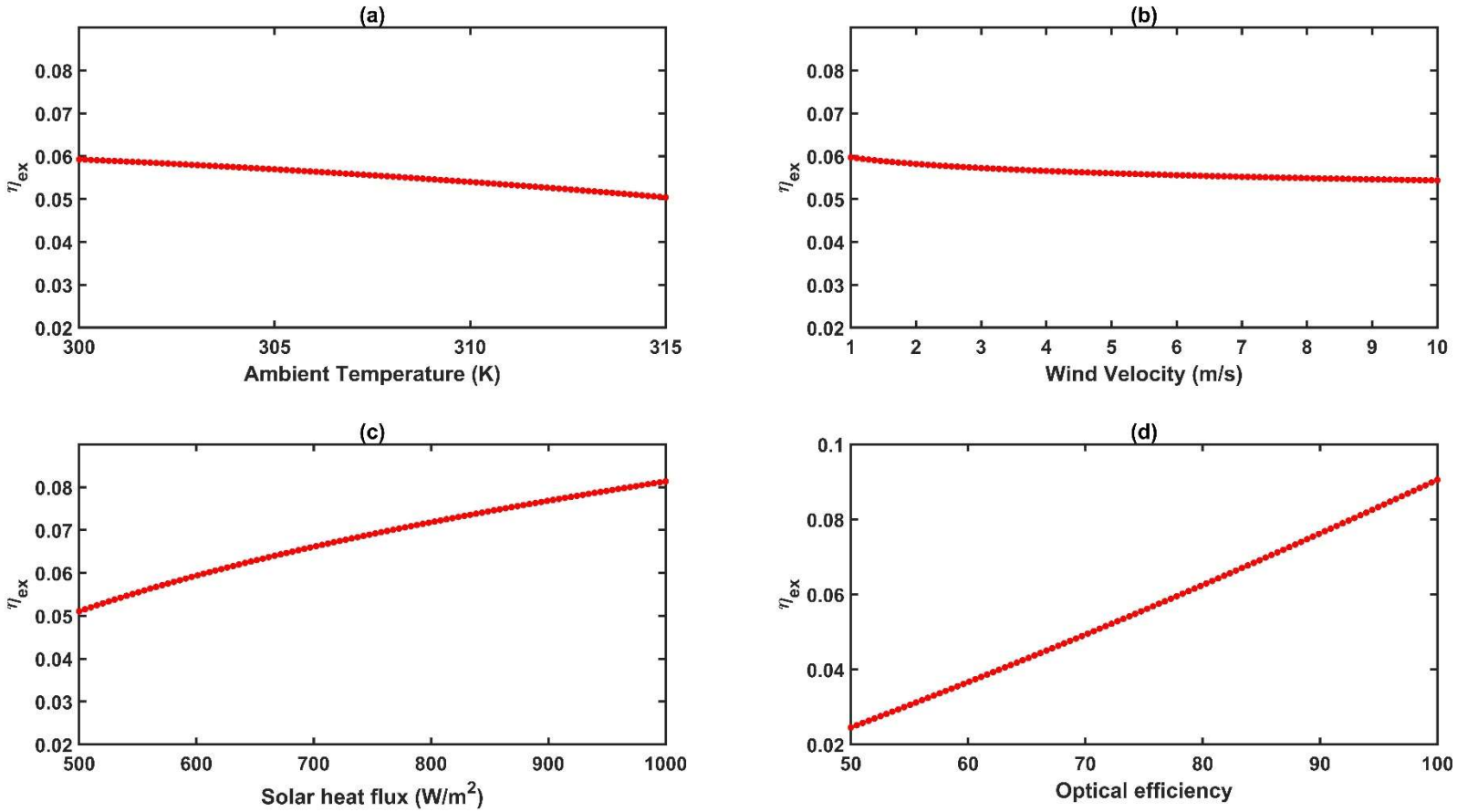

Fig. 7.5. Effect of environmental conditions on exergy efficiency (a) ambient temperature, (b) wind speed, (c) incident solar heat flux, and (d) optical efficiency

Single objective optimization

The statistical table representing the best, worst, mean, median, and standard deviation of the results reported by each algorithm for maximizing mean exergy efficiency in all the runs is provided in Table 7.4. The best value under each statistical parameter is highlighted with boldface font. It is evident from Table 7.4 that the performance of WCA is superior compared to all the other algorithms in every statistical parameter. It should be noted that the best and median statistics of WCA are the same value, and the mean value is also close to the reported best objective function value, which further indicates that WCA determined the optima in most of the runs. Apart from WCA, DNLPSO and MPEDE also determine the optimal solution in at least one run. On comparing the standard deviation of each algorithm, it is found that SHO determined the worst value. Likewise, the mean objective function value of SHO is also worse among the other algorithms, and thus the overall performance of SHO on determining the maximum mean exergy efficiency is not satisfactory. Even though the mean and median values reported by SHTS is better than GA, GA provided better values than SHTS in all other statistics.

Table 7.4. Statistical analysis for single-objective optimization

Algorithms	Objective: Maximize η_{ex}					Objective: Minimize A_p				
	Best	Worst	Mean	Median	SD	Best	Worst	Mean	Median	SD
SHTS	0.05921	0.05801	0.05889	0.05892	2.40E-04	1	1	1	1	0
SHO	0.05911	0.05691	0.05844	0.05865	5.90E-04	1	1	1	1	0
WCA	**0.05926**	**0.05913**	**0.05925**	**0.05926**	**2.00E-05**	1	1	1	1	0
DNLPSO	**0.05926**	0.05887	0.05917	0.05921	9.00E-05	1	1.25	1.01	1	0.05
MPEDE	**0.05926**	0.05904	0.05923	0.05924	4.00E-05	1	1	1	1	0
GA	0.05922	0.05842	0.05887	0.05887	2.20E-04	1	1.36	1.03	1	0.09

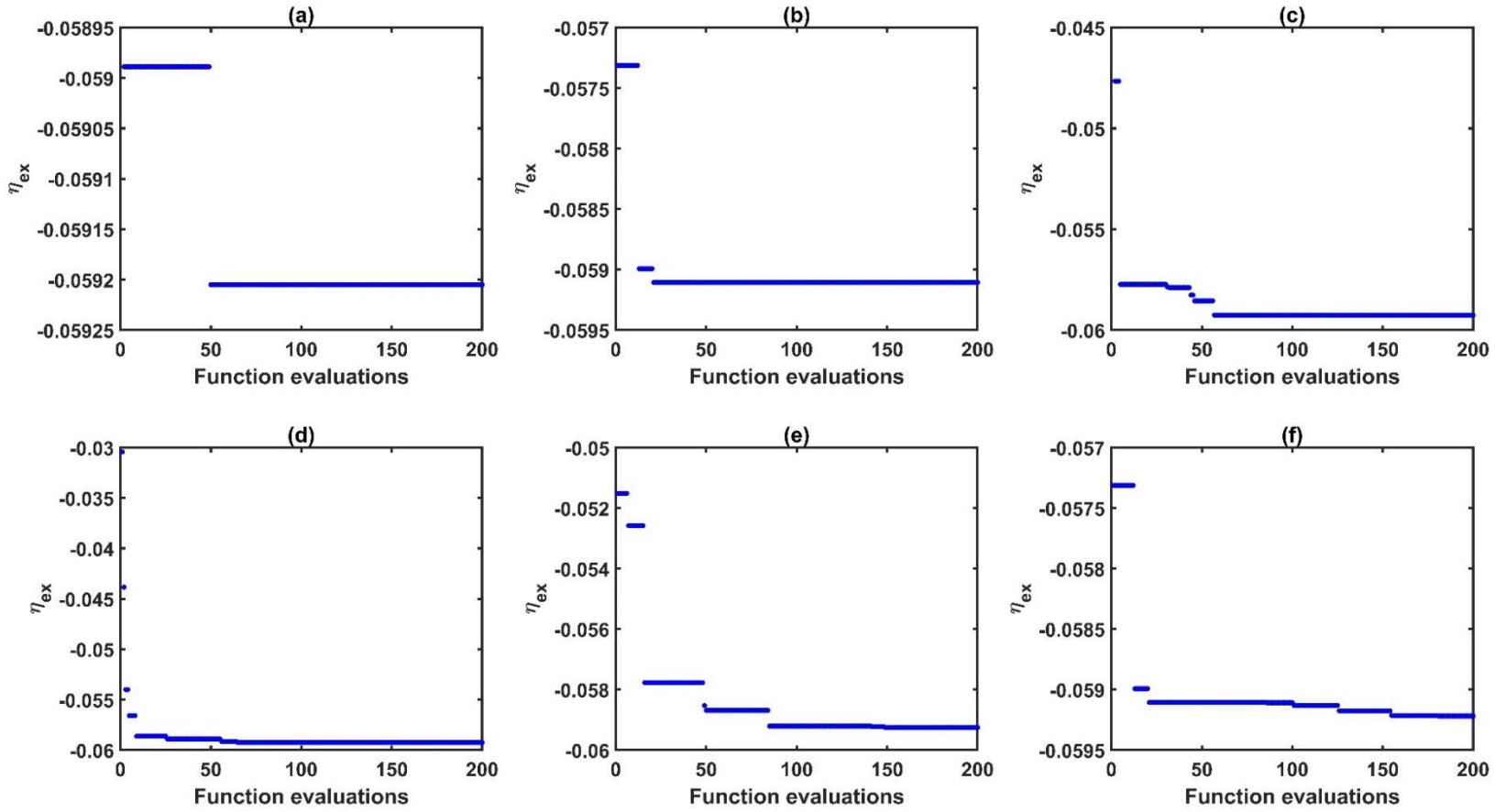

Fig. 7.6. Convergence curve of the best run for maximization of mean exergy efficiency

(a) SHTS, (b) SHO, (C) WCA, (d) DNLPSO, (e) MPEDE, (f) GA

The convergence obtained by each algorithm for their best solution is represented in Fig. 7.6, where the x-axis represents the function evaluations, and their corresponding best value of mean exergy efficiency is given on the y-axis. All the considered algorithms are based on minimizing an objective function, and the maximization of mean exergy efficiency is calculated by multiplying with (-1). The following inferences are depicted from the convergence plots: Among all the algorithms considered, SHO converges quickly to the final solution; however, it is not able to determine the best solution. SHTS converges to a sub-optimal solution within 25% of the maximum function evaluations and do not show any further improvement. A similar trend of convergence is shown by SHO, while the final solution reported by SHTS is better than SHO. DLNPSO and WCA are able to determine the optimal solution using slightly more than 25% of the function evaluations.

MPEDE also reports the optima by utilizing almost 75% of the functional evaluations. Considering all the algorithms, GA shows poor convergence and is not able to converge even after completing the termination criterion. The mean CPU time for determining the single objective solution for each algorithm is given in Table 7.2. Among all the algorithms, SHO is the fastest, whereas SHTS is the slowest in determining the optima. The statistical results for the single objective case with minimizing the absorber plate area are given in Table 7.4.

The best, worst, mean, median, and standard deviation values are the same for all algorithms except DNLPSO and GA, which indicates optimal solution determination in all the runs. The mean values of DNLPSO and GA state the determination of suboptimal solutions in at least one of the runs. The convergence of the best solution determined by each algorithm for the objective of the minimum absorber plate area is shown in Fig. 7.7.

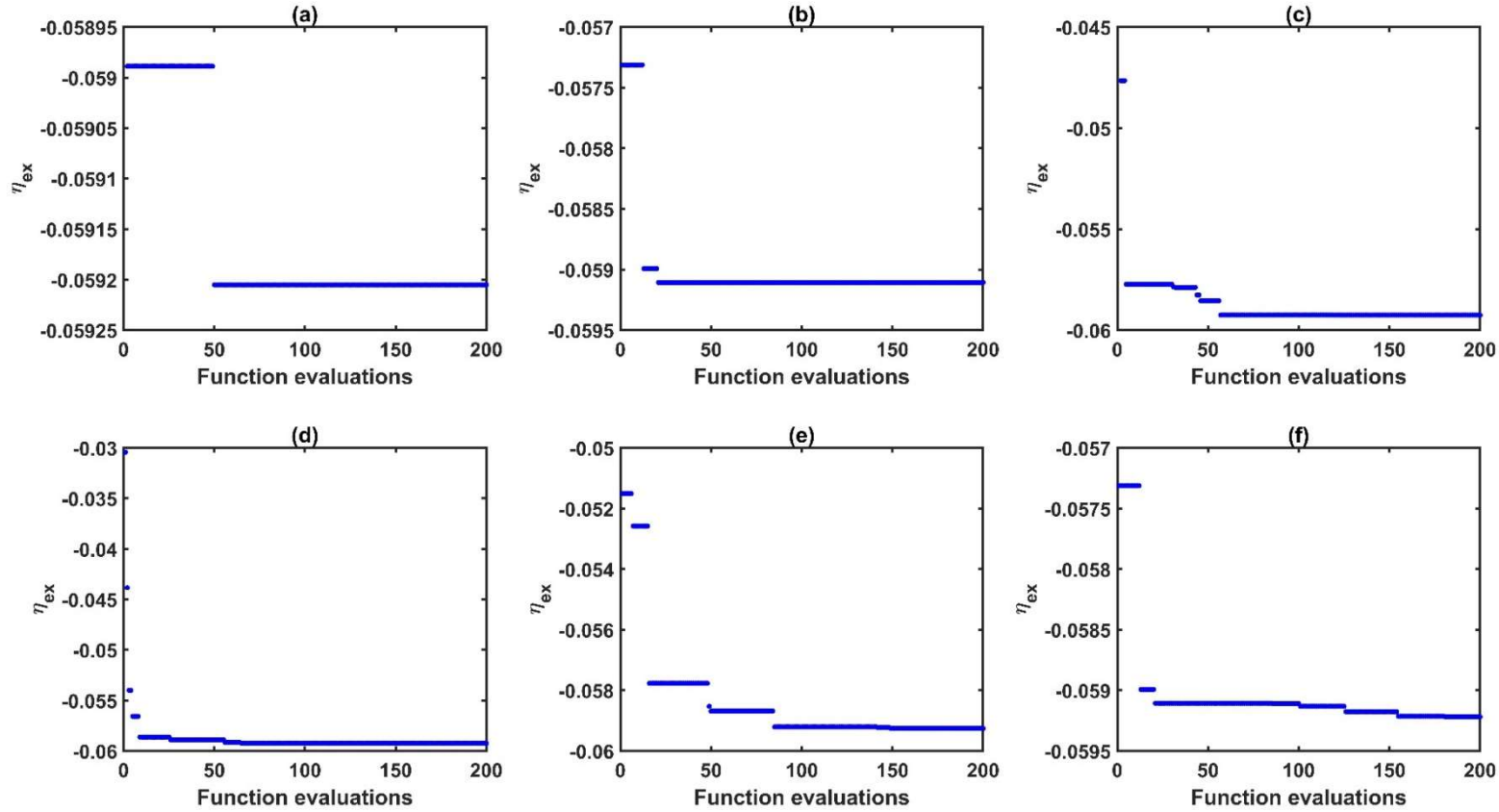

Fig. 7.7. Convergence curve of the best run for minimization of absorber plate area

(a) SHTS, (b) SHO, (C) WCA, (d) DNLPSO, (e) MPEDE, (f) GA

All the algorithms are able to converge within the termination criterion. All algorithms expect DNLPSO and GA show quick convergence and reach the final solution within 25% of the functional evaluations.

Multi-objective optimization

The global Pareto of any real-time problems is determined by selecting the non-dominated solutions from the set of Pareto solutions reported by all the algorithms. Fig. 7.8 represents the Pareto obtained by each algorithm along with the non-dominated solutions determined in all the runs and the global Pareto of the problem. It is evident from Fig. 7.8 that the Pareto front of MOWCA and MOGA overlapped with the global Pareto front. It implies that most of the non-dominated points determined by MOWCA and MOGA are present in the global Pareto. All other algorithms, except MOWCA, are not able to determine the corner point corresponding to maximum mean exergy efficiency (with maximum absorber plate area).

On analyzing the convergence of the obtained Pareto to the global Pareto, the performance of MSSA is not satisfactory. The mean CPU time of MODE is observed to be the lowest among all, whereas FYYPO consumes more time in determining non-dominating solutions. The convergence of Pareto solutions with respect to 50, 100, 150, and 200 function evaluations determined by MOWCA for the best run is provided in Fig. 7.9. It is evident from Fig. 7.9 that MOWCA improves the convergence of non-dominated solutions with an increase in function evaluations. The corner solution representing the minimum absorber is obtained within 75 % of the function evaluations. The number of solutions in the region indicating minimum area (minimum mean exergy efficiency) is lesser than the region representing maximum mean exergy efficiency (maximum absorber plate area).

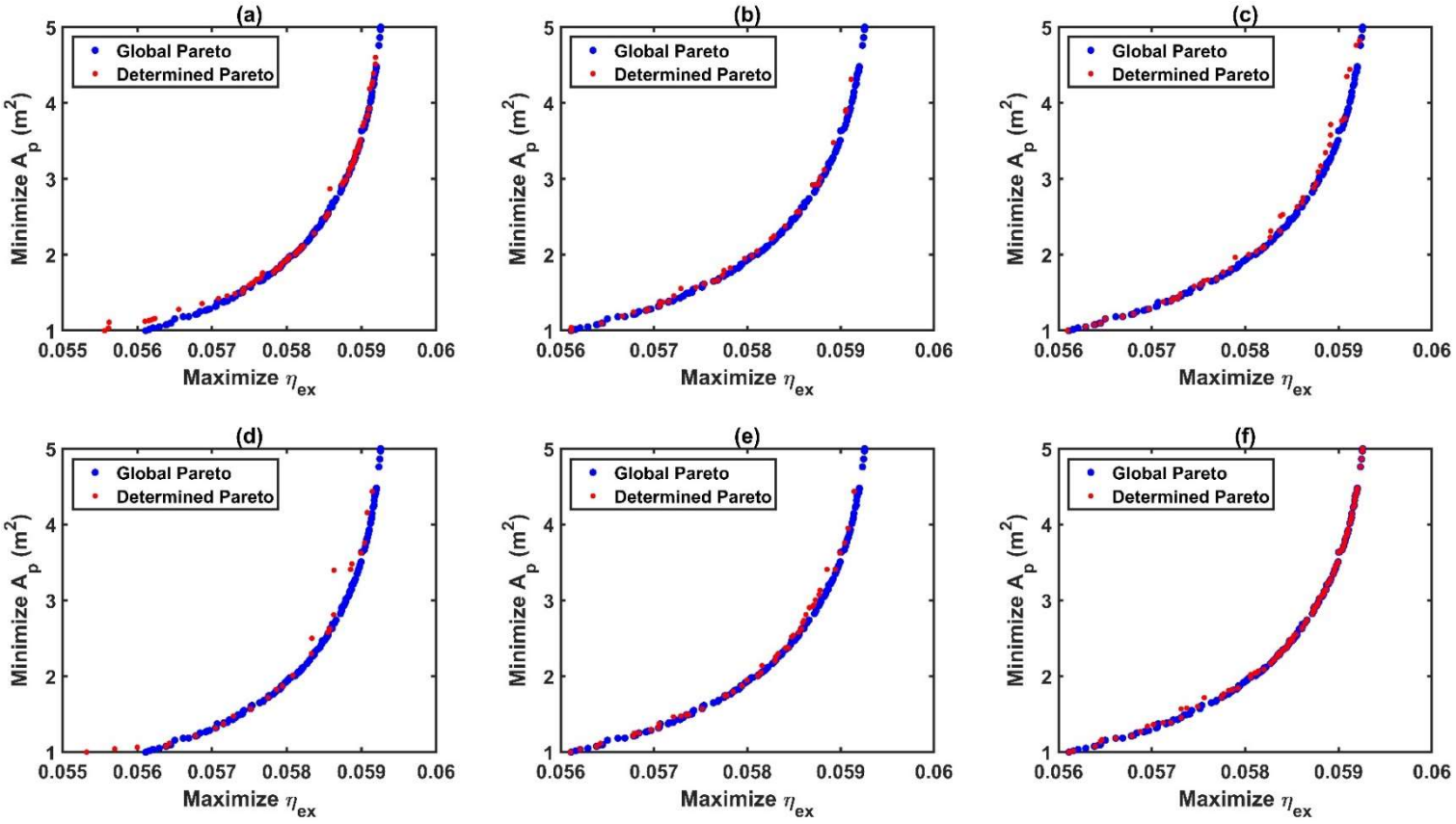

Fig. 7.8. Pareto front between maximization of η_{ex} and minimization of A_p

(a) SHTS, (b) SHO, (C) WCA, (d) DNLPSO, (e) MPEDE, (f) GA

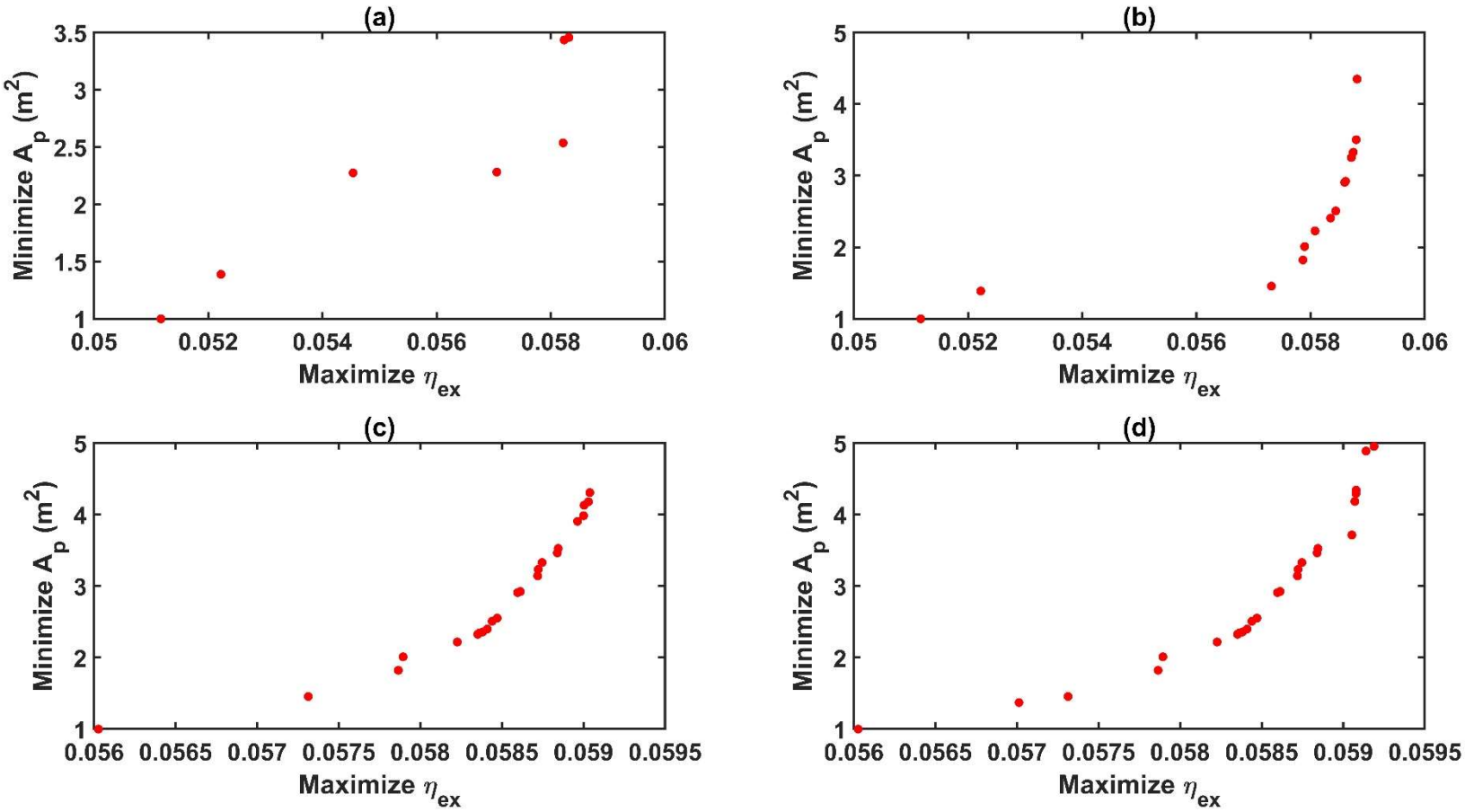

Fig. 7.9. Convergence of the Pareto front in the best run of MOWCA corresponding to (a) 50, (b) 100, (c) 150 and (d) 200 function evaluations

Optimization toolkit

The implementation of a mathematical model into an optimization simulation environment is challenging for many users. The final solution of such an optimization problem requires modeling and simulation of all the equations into an objective function and using it appropriately for optimization algorithms. It also requires good proficiency in simulation software. In this regard, a GUI-based toolkit is highly beneficial in reducing user difficulties in determining the optimal solution. One of the essential benefits of such toolkits is demonstrating the sensitivity of the model with varying operational and design conditions using minimal knowledge of model or software components. An optimization tool kit using MATLAB GUI is developed in this study, and the interface is given in Fig. 7.10. The initial interface of the GUI provides the bounds for nine decision variables used in this study, a schematic of the solar water collector model, and a choice of different metaheuristic techniques for both single and multi-objective optimizations.

The toolkit provides the benefits of changing the (a) operational bounds, (b) model parameters, (c) selection of single or multi-objective model, (d) optimization using one or more metaheuristic techniques, (e) termination criterion, and (f) number of simulations. The model parameters used for this toolkit are provided in a Microsoft spreadsheet. The model parameters can be easily accessed and modified by clicking the *'Change model parameters'* button. The *'Start'* and *'Stop'* buttons are used to initiate or terminate the simulations. The *'Reset'* button sets all the model parameters to the default values, as displayed in the initial GUI interface. On completion of the optimization, the single objective model of the GUI displays the results, such as the convergence curve corresponding to the best run and best optimal solution among all simulations.

(a)

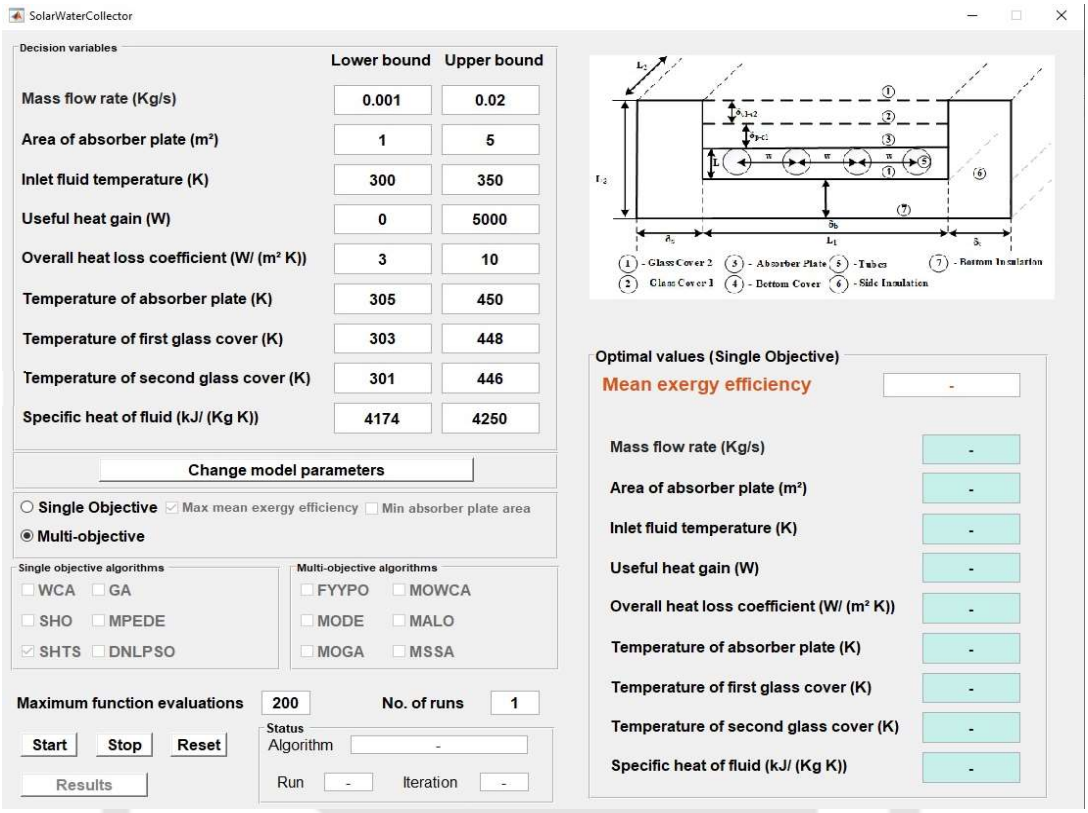

(b)

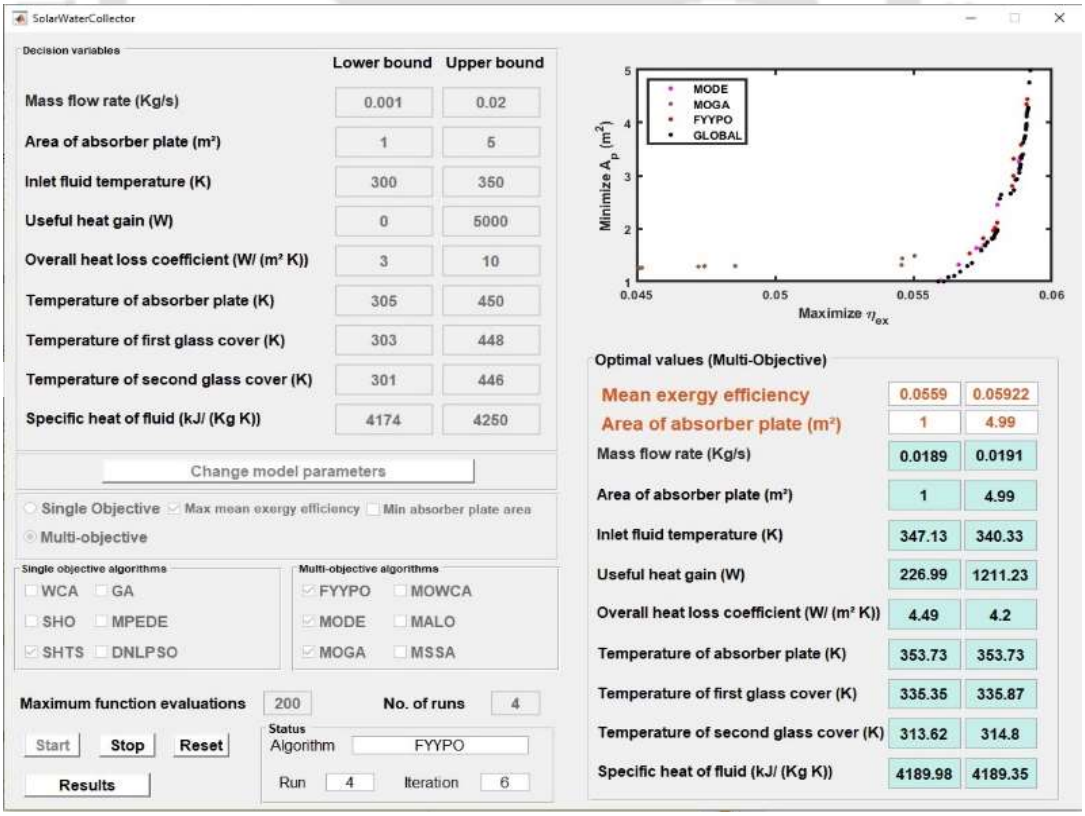

Fig. 7.10. Interface of the optimization toolkit (a) model initialization (b) model optimization

In the multi-objective optimization scenario, the panel displays a plot for Pareto solutions obtained by each algorithm along with the global Pareto front and corner solutions for determining the global Pareto front. All the figures displayed in the panel for different optimization criteria are saved into a jpeg format for future analysis by the users. Apart from displaying the optimal solutions, the GUI also saves the solutions/Pareto solutions and statistical analysis results/corner solutions determined by all the algorithms for single/multi-objective optimization into a spreadsheet. If required, the users can also perform an additional analysis using all simulation results, which are saved using MATLAB compatible 'mat' file format. A snapshot of different optimized results obtained from the tool kit is given in Appendix 1, and the toolkit can be accessed from https://bit.ly/3dy5pde

7.6. Conclusion

An exergetic optimization of flat plate solar water collectors was performed using hourly solar irradiation data over a year for humid subtropical climatic conditions to calculate the optimal performance and design conditions. The proposed model predicts exergy efficiency by considering various factors affecting the exergy losses. Recent metaheuristic techniques were used for determining the optimal values of all decision variables for maximum exergy efficiency as the single objective and maximum exergy efficiency and the minimum absorber plate area as multi-objective on a case study based on Guwahati city climatic conditions. SHTS, SHO, WCA, GA, MPEDE, and DNLPSO were used to optimize the single objective optimization model, whereas the multi-objective model was solved using MOGA, MODE, FYYPO, MOWCA, MALO, and MSSA.

The parameters affecting the design, operational and environmental conditions such as mass flow rate of fluid, fluid inlet temperature, absorber plate area, absorber plate temperature, and

glass cover temperatures, ambient temperature, wind velocity, incident solar heat flux, and optical efficiency on mean exergy efficiency for other constant optimal values were analyzed. The performance of WCA in solving the solar model is superior compared to all the other algorithms, while the corner points reported by MOWCA were better or non-dominating to all corner points reported by other algorithms. The multi-objective study proposed in this chapter proves the occurrence of higher exergy efficiency with a lower absorber plate area. An optimization tool kit using MATLAB GUI is provided to design a flat plate solar water collector with maximum exergetic efficiency and minimum absorber plate area for humid subtropical climatic conditions.

Chapter 8

Conclusion and scope of future work

With increasing population and consistent developments in various sectors such as transportation, construction, industrial, space exploration, etc., there is a continuous growth in energy requirements. The energy demand has been largely dependent on fossil-based energy sources, which contribute to high carbon emissions. On this account, a carbon-free green economy is desired. Worldwide researchers and policymakers have been trying to achieve this goal in a sustainable framework. Renewable resources, such as solar energy, wind energy, geothermal energy, and biofuels, can substantially help to address the challenges as these are available in abundance. However, energy harvesting from renewable sources is still in the development stage, and apart from government subsidies and incentives, commercialization will need optimal decisions starting from the design stage to the final delivery stages. In this context, this thesis provides optimal frameworks for designing biofuel supply chains and solar-based energy systems. This chapter summarizes the primary contributions of this thesis along with possible future research directions.

8.1. Research outcomes for Biorefinery superstructures

This thesis first proposed an efficient optimization framework using metaheuristic techniques to solve the biorefinery supply chain network that includes nonlinearities. The strategies employed in the framework efficiently handle the equality constraints and aid the metaheuristic techniques in searching for the optimal solution. Multiple repair operators are also incorporated into the framework to improve potential solutions that violate the bound constraints on the flow rates and the processing capacity. The proposed strategy is tested on a case study with nonlinear cost functions using six metaheuristic techniques to minimize the total life cycle cost. The techniques were able to determine feasible solutions for all the independent runs, representing the robustness of the proposed strategy. The use of the standard approach for solving the case

study resulted in infeasible solutions. The proposed solution strategy will help guide the researchers in employing metaheuristic techniques to optimize the supply chain in biorefineries and other domains involving mass balances.

The framework is extended to a multi-unit strategy-based framework to tackle the processing capacity restrictions in biorefineries. The framework includes a heuristic mechanism to help in the capacity planning of the biorefineries by implementing multiple units of the selected technology within the capacity domain. The performance analysis of the framework using eight metaheuristic techniques exhibited its benefit by determining reduced total lifecycle cost compared to the single unit case. All the techniques were able to determine feasible solutions for the multi-unit supply chain case study in every independent run. The approach used multiple units of processing technologies at the main and secondary processing facilities, increasing the economic gains over the single-unit supply chain. The proposed framework is expected to aid researchers in addressing capacity planning in the supply-chain network of biorefineries and optimizing them using metaheuristic techniques.

The multi-unit strategy was found to be beneficial for the biorefinery superstructures while optimizing using the metaheuristic techniques. As a large section of the researchers uses the mixed integer linear programming-based models for solving biorefinery superstructures, hence this research proposed a multi-unit strategy-based mixed-integer linear programming framework for a biorefinery supply chain network that supports multiple technological choices for each type of biomass, domain constraints related to the capacity selection of the processing technologies, and biofuel distributions. A single-unit model of a distributed biorefinery superstructure available in the literature is improved to accommodate the decisions for multiple technologies. The improved single-unit model is extended to a multi-unit model that can implement multiple process units of selected technologies.

The efficacy of the proposed model is demonstrated in a case study using the total life cycle analysis approach with linear approximations for the capital cost calculations. The optimal solution of the multi-unit model has a reduced total life cycle cost of 1.25% compared to the single-unit model. The proposed model is generic to implement the idea of the multi-unit strategy and can be used in other process industries.

The biorefinery superstructures are prone to seasonal unavailability of biomass and hence use storage structures to use additional biomass in the peak demand or in case of biomass unavailability. This requires a periodic assessment of the biorefineries, and in that case, the selection of a single unit of higher-capacity facility might become redundant in a period of low biomass availability and market demand. The effect of a multi-unit strategy on a periodic supply chain is analyzed in this research by proposing a mixed-integer linear programming framework that adopts a multi-period distributed biorefinery supply chain network and integrates the multi-unit strategy. The proposed model uses multiple objectives, such as the maximization of profit and the maximization of social impact, to demonstrate the efficacy of the multi-unit strategy on a periodic biorefinery superstructure. The multi-unit model has improved the profit by 4.73% and has generated 78 additional jobs in the analysis performed over 12 months compared to the single-unit strategy. This research also analyzed the effect of implementing multiple units on the profit and additionally performed a sensitivity analysis towards demand variation from 50 to 150%. The profit increment obtained by varying the demand from 50 to 150% of its actual value is observed to be from 3.96 to 4.76%.

8.2. Research outcomes: Solar-based energy systems

This research developed a bi-level framework that employs metaheuristic techniques for optimizing simple and finned solar air collectors. The optimization strategy eliminates all the thermodynamically infeasible solutions using constraints on the operating conditions of the system. It was found that the probabilistic selection on upper and lower bounds of decision variables in the optimization procedure can affect the optima in finned air collectors. The performance and accuracy of the results obtained by solving the energy balance equations governing the performance of the simple solar air collector system were validated against the literature. The simulation of the current model showed a better consistency between the present results and those reported in the literature. The maximum energy and exergy efficiency is achieved in the case of finned air collectors (case 2) with a yearly optimal average energy and exergy efficiency of 43% and 6.10%, respectively, for an optimal collector area of 5 m^2 and yearly optimal average heat flux of 601 W/m2 for humid subtropical climatic conditions (Guwahati, India).

A second framework was developed for a multi-objective solar water collector using metaheuristic techniques. The framework has efficient optimization strategies and includes additional constraints on the operating conditions of the solar water collector to ensure its thermodynamic feasibility. Multiple metaheuristic techniques were used for determining the optimal values of all decision variables for maximum exergy efficiency as the single objective case and maximum exergy efficiency and the minimum absorber plate area as multi-objective on a case study based on Guwahati City climatic conditions. The multi-objective study proposed in this article proved the occurrence of higher exergy efficiency with a lower absorber plate area. An optimization toolkit using MATLAB GUI is developed to analyze the effect of various operational parameters on the solar water collector framework.

8.3. Future research directions

The current research on efficient optimization strategies for renewable energy systems can be extended into multiple aspects. Biorefineries are complex structures where biomass to biofuel generation is undertaken using multiple stages. Although the technologies involved in the conversion of various biomass into biofuel involve nonlinearities, the major supply chain networks use approximations in terms of a conversion factor and solve using mixed integer linear programming techniques. The use of the metaheuristic technique is often not explored due to the absence of inherent constraint-handling capabilities and poor performance in the presence of equality-type constraints. The strategy provided in this research could be used to explore the application of metaheuristic techniques for complete supply chain networks, avoiding the approximation of nonlinearities. The constraint handling strategies for the equality constraints presented in this research can be used for other process industries involving mass balances, and metaheuristic-based optimization solutions can be suggested.

The application of a multi-unit strategy is observed to be beneficial for biorefinery superstructures using metaheuristic frameworks, and mixed integer linear programming models can be explored for pre-treatment facilities at harvesting locations. The current study does not incorporate the use of pre-treatment facilities and assumes a single mode of transportation system. The multi-unit strategy can be used for the pre-treatment facilities-based biorefinery superstructures and capacity-based multi-mode transportation systems. Further, the models can be explored for stochastic optimization problems that include uncertainties in various stages of the supply chain network. The current research has used the maximization of profit and maximization of social impact as two conflicting objectives and demonstrated the benefits of a multi-unit strategy for a periodic supply chain. This can be extended to use different environmental objectives such as land and water footprint, waste management, and

economic objectives such as net present value, internal rate of return, etc. The proposed multi-unit concept is generic, and its applicability can also be explored for other manufacturing industries.

The research presented for solar energy-based systems has used the subtropical climatic conditions of Guwahati as the case study. However, the system can be explored for other geographical conditions. The current systems can be integrated with photovoltaic thermal collectors that could increase the performance of both the photovoltaic panel and the solar collectors. The current models can be integrated with various solar combi systems, such as solar refrigeration systems and solar heat pumps, to analyze the commercial potential of the systems. Additionally, the integration with solar thermal storage systems can be explored to satisfy intermittent energy requirements.

Research Publications

Journal articles

- **Maharana, D**., Kommadath, R., & Kotecha P. A multi-unit model for the biorefinery supply chain focusing on life cycle analysis-based capacity planning for the processing units. Biomass conversion and biorefinery (Accepted)
- **Maharana D**, Kommadath R, Kotecha P. An innovative approach to the supply-chain network optimization of biorefineries using metaheuristic techniques. Eng Optim 2022. https://doi.org/10.1080/0305215X.2022.2080204.
- **Maharana D**, Kommadath R, Kotecha P. A mixed-integer linear programming model with multi-unit strategy for distributed biorefinery superstructures with economic and social benefits. Clean Technol Environ Policy 2022. https://doi.org/10.1007/s10098-022-02296-z.
- **Maharana D**, Bhattacharya T, Kotecha P, Anandalakshmi R. Exergetic optimization of simple and finned solar air collectors for humid subtropical regions. Environ Sci Pollut Res 2022 2022;1:1–17. https://doi.org/10.1007/S11356-021-18070-5.
- **Maharana D**, Bhattacharya T, Kotecha P, Anandalakshmi R. Exergetic optimization of solar water collectors using computational intelligence techniques. Clean Technol Environ Policy 2021;23:1737–68. https://doi.org/10.1007/s10098-021-02057-4.
- **Maharana, D**, Kommadath, R, & Kotecha P, A novel multi-unit metaheuristic framework for the capacity planning of distributed biorefineries. (Manuscript under review)

Book chapters

- **Maharana D**, Maheshka S, Kotecha P. Multi-objective league championship algorithms and its applications to optimal control problems. Adv. Intell. Syst. Comput., vol. 669, 2019, p. 35–46. https://doi.org/10.1007/978-981-10-8968-8_4.
- **Maharana D**, Kotecha P. Optimization of job shop scheduling problem with grey wolf optimizer and JAYA algorithm. Adv. Intell. Syst. Comput., vol. 669, 2019, p. 47–58. https://doi.org/10.1007/978-981-10-8968-8_5.

Conferences proceedings

- **Maharana D**, Kotecha P. Simultaneous Heat Transfer Search for single objective real-parameter numerical optimization problem. IEEE Reg 10 Annu Int Conf Proceedings/TENCON 2017:2138–41. https://doi.org/10.1109/TENCON.2016.7848404.
- **Maharana D**, Kommadath R, Kotecha P. Dynamic Yin-Yang Pair Optimization and its performance on single objective real parameter problems of CEC 2017. 2017 IEEE Congr Evol Comput CEC 2017 - Proc 2017:2390–6. https://doi.org/10.1109/CEC.2017.7969594.
- **Maharana D**, Choudhary P, Kotecha P. Optimization of bio-refineries using genetic algorithm. ACM Int Conf Proceeding Ser 2017;Part F127854:26–30. https://doi.org/10.1145/3059336.3059360.

- **Maharana D**, Kotecha P. Simultaneous heat transfer search for computationally expensive numerical optimization. 2016 IEEE Congr Evol Comput CEC 2016 2016:2982–8. https://doi.org/10.1109/CEC.2016.7744166

Other research publications

Journal articles

- Kommadath R, **Maharana D**, Kotecha P. A metaheuristic-based efficient strategy for multi-unit production planning with unique process constraints. Appl Soft Comput 2023;134:109871. https://doi.org/10.1016/J.ASOC.2022.109871.
- Kommadath R, **Maharana D**, Anandalakshmi R, Kotecha P. Multi-objective scheduling in the vegetable processing and packaging facility using metaheuristic based framework. Food Bioprod Process 2023;137:1–19. https://doi.org/10.1016/J.FBP.2022.10.005.
- Kommadath R, **Maharana D**, Kotecha P. An effective strategy for solving single and multi-unit production planning models with unique process constraints using metaheuristic techniques. Expert Syst Appl 2023;224:119813. https://doi.org/10.1016/J.ESWA.2023.119813.
- Swarna Nagraj M, **Maharana D**, Kotecha P, Anandalakshmi R. Thermoeconomic and environmental analyses based single objective optimization of subcooled compression-absorption cascaded refrigeration system using evolutionary techniques. Energy Sources, Part A Recover Util Environ Eff 2023;45:10764–88. https://doi.org/10.1080/15567036.2023.2244909
- Nagraj MS, **Maharana D**, Kotecha P, Anandalakshmi R. Thermoeconomic optimization of cascade refrigeration system using computational intelligence techniques. J Therm Anal Calorim 2022;147:13805–27. https://doi.org/10.1007/s10973-022-11516-z.
- Santra S, **Maharana D**, Kotecha P, Banerjee T. Process Simulation and Multiobjective Optimization for High-Purity Hexane Recovery Using Deep Eutectic Solvent. Ind Eng Chem Res 2022;61:13929–43. https://doi.org/10.1021/acs.iecr.2c01028
- Kommadath R, **Maharana D**, Sivadurgaprasad C, Kotecha P. Parallel computing strategies for Sanitized Teaching Learning Based Optimization. J Comput Sci 2022;63:101766. https://doi.org/10.1016/J.JOCS.2022.101766.
- Kommadath R, **Maharana D**, Kotecha P. Efficient scheduling of jobs on dissimilar parallel machines using heuristic assisted metaheuristic techniques. Chem Eng Res Des 2022;188:916–34. https://doi.org/10.1016/J.CHERD.2022.10.011.
- Kommadath R**, Maharana D**, Kotecha P, Anandalakshmi R. An efficient optimization strategy for vapor compression–absorption-based cascaded refrigeration system using various evolutionary techniques. Int. J. Green Energy. 2023. https://doi.org/10.1080/15435075.2023.224404

Conferences proceedings

- Kommadath, R., Nagraj, M.S., Maharana, D., Kotecha, P. (2023). Efficient Bounding Strategy for CEC 2020 Winner Algorithms in Solving Production Planning Problems. In: Senjyu, T., So-In, C., Joshi, A. (eds) Smart Trends in Computing and Communications. SmartCom 2023. Lecture Notes in Networks and Systems, vol 650. Springer, Singapore. https://doi.org/10.1007/978-981-99-0838-7_16.

Presentations

- D. Maharana, and P. Kotecha," Optimal Pollutant Trading for Mercury Waste Management in Water Bodies using ABC, SFO and YYPO", presented at Indian Process System Engineering, IIT Madras, 18-19 August, 2019
- D. Maharana, G. Sharma and P. Kotecha, "Optimal Pollutant Trading for Mercury Waste Management in Water Bodies using SHO, sTLBO and SCA," presented at the REFLUX 2019, IIT Guwahati, India, 2019
- D. Maharana and P. Kotecha, "Optimal Control of Chemical Reactors using Computational Intelligence Techniques," presented at the REFLUX 2017, IIT Guwahati, India, 2017

Referrences

Aboytes-Ojeda, M., Castillo-Villar, K. K., & Eksioglu, S. D. (2019). Modeling and optimization of biomass quality variability for decision support systems in biomass supply chains. *Annals of Operations Research*. https://doi.org/10.1007/s10479-019-03477-8

Aboytes-Ojeda, M., Castillo-Villar, K. K., & Roni, M. S. (2020). A decomposition approach based on meta-heuristics and exact methods for solving a two-stage stochastic biofuel hub-and-spoke network problem. *Journal of Cleaner Production*, *247*, 119176. https://doi.org/10.1016/j.jclepro.2019.119176

Aguitoni, M. C., Pavão, L. V., Siqueira, P. H., Jiménez, L., & Ravagnani, M. A. da S. S. (2018). Heat exchanger network synthesis using genetic algorithm and differential evolution. *Computers & Chemical Engineering*, *117*, 82–96. https://doi.org/10.1016/J.COMPCHEMENG.2018.06.005

Akhtari, S., & Sowlati, T. (2020). Hybrid optimization-simulation for integrated planning of bioenergy and biofuel supply chains. *Applied Energy*, *259*, 114124. https://doi.org/10.1016/j.apenergy.2019.114124

Alpanda, S., & Peralta-Alva, A. (2010). Oil crisis, energy-saving technological change and the stock market crash of 1973–74. *Review of Economic Dynamics*, *13*(4), 824–842. https://doi.org/10.1016/j.red.2010.04.003

Alta, D., Bilgili, E., Ertekin, C., & Yaldiz, O. (2010). Experimental investigation of three different solar air heaters: Energy and exergy analyses. *Applied Energy*, *87*(10), 2953–2973. https://doi.org/10.1016/j.apenergy.2010.04.016

Ammar, M., Mokni, A., Mhiri, H., & Bournot, P. (2021). Performance optimization of flat plate solar collector through the integration of different slats arrangements made of transparent insulation material. *Sustainable Energy Technologies and Assessments*, *46*, 101237. https://doi.org/10.1016/J.SETA.2021.101237

Atashbar, N. Z., Labadie, N., & Prins, C. (2016). Modeling and optimization of biomass supply chains: A review and a critical look. *IFAC-PapersOnLine*, *49*(12), 604–615. https://doi.org/10.1016/j.ifacol.2016.07.742

Atia, D. M., Fahmy, F. H., Ahmed, N. M., & Dorrah, H. T. (2012). Optimal sizing of a solar water heating system based on a genetic algorithm for an aquaculture system. *Mathematical and Computer Modelling*, *55*(3), 1436–1449. https://doi.org/10.1016/j.mcm.2011.10.022

Ayoub, N., Elmoshi, E., Seki, H., & Naka, Y. (2009). Evolutionary algorithms approach for integrated bioenergy supply chains optimization. *Energy Conversion and Management*, *50*(12), 2944–2955. https://doi.org/10.1016/j.enconman.2009.07.010

Ba, B. H., Prins, C., & Prodhon, C. (2016). Models for optimization and performance evaluation of biomass supply chains: An Operations Research perspective. *Renewable Energy*, *87*, 977–989. https://doi.org/10.1016/j.renene.2015.07.045

Bala, J. D., Lalung, J., Al-Gheethi, A. A. S., & Norli, I. (2016). A review on biofuel and bioresources for environmental applications. In *Renewable Energy and Sustainable Technologies for Building and Environmental Applications: Options for a Greener Future* (pp. 205–226). Springer International Publishing. https://doi.org/10.1007/978-3-319-31840-0_13

Basile, F., Pilotti, L., Ugolini, M., Lozza, G., & Manzolini, G. (2022). Supply chain optimization and GHG emissions in biofuel production from forestry residues in Sweden. *Renewable Energy*, *196*, 405–421. https://doi.org/10.1016/J.RENENE.2022.06.095

Bejan, A, Kearney, D. W., & Kreith, F. (1981). Second Law Analysis and Synthesis of Solar Collector Systems. *Journal of Solar Energy Engineering*, *103*(1), 23–28. https://doi.org/10.1115/1.3266200

Bejan, Adrian. (2002). Fundamentals of exergy analysis, entropy generation minimization, and the generation of flow architecture. *International Journal of Energy Research*, *26*(7), 0–43. https://doi.org/10.1002/er.804

Bowling, I. M., Ponce-Ortega, J. M., & El-Halwagi, M. M. (2011). Facility location and supply chain optimization for a biorefinery. *Industrial and Engineering Chemistry Research*, *50*(10), 6276–6286. https://doi.org/10.1021/ie101921y

Carrillo Caballero, G. E., Mendoza, L. S., Martinez, A. M., Silva, E. E., Melian, V. R., Venturini, O. J., & del Olmo, O. A. (2017). Optimization of a Dish Stirling system working with DIR-type receiver using multi-objective techniques. *Applied Energy*, *204*, 271–286. https://doi.org/10.1016/j.apenergy.2017.07.053

Castillo-Villar, K. K., Eksioglu, S., & Taherkhorsandi, M. (2017). Integrating biomass quality variability in stochastic supply chain modeling and optimization for large-scale biofuel production. *Journal of Cleaner Production*, *149*, 904–918. https://doi.org/10.1016/j.jclepro.2017.02.123

Chandel, A. K., Garlapati, V. K., Singh, A. K., Antunes, F. A. F., & da Silva, S. S. (2018). The path forward for lignocellulose biorefineries: Bottlenecks, solutions, and perspective on commercialization. *Bioresource Technology*, *264*, 370–381. https://doi.org/10.1016/j.biortech.2018.06.004

Chauhan, S. S., & Kotecha, P. (2018). An efficient multi-unit production planning strategy based on continuous variables. *Applied Soft Computing*, *68*, 458–477. https://doi.org/10.1016/j.asoc.2018.03.012

Chauhan, S. S., Sivadurgaprasad, C., Kadambur, R., & Kotecha, P. (2018). A novel strategy for the combinatorial production planning problem using integer variables and performance evaluation of recent optimization algorithms. *Swarm and Evolutionary Computation*, *43*, 225–243. https://doi.org/10.1016/j.swevo.2018.04.004

Cheng, Z.-D., He, Y.-L., Du, B.-C., Wang, K., & Liang, Q. (2015). Geometric optimization on optical performance of parabolic trough solar collector systems using particle swarm optimization algorithm. *Applied Energy*, *148*, 282–293. https://doi.org/10.1016/j.apenergy.2015.03.079

Chopra, K., Tyagi, V. V., Pandey, A. K., & Sari, A. (2018). Global advancement on experimental and thermal analysis of evacuated tube collector with and without heat pipe systems and possible applications. *Applied Energy*, *228*, 351–389. https://doi.org/10.1016/j.apenergy.2018.06.067

Coello Coello, C. A. (2002). Theoretical and numerical constraint-handling techniques used with evolutionary algorithms: a survey of the state of the art. *Computer Methods in Applied Mechanics and Engineering*, *191*(11–12), 1245–1287. https://doi.org/10.1016/s0045-7825(01)00323-1

Das, R. (2015). Application of simulated annealing for inverse analysis of a single-glazed solar collector. In E.-S. M. El-Alfy, S. M. Thampi, H. Takagi, S. Piramuthu, & T. Hanne (Eds.), *Advances in Intelligent Systems and Computing* (Vol. 320, pp. 267–275). Springer International Publishing. https://doi.org/10.1007/978-3-319-11218-3_25

Deb, K, Pratap, A., Agarwal, S., & Meyarivan, T. (2002). A fast and elitist multiobjective genetic algorithm: NSGA-II. *IEEE Transactions on Evolutionary Computation*, *6*(2), 182–197. https://doi.org/10.1109/4235.996017

Deb, Kalyanmoy. (2000). An efficient constraint handling method for genetic algorithms. *Computer Methods in Applied Mechanics and Engineering*, *186*(2–4), 311–338. https://doi.org/10.1016/S0045-7825(99)00389-8

Debnath, S., Reddy, J., Jagadish, & Das, B. (2019). An expert system-based modeling and optimization of corrugated plate solar air collector for North Eastern India. *Journal of the Brazilian Society of Mechanical Sciences and Engineering*, *41*(7). https://doi.org/10.1007/s40430-019-1782-z

Dickson, R., Mancini, E., Garg, N., Woodley, J. M., Gernaey, K. V., Pinelo, M., Liu, J., & Mansouri, S. S. (2021). Sustainable bio-succinic acid production: superstructure optimization, techno-economic, and lifecycle assessment. *Energy & Environmental Science*, *14*(6), 3542–3558. https://doi.org/10.1039/D0EE03545A

Dixit, M., & Kumar, H. (2015). *Tata McGraw Hill Education Private Limited*. Indian Institute of Management, Ahmedabad. https://doi.org/10.4135/9781473974463

El-Halwagi, A. M., Rosas, C., Ponce-Ortega, J. M., Jiménez-Gutiérrez, A., Mannan, M. S., & El-Halwagi, M. M. (2013). Multiobjective optimization of biorefineries with economic and safety objectives. *AIChE Journal*, *59*(7), 2427–2434. https://doi.org/10.1002/aic.14030

Elfasakhany, A. (2015). Investigations on the effects of ethanol–methanol–gasoline blends in a spark-ignition engine: Performance and emissions analysis. *Engineering Science and Technology, an International Journal*, *18*(4), 713–719. https://doi.org/10.1016/j.jestch.2015.05.003

Espinoza Pérez, A. T., Camargo, M., Narváez Rincón, P. C., & Alfaro Marchant, M. (2017). Key challenges and requirements for sustainable and industrialized biorefinery supply chain design and management: A bibliographic analysis. *Renewable and Sustainable Energy Reviews*, *69*, 350–359. https://doi.org/10.1016/j.rser.2016.11.084

Farahani, R. Z., Rezapour, S., Drezner, T., & Fallah, S. (2014). Competitive supply chain network design: An overview of classifications, models, solution techniques and applications. *Omega*, *45*, 92–118. https://doi.org/10.1016/j.omega.2013.08.006

Farahat, S., Sarhaddi, F., & Ajam, H. (2009). Exergetic optimization of flat plate solar collectors. *Renewable Energy*, *34*(4), 1169–1174. https://doi.org/10.1016/j.renene.2008.06.014

Garg, H. P., & Garg, S. N. (1985). Correlation of monthly-average daily global, diffuse and beam radiation with bright sunshine hours. *Energy Conversion and Management*, *25*(4), 409–417. https://doi.org/10.1016/0196-8904(85)90004-4

Gautam, S., LeBel, L., & Carle, M. A. (2017). Supply chain model to assess the feasibility of incorporating a terminal between forests and biorefineries. *Applied Energy*, *198*, 377–384. https://doi.org/10.1016/j.apenergy.2017.01.021

Ge, Y., & Li, L. (2018). System-level energy consumption modeling and optimization for cellulosic biofuel production. *Applied Energy*, *226*, 935–946. https://doi.org/10.1016/j.apenergy.2018.06.020

Ge, Y., Li, L., & Yun, L. (2021). Modeling and economic optimization of cellulosic biofuel supply chain considering multiple conversion pathways. *Applied Energy*, *281*, 116059. https://doi.org/10.1016/J.APENERGY.2020.116059

Geraili, A., Sharma, P., & Romagnoli, J. A. (2014). A modeling framework for design of nonlinear renewable energy systems through integrated simulation modeling and metaheuristic optimization: Applications to biorefineries. *Computers & Chemical Engineering*, *61*, 102–117. https://doi.org/10.1016/j.compchemeng.2013.10.005

Giarola, S., Zamboni, A., & Bezzo, F. (2012). Environmentally conscious capacity planning and technology selection for bioethanol supply chains. *Renewable Energy*, *43*, 61–72. https://doi.org/10.1016/j.renene.2011.12.011

Goldberg, D. E. (1989). Genetic algorithms in search, optimization, and machine learning. In *Choice Reviews Online* (Vol. 27, Issue 02). Addison-Wesley Longman Publishing Co., Inc. https://doi.org/10.5860/choice.27-0936

Gopinathan, K. K. (1988). A general formula for computing the coefficients of the correlation connecting global solar radiation to sunshine duration. *Solar Energy*, *41*(6), 499–502. https://doi.org/10.1016/0038-092X(88)90052-7

Griffel, D. (2003). Multi-objective optimization using evolutionary algorithms, by Kalyanmoy Deb, Pp.487. £60. 2001. ISBN 0 471 87339 X (Wiley). *The Mathematical Gazette*, *87*(509), 409–410. https://doi.org/10.1017/s0025557200173498

Gueymard, C. (2000). Prediction and Performance Assessment of Mean Hourly Global Radiation. *Solar Energy*, *68*(3), 285–303. https://doi.org/10.1016/S0038-092X(99)00070-5

Hà, M. H., Bostel, N., Langevin, A., & Rousseau, L.-M. (2014). An exact algorithm and a metaheuristic for the generalized vehicle routing problem with flexible fleet size. *Computers & Operations Research*, *43*, 9–19. https://doi.org/10.1016/j.cor.2013.08.017

Hatefi, S. M., Moshashaee, S. M., & Mahdavi, I. (2019). A bi-objective programming model for reliable supply chain network design under facility disruption. *International Journal of Integrated Engineering*, *11*(6), 080–092. https://doi.org/10.30880/ijie.2019.11.06.009

Hedayatizadeh, M., Sarhaddi, F., Safavinejad, A., Ranjbar, F., & Chaji, H. (2016). Exergy loss-based efficiency optimization of a double-pass/glazed v-corrugated plate solar air heater. *Energy*, *94*, 799–810. https://doi.org/10.1016/j.energy.2015.11.046

Hernández-Pérez, L. G., Sánchez-Tuirán, E., Ojeda, K. A., El-Halwagi, M. M., & Ponce-Ortega, J. M. (2019). Optimization of Microalgae-to-Biodiesel Production Process Using a Metaheuristic Technique. *ACS Sustainable Chemistry and Engineering*, *7*(9), 8490–8498. https://doi.org/10.1021/acssuschemeng.9b00274

Hollands, K. G. T., Unny, T. E., Raithby, G. D., & Konicek, L. (1976). Free convective heat transfer across inclined air layers. *Journal of Heat Transfer*, *98*(2), 189–193. https://doi.org/10.1115/1.3450517

How, B. S., & Lam, H. L. (2018). PCA Method for Debottlenecking of Sustainability Performance in Integrated Biomass Supply Chain. *Process Integration and Optimization for Sustainability*, *3*(1), 43–64. https://doi.org/10.1007/s41660-018-0036-3

Jadhav, I. B., Bose, M., & Bandyopadhyay, S. (2020). Optimization of solar thermal systems with a thermocline storage tank. *Clean Technologies and Environmental Policy*, *22*(5), 1069–1084. https://doi.org/10.1007/s10098-020-01849-4

Jalilian, M., Kargarsharifabad, H., Abbasi Godarzi, A., Ghofrani, A., & Shafii, M. B. (2016). Simulation and optimization of pulsating heat pipe flat-plate solar collectors using neural networks and genetic algorithm: a semi-experimental investigation. *Clean Technologies and Environmental Policy*, *18*(7), 2251–2264. https://doi.org/10.1007/s10098-016-1143-x

Katsaprakakis, D. (2019). Introducing a solar-combi system for hot water production and swimming pools heating in the Pancretan Stadium, Crete, Greece. *Energy Procedia*, *159*, 174–179. https://doi.org/10.1016/j.egypro.2018.12.047

Kennedy, J., & Eberhart, R. (1995). Particle swarm optimization. *Neural Networks, 1995. Proceedings., IEEE International Conference On*, *4*, 1942–1948 vol.4. https://doi.org/10.1109/ICNN.1995.488968

Khishtandar, S. (2019). Simulation based evolutionary algorithms for fuzzy chance-constrained biogas supply chain design. *Applied Energy*, *236*, 183–195. https://doi.org/10.1016/j.apenergy.2018.11.092

Kim, J., Hong, T., Jeong, J., Lee, M., Koo, C., Lee, M., Ji, C., & Jeong, J. (2016). An integrated multi-objective optimization model for determining the optimal solution in the solar thermal energy system. *Energy*, *102*, 416–426. https://doi.org/10.1016/j.energy.2016.02.104

Kommadath, R., Sivadurgaprasad, C., & Kotecha, P. (2016). Single phase multi-group teaching learning algorithm for computationally expensive numerical optimization (CEC 2016). *2016 IEEE Congress on Evolutionary Computation, CEC 2016*, 2989–2995. https://doi.org/10.1109/CEC.2016.7744167

Lim, C. H., & Lam, H. L. (2016). Biomass supply chain optimisation via novel Biomass Element Life Cycle Analysis (BELCA). *Applied Energy*, *161*, 733–745. https://doi.org/10.1016/J.APENERGY.2015.07.030

Lugo, S., Morales, L. I., Best, R., Gómez, V. H., & García-Valladares, O. (2019). Numerical simulation and experimental validation of an outdoor-swimming-pool solar heating system in warm climates. *Solar Energy*, *189*, 45–56. https://doi.org/10.1016/j.solener.2019.07.041

Luminosu, I., & Fara, L. (2005). Thermodynamic analysis of an air solar collector. *International Journal of Exergy*, *2*(4), 385–408. https://doi.org/10.1504/IJEX.2005.007788

Maharana, D, & Kotecha, P. (2016). Simultaneous Heat Transfer Search for single objective real-parameter numerical optimization problem. *2016 IEEE Region 10 Conference (TENCON)*, 2138–2141. https://doi.org/10.1109/TENCON.2016.7848404

Maharana, Debasis, Kommadath, R., & Kotecha, P. (2017). Dynamic Yin-Yang Pair Optimization and its performance on single objective real parameter problems of CEC 2017. *2017 IEEE Congress on Evolutionary Computation, CEC 2017 - Proceedings*, 2390–2396. https://doi.org/10.1109/CEC.2017.7969594

Maharana, Debasis, Kommadath, R., & Kotecha, P. (2022a). A mixed-integer linear programming model with multi-unit strategy for distributed biorefinery superstructures with economic and social benefits. *Clean Technologies and Environmental Policy*. https://doi.org/10.1007/s10098-022-02296-z

Maharana, Debasis, Kommadath, R., & Kotecha, P. (2022b). An innovative approach to the supply-chain network optimization of biorefineries using metaheuristic techniques. *Engineering Optimization*. https://doi.org/10.1080/0305215X.2022.2080204

Mavrotas, G. (2009). Effective implementation of the ε-constraint method in Multi-Objective Mathematical Programming problems. *Applied Mathematics and Computation*, *213*(2), 455–465. https://doi.org/10.1016/j.amc.2009.03.037

Mezura-Montes, E., & Coello Coello, C. A. (2011). Constraint-handling in nature-inspired numerical optimization: Past, present and future. *Swarm and Evolutionary Computation*, *1*(4), 173–194. https://doi.org/10.1016/J.SWEVO.2011.10.001

Mirjalili, S., Mirjalili, S. M., & Lewis, A. (2014). Grey Wolf Optimizer. *Advances in Engineering Software*, *69*, 46–61. https://doi.org/10.1016/j.advengsoft.2013.12.007

Mitkidis, G., Magoutas, A., & Kitsios, F. (2018). Market and economic feasibility analysis for the implementation of 2nd generation biofuels in Greece. *Energy Strategy Reviews*, *19*, 85–98. https://doi.org/10.1016/j.esr.2017.12.006

Mohseni-Languri, E., Taherian, H., Masoodi, R., & Reisel, J. R. (2009). An energy and exergy study of a solar thermal air collector. *Thermal Science*, *13*(1), 205–216. https://doi.org/10.2298/TSCI0901205M

Moncada B., J., Aristizábal M., V., & Cardona A., C. A. (2016). Design strategies for sustainable biorefineries. *Biochemical Engineering Journal*, *116*, 122–134. https://doi.org/10.1016/j.bej.2016.06.009

Mutenure, M., Čuček, L., Egieya, J., Isafiade, A. J., & Kravanja, Z. (2018). Optimization of bioethanol and sugar supply chain network: a South African case study. *Clean Technologies and Environmental Policy*, *20*(5), 925–948. https://doi.org/10.1007/s10098-018-1535-1

Nájera-Trejo, M., Martin-Domínguez, I. R., & Escobedo-Bretado, J. A. (2016). Economic Feasibility of Flat Plate vs Evacuated Tube Solar Collectors in a Combisystem. *Energy Procedia*, *91*, 477–485. https://doi.org/10.1016/j.egypro.2016.06.181

Naphon, P. (2005). On the performance and entropy generation of the double-pass solar air heater with longitudinal fins. *Renewable Energy*, *30*(9), 1345–1357. https://doi.org/10.1016/J.RENENE.2004.10.014

Ng, R. T. L., & Maravelias, C. T. (2017). Design of biofuel supply chains with variable regional depot and biorefinery locations. *Renewable Energy*, *100*, 90–102. https://doi.org/10.1016/j.renene.2016.05.009

Olivares-Benitez, E., Ríos-Mercado, R. Z., & González-Velarde, J. L. (2013). A metaheuristic algorithm to solve the selection of transportation channels in supply chain design. *International Journal of Production Economics*, *145*(1), 161–172. https://doi.org/10.1016/j.ijpe.2013.01.017

Ortiz-Sanchez, M., Solarte-Toro, J.-C., González-Aguirre, J.-A., Peltonen, K. E., Richard, P., & Cardona Alzate, C. A. (2020). Pre-feasibility analysis of the production of mucic acid from orange peel waste under the biorefinery concept. *Biochemical Engineering Journal*, *161*, 107680. https://doi.org/10.1016/j.bej.2020.107680

Parajuli, R., Dalgaard, T., Jørgensen, U., Adamsen, A. P. S., Knudsen, M. T., Birkved, M., Gylling, M., & Schjørring, J. K. (2015). Biorefining in the prevailing energy and materials crisis: a review of sustainable pathways for biorefinery value chains and sustainability assessment methodologies. *Renewable and Sustainable Energy Reviews*, *43*, 244–263. https://doi.org/10.1016/j.rser.2014.11.041

Pierezan, J., & Dos Santos Coelho, L. (2018, September). Coyote Optimization Algorithm: A New Metaheuristic for Global Optimization Problems. *2018 IEEE Congress on Evolutionary Computation, CEC 2018 - Proceedings*. https://doi.org/10.1109/CEC.2018.8477769

Ponce-Ortega, J. M., & Santibañez-Aguilar, J. E. (2019). Introduction. In *Strategic Planning for the Sustainable Production of Biofuels* (pp. 1–7). Elsevier. https://doi.org/10.1016/b978-0-12-818178-2.00001-8

Potrč, S., Čuček, L., Martin, M., & Kravanja, Z. (2020). Synthesis of European Union Biorefinery Supply Networks Considering Sustainability Objectives. *Processes 2020, Vol. 8, Page 1588*, *8*(12), 1588. https://doi.org/10.3390/PR8121588

Punnathanam, V., & Kotecha, P. (2016). Yin-Yang-pair Optimization: A novel lightweight optimization algorithm. *Engineering Applications of Artificial Intelligence*, *54*, 62–79. https://doi.org/10.1016/j.engappai.2016.04.004

Rasoul Asaee, S., Ismet Ugursal, V., & Beausoleil-Morrison, I. (2016). Techno-economic study of solar combisystem retrofit in the Canadian housing stock. *Solar Energy*, *125*, 426–443. https://doi.org/10.1016/j.solener.2015.12.037

Reche-López, P., Ruiz-Reyes, N., García Galán, S., & Jurado, F. (2009). Comparison of metaheuristic techniques to determine optimal placement of biomass power plants. *Energy Conversion and Management*, *50*(8), 2020–2028. https://doi.org/10.1016/j.enconman.2009.04.008

Reche López, P., Jurado, F., Ruiz Reyes, N., García Galán, S., & Gómez, M. (2008). Particle swarm optimization for biomass-fuelled systems with technical constraints. *Engineering Applications of Artificial Intelligence*, *21*(8), 1389–1396. https://doi.org/10.1016/j.engappai.2008.04.013

Reddy, J., Roy, S., Das, B., & Jagadish. (2021). Performance evaluation of sand coated absorber based solar air collector. *Journal of Building Engineering*, *44*, 102973. https://doi.org/10.1016/J.JOBE.2021.102973

Rentizelas, A. A., Tatsiopoulos, I. P., & Tolis, A. (2009). An optimization model for multi-biomass tri-generation energy supply. *Biomass and Bioenergy*, *33*(2), 223–233. https://doi.org/10.1016/j.biombioe.2008.05.008

Rey, A., & Zmeureanu, R. (2018). Multi-objective optimization framework for the selection of configuration and equipment sizing of solar thermal combisystems. *Energy*, *145*, 182–194. https://doi.org/10.1016/j.energy.2017.10.125

Sakoda, A., & Suzuki, M. (1986). Simultaneous transport of heat and adsorbate in closed type adsorption cooling system utilizing solar heat. *Journal of Solar Energy Engineering, Transactions of the ASME*, *108*(3), 239–245. https://doi.org/10.1115/1.3268099

Sánchez-Bautista, A. de F., Santibañez-Aguilar, J. E., Ponce-Ortega, J. M., Nápoles-Rivera, F., Serna-González, M., & El-Halwagi, M. M. (2014). Optimal design of domestic water-heating solar systems. *Clean Technologies and Environmental Policy*, *17*(3), 637–656. https://doi.org/10.1007/s10098-014-0818-4

Santibañez-Aguilar, J. E., González-Campos, J. B., Ponce-Ortega, J. M., Serna-González, M., & El-Halwagi, M. M. (2011). Optimal planning of a biomass conversion system considering economic and environmental aspects. *Industrial and Engineering Chemistry Research*, *50*(14), 8558–8570. https://doi.org/10.1021/ie102195g

Santibañez-Aguilar, J. E., González-Campos, J. B., Ponce-Ortega, J. M., Serna-González, M., & El-Halwagi, M. M. (2014). Optimal planning and site selection for distributed multiproduct biorefineries involving economic, environmental and social objectives. *Journal of Cleaner Production*, *65*, 270–294. https://doi.org/10.1016/j.jclepro.2013.08.004

Sarhaddi, F., Farahat, S., Ajam, H., & Behzadmehr, A. (2009). Exergetic Optimization of a Solar Photovoltaic Array. In *Journal of Thermodynamics* (Vol. 2009). https://doi.org/10.1155/2009/313561

Sarker, B. R., Wu, B., & Paudel, K. P. (2019). Modeling and optimization of a supply chain of renewable biomass and biogas: Processing plant location. *Applied Energy*, *239*, 343–355. https://doi.org/10.1016/j.apenergy.2019.01.216

Schwefel, H.-P. P. (1993). *Evolution and Optimum Seeking: The Sixth Generation*. John Wiley & Sons, Inc. http://portal.acm.org/citation.cfm?id=529401&coll=GUIDE&dl=GUIDE&CFID=62411977&CFTOKEN=26586097

Shahbaz, M., Al-Ansari, T., Aslam, M., Khan, Z., Inayat, A., Athar, M., Naqvi, S. R., Ahmed, M. A., & McKay, G. (2020). A state of the art review on biomass processing and conversion technologies to produce hydrogen and its recovery via membrane separation. *International Journal of Hydrogen Energy*, *45*(30), 15166–15195. https://doi.org/10.1016/j.ijhydene.2020.04.009

Shastri, Y. N., Rodriguez, L. F., Hansen, A. C., & Ting, K. C. (2011). Impact of distributed storage and pre-processing on Miscanthus production and provision systems. *Biofuels, Bioproducts and Biorefining*, *6*(1), 21–31. https://doi.org/10.1002/bbb.326

Shirazi, A., Taylor, R. A., Morrison, G. L., & White, S. D. (2018). Solar-powered absorption chillers: A comprehensive and critical review. *Energy Conversion and Management*, *171*, 59–81. https://doi.org/10.1016/j.enconman.2018.05.091

Shojaeizadeh, E., Veysi, F., & Kamandi, A. (2015). Exergy efficiency investigation and optimization of an Al2O3–water nanofluid based Flat-plate solar collector. *Energy and Buildings*, *101*, 12–23. https://doi.org/10.1016/J.ENBUILD.2015.04.048

Siddhartha, Sharma, N., & Varun. (2012). A particle swarm optimization algorithm for optimization of thermal performance of a smooth flat plate solar air heater. *Energy*, *38*(1), 406–413. https://doi.org/10.1016/J.ENERGY.2011.11.026

Soren, A., & Shastri, Y. (2021). Resiliency considerations in designing commercial scale systems for lignocellulosic ethanol production. *Computers & Chemical Engineering*, *147*, 107239. https://doi.org/10.1016/J.COMPCHEMENG.2021.107239

Storn, R., & Price, K. (1997). No Title. *Journal of Global Optimization*, *11*(4), 341–359. https://doi.org/10.1023/a:1008202821328

Struhs, E., Mirkouei, A., You, Y., & Mohajeri, A. (2020). Techno-economic and environmental assessments for nutrient-rich biochar production from cattle manure: A case study in Idaho, USA. *Applied Energy*, *279*, 115782. https://doi.org/10.1016/j.apenergy.2020.115782

Sustar, J. L., Burch, J., & Krarti, M. (2015). Performance Modeling Comparison of a Solar Combisystem and Solar Water Heater. *Journal of Solar Energy Engineering*, *137*(6). https://doi.org/https://doi.org/10.1115/1.4031044

Tirkolaee, E. B., Mardani, A., Dashtian, Z., Soltani, M., & Weber, G.-W. (2020). A novel hybrid method using fuzzy decision making and multi-objective programming for sustainable-reliable supplier selection in two-echelon supply chain design. *Journal of Cleaner Production*, *250*, 119517. https://doi.org/10.1016/j.jclepro.2019.119517

Torres-Reyes, E., Cervantes-de Gortari, J. G., Ibarra-Salazar, B. A., & Picon-Nuñez, M. (2001). A design method of flat-plate solar collectors based on minimum entropy generation. *Exergy, An International Journal*, *1*(1), 46–52. https://doi.org/10.1016/S1164-0235(01)00009-7

Varun, Sharma, N., Bhat, I. K., & Grover, D. (2011). Optimization of a smooth flat plate solar air heater using stochastic iterative perturbation technique. *Solar Energy*, *85*(9), 2331–2337. https://doi.org/10.1016/j.solener.2011.06.022

Varun, & Siddhartha. (2010). Thermal performance optimization of a flat plate solar air heater using genetic algorithm. *Applied Energy*, *87*(5), 1793–1799. https://doi.org/10.1016/J.APENERGY.2009.10.015

Vera, D., Carabias, J., Jurado, F., & Ruiz-Reyes, N. (2010). A Honey Bee Foraging approach for optimal location of a biomass power plant. *Applied Energy*, *87*(7), 2119–2127. https://doi.org/10.1016/J.APENERGY.2010.01.015

Wang, Z., Yang, W., Qiu, F., Zhang, X., & Zhao, X. (2015). Solar water heating: From theory, application, marketing and research. *Renewable and Sustainable Energy Reviews*, *41*, 68–84. https://doi.org/10.1016/j.rser.2014.08.026

Wolpert, D. H., & Macready, W. G. (1997). No free lunch theorems for optimization. *IEEE Transactions on Evolutionary Computation*, *1*(1), 67–82. https://doi.org/10.1109/4235.585893

Wood, G. (2019). Fossil Fuels in a Carbon-Constrained World. In *The Palgrave Handbook of Managing Fossil Fuels and Energy Transitions* (pp. 3–23). Springer International Publishing. https://doi.org/10.1007/978-3-030-28076-5_1

Yıldırım, C., & Aydoğdu, İ. (2017). Artificial bee colony algorithm for thermohydraulic optimization of flat plate solar air heaters. *Journal of Mechanical Science and Technology*, *31*(7), 3593–3602. https://doi.org/10.1007/s12206-017-0647-6

Yue, D., You, F., & Snyder, S. W. (2014). Biomass-to-bioenergy and biofuel supply chain optimization: Overview, key issues and challenges. *Computers & Chemical Engineering*, *66*, 36–56. https://doi.org/10.1016/J.COMPCHEMENG.2013.11.016

Zayed, M. E., Zhao, J., Elsheikh, A. H., Li, W., & Elaziz, M. A. (2020). Optimal design parameters and performance optimization of thermodynamically balanced dish/Stirling concentrated solar power system using multi-objective particle swarm optimization. *Applied Thermal Engineering*, *178*, 115539. https://doi.org/10.1016/j.applthermaleng.2020.115539

Zhang, F., Wang, J., Liu, S., Zhang, S., & Sutherland, J. W. (2017). Integrating GIS with optimization method for a biofuel feedstock supply chain. *Biomass and Bioenergy*, *98*, 194–205. https://doi.org/10.1016/j.biombioe.2017.01.004

Zhang, J., Osmani, A., Awudu, I., & Gonela, V. (2013). An integrated optimization model for switchgrass-based bioethanol supply chain. *Applied Energy*, *102*, 1205–1217. https://doi.org/10.1016/j.apenergy.2012.06.054

Appendix

Appendix A: Salient features of the metaheuristic techniques

Table A1. Features of single objective metaheuristic techniques

Algorithm	Inspiration	Potential solution	Selection strategy	User-defined parameters
COA	Social structure and the experience sharing of coyote packs	Coyote	Greedy selection and (μ, λ)	Population size, termination criteria, number of coyote in a pack
DE	Parallel direct search	Parameter vector	Greedy selection	Population size, termination criteria, crossover probability, scaling factor
DYYPO	Balance between conflicting forces	Points representing the centre of hyper spheres	(μ+λ)	Termination criteria, expansion /contraction factor, minimum and maximum number of archive updates
GA	Natural genetics	Chromosome	(μ+λ)	population size, termination criteria, reproduction operator, crossover and mutation operator, crossover and mutation probabilities
GWO	Leadership hierarchy and hunting strategy of grey wolves	Search agents	(μ, λ)	Population size, termination criteria
PSO	Bird flocking and fish schooling	Particles	(μ, λ)	Population size, termination criteria, acceleration coefficients, inertia weight
SHTS	Heat transfer among molecules	Molecules	(μ, λ)	Population size, termination criteria

Appendix A: Salient features of the metaheuristic techniques

Algorithm	Inspiration	Potential solution	Selection strategy	User-defined parameters
SPMGTLO	Teaching and learning process	Students	Greedy selection	Population size, termination criteria, number of groups
SHO	Searching, encircling, hunting of spotted hyenas	Search agents	(μ+λ) selection	Population size, Termination criteria
WCA	The downhill flow of rivers and streams towards the sea	Raindrop	Position update using (μ, λ) Keep track of elite solutions (rivers and sea)	Population size, Termination criteria, Number of rivers + sea, Search intensity near the sea
DNLPSO	Bird flocking in search of food	Particles	(μ, λ) selection	Population size, Termination criteria, Maximum and minimum value of inertia factor, Acceleration coefficients corresponding to the personal best and global best position, Learning probability
MPEDE	Parallel direct search using n-dimensional vector	Candidate solution	Greedy selection	Population size, Termination criteria, Percentage of indicator population, Generation gap, Scaling factor, Crossover probability

Table A2. Features of multi-objective metaheuristic techniques

Algorithm	Inspiration	Potential solution	Selection strategy	User-defined parameters
MOGA	Natural genetics and natural selection	Chromosome	Non-dominated sorting and crowding distance	Population size, Termination criteria, Reproduction operator, Crossover and mutation operator, Crossover and mutation probabilities,
MO-MODE	Parallel direct search using n-dimensional vector	Candidate solution	Non-dominated sorting	Population size, Termination criteria, Scaling factor, Crossover probability
FYYPO	Yin Yang philosophy of balance between conflicting forces	Solution	Non-dominated sorting and crowding distance	Termination criteria, Bounds for archive update interval, Expansion or contraction factor
MSSA	Swarming behaviour of salps	Salp position	Non-dominated sorting based archive and distance-based roulette wheel selection	Population size, Termination criteria, Archive size
MALO	Hunting mechanism of ant lions	Ant position	Niching based archive update	Population size, Termination criteria, Archive size
MOWCA	The downhill flow of rivers and streams towards the sea	Raindrop	Non-dominated sorting and crowding distance	Population size, Termination criteria, Number of rivers + sea, Search intensity near the sea

Appendix B: Additional analysis of the results

B1. Wilcoxon signed rank test analysis

The Wilcoxon signed-rank test is a non-parametric hypothesis test, which analyses whether results obtained from two algorithms (samples) are statistically different or not with a significance level (α), which is taken as 5% in this article. The Wilcoxon test checks the null hypothesis, stating that the differences between the two samples are derived from a zero median distribution. The total cost determined at the end of each independent run corresponding to each algorithm is considered as a sample for this work. Table B1 provides the Wilcoxon signed-rank test results among each algorithm on solving the multi-unit framework.

Table B1. Results of Wilcoxon signed rank test for multi-unit framework

	COA			DE			DYYPO			GA		
	p-value	R+	R–	p-value	R+	R–	p-value	R+	R–	p-value	R+	R–
COA	-	-	-	**6.5E-05**	14	311	**1.2E-05**	0	325	**1.2E-05**	0	325
DE	**6.5E-05**	311	14	-	-	-	**1.2E-05**	0	325	**1.4E-05**	1	324
DYYPO	**1.2E-05**	325	0	**1.2E-05**	325	0	-	-	-	**1.6E-05**	323	2
GA	**1.2E-05**	325	0	**1.4E-05**	324	1	**1.6E-05**	2	323	-	-	-
GWO	**3.7E-02**	240	85	**7.4E-03**	63	262	**1.2E-05**	0	325	**1.4E-05**	1	324
PSO	**1.4E-05**	324	1	5.8E-02	233	92	**1.2E-05**	0	325	**2.3E-05**	5	320
SHTS	**1.3E-04**	305	20	6.5E-02	231	94	**1.2E-05**	0	325	**5.8E-05**	13	312
SPMGTLO	**2.2E-04**	25	300	**1.2E-05**	0	325	**1.2E-05**	0	325	**1.2E-05**	0	325
	GWO			PSO			SHTS			SPMGTLO		
	p-value	R+	R–	p-value	R+	R–	p-value	R+	R–	p-value	R+	R–
COA	**3.7E-02**	85	**240**	**1.4E-05**	1	**324**	**1.3E-04**	20	**305**	**2.2E-04**	**300**	25
DE	**7.4E-03**	**262**	63	5.8E-02	92	233	6.5E-02	94	231	**1.2E-05**	**325**	0
DYYPO	**1.2E-05**	**325**	0	**1.2E-05**	**325**	0	**1.2E-05**	**325**	0	**1.2E-05**	**325**	0
GA	**1.4E-05**	**324**	1	**2.3E-05**	**320**	5	**5.8E-05**	**312**	13	**1.2E-05**	**325**	0
GWO	-	-	-	**6.0E-04**	35	**290**	**2.1E-03**	48	**277**	**1.2E-05**	**325**	0
PSO	**6.0E-04**	**290**	35	-	-	-	7.8E-01	152	173	**1.2E-05**	**325**	0
SHTS	**2.1E-03**	**277**	48	7.8E-01	173	152	-	-	-	**1.2E-05**	**325**	0
SPMGTLO	**1.2E-05**	0	**325**	**1.2E-05**	0	**325**	**1.2E-05**	0	**325**	-	-	-

If the p-value among two algorithms is less than the significance level (α =0.05), then the null hypothesis is rejected, indicating the results provided by the pair-wise compared algorithms are statistically different. The Wilcoxon test ranks the difference between the results provided

by the algorithms in each run. The R– represents the sum of ranks corresponding to the negative differences, and R+ indicates the sum of ranks of positive differences. In Table 3, the p-value less than the significance level and the higher value among R+ and R– are highlighted using bold type-face font. The p-value obtained in each pair-wise comparison of algorithms is less than the significance level of 0.05, indicating the results provided by all algorithms are statistically different from each other. Such an inference is not observed on comparing the p-value of DE with SHTS and PSO. The R– corresponding to SPMGTLO against all the algorithms is large, indicating SPMGTLO outperformed all other algorithms. The lower R– value of DYYPO in comparison to all the algorithms indicates its poor performance.

B2. Analysis of fitness for the final population

The fitness value corresponding to the total life cycle cost of the converged feasible population after utilizing the maximum function evaluations is shown in Fig. B1. The solution profile shown in Fig. B1 excludes DYYPO as it works only using two solutions and is independent of population size. The final population analysis helps in getting a set of converged solutions that show a trade-off in their fitness value and can be used for cases where the optimal solution is limited by operational constraints. The techniques DE, SPMGTLO, GA and COA could determine feasible solutions for all the population members, whereas for GWO, PSO and SHTS, infeasible solutions were also found in the population. Among the techniques, GA has converged to a single solution for the feasible population. A significant deviation in the fitness value is observed among solutions in the population for SHTS, COA, SPMGTLO, and DE.

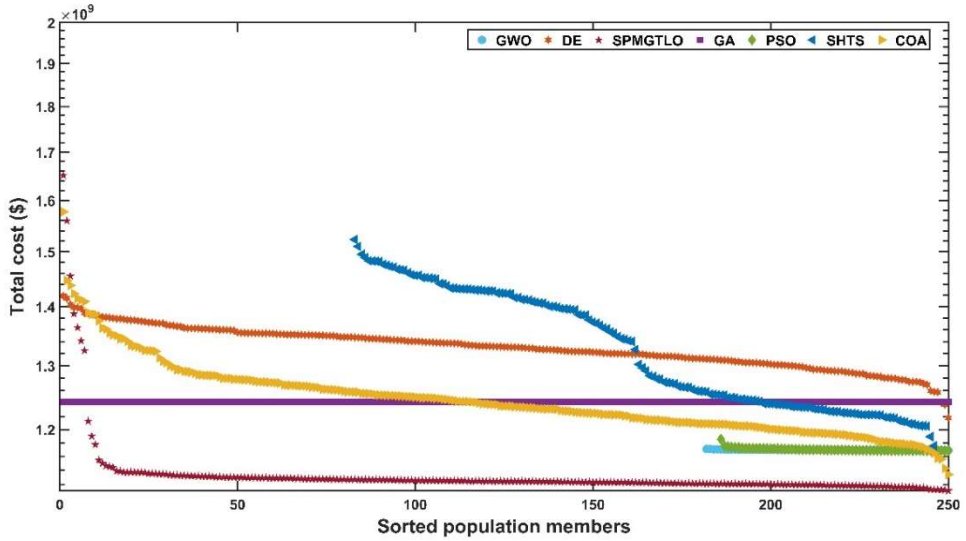

Fig. B1 Fitness analysis of the final population

Appendix C: Data used for the case studies of Chapters 2-4

Table C1. Raw material availability per month (tonnes/month)

	Harvesting sites	Wood Chips	sugar cane	Grain corn	Grain sorghum	Sweet sorghum
H 1	Northwest region	5084	327174	486858	79019	137598
H 2	South region	1701	558791	123441	7439	928
H 3	Centre west region	3311	698934	425502	164005	83629
H 4	Northeast region	4213	0	116917	11376	137737
H 5	East region	779	2259889	245245	248035	4469
H 6	Centre region	779	155737	139095	20614	1595

Table C2. Cost of raw material at source

	Raw material	$/tonnes
Raw 1	Wood Chips	86.6
Raw 2	Sugar cane	28.98
Raw 3	Grain corn	207.4
Raw 4	Grain sorghum	167.77
Raw 5	Sweet sorghum	31.11

Table C3. Product demand (tonnes/month)

	User 1	User 2
SPU 1	2021.78	901.02
SPU 2	1268.3	1065.1

Table C4. Data related to the available technologies for the MPU

Biomass	Technology	Mass ratio (/ tonne)	Fixed cost coefficient ($)	Variable cost coefficient ($/tonne)	Processing cost ($/tonne)
Wood Chips	Pretreatment, acid hydrolysis and Fermentation	0.1669	7000000	0.007	80
Wood Chips	Gasification and biosynthesis	0.2625	7000000	0.007	80
Wood Chips	Gasification and chemical synthesis	0.1887	7000000	0.007	80
sugar cane	Pretreatment, acid hydrolysis and Fermentation	0.0592	2766400	0.0027664	31.616
Grain corn	Pretreatment, acid hydrolysis and Fermentation	0.3149	5083260	0.00508326	58.0944
Grain sorghum	Pretreatment, acid hydrolysis and Fermentation	0.2999	3984120	0.00398412	45.5328
Sweet sorghum	Pretreatment, acid hydrolysis and Fermentation	0.0553	1421000	0.001421	16.24

Table C5. Data related to the available technologies for the SPU

Biomass	Technology	Mass ratio (/tonne)	Fixed cost coefficient ($)	Variable cost coefficient ($/tonne)	Processing cost ($/tonne)
Wood Chips	Pretreatment, acid hydrolysis and Fermentation	0.1669	10000000	0.01	100
Wood Chips	Gasification and biosynthesis	0.2625	10000000	0.01	100
Wood Chips	Gasification and chemical synthesis	0.1887	10000000	0.01	100
sugar cane	Pretreatment, acid hydrolysis and Fermentation	0.0592	3952000	0.003952	39.52
Grain corn	Pretreatment, acid hydrolysis and Fermentation	0.3149	7261800	0.0072618	72.618
Grain sorghum	Pretreatment, acid hydrolysis and Fermentation	0.2999	5691600	0.0056916	56.916
Sweet sorghum	Pretreatment, acid hydrolysis and Fermentation	0.0553	2030000	0.00203	20.3

Table C6. Biomass transportation cost ($/tonne)

	MPU	SPU 1	SPU 2
Northwest region	157.68	141.63	157.68
South region	118.31	158.39	118.31
Center west region	17.34	56.28	17.34
Northeast region	67.04	27.43	67.04
East region	13.39	34.07	13.39
Center region	23.81	63.88	23.81

Table C7. Allowable flow rates for transportation (tonnes/month)

	Minimum	Maximum
Biomass flow to the MPU	140	1400
Biomass flow to SPU	140	1400
Fuel flow from the MPU to SPU	140	1400

Table C7. Allowable processing capacity for MPU(tonnes/month)

	Minimum	Maximum
Biomass flow to the MPU	140	1400
Biomass flow to SPU	140	1400
Fuel flow from the MPU to SPU	140	1400

Table C8. Allowable processing capacity for MPU (tonnes/month)

Biomass	Technology	Minimum	Maximum
Wood Chips	Pretreatment, acid hydrolysis and Fermentation	95.32	9532.23
Wood Chips	Gasification and biosynthesis	95.32	9532.23
Wood Chips	Gasification and chemical synthesis	95.32	9532.23
sugar cane	Pretreatment, acid hydrolysis and Fermentation	116.61	11661.11
Grain corn	Pretreatment, acid hydrolysis and Fermentation	60.46	6046.45
Grain sorghum	Pretreatment, acid hydrolysis and Fermentation	35.50	3550.92
Sweet sorghum	Pretreatment, acid hydrolysis and Fermentation	89.10	8910.71

Table C9. Allowable processing capacity for SPU (tonnes/month)

Biomass	Technology	Minimum	Maximum
Wood Chips	Pretreatment acid hydrolysis and Fermentation	76.25	7625.78
Wood Chips	Pretreatment gasification and biosynthesis	76.25	7625.78
Wood Chips	Pretreatment gasification and chemical synthesis	76.25	7625.78
sugar cane	Hydrolysis and fermentation with black fermentation	93.28	9328.89
Grain corn	Catalytic Pyrolysis with LA/AL_2O_3	48.37	4837.16
Grain sorghum	Catalytic pyrolysis with GAMMA/AL_2O_3	28.40	2840.73
Sweet sorghum	Catalytic pyrolysis with CR_2O_3	71.28	7128.57

Note: For the main processing unit of the biorefinery case study used in chapters 3 and 4, an increased investment cost of 20% is applied.

Table C10. Algorithmic parameters for the metaheuristic algorithms

Algorithm	User-defined parameter	Value
GA	Tournament size	2
	Crossover distribution index mean	10
	Mutation distribution index mean	10
	Crossover probability	0.8
	Mutation probability	0.2
DE	Crossover probability	0.8
	Scaling factor	0.6
PSO	Inertia weight	0.7
	Acceleration coefficient 1	1.5
	Acceleration coefficient 2	1.5
SPMGTLO	Number of groups	4
DYYPO	Minimum value for archive update	1
	Maximum value for archive update	10
	Expansion/contraction factor	10

Appendix D: Detailed solution and data for the case study used in Chapter 5

Table D1. Conversion factors, Unit costs, Eco-indicator99 and jobs for each feedstock

Product	Raw Material	Cost ($/tonne)	Processing Route	Mass Ratio (/tonne)
Ethanol	Wood Chips	86.6	Pretreatment, acid hydrolysis and fermentation	0.1669
Ethanol	Wood Chips	86.6	Gasification and Biosynthesis	0.2625
Ethanol	Wood Chips	86.6	Gasification and Chemical synthesis	0.1887
Ethanol	Sugar cane	28.98	Pretreatment, acid hydrolysis and fermentation	0.0592
Ethanol	Corn grain	207.4	Pretreatment, acid hydrolysis and fermentation	0.3149
Ethanol	Sorghum grain	167.77	Pretreatment, acid hydrolysis and fermentation	0.2999
Ethanol	Sweet sorghum	31.11	Pretreatment, acid hydrolysis and fermentation	0.0553
Biodiesel	African Palm Oil	66.31	Extraction and transesterification with methanol	0.2064
Biodiesel	Jatropha	110.4	Extraction and transesterification with methanol	0.3268
Biodiesel	Sawflower	269.07	Extraction and transesterification with methanol	0.285

Table D2. Processing costs, Eco-indicator99 and jobs for each feedstock

Raw Material	Processing cost at main unit ($/tonne)	Processing cost at secondary unit ($/tonne)	Eco-indicator 99/tonne	Jobs/tonne biomass processed
Wood Chips	80	100	39.31	5.93E-04
Wood Chips	80	100	9.9	5.93E-04
Wood Chips	80	100	10.39	5.93E-04
Sugar cane	30.4	39.52	1.84	5.93E-04
Corn grain	55.86	72.618	17.16	6.41E-06
Sorghum grain	53.2	56.916	5.85	5.93E-04
Sweet sorghum	16.1	20.93	5.85	5.93E-04
African Palm Oil	55.05	71.565	10.56	1.19E-03
Jatropha	87.16	113.308	16.72	1.19E-03
Sawflower	76.01	98.813	14.58	1.19E-03

Table D3. Feedstock availability at the harvesting locations (tonnes)

Raw material	Harvesting locations	Jan	Feb	Mar	Apr	May	Jun	Jul	Aug	Sep	Oct	Nov	Dec
Wood Chips	H1	5084	5084	5084	5084	5084	5084	5084	5084	5084	5084	5084	5084
	H2	1701	1701	1701	1701	1701	1701	1701	1701	1701	1701	1701	1701
	H3	3311	3311	3311	3311	3311	3311	3311	3311	3311	3311	3311	3311
	H4	4213	4213	4213	4213	4213	4213	4213	4213	4213	4213	4213	4213
	H5	779	779	779	779	779	779	779	779	779	779	779	779
	H6	779	779	779	779	779	779	779	779	779	779	779	779
Sugar cane	H1	533008	395977	775646	529242	744649	558202	389363	0	0	0	0	0
	H2	3025668	1094683	2184954	1669491	1334888	282295	113518	0	0	0	0	0
	H3	2748833	1116699	1470949	1820716	752872	366686	110452	0	0	0	0	0
	H4	0	0	0	0	0	0	0	0	0	0	0	0
	H5	6219260	4458579	5769145	5178078	3426659	682132	1384818	0	0	0	0	0
	H6	594493	258901	348528	296504	370420	0	0	0	0	0	0	0
Corn	H1	194	222	29763	84305	1785225	3224777	89881	3778	7337	281066	111428	224323
	H2	11805	58713	62752	65346	57243	10311	16306	12392	4203	223921	497902	460400
	H3	1319	255	5180	78290	37821	1319	8037	1079	225	603659	1787921	2580913
	H4	0	0	0	0	270.00	1705	0	1419	0	241662	1047587	110359
	H5	9633	15896	30375	108580	237199	85922	242639	190775	45317	304867	1056438	615297
	H6	0	0	0	1490	1289	914	1307	478	170	55190	612789	995510
Sorghum	H1	0	1000	9466	215244	8045	23186	394771	59919	44783	7791	80092	103934
	H2	0	747	7864	27216	13364	10315	3773	597	130	1117	7023	17127
	H3	896	16	1993	15101	7849	3680	428	492	2959	456005	959629	519013
	H4	0	0	0	0	0	19066	4400	10059	1243	22183	52547	27017
	H5	480	0	19865	85780	45188	1893824	501646	1821	9927	881	87819	329187
	H6	0	0	0	0	0	0	0	0	0	13641	191951	41774

Raw material	Harvesting locations	Jan	Feb	Mar	Apr	May	Jun	Jul	Aug	Sep	Oct	Nov	Dec
Sweet sorghum	H1	7625	58755	12414	84221	25722	45410	48943	199258	424088	227577	332236	184921
	H2	0	0	4787	1852	1060	1095	0	220	317	406	1039	365
	H3	17786	6151	38791	113274	9782	10491	3519	3409	5476	229133	257755	307985
	H4	0	0	0	0	180	50413	39083	475238	304165	346089	253728	183950
	H5	0	595	2755	4600	7115	0	2725	4000	7289	3581	16410	4560
	H6	0	0	0	225	1105	233	447	4743	1148	2256	3046	5933
African palm	H1	0	0	0	0	0	0	0	0	0	0	0	0
	H2	24517	24517	24517	24517	24517	24517	24517	24517	24517	24517	24517	24517
	H3	0	0	0	0	0	0	0	0	0	0	0	0
	H4	0	0	0	0	0	0	0	0	0	0	0	0
	H5	6129	6129	6129	6129	6129	6129	6129	6129	6129	6129	6129	6129
	H6	0	0	0	0	0	0	0	0	0	0	0	0
Jatropha	H1	0	0	0	0	0	0	0	0	0	0	0	0
	H2	44150	44150	44150	44150	44150	44150	44150	44150	44150	44150	44150	44150
	H3	44150	44150	44150	44150	44150	44150	44150	44150	44150	44150	44150	44150
	H4	44150	44150	44150	44150	44150	44150	44150	44150	44150	44150	44150	44150
	H5	0	0	0	0	0	0	0	0	0	0	0	0
	H6	0	0	0	0	0	0	0	0	0	0	0	0
Sawflower	H1	0	0	3817	4113	73	14809	41327	1608	6836	0	0	0
	H2	0	0	0	0	0	0	0	0	0	0	0	0
	H3	0	0	128	352	3372	6301	118	44	750	0	0	0
	H4	0	0	0	0	0	90	0	0	0	0	15	0
	H5	0	0		2662	9826	1227	977	0	0	0	0	0
	H6	0	0	0	0	0	0	0	0	0	0	0	0

Table D4. Demand of bioethanol in each market (tonnes)

	Bioethanol					Biodiesel				
	MK1	MK2	MK3	MK4	MK5	MK1	MK2	MK3	MK4	MK5
January	181960	81091	114146	95858	70515	25709	13482	20469	17289	12631
February	121307	54061	76097	63905	47010	51419	26963	40938	34578	25261
March	90980	40545	57073	47929	35257	38564	20223	30703	25933	18946
April	75817	33788	47561	39941	29381	19282	10111	15352	12967	9473
May	75817	33788	47561	39941	29381	16068	8426	12793	10806	7894
June	60653	27030	38049	31953	23505	16068	8426	12793	10806	7894
July	60653	27030	38049	31953	23505	12855	6741	10234	8644	6315
August	75817	33788	47561	39941	29381	12855	6741	10234	8644	6315
September	75817	33788	47561	39941	29381	12855	6741	10234	8644	6315
October	90980	40545	57073	47929	35257	16068	8426	12793	10806	7894
November	121307	54061	76097	63905	47010	16068	8426	12793	10806	7894
December	181960	81091	114146	95858	70515	19282	10111	15352	12967	9473

Table D5. Unit costs, Eco-indicator99 for the products

Product	Cost ($/tonne)	Eco-indicator99/tonne
Bioethanol	796.82	32.12
Biodiesel	841	10.15

Table D6. Biomass transportation costs from main processing unit to secondary processing locations ($/tonne)

	Sec 1	Sec 2	Sec 3	Sec 4	Sec 5
Main unit	14.16359601	54.61732644	33.25518207	40.20708141	54.51152986

Table D7. Biomass transportation costs from harvesting location to processing locations ($/tonne)

	Main unit	Sec 1	Sec 2	Sec 3	Sec 4	Sec 5
H1	171.6871862	157.68448	141.6334461	176.2182845	212.0939664	224.390158
H2	104.3993111	118.3125	158.3906223	113.084026	64.7556434	83.88040926
H3	31.34646158	17.344379	56.27188474	49.37382271	71.30313689	85.23197618
H4	11.98568796	67.036843	27.42572807	62.63658178	116.4281941	128.4727275
H5	20.94021009	13.38984	34.06774986	27.17031385	60.8968854	74.8257247
H6	10.95777092	23.806734	63.88485619	38.53812476	37.38813475	51.31697404

Table D8. Jobs for biomass transportation

/tonne biomass transport	5.87E-04

Table D9. Eco-indicator 99/tonne transportation of biomass from harvesting to the processing locations

	Main unit	Sec 1	Sec 2	Sec 3	Sec 4	Sec 5
H1	2.248704535	2.0653015	1.85507014	2.30805143	2.77793978	2.938991413
H2	1.367389201	1.5496198	2.074550341	1.481138783	0.848148963	1.098639106
H3	0.410566053	0.2271712	0.737031372	0.646682735	0.933905965	1.116341503
H4	0.156984755	0.8780274	0.359213524	0.820394164	1.524939711	4.682695205
H5	0.274268258	0.1753759	0.446208627	0.355868189	0.79760817	0.980043707
H6	0.143521422	0.3118131	0.836743668	0.504760185	0.489697979	0.672133517

Table D10. Eco-indicator 99/tonne transportation of product from processing locations to the markets

	Main unit	Sec 1	Sec 2	Sec 3	Sec 4	Sec 5
MK1	0.145912119	0.3118131	0.836743668	0.504760185	0.489697979	0.572133517
MK2	0.750035541	0.5762913	0.02131831	0.493158105	1.198523588	1.380959125
MK3	0.436452572	0.2271712	0.737031372	0.646682735	0.933905965	1.116341503
MK4	2.091520946	2.0653015	1.85507014	2.30805143	2.772036248	2.1482297
MK5	0.858401431	1.5496198	2.074550341	1.481138783	0.848748963	1.098639106

Table D11. Eco-indicator 99/tonne transportation of product from main processing unit to secondary processing units

	Sec 1	Sec 2	Sec 3	Sec 4	Sec 5
Eco-indicator 99	0.185510294	0.7153605	0.435565871	0.526619652	0.7139748

Table D12. Biomass production at the harvesting locations (tonne/month)

Harvesting locations	Raw material	Jan	Feb	Mar	Apr	May	June	July	Aug	Sept	Oct	Nov	Dec
H3	Wood Chips	3310.80	3310.80	3310.80	3310.80	3310.80	3310.80	3310.80	3310.80	3310.80	3310.80	3310.80	3310.80
	Jatropha	44150	44150	44150	44150	44150	44150	44150	44150	44150	44150	44150	44150
H4	Wood Chips	4213.21	4213.21	4213.21	4213.21	4213.21	4213.21	4213.21	4213.21	4213.21	4213.21	4213.21	4213.21
	Grain Sorghum	0	0	0	0	0	19066	0	0	0	22183	0	27017
	Jatropha	44150	44150	44150	44150	44150	44150	44150	44150	44150	44150	44150	44150
H5	Wood Chips	779.46	779.46	779.46	779.46	779.46	779.46	779.46	779.46	779.46	779.46	779.46	779.46
	Grain Sorghum	0	0	0	85780	45188	1416443	501646	0	0	0	0	0
	African palm Oil	6129	6129	6129	6129	6129	6129	6129	6129	6129	6129	6129	6129
H6	Wood Chips	779.46	779.46	779.46	779.46	779.46	779.46	779.46	779.46	779.46	779.46	779.46	779.46
	Grain Sorghum	0	0	0	0	0	0	0	0	0	13641	0	41774

Table D13. Biomass transported to processing plants (tonne/month)

	Raw material	Jan	Feb	Mar	Apr	May	June	July	Aug	Sept	Oct	Nov	Dec
H3-C	Wood Chips	9932.41	3310.80	3310.80	3310.80	3310.80	3310.80	3310.80	3310.80	3310.80	3310.80	0	0
	Jatropha	27806.80	12583.00	44150	44150	44150	44150	44150	44150	44150	1148.08	0	0
H3-SP1	Jatropha	111265.70	31567.00	0	0	0	0	0	0	0	36379.42	0	0
H3-C	Wood Chips	12639.64	4213.21	4213.21	4213.21	4213.21	4213.21	4213.21	4213.21	4213.21	4213.21	0	0
	Grain Sorghum	27017	0	0	0	0	19066	0	0	0	22183	0	0
	Jatropha	132450	44150	44150	44150	44150	44150	44150	44150	44150	44150	0	0
H5-C	Wood Chips	2338.39	779.46	779.46	779.46	779.46	779.46	779.46	779.46	779.46	779.46	0	0
	Grain Sorghum	0	0	0	0	0	16443.2	0	0	0	0	0	0
	African palm Oil	18387	6129	6129	6129	6129	6129	6129	6129	6129	6129	0	0
H5-SP1	Grain Sorghum	0	0	0	85780	45188	1400000	501646	0	0	0	0	0
H6-C	Wood Chips	2338.39	779.46	779.46	779.46	779.46	779.46	779.46	779.46	779.46	779.46	0	0
	Grain Sorghum	41774	0	0	0	0	0	0	0	0	13641	0	0
SP1-C	Jatropha	0	111265.70	31567.00	0	0	0	0	0	0	0	36379.42	0

Table D14. Biomass stored at various storage facilities (tonne//month)

Storage location	Raw material	Jan	Feb	Mar	Apr	May	June	July	Aug	Sept	Oct	Nov	Dec
H3	Wood Chips	0	0	0	0	0	0	0	0	0	0	3310.80	6621.60
	Jatropha	0	0	0	0	0	0	0	0	0	6622.5	50772.50	94922.50
H4	Wood Chips	0	0	0	0	0	0	0	0	0	0	4213.21	8426.43
	Grain Sorghum	0	0	0	0	0	0	0	0	0	0	0	27017
	Jatropha	0	0	0	0	0	0	0	0	0	0	44150	88300
H5	Wood Chips	0	0	0	0	0	0	0	0	0	0	779.46	1558.92
	African Palm Oil	0	0	0	0	0	0	0	0	0	0	6129	12258
H6	Wood Chips	0	0	0	0	0	0	0	0	0	0	779.46	1558.92
	Grain Sorghum	0	0	0	0	0	0	0	0	0	0	0	41774
C	Jatropha	0	0	0	0	0	0	0	0	0	0	0	36379.42

Table D15. Biomass processed at various processing plants (tonne/month)

Plant	Raw material	Jan	Feb	Mar	Apr	May	June	July	Aug	Sept	Oct	Nov	Dec
SP1	Grain Sorghum	0	0	0	0	85780	45188	1400000	501646	0	0	0	0
C	Wood Chips	0	27248.82	9082.94	9082.94	9082.94	9082.94	9082.94	9082.94	9082.94	9082.94	9082.94	0
	Grain Sorghum	0	68791	0	0	0	0	35509.2	0	0	0	35824	0
	African Palm Oil	0	18387	6129	6129	6129	6129	6129	6129	6129	6129	6129	0
	Jatropha	36379.42	160256.80	167998.70	119867	88300	88300	88300	88300	88300	88300	45298.08	0

Table D16. Product transport to different markets (tonne/month)

		Product	Jan	Feb	Mar	Apr	May	June	July	Aug	Sept	Oct	Nov	Dec
SP1	C	Ethanol	0	0	0	0	0	0	0	221470.73	150443.64	0	0	0
	MK1		0	0	0	0	0	0	0	75817	0	0	0	0
	MK2		0	0	0	0	0	0	0	33788	0	0	0	0
	MK3		0	0	0	0	0	25725.42	13551.88	47561	0	0	0	0
	MK4		0	0	0	0	0	0	0	24875.75	0	0	0	0
	MK5		0	0	0	0	0	0	0	16347.52	0	0	0	0
C	MK1	Ethanol	13127.89	0	27783.24	2384.27	2384.27	2384.27	2384.27	0	90980	121307	2384.27	0
		Biodiesel	16068.44	11888.80	16068	16068	12855	12855	12855	6068	9254.47	1982	5709	0
	MK2	Ethanol	0	0	0	0	0	0	0	0	40545	0	0	0
		Biodiesel	0	0	8426	8426	6741	717.4656	717.4656	8426	0	3314.47	0	0
	MK3	Ethanol	0	0	0	0	0	0	0	0	57073	31520.91	0	0
		Biodiesel	0	0	12973	12973	10234	10234	10234	12793	12973	15352	20469	0
	MK4	Ethanol	0	0	0	0	0	0	0	0	0	0	0	0
		Biodiesel	0	0	10806	10806	4292.56	0	0	0	0	0	0	0
	MK5	Ethanol	0	0	0	0	0	0	0	13033.48	35257	0	0	0
		Biodiesel	0	0	7894	7894	6315	6315	6315	2834.47	7894	9473	3943.47	0

Table D17. Product stored at storage locations (tonne/month)

	Product	Jan	Feb	Mar	Apr	May	June	July	Aug	Sept	Oct	Nov	Dec
C	Ethanol	0	0	0	0	0	0	0	0	0	0	0	13127.89
	Biodiesel	0	0	0	0	0	0	0	0	0	0	0	16068.44

Table D18. Product sold at different markets (tonne/month)

Markets	Product	Jan	Feb	Mar	Apr	May	June	July	Aug	Sept	Oct	Nov	Dec
MK1	Ethanol	0	13127.89	0	27783.24	2384.27	2384.27	2384.27	2384.27	75817	90980	121307	2384.27
	Biodiesel	0	16068.44	11888.80	16068	16068	12855	12855	12855	6068	9254.47	1982	5709
MK2	Ethanol	0	0	0	0	0	0	0	0	33788	40545	0	0
	Biodiesel	0	0	0	8426	8426	6741	717.47	717.47	8426	0	3314.47	0
MK3	Ethanol	0	0	0	0	0	0	25725.422	13551.881	47561	57073	31520.91	0
	Biodiesel	0	0	0	12973	12973	10234	10234	10234	12793	12973	15352	20469
MK4	Ethanol	0	0	0	0	0	0	0	0	24875.753	0	0	0
	Biodiesel	0	0	0	10806	10806	4292.56	0	0	0	0	0	0
MK5	Ethanol	0	0	0	0	0	0	0	0	29381	35257	0	0
	Biodiesel	0	0	0	7894	7894	6315	6315	6315	2834.47	7894	9473	3943.47